A REDUCED ORDER MODELING METHODOLOGY FOR THE PARAMETRIC ESTIMATION AND OPTIMIZATION OF AVIATION NOISE

A Dissertation
Presented to
The Academic Faculty

By

Ameya Ravindra Behere

In Partial Fulfillment
of the Requirements for the Degree
Doctor of Philosophy in the
School of Aerospace Engineering

Georgia Institute of Technology

December 2022

A REDUCED ORDER MODELING METHODOLOGY FOR THE PARAMETRIC ESTIMATION AND OPTIMIZATION OF AVIATION NOISE

Thesis committee:

Prof. Dimitri N. Mavris, Advisor
School of Aerospace Engineering
Georgia Institute of Technology

Dr. Michelle R. Kirby
School of Aerospace Engineering
Georgia Institute of Technology

Prof. Lakshmi N. Sankar
School of Aerospace Engineering
Georgia Institute of Technology

Dr. Rudramuni K. Majjigi
Office of Environment and Energy – Noise Division
Federal Aviation Administration

Prof. Daniel P. Schrage
School of Aerospace Engineering
Georgia Institute of Technology

Date approved: August 19, 2022

To my parents...

ACKNOWLEDGMENTS

The experience of undertaking original research and writing this dissertation has been a challenging yet fulfilling endeavor, which would be unthinkable without the support, encouragement, and mentorship of many individuals. Here, I would like to acknowledge all those who supported me through this journey.

First, I would like to thank my advisor Dr. Dimitri Mavris for his constant support, guidance, and advice which made graduate school a wonderfully enriching experience. I especially thank him for providing me with the freedom and stability with which I could work on a topic of my interest. His insights and experience helped me greatly when I was in the exploration stage of my research, and there are many life-lessons that I will take with me throughout my career. The PhD program at ASDL has honed my analytical, reasoning, and argumentation skills. I will forever be thankful to Dr. Mavris for creating a fun and welcoming environment at ASDL, which has resulted in many friendships and a relatively stress-free graduate life.

I would also like to thank all members of my defense committee: Dr. Michelle Kirby, Prof. Lakshmi Sankar, Prof. Daniel Schrage, and Dr. Rudramuni Majjigi for taking time out of their busy schedules to be on my committee. Their feedback and comments have proved invaluable in steering me in the right direction and bettering this dissertation. I also want to thank Dr. Kirby for providing me with a research home at ASDL, her mentorship, support and encouragement, and for providing me with ample opportunities to grow as a researcher.

I would like to thank all my friends and colleagues at ASDL, who have made the graduate school life enjoyable and fulfilling. Starting with the friendships from the 'bootcamp' first year of graduate school, I would like thank Ruxandra Duca, Kenneth Decker, Lea Harris, Edan Baltman, Chelsea Johnson, Matt Rines, Adam Baker, Marlin Ballard, Shawn Wesley Skinner, and many more. I also thank Dongwook Lim for his

mentorship and encouragament. I also want to thank my colleague Jirat Bhanpato for all our collaboration on publications. I would also like to express my gratitude to my close friends and colleagues Tejas Puranik, Mayank Bendarkar, and Dushyyanth Rajaram for the long coffee walks, research collaborations, great times, and advice throughout the PhD journey. I must also thank Tanya Ard-Smith and Adrienne Durham for patiently answering my incessant queries about grad school logistics.

I have had the good fortune of meeting some amazing people throughout my time at graduate school with many wonderful new friendships forged, and old friendships strengthened. I would like to thank Achyut Panchal, Pushkar Godbole, Indranil Karandikar, Ketan Patwardhan, and Aditya Pophale for their friendship. I would like to thank Devika Gokhale, Sagar Patil, Prerna Singh, Eashwar Sriram, Pranjali Borkar, Juilee Rege, Deep Chitale, Aditya Bhatambrekar, and Priya Kandharkar for their strong friendships, constant encouragement and support. I also thank Moumita Dey, Darshan Sarojini, and Nitish Sontakke for their companionship along the PhD journey.

I am exceedingly fortunate to have shared this PhD experience with my most wonderful and amazing girlfriend, Sriramya Bhamidipati. Thank you for supporting me through all of life's twists and turns, for your limitless love and companionship. Thank you to Sirisha Bhamidipati, Charan Reddy Enugala, Surabhi Abhyankar, and Chirag Mirani for providing me with a home away from home and for always treating me like family. Thank you Dhruvika, Shruti, and Sandhya for always bringing a smile to my face.

Finally, I express the utmost gratitude for my parents, Ravindra Behere and Anita Behere to whom this thesis is dedicated. Your support, belief in my abilities, and pride in my achievements motivates me to be better each day. Thank you for setting me up to be successful in my personal and professional life and for all the sacrifices you make for your children. I also thank my sister Aditi Behere, brother-in-law Kunal Kulkarni, and nephew Advay for their love and support, and for being role models I could always look up to.

TABLE OF CONTENTS

LIST OF TABLES

LIST OF FIGURES

SUMMARY

Sustainability is one of the most important modern challenges faced by the aviation industry, with proposed solutions ranging from novel aircraft architectures to sustainable aviation fuels. A key barrier to robust long-term growth is the successful mitigation of aviation noise at airports. In addition to infrastructure constraints, community noise exposure remains a crucial limiting factor on capacities at most global large airports. With increasing urbanization and robust growth in air traffic passenger volumes, community noise exposure is expected to be of ever-increasing concern. The consequences of aviation noise can be categorized as direct and indirect health effects, effects on the human and non-human environments, and economic effects. These effects range from sleep disturbances, lower learning outcomes in schools, and declining real-estate valuations.

Various stakeholders have proposed a wide variety of mitigation measures to abate the consequences of aviation noise. The International Civil Aviation Organization (ICAO)'s Balanced Approach classifies these measures into four broad categories – reduction of aircraft noise at source through the development of new technologies, land-use planning and management, noise abatement operational procedures, and operating restrictions. While technology development is limited to aircraft and engine manufacturers, airports may employ a combination of operational measures. With a variety of options available, it is crucial that the potential noise outcomes of each option be accurately analyzed.

Existing methods and tools to quantify aviation noise rely on two fundamental capabilities – the ability to model aircraft operations in the terminal airspace to obtain trajectories and performance information, and the ability to use the generated trajectory and performance to compute various noise metrics. The first capability is usually achieved through point-mass aircraft performance and dynamics models. The second capability is usually based on Noise-Power-Distance (NPD) curves, which use lookup tables to interpolate noise metrics using the computed thrust and separation of the aircraft to the

observer at multiple points in the trajectory. These physics-based and semi-empirical methods used by traditional aviation noise modeling methods and tools are computationally expensive. Considering the wide variety of factors which can influence aviation noise, such as ambient temperature, wind, choice of operational profile etc., it is infeasible to comprehensively evaluate all possible factors. This leads to simplifying assumptions which limit the accuracy and applicability of the model at non-assumed conditions.

The fundamental cause of computational complexity is the high-dimensionality of the output to be calculated. Community noise exposure analysis inevitably involves the computation of noise metrics on a large grid of points surrounding the airport. Traditional surrogate modeling methods that attempt to speed up the noise computation process suffer from the same high-dimensional outputs, and are therefore unable to make meaningful improvements to computational speed; or must make similar simplifying assumptions to make the problem tractable which limits the proposed model's accuracy and applicability. The secondary problem is that some averaged assumptions such as the flight profile of an aircraft are difficult to represent with numeric parameters and are often handled using categorical variables.

The overarching objective of this dissertation is to develop a methodology that addresses these two problems with traditional aviation noise quantification models. First, a parametric definition for the representation of aircraft trajectories and flight characteristics is proposed. It is shown that the developed parametric definition can reasonably present the variation present in real-world trajectory data. Next, a method is proposed by which real-world time-series flight data, which are typically difficult to model for aviation noise results, can be mapped onto a parametric definition. A supplementary method is also developed based on the unsupervised machine learning technique of clustering which is used to group similar real-world flights together, so that only the median representatives of the identified groups need to be modeled.

Next, the identified parameters are screened for their influence on aviation noise

metrics. Using a step-wise regressions, the parameters with the most influence on the noise results are identified. This information is of importance when performing parametric trade-off analyses and optimization studies, where the design space of aircraft trajectories can be explored efficiently, given a ranked list of parameters based on their influence. Additionally, the parameters which do not have a significant impact are also identified. These least influential parameters can be safely set to default values when performing the aforementioned many-query studies.

Finally, the high-dimensional complexity of the noise output is addressed with the use of Model Order Reduction techniques. The Principal Component Analysis method is adapted for use with aviation noise outputs. This method works by reorienting the high-dimensional data along identified principal directions or axes. With this reorientation, the variability within the dataset can be explained just using the first few directions, and all other directions can be discarded. This effectively results in a projection of the high-dimensional data onto a lower-dimensional hyperplane. With the dimensionality reduction complete, the final problem of predicting the coordinates of the projected data is tackled. A predictive regression model based on the Boosted Tree algorithm is generated. This developed prediction model can accurately quantify the coordinates of the projected lower-dimensional data based on input parameter values. The model order reduction combined with the surrogate modeling in lower-dimensional space is collective referred to as Reduced Order Modeling or Field Surrogate Modeling. Thus, given a set of parameters, and the developed field surrogate model, complete noise grids can be accurately predicted with near real-time computational speed.

The conclusion of the research effort yielded a methodology that encapsulates the contributions of both research areas and provides an integrated platform for the rapid, accurate, and parametric quantification of aviation noise metrics. Thus, the developed methodology fulfils the research objective and answers the motivating research question of this dissertation. The application of this methodology is shown in a case study, where

a large set of real-world flights are analyzed for their sound exposure level. Additionally, this methodology can also be employed for many-query applications such as parametric trade-off analyses and optimization efforts.

CHAPTER 1
INTRODUCTION

As the commercial aviation industry progresses towards sustainable growth, some key barriers need to be overcome. This chapter provides details about these barriers, their consequences, and attempts at their mitigation. The chapter concludes with a motivating research question and a research objective which guide the research in this dissertation.

1.1 Sustainable Aviation

1.1.1 Growth of the Global Aviation Industry

The modern civil aviation industry since its inception in the early 20th century has witnessed strong and robust long-term growth. Initial demand for air travel was limited to the capabilities of the aircraft of the time. As technologies continued to mature, aircraft became safer, more economical, and could fly farther and faster, thereby increasing accessibility to the skies. Current air travel growth is strongly correlated with economic and demographic growth. Over the past few decades, the civil aviation industry has continued to maintain robust long-term growth globally, despite powerful short-term shocks to the market. This trend is expected to continue into the future, driven by modest growth in developed markets, and rapid growth in newly industrializing countries.

Growth forecasts and analyses performed by different stakeholders provide the data to back up these predictions. The Boeing Company's Commercial Market Outlook for 2021-2040 predicts a global averaged fleet growth rate of 3.1% and an air traffic growth rate of 4.0% per year [1]. Similarly, the Global Market Forecast released by Airbus for 2021-2040 predicts an average annual growth rate of 3.9% [2]. These predictions by the aircraft manufacturers are corroborated by reports from governmental agencies. The

Federal Aviation Administration (FAA) estimates a average growth rate over 2021-2040 to be 2.3% for the US domestic market, after a recovery to pre-pandemic levels [3]. EUROCONTROL's predictions in its Aviation Outlook 2050 report range from 0.6% to 1.8% depending on the scenario [4]. As noted previously, the lower growth numbers for the developed US and European aviation markets are to be expected.

Although this growth in passenger numbers and fleet sizes is robust over the long-term, it is not always steady. Figure 1.1 shows the number of scheduled passengers boarded by the global airline industry from 2004 to 2022. While most years from this chart show growth, there are two notable exceptions. There is a slight contraction in passenger numbers between 2008 and 2009, attributed to the economic recession of that time and volatility in fuel costs, among other factors [5]. The industry recovered quickly, and passenger numbers were rising again by 2010. A much more drastic contraction occurred due to the Covid-19 global pandemic which suspended almost all global commercial aviation, especially international travel, and crippled the airline industry. As both business and leisure travel plummeted, the actual number of global passengers post-Covid ended up being 1.8 billion, about 40% of the expected 4.7 billion. Passenger numbers recovered slightly in 2021, and are expected to continue their recovery in 2022. In the near-future, the International Air Transport Association (IATA) forecasts a steady recovery, with overall passenger numbers reaching 94% of 2019 levels in 2023, 103% in 2024, and 111% in 2025 [6]. EUROCONTROL's Forecast Update for 2021-2027 outlines the potential recovery timelines for European markets in three scenarios [7]. In the 'low' scenario, recovery to pre-pandemic levels is delayed until 2027, but in the baseline and high scenarios, can happen as soon as 2023. The prospects of recovery have also been studied by academia, with similar predicted outcomes [8, 9].

The robust long-term growth of commercial aviation is complimented by the potential growth from new air-transportation concepts that are currently being developed. The Urban Air Mobility (UAM) is an emerging concept where small vehicles operate as air taxi

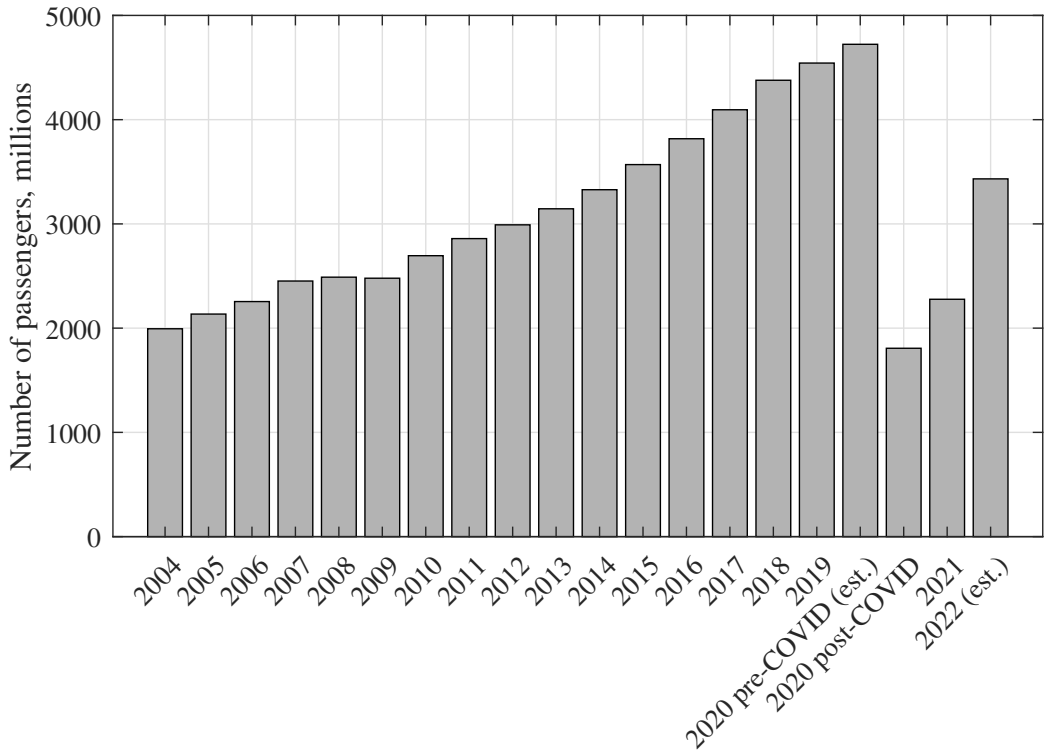

Figure 1.1: Number of scheduled passengers boarded by the global airline industry from 2004 to 2022, created with data from Statista [10]

services. There are several companies developing vehicles which range from piloted to autonomous, and from single-seater to multi-seater configurations. Propulsion systems are usually battery-electric, and lift generation is either through rotors, or through a combination of rotors and lift-generating surfaces. These concepts have the potential to open up new areas in the aviation market, and their ability to generate demand has been studied extensively [11, 12, 13]. According to findings by NASA-commissioned market studies, the annual demand by 2030 could be as high as 500 million flights for package delivery services and 750 million flights for passenger services, which have the potential to make the UAM concept profitable and relevant [14]. Additionally, general aviation and transport category aircraft are also being investigated for potential electrification with a research emphasis on safety analysis [15, 16] and certification [17, 18].

The re-emergence of supersonic aircraft is another concept which has the potentially to significantly impact the industry. With supersonic flight over land unlikely to be

approved, a large amount of resources have been invested in demand forecasting and routing models [19]. Conventionally, the demand for supersonic travel has been seen as a premium segment, and studies have attempted to estimate the market potential for these aircraft by analyzing the premium ticket market globally [20]. Indeed, the most promising initial application of supersonic flight in the near future is likely to be in the business jet market [21, 22]. This mode of flight will likely attract subsonic business travel, and not necessarily induce new demand. Nevertheless, the environmental impacts of supersonic aircraft are typically higher than subsonic aircraft, and must be a part of the consideration for sustainable aviation [23, 24, 25].

1.1.2 Environmental Effects of Aviation

The predicted long-term growth of traditional commercial aviation and the emergence of new concepts have several barriers which will need to be overcome. Increasing demand for air travel is expected to be met by airlines through a combination of measures. These measures include the addition of new city-pair operations to existing airline networks, the 'upgauging' of routes so that higher capacity aircraft are deployed, and an increase in the frequency of operations on existing routes. There are several challenges associated with accommodating these additional operations – airspace congestion, allocation of slots at busy airports, ground handling logistics and infrastructure, and so on.

Other key concerns are about the associated environmental impacts from the growing aviation industry [26, 27, 28, 29]. Environmental impacts from aviation can be classified into three categories – exposure of people living near airports to noise from aircraft, pollutant discharge in storm water runoff from airports, and aircraft engine emissions into the atmosphere [30]. The mitigation of these environmental effects is a key enabler to sustainable aviation growth. This has given rise to major areas of research with with interest from governmental agencies, academia, and the industry.

In order to mitigate these effects, several aggressive goals have been set by various

stakeholders in the aviation industry. The Environmentally Responsible Aviation (ERA) program by the National Aeronautics and Space Administration (NASA) was created to focus on the development and demonstration of integrated systems technologies to Technology Readiness Levels (TRL) of 4 to 6 which could simultaneously reduce CO_2, NO_x, and noise emissions on a system level [31]. Aggressive targets were assigned progressively over three generations, called N+1, N+2, and N+3. These targets are summarized in Table 1.1. The goals represent projected benefits in metric values once multiple technologies are matured and implemented by the industry. For example, some of the technologies considered are drag reduction through laminar flow, weight reductions with advanced composite structures, Low NO_x and fuel-flexible combustors, and the integration of advanced ultra high bypass engines. The reference aircraft for the N+1 and N+3 values is a Boeing 737-800 aircraft with CFM56-7B engines, whereas the reference aircraft for the N+2 values is a Boeing 777-200 with GE90 engines.

Table 1.1: NASA ERA Goals for Subsonic Transport System Level Metrics [31]

	Technology Generations (TRL 4-6)		
Technology Benefits	N+1	N+2	N+3
Noise (cumulative below Stage 4)	-32 dB	-42 dB	-71 dB
LTO NOx Emissions (below CAEP 6)	-60%	-75%	-80%
Cruise NOx Emissions (relative to 2005 best in class)	-55%	-70%	-80%
Aircraft Fuel/Energy Consumption (relative to 2005 best in class)	-33%	-50%	-60%

Similarly, the International Air Transport Association (IATA) has created a roadmap to identify a timeline for potential CO_2 reductions by 2050 as shown in Figure 1.2 [32]. This roadmap also outlines the various avenues of improvement through which the target of -50% CO_2 emissions can be achieved. These include a mix of existing technologies,

economic measures, and alternative fuels. In 2009, various stakeholders committed to a set of ambitious climate goals including 1.5% fuel efficiency improvements per year, reaching net carbon neutrality by 2020, and reducing the global net carbon emissions by 50% in the year 2050, when compared to a baseline of 2005. Along similar lines, the International Civil Aviation Organization (ICAO) in 2017 with the help of industry and governments, developed and adopted the new aircraft CO_2 emissions standard in order to reduce the impact of aviation greenhouse gas emissions on the global climate [33].

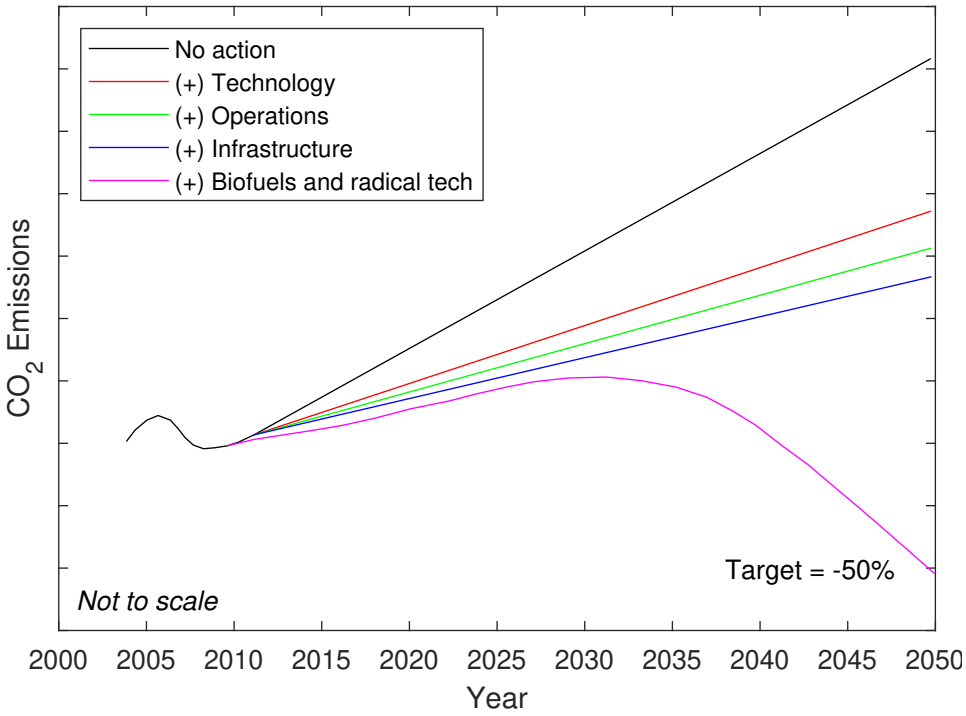

Figure 1.2: Schematic Roadmap for CO_2 emissions reductions by IATA (based on [32])

1.2 Aviation Noise

In addition to concerns over fuel consumption and pollutants, the International Civil Aviation Organization has identified aircraft noise as "the most significant cause of adverse community reaction related to the operation and expansion of airports." To this effect, one of ICAO's main priorities and key environmental goals is limiting or reducing the number of people affected by significant aircraft noise. As part of the CAEP/11 update to the

ICAO Global Environmental Trends in 2019, a range of scenarios was developed for the assessment of future noise trends. The high level indicator used for this assessment was the total contour area and population contained within the 55 DNL dB contour at 315 airports worldwide. This assessment captured about 80% of global traffic. The trends for various scenarios are shown in Figure 1.3.

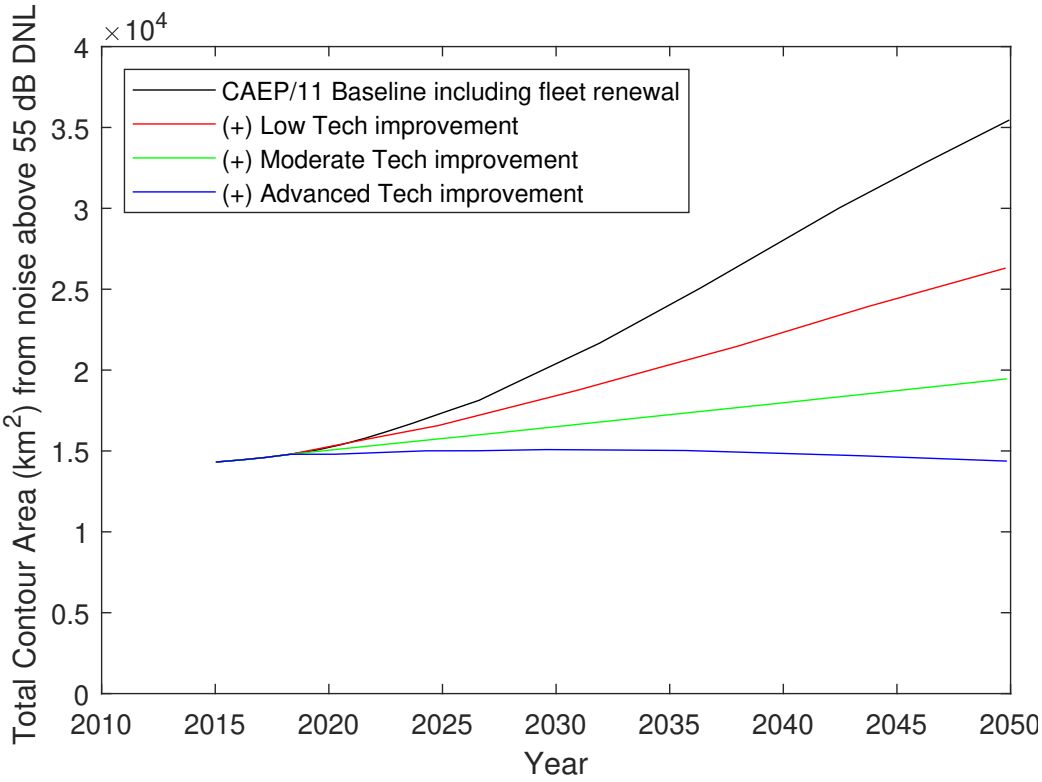

Figure 1.3: Total aircraft noise contour area above 55 DNL dB for 315 global airports (based on [34])

Aviation noise consists of several sources, related to both the engine and the airframe itself. The noise at source then propagates through the atmosphere before reaching a receptor. A breakdown of the sources and the atmospheric effects on propagation is shown in Figure 1.4.

ICAO's main overarching policy on aircraft noise is the Balanced Approach to Aircraft Noise Management [36]. This policy consists of identifying the noise problem at a specific airport and assessing the different measures available to reduce noise. These reduction measures are classified into four principal elements – reduction of noise at

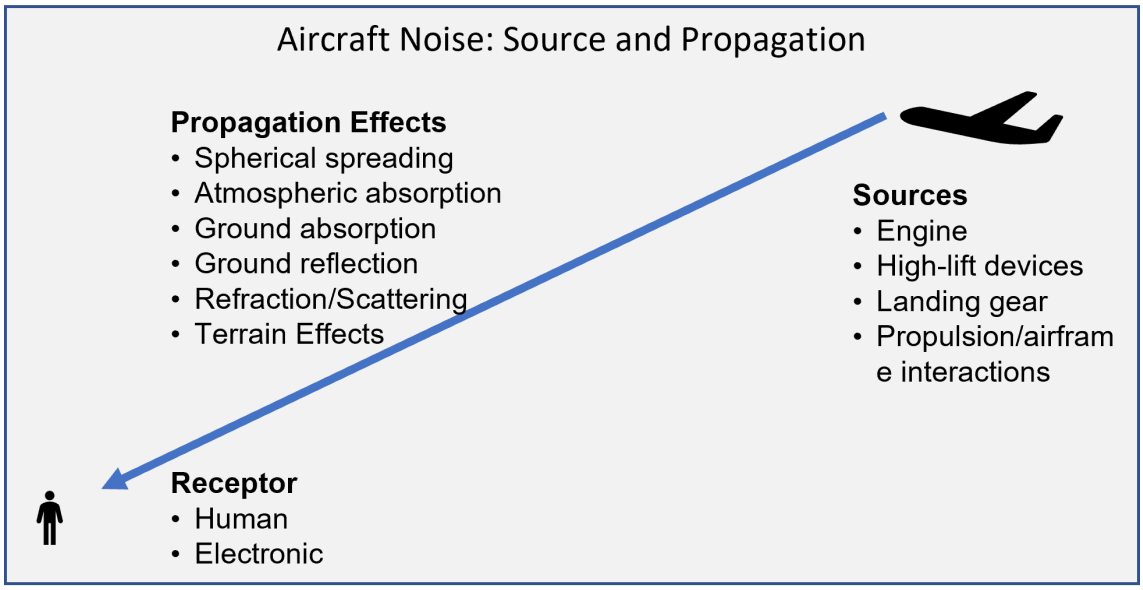

Figure 1.4: Breakdown of typical noise sources for a fixed-wing aircraft (based on [35])

source (technology standards), land-use planning and management, noise abatement operational procedures, and operating restrictions. The noise problem is addressed on an individual airport basis, by identifying the noise-related measures that achieve maximum environmental benefit while also being the most cost-effective. This cost-benefit analysis should be performed using objective and measurable criteria.

1.2.1 Consequences of Aviation Noise

There are several undesirable consequences of aviation noise to society. Many major airports across the world already consider noise to be the largest major concern for their operations in the near-term and long-term future. This problem will continue with increasing air traffic and will be further exacerbated by increasing levels of global urbanization. In a 2010 survey by the US Government Accountability Office, addressing noise issues was the most commonly cited environmental issue that led to delay in implementing operational changes [37].

The impacts of aviation noise can be categorized as direct health effects, effect of noise on human environments, effect of noise to non-human environment, and the economic

effects of noise [38, 39, 40, 41, 42, 43].

The most direct concern arising from aviation noise is related to the potential effects is might have on the health of the community. It is difficult to establish conclusive causal correlations between effects and aviation noise, due to the large amount of other confounding variables which can often not be accounted for. Nevertheless, there is some scientific evidence to suggest that aviation noise exposure can induce hearing impairment and cardiovascular conditions [44]. Additionally, noise disturbs the sleeping patterns of residents in neighboring communities. In fact, most noise-exposed populations in the vicinity of airports cite sleep disturbance as a common complaint [42]. Repeated exposure to noise events impairs sleep quality by delayed sleep onset, early awakenings, more time spent in superficial sleep stages, and overall poor quality of sleep [39, 45].

Beyond direct health effects, noise also has other effects on people's living and working environment [46]. These other effects are related to annoyance and interference. Although it is subjective, annoyance is the most widespread and well document response to noise. Annoyance can be described as a feeling of resentment, discomfort, or dissatisfaction which occurs when noise interferes with thoughts, feelings, and daily activities. There are several factors which affect annoyance, including the sound itself (amplitude, pitch, duration, temporal profile) and psychological factors [47, 48]. Speech interference is a major contributor to annoyance. Additionally, there is a considerable amount of research on the effect that noise has on the learning abilities of children. Two studies spaced three years apart at the Munich airport demonstrated that in areas with high noise, there was evidence of poor persistence for challenging tasks [49]. The switch of airports at Munich in 1998 provided researchers with a unique opportunity. Researchers collected data from areas around the old and new airports, before and after the switch. They found that long-term memory and reading skills were impaired in children at the new airport, while there was improvement in children at the old airport, who were no longer exposed to aviation noise [50]. An improvement in short-term memory was also observed after closure of the

old airport, while speech perception suffered in the children newly exposed to noise at the new airport.

The effects of aviation noise are not limited to humans alone, and extend to both domesticated animal species and wildlife [51]. It has been noted in literature that noise alone can be a minor disturbance, but in combination with the visual stimulus can trigger a reaction [52]. Most prior research in this area has been performed in controlled laboratory conditions to maintain accurate measures of noise levels and changes in the animal's response. Therefore, the results cannot always be applied directly to wildlife species. However, further research in this area has been encouraged with potential adverse effects including habitat changes, predator-prey relationships, reproductive failure, intra- and inter-species behavior patterns, and nutritional deficiencies [53].

Lastly, there are a large variety of economic effects which arise from aviation noise [54, 55]. These effects range from lost economic output due to land-use compatibility and real-estate valuations to actual spending on noise mitigation programs such as home insulation grants. Balancing this lost economic output with the economic boosts that airports provide is a key challenge faced by many airport operators. Loss of economic output often affects entire communities which are located in the airport vicinity. Increases in noise levels over time also drive down real estate prices, and can also make the sale of a property more difficult [56]. This is usually true for residential zoned land, while some commercial zones such as business centers may favor proximity to the airport [57]. Noise management programs can also have expensive components such as funding for noise insulation or acquisition of non-compatible land. Since the start of the Airport Noise Compatibility Planning program in 1982, the FAA has spent almost $6 billion for Part 150 studies and implementation [58]. This funding is typically obtained either through passenger fees or through federal taxes. Airports can also impose landing fees or surcharges on airlines, which would ultimately pass the costs on to the passengers.

Aviation noise has long been an undesirable consequence of aviation. Technology has

certainly improved over the years, and reduced noise levels at the individual aircraft level. However, at a systems level, increased number of air operations have ensured that noise mitigation remains a key issue at most major airports. To enable sustainable aviation, it is important to understand the effects of noise as well as investigating potential mitigation strategies.

1.2.2 Noise Mitigation and Management Programs

There are several measures for noise control and management which have been categorized by ICAO's Balanced Approach for airport noise management into four major categories – reduction of noise at source (technology standards), land-use planning and management, noise abatement operational procedures, and operating restrictions [36]. These guidelines are general, as ICAO recognized the need for the solution each airport's noise problem to be developed in accordance with the specific characteristics of the airport. However, similar solutions can be applied if similar noise problems are identified at airports. An analysis of noise management practices at airports revealed no fewer than 18 measures, with many airports implementing a combination of features based on their suitability and efficacy [59, 60, 61, 62]. These measures are discussed in detail according to the ICAO categories in this subsection.

The reduction of noise at the aircraft source is one of the most effective solutions available for long-term improvement [63]. Jet-powered aircraft have benefited from a large reduction in engine noise, as engine architectures have moved from inefficient turbojet to low-bypass turbofan to high-bypass turbofan engines which are present on all modern aircraft designs [64, 65]. A higher bypass engine pushes a larger volume of air at a lower exit velocity, thereby reducing jet noise. A comprehensive assessment of the noise impact of technologies discussed in NASA ERA Projects ranging in levels from component to single event to multi-event is presented in [66]. The development of these technologies usually occurs concurrently with new aircraft or engine model programs. Recent examples

of this include the nacelle chevrons [67] included on most modern Boeing commercial aircraft starting with the 787 aircraft family which entered commercial service in 2011 and the geared turbofan architecture [68] developed by Pratt and Whitney which entered into commercial service in 2016 as an engine option for the Airbus A320 NEO family. New technologies can also be deployed on older aircraft through retrofits also known as "hushkits" [69]. However, these solutions often exacerbate the problem by only reducing the noise levels to the permissible limit, which then adds several years to the operational life of the older aircraft. While technologies are certainly effective, developing them is a time and capital intensive process. Even technologies which are selected for deployment on production aircraft may take several years to make a pronounced effect – aircraft fleet replacement is a time-consuming and capital-intensive proposition for airlines.

The second major category is land-use planning and management which is primarily undertaken by the airport operator and local government. Noise insulation programs fall under this category which may include structural changes to buildings such as insulated sidings, solid core doors, and double pane windows [70, 71]. These programs typically include homes which are deemed to be exposed to a significant level of noise exposure. The area of significant noise exposure is determined by overlaying contours of noise metrics on maps. With the help of appropriate zoning laws, these contours help prevent or discourage incompatible development of property within the contour without the proper notice and documentation. Another strategy can be to provide purchase assurance to homeowners located within the airport noise contours, or for airport operators to acquire incompatible land in the airport vicinity [72, 73, 74, 75]. Under purchase assurance programs, the airport proprietor agrees to be a last resort option for the homeowner, if the house cannot be sold in the open market.

Noise abatement procedures and operational changes are also important tools for noise mitigation. These allow airport operators to make relatively quick changes (as compared to land use policies and new technologies) to aircraft operations and observe benefits. These

can include simple measures such as operating quotas based on the time of the year, aircraft type, time of the day etc. Preferential runway and ground track assignments can also help by directing traffic away from populated areas, if Air Traffic Control, weather, and safety conditions permit [76, 77]. For example, in many coastal areas, departures may be flown out over water bodies where the exposure to humans is limited. Finally, noise abatement procedures are utilized by airlines and sometimes recommended by airports which alter the aircraft's departure or arrival trajectory and thrust variation to suitably tailor the noise footprint of each operation.

Operating restrictions and legislative measures are the final category of noise management measures. These include various types of restrictions on aircraft operations imposed by individual airports and also more coordinated efforts such has increasingly stringent noise certification standards. Some airports may choose to implement engine run-up or APU restrictions which may limit where and how an aircraft can perform a run-up or use its APU respectively. An airport may have to offer additional accommodations in order to implement these limits. For example, limiting the use of the APU would require the airport to have ground power units available. The airport may impose curfews or quiet hours where operations are not allowed, usually during night time or on weekends. Noise charges may also be imposed on airlines whose aircraft exceed the allowable values of noise [78]. The amount of this charge can be flexible based on the severity by which the noise limit is exceeded. These fees can help airports fund other noise mitigation efforts. An airport may also choose to have a noise "budget" which involves assigning departure and arrival slots to different aircraft in order to meet a pre-defined noise metric target. Finally, airports may choose to outright ban certain types of aircraft from operating. Such bans may be imposed for older aircraft which were not certified according to the latest noise certification standards recommended by ICAO or FAA.

In the US, aircraft noise standards are defined in Part 36 of the noise certification requirements of the United States Code of Federal Regulations (CFR) Title 14 [79].

Certified noise levels are published by the FAA in Advisory Circular 36-1H – Noise Levels for U.S. Certificated and Foreign Aircraft [80]. The implementation of noise certification requirements and standards ensures that the latest improvements in noise reduction technology are incorporated into the aircraft design process. The current standard for jet and large turboprop aircraft is Stage 5, which is equivalent to ICAO's Chapter 14 standards. Noise certification standards are defined as a limit on the total EPNdB calculated at three reference points. These reference points are shown in Figure 1.5 and described below –

- Fly-over – 6.5 km from the brake-release point, under the take-off flight path.
- Sideline – the highest noise measurement recorded at any point 450 m from the runway axis during take-off.
- Approach – 2 km from the runway threshold, under the approach flight path.

The permissible EPNdB level is a function of the aircraft's gross takeoff weight – heavier aircraft have higher permissible noise levels. As technology improves, standards are updated accordingly. The progression of ICAO's noise certification standards is seen in Figure 1.6. The horizontal axis is the aircraft's Maximum Take-Off Mass on a logarithmic scale. The vertical axis represents the maximum allowable cumulative EPNdB. The trend of smaller permissible noise limits for certification is observed in this figure. Notably, the most recent Chapter 14 adopted in 2013 represents an improvement of at least 7 cumulative EPN dB over the previous Chapter 4. Lighter aircraft, those below 10.0 tonnes will need to make an even larger improvement to be certified.

As mentioned previously, airports may choose a combination of measures best suited to their situation [82]. Many of these measures are complementary, and it has been found that there exists a significant correlation between not only the applied Noise Abatement Measures (NAMs) and particular airport-related characteristics, but also between NAMs themselves [83].

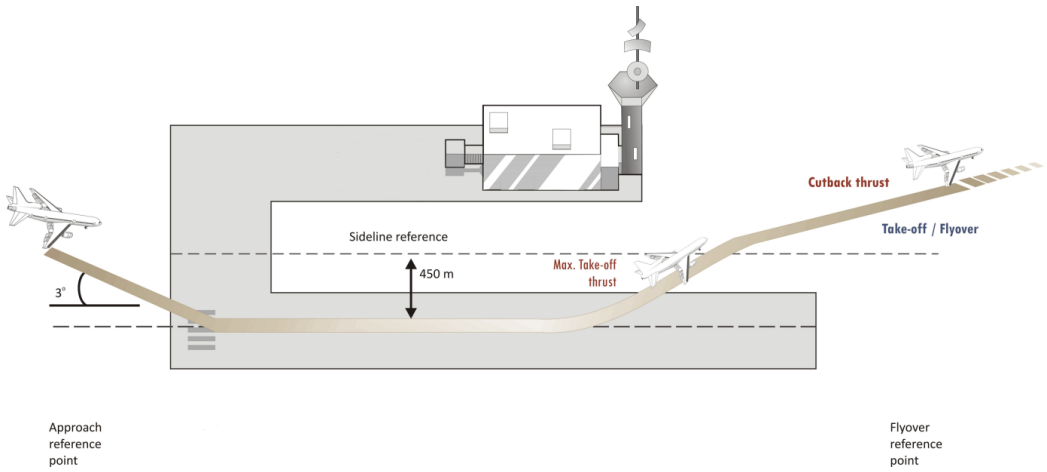

Figure 1.5: Reference points used to measure noise for aircraft noise certification (Image source: ICAO website [81])

For example, consider the Noise Action Plan created by the London City Airport [84]. Some of the measures undertaken by the airport for noise mitigation are – imposition of limits on aircraft movements, limitation of noise contours to a fixed area, improvements to flight tracks and noise monitoring systems, imposition of incentives and penalties, measures to reduce noise from aircraft ground movements, a scheme to classify aircraft into new noise categories, and enhancements to the sound insulation scheme. The combination of these measures aims to mitigate the effects of noise exposure to the surrounding communities.

1.3 Need for Rapid Noise Models

As outlined in the previous section, a large number of noise abatement measures are available for airports to implement. Some of these measures relate directly to aircraft movements, such as operating restrictions, and flight paths. Other measures do not directly affect aircraft movements, such as the installation of sound insulation at homes and businesses. In order to make the correct decisions on which measures to implement, stakeholders must be able to perform quantitative cost-benefit analyses for each measure. In order to help with such decision making, various stakeholders have developed quantitative

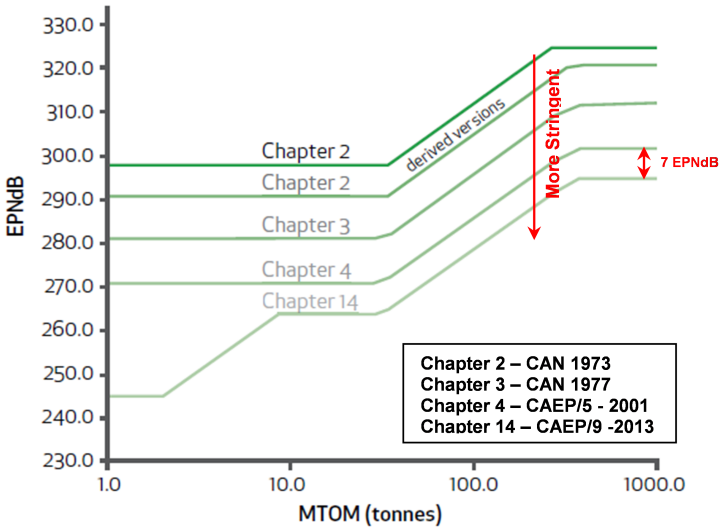

Figure 1.6: Progression of ICAO's aircraft noise standards (Image source: ICAO website [81])

tools for noise assessment.

Traditional aviation noise quantification tools such as the Integrated Noise Model (INM) or the Aviation Environmental Design Tool (AEDT) can be used to perform such analyses. However, due to the large amount of variables involved, it is often not feasible to evaluate a comprehensive set of scenarios. The quantification of a single scenario involves knowledge of the airport layout, population distribution in the surrounding communities, operational counts of aircraft types, and the departure and arrival trajectories flown by each aircraft. Furthermore, even if all these parameters are known, the noise impact varies from day to day due to changing weather conditions which affect both the aircraft performance and trajectory, and also noise propagation through the atmosphere. Thus, the evaluation of aviation noise is a very high dimensional problem leading to computationally expensive models.

A proven solution to address the problem of computationally expensive models is the use of surrogate models. Surrogate models or *models of models* are, broadly speaking, mathematical constructs which are computationally inexpensive to evaluate, and approximate the original model with sufficient accuracy over the domain for which they are

created. It should be noted that although the cost of evaluating a surrogate model is very low, the cost of creating or *training* it may be quite high. This distinction is often referred to in the literature as *offline* and *online* costs. Offline costs refer to the often large investment made to train the model, whereas online costs refers to the evaluation cost of a trained model. Typically, a high offline cost may be acceptable, as it is a one-time occurrence, if there is sufficiently acceptable improvement in the online costs.

However, in the context of aviation noise estimation, scalar surrogate models (which estimate scalar-valued functions evaluated on a set of parameters) have typically fallen short. These shortcomings typically arise from the inherent complexity of the aviation noise estimation problem and are examined in detail in chapter 2. The shortcomings typically lie on either of end of the following spectrum – a simple surrogate model will have low offline cost, but will inevitably contain simplifying assumptions which will greatly limit the usability of the model. A more general model with fewer assumptions will typically not be much faster to evaluate than the original model, and thus will not justify the offline training efforts.

A different class of models called Reduced Order Models (ROMs) show promise in this application. ROMs are well suited to the prediction of field quantities, such as pressure, temperature etc. Fundamentally, noise is unwanted sound which manifests through changes in air pressure. ROMs are well suited to problems with high dimensional data, as the first step of a ROM is to perform Model Order Reduction (MOR). In this step, the high dimensional data is transformed into a lower dimensional space. The MOR is performed so as to minimize the errors related to this transformation, and several different algorithms exist for this purpose. The lower order data are then treated as the input data for interpolation/regression schemes, which link the transformed data to the input parameters. With the correct implementation, results for different parameter combinations can be obtained in near real-time speed, while maintaining acceptable levels of accuracy. These models are investigated in detail in chapter 2.

In addition to the problem of high dimensionality and ill-suited scalar-valued surrogate models, aviation noise estimation models also inevitably include various categorical variables as inputs. Some inputs, such as the ambient temperature and pressure can be easily represented numerically. Other inputs, such as the flight path and trajectory of the aircraft are difficult to represent numerically. In traditional analyses, such inputs have been defined as categorical variables. Categorical variables have values which do not have an intrinsic numerical meaning. Instead, their values are treated as labels with no implicit ordering. For example, a departure operation out of an airport will follow a pre-determined procedure. This procedure is often labeled as 'NADP-1' or 'NADP-2', which do not provide much numeric information about the operation.

The problem with categorical variables is that they are not conducive to being used as inputs to a surrogate modeling process. Therefore, when dealing with categorical variables, multiple surrogate models have to be developed. Usually, this takes the form of one model per value (label) that the categorical variable takes. An internal *if-then* logic is then used to determine the appropriate model to be applied. This sort of break-down into smaller surrogate model often compromises the ability to train fast and accurate models, and thus poses a major problem in the context of aviation noise estimation.

1.4 Summary

As commercial aviation activity returns to its long-term growth trajectory, the mitigation of aviation noise remains an increasingly important facet of sustainable aviation. The mitigation of aviation noise is a topic of research for various stakeholders, and several solutions have been developed ranging from technology improvements to operational measures to stringent regulations. Due to the large number of potential solutions and variables which affect aircraft noise, the quantitative evaluation and comparison of airport mitigation strategies is crucial. Current aviation noise analysis inevitably involves simplifying assumptions and localized efforts due to the immense complexity of the

problem.

Existing research in the literature has attempted to address these inherent complexities with the help of surrogate models, with limited success. The complexities of the aviation noise quantification process inevitably lead to surrogate models that are either too complex and time-consuming to provide any benefit, or models that end up with too many simplifying assumptions to make the problem tractable, at the expense of model accuracy and applicability.

At this point, the motivation for the subsequent research is clear and the motivating research question can be stated.

Motivating Research Question

How can the process of aviation noise quantification be improved to enable rapid quantification of noise metrics to facilitate parametric trade-off analyses and optimization efforts?

In order to address the motivating research question and guide subsequent research, the overall research objective is stated here.

Research Objective

Develop a methodology to address inherent complexities in the aviation noise computation problem, thereby enabling rapid quantification of noise metrics in a variety of scenarios, thus facilitating parametric trade-off analyses and optimization efforts.

The Motivating Research Question and the Research Objective inform the subsequent research presented in this dissertation.

1.5 Document Outline

The remainder of this dissertation is organized as follows –

- Chapter 2 provides a detailed background of the noise quantification process and optimization efforts in the literature. Various efforts by researchers on creating parametric rapid noise assessments tools are also studied and described.

- Chapter 3 contains the formal problem formulation and research questions based on gaps identified in the literature. The high level research questions are decomposed into specific sub research questions. Hypotheses are developed to answer these research questions, and experiments are designed to support hypotheses.

- Chapters 4 and 5 provide details of the execution of the research plan. Results from the experiments which support the formulated hypotheses are included in these chapters.

- Chapter 6 documents the overall methodology and the results of a case study which was conducted to demonstrate the modeling capabilities of the developed methodology.

- Chapter 7 contains the summary, conclusions, and contributions of the work undertaken in this dissertation. Potential avenues for future research are also identified and included.

CHAPTER 2
BACKGROUND AND LITERATURE REVIEW

The stated motivating research question and the research objective in the previous chapter serve as the starting point for subsequent literature review. In this chapter, findings from the review of literature are described and major observations are highlighted explicitly. This chapter is divided into several sections, each addressing a key part of the overall objective. The chapter ends with a summary of the observations, and a formalization of the gaps to be addressed in this dissertation.

2.1 Aviation Noise Modeling

The many facets of aviation noise modeling are covered in this section. First, a list of noise metrics is discussed. Next, the process of noise exposure calculation is covered supplemented by a discussion of available state-of-the-art noise tools. A comprehensive literature review of methods for rapid noise computation is discussed next.

2.1.1 Noise Metrics

There are several different metrics developed to quantify aviation noise, with usage depending on the context. The harmful effects of aviation noise which were described in subsection 1.2.1 correlate to different noise metrics [85, 86, 87]. A list of noise metrics and their use cases described in literature is presented here [88, 89, 90] –

1. Instantaneous sound level metrics

    (a) Frequency weighted metrics – The human ear responds differently to sounds of different frequencies, even if they are of the same amplitude. This leads to some frequencies being perceived as louder or more annoying than others. To

account for this sensitivity of the human ear, various frequency weightings have been developed. These are summarized in Table 2.1. The absence of frequency weighting is referred to as a "flat" response.

Table 2.1: Summary of different frequency weightings for sound pressure level

Weighting	Definition	Purpose
A	SPL modified to de-emphasize low frequency portion of sounds	Approximate the relative "noisiness" or "annoyance" of many commonly occurring sounds
B	Similar to A but different weighting	No longer in common use
C	SPL modified to limit the low and high frequency portion of sounds	Primarily used to approximate overall SPL where the frequency range of interest is between 31.5 Hz and 8000 Hz
D	SPL modified to de-emphasize low frequency portion and emphasize high frequency of sounds	Developed as a simple approximation of perceived noise level, intended to be more accurate than A-weighting for many commonly occurring sounds
E	SPL modified to de-emphasize low frequency portion and emphasize high frequency of sounds	Designed to measure the noisiness or loudness of sounds such as aircraft flyovers

(b) Computed metrics

i. Perceived Noise Level (PNL) is the rating of the noisiness of a sound computed from SPL measured in octave or one-third octave frequency bands. It is mainly used for ranking the relative annoyance or disturbance caused by aircraft flyover noise.

ii. Tone Corrected Perceived Noise Level (PNLT) adds a tone correction factor to the PNL level. The intent of the correction is to account for the added annoyance due to discrete frequency components such as tones.

2. Single event metrics

   (a) Maximum Sound Level (L_{max}) accounts for only the amplitude and represents the maximum sound amplitude at some time during the event.

   (b) Effective Perceived Noise Level (EPNL) is PNL of a single event with adjustments for both tonal corrections and for added annoyance due to duration. As it takes the entire event into account, it is used to measure subsonic aircraft flyovers. This metric forms the basis for the FAA's procedure for aircraft noise certification [79, 80].

   (c) Sound Exposure Level (SEL) is an energy averaged metric which represents A-weighted sound level over the specified duration of time referenced as one second. The relation between SPL, L_{max}, Equivalent Sound Level, and SEL is shown in Figure 2.1.

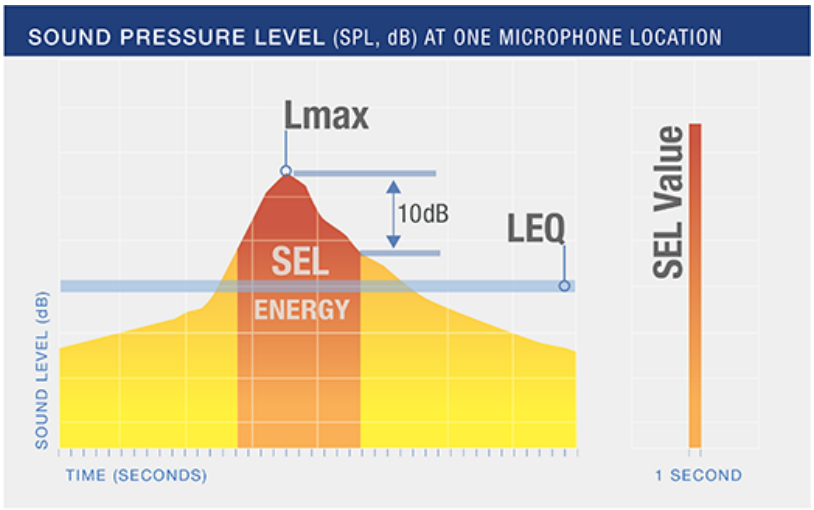

Figure 2.1: Relation between SPL, L_{max}, Equivalent Sound Level, and SEL (Image source: FAA website [91])

   (d) Single Event Noise Exposure Level (SENEL) is a subset of the SEL and is calculated. similarly. The difference is that for SENEL, only the sound level above a certain threshold is used.

3. Multiple event metrics

(a) Equivalent Continuous Sound Level (LEQ) is the level of A-weighted sound energy which is averaged over a period of time. It is useful in assessing people's reactions to aircraft and vehicular traffic noise, and correlates with annoyance, speech interference, and sleep interference.

(b) Hourly Noise Level (HL) is the level of mean-square A-weighted sound pressure over a one hour period. It is similar to QL calculated for one hour.

(c) Time Above Threshold (TA) measues the amount of time of noise exposure above a pre-selected threshold of A-weighted sound level.

(d) Composite Noise Rating (CNR) is calculated over a 24-hour period based on the perceived noise levels of all events during that period. Different ratings are calculated for flight and for run-up operations. Adjustments are typically made for the time of day, type of aircraft, and the number of operations.

(e) Noise Exposure Forecast (HEF) is based on the effective perceived noise levels over a 24-hour period. Adjustments similar to those for CNR are made.

(f) Day-Night Average Sound Level (DNL) is the energy averaged A-weighted sound level over a 24 hour period with a 10dB penalty added for night time operations as shown in Figure 2.2. Operations between 10:00 pm and 7:00 am are penalized to account for the increased sensitivity to noise intrusions during night time hours. This measure is used for creating noise exposure maps (NEMs) and for assessing land-use compatibility and making zoning recommendations. As the DNL metric is based on the total noise energy over a 24-hour period, it accounts for both the number of operations and the noisiness of each operation. Thus, there are several different combinations of operations which can result in the same DNL level. This also implies that given a DNL limit or target, a quieter aircraft can fly more operations than a louder one, as shown in Figure 2.3. There is a correlation between the annoyance experienced

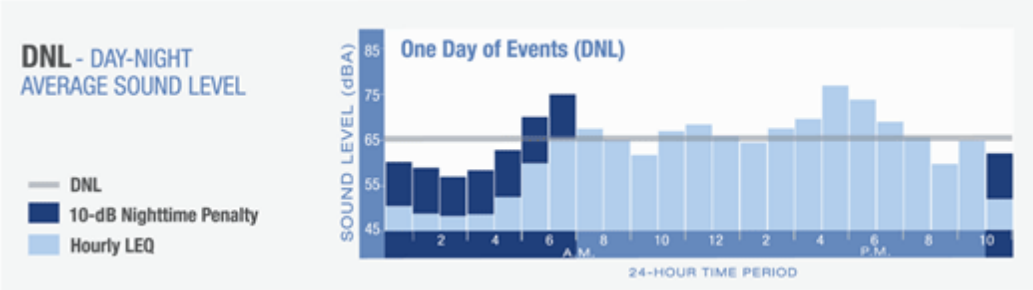

Figure 2.2: Calculation of DNL from hourly LEQ (Image source: FAA website [91])

by a human towards a certain noise event and the DNL value of the noise event, as shown in Figure 2.4.

(g) Community Noise Equivalent Level (CNEL) is computed similarly to the DNL but an additional penalty is added for evening operations between 7:00 pm and 10:00 pm. This metric is used instead of the DNL in the state of California for land-use compatibility assessments and zoning recommendations.

(h) Noise and Number Index (NNI) is based on the average maximum perceived noise level for aircraft flyovers in a given time period.

(i) Weighted Equivalent Continuous Perceived Noise Level (WECPNL) is a cumulative rating based on the EPNL. Adjustments are made based on the variables associated with aircraft noise such as discrete tones, time of day, and season of the year.

4. Speech communication metrics

(a) Articulation Index (AI) is based on a weighted measure of the difference between the background noise and the speech signal to estimate the proportion of normal speech which can be understood by a listener. It is expressed as a number between 0 and 1, where 1 indicates complete speech intelligibility.

(b) Speech Interference Level (SIL) is the arithmetic average of the sound pressure levels in four octave bands centered on 500 Hz, 1000 Hz, 2000 Hz, and 4000 Hz. It is used to determine the expected vocal effort for face-to-face communication.

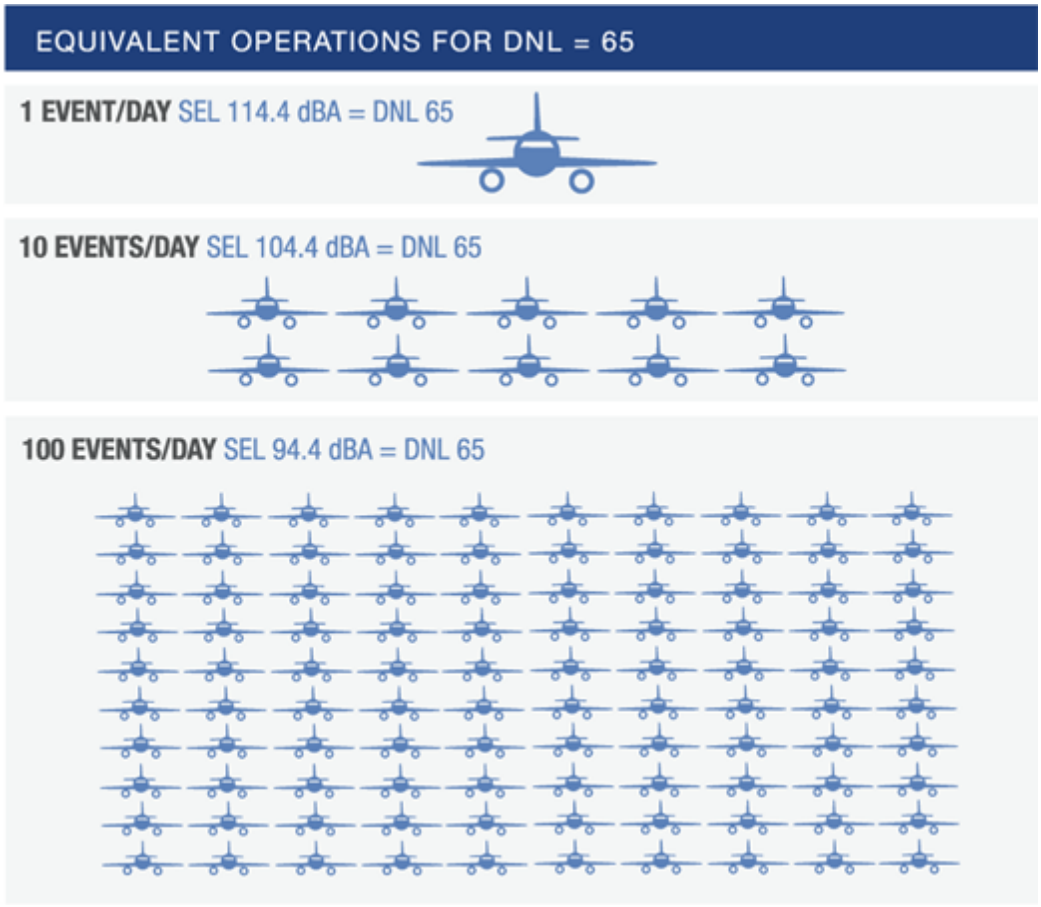

Figure 2.3: Combination of operations yielding the same DNL value (Image source: FAA website [91])

Although the noise metrics described here are numerous, this list should not be considered as comprehensive. In order to adequately capture noise impacts from emerging technologies such as Urban Air Mobility concepts for cargo and passenger operations, new metrics may need to be defined. For example, recent research has proposed creating an alternate noise weighting to account for the unique noise signatures arising from Urban Air Mobility operations [93].

Each of these numerous noise metrics described above have their own formulations and use-cases. A commonly used noise metric for community noise exposure is the DNL, which is used to create Noise Exposure Maps (NEMs) as per 14 CFR Part 150. NEMs are used to inform the public about noise exposure and land use in the vicinity of airports. A typical NEM consists of DNL noise contours overlaid on a map, as shown in Figure 2.5. To

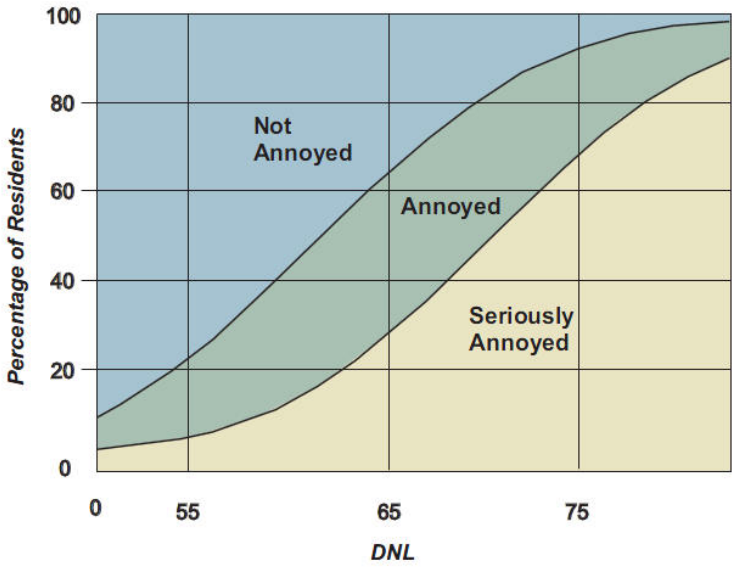

Figure 2.4: Relationship between the percentage of the population which is annoyed and the DNL value of the noise event (Image reproduced from [92])

show the noise variation over an extended area, noise metrics shown as contours are more useful than point valued depictions. Such contours are created by computing noise levels over a collection of points and then joining points with the same noise levels to create a closed shape.

When creating NEMs, the noise metric has to be computed over a number of locations, most commonly structured as a two dimensional grid. In this context, the calculated value of the noise metric changes not only with the noise event scenario, but also the location of the receptor. Additionally, all noise metrics are based fundamentally on sound manifested as temporal variations of air pressure. This temporal variation accounts for both the sound level (amplitude) and frequency (pitch). Figure 2.1 and Figure 2.2 show how the computation of the SEL and DNL metrics can be traced back to the time varying SPL. Thus, for the purposes of creating NEMs, noise metrics can be considered to be functions of the spatial and temporal variations of air pressure.

Observation 1: Noise metrics are functions of the spatial and temporal variations of atmospheric pressure, and are field quantities.

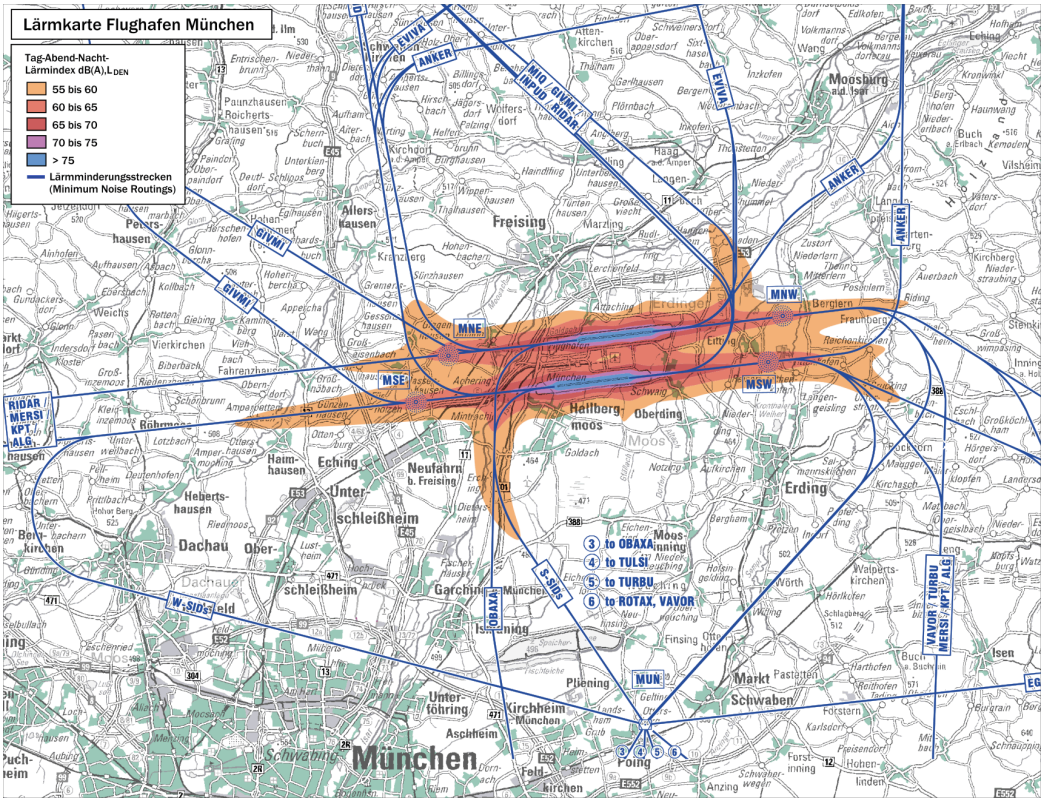

Figure 2.5: 2016 Noise Exposure Map for Munich airport (Image source: Wikimedia Commons.

2.1.2 Tools for computation of aviation noise

The basis of any noise mitigation effort is the ability to accurately predict relevant noise metrics in a variety of scenarios. Methods for the quantification of aviation noise have been developed by SAE International [94], ICAO [95], and the European Civil Aviation Conference (ECAC) [96]. Using such methods, several noise quantification tools have been developed by regulators, researchers, and other stakeholders. Some of the commonly used tools in the U.S. are discussed here. Other tools addressing parts or whole of the noise quantification problem include the SysTem for AirPort noise Exposure Studies (STAPES) [97], Aircraft Noise Control Model (ANCON) [98, 99], Integrated aircraft noise and emissions modelling platform (IMPACT) [100], Parametric Aircraft Noise Analysis Module (PANAM) [101], Nord2000 [102]. Note that although not all tools are discussed in detail here, the fundamental idea and process of noise quantification is similar among

them.

NASA's Aircraft Noise Prediction Program (ANOPP) along with its next generation version ANOPP2 [103] provide the capability to model noise from aircraft including source noise, propagation, and metrics. It predicts total aircraft noise accounting for both propulsion and airframe sources. It can also be used to model aircraft components individually. Propagation effects such as spherical spreading, atmospheric absorption, ground absorption and reflection, terrain effects, and refraction/scattering effects are modeled in ANOPP.

The Integrated Noise Model (INM) [104, 105] was developed to evaluate aircraft noise impacts in the vicinity of airports, used for FAR Part 150 noise compatibility planning studies and FAA Order 1050 environmental assessments and environmental impact statements. INM was based on the algorithm and framework outlined in the SAE-AIR-1845 standard "Procedure for the calculation of airplane noise in the vicinity of airports" [94]. This framework used Noise-Power-Distance (NPD) data to estimate noise by taking into consideration aircraft specific data, thrust setting, separation between source and receiver, and environmental factors. INM has now been replaced by the Aviation Environmental Design Tool (AEDT).

AEDT [106, 107] was developed to replace legacy tools INM, Noise Integrated Routing System (NIRS), and the Emissions and Dispersion Modeling System (EDMS). AEDT is the official tool used for quantifying the environmental impacts of aviation in the US and is used for informing policy decisions, domestic planning, environmental compliance, and research analyses. Users include domestic and international regulatory agencies, airlines, airports, academic institutions, aircraft and engine manufacturers, environmental organizations, and consultants. AEDT utilizes aircraft performance models to compute aircraft trajectories and performance characteristics in space and time to produce environmental metrics such as fuel burn, emissions, and noise. The scope of modeling ranges from single flight departure/arrival/gate-to-gate operations to airport level

modeling consisting of several types of aircraft and operations. AEDT is under continuous development to improve modeling accuracy and capabilities, recent improvements include the inclusion of the BADA4 performance model developed by EUROCONTROL [108]. The tool itself has also been to various modeling validation studies to assess the impact of its assumptions [109, 110, 111].

A typical study in AEDT is built-up by assigning aircraft operations to specific airport layouts. Aircraft trajectories can either be directly imported or pre-defined operations can be used. The tool then uses an aircraft performance model to compute the aircraft's position and state in space and time. Position information contains both the aircraft's absolute position such as MSL altitude, latitude, and longitude and relative position such as AFE altitude and cumulative ground track distance. The state information contains aircraft's speed, thrust level, fuel flow to the engines, etc. The computed position and state information serves as the input to various environmental models. The noise model in AEDT uses NPD data to estimate the noise impact. AEDT can also combine operation level results to create airport level analyses. A combination of physics-based and empirical models are used throughout this process. For example, the trajectory of the aircraft is calculated using physics-based equations of motion, while the calculation of aircraft thrust are based on empirical equations with supporting coefficients. A simplified flowchart is shown in Figure 2.6.

The core process of computations in AEDT is performed by modules that rely on many databases. These databases can be grouped according to three categories –

1. Weather data consists of weather parameters such as temperature, humidity, pressure, density, and wind speed. These parameters affect not only the performance of the aircraft, but also the noise propagation through atmospheric absorption.

2. Aircraft data – In order to compute the trajectory of the aircraft, several aircraft-specific parameters are required. The thrust and aerodynamic coefficients are required in order to compute the aircraft's trajectory through fundamental performance

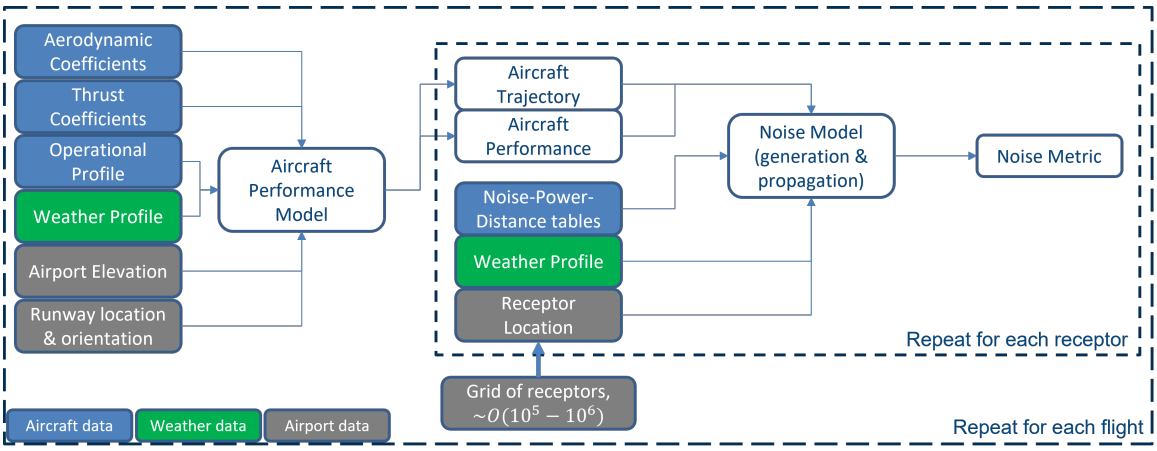

Figure 2.6: Generic process for calculating aviation noise metrics

equations. Additionally, the operational data relating to how a pilot might fly the aircraft is encoded through the profile, weight, and runway assignments.

3. Airport data – the airport runways provide an anchor for the computed aircraft trajectory. Additionally, the airport also affects the weather through elevation, and historical weather data.

From Figure 2.6, it is evident that quantifying noise metrics involves many computationally expensive processes which are necessary to guarantee a high degree of confidence in the results. Additionally, due to the underlying dependencies on a large amount of variables and data, the parameters which can influence the noise result are numerous.

Observation 2: The process of calculating aviation noise is reliant on computationally expensive physics-based and semi-empirical models.

Observation 3: The input space of parameters which can influence the value of aviation noise metrics is very high dimensional.

These observations indicate that tools like AEDT are very useful for quantifying noise metrics in specific scenarios, where only a small subspace of the complete input space needs to be evaluated. For comprehensive analyses spanning a larger subspace of the input space, the usage of a full order model like AEDT is infeasible. This problem of computational intractability has been identified by the research community and there are

several strategies documented in literature which attempt to address this problem. These strategies are discussed in section 2.2.

2.2 Methods for rapid noise evaluation

In order to make improvements on the computational time for aviation noise quantification, several different methods have been proposed and tools have been created. This section provides an overview of these methods, including their improvement strategies, underlying assumptions, documented applications, and limitations.

2.2.1 Airport Noise Grid Interpolation Method

The Airport Noise Grid Interpolation Method was developed by Bernardo [38] for the rapid computation of noise grids and contours, thereby enabling the evaluation of a more exhaustive set of scenarios. The core improvement is the creation of a library of pre-computed vehicle-level SEL noise grids which remove the requirement of running through the aircraft performance model, NPD lookups and interpolation, and noise propagation models.

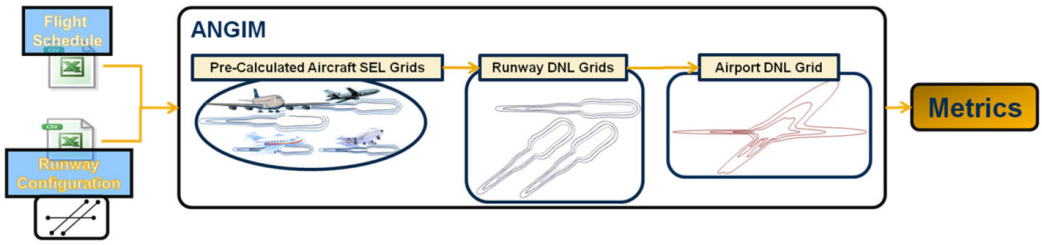

Figure 2.7: Process overview of the Airport Noise Grid Interpolation Method (ANGIM) [38]

The overall process behind ANGIM is shown in Figure 2.7, with the steps described in detail below –

1. First, the single-event aircraft-level noise grids are computed using the INM tool. Separate computations are performed for departure and arrival operations, and for

each stage length defined within those operations. By centering the grid about the runway axis, and assuming a straight ground track, only half of the noise grid needs to be stored, due to symmetry. An adequately sized and finely spaced grid is defined, and the results are stored. This step is only performed once and after this step, INM is no longer required.

2. The second step is the computation of runway DNL grids by using the pre-computed single-event noise grids. Two inputs are required for this – the flight schedule and the runway geometry. The flight schedule provides the number and type of operations for each aircraft, the runway used to perform that operation, and the time of operation (required to impose the night-time operation penalty for the DNL noise metric). The runway geometry is defined by the anchoring Cartesian coordinates for the runway end, and the heading direction. These inputs modify the pre-computed noise grids to calculate the runway level grids.

   (a) Single-event SEL grids are converted to Sound Exposure Ratio at each grid point using Equation 2.2. Unlike SEL, the exposure ratio is linear, and therefore can be scaled and summed across different operations at the same grid point.

$$SEL_{ac} = 10\log_{10}\left\{\frac{\int_{t_1}^{t_2} p_A^2(t)dt}{p_0^2 t_0}\right\} = 10\log_{10}(E_{ac}) \tag{2.1}$$

$$E_{ac} = 10^{\frac{SEL_{ac}}{10}} \tag{2.2}$$

   (b) The exposure ratio is scaled by the number of operations for an aircraft assigned to the runway. Night-time and day-time operations are handled separately at this stage.

   (c) The scaled exposure ratios are summed across operation types, thus combining all arrivals and departures across all different aircraft types.

(d) The runway level exposure metric is then converted to the DNL metric for each receptor point in the grid using Equation 2.3.

$$DNL_{rwy} = 10\log_{10}\left(E_{rwy,day} + 10 \times E_{rwy,night}\right) - 49.4 \tag{2.3}$$

(e) Finally, the DNL noise grid is mirrored across the runway axis to obtain the symmetric noise grid for the runway.

3. Next, the runway noise grids are rotated and translated to achieve the correct relative positioning across the different runways. Standard Cartesian rotation and translation operations are applied, in that order.

4. Finally, the runway level grids are combined by first interpolating the rotated and translated runway grids onto a common airport grid, and then summing the noise values logarithmically. The interpolation is performed logarithmically from the nearest neighbor. The summation formula is shown in Equation 2.4.

$$DNL_{apt} = 10\log_{10}\left(\sum_{rwy} 10^{\left(\frac{DNL_{rwy}}{10}\right)}\right) \tag{2.4}$$

5. Once the airport level DNL grids are calculated, post-processing can be performed to obtain contour area, population exposure etc.

In summary, the development of ANGIM enabled the creation of rapid fleet-level analyses, by using clever superimposition of pre-computed noise grid data. The benchmarking of ANGIM against INM was done in a verification and validation study which showed large improvements in computation time [112]. For example, in a case study with four parallel runways including crossflow traffic patterns, the ANGIM runtime was 5.92 minutes as compared to the INM runtime of 56.6 minutes. Similar levels of improvements were observed for a wide range of cases which were tested. The study also reported acceptable accuracy when the underlying assumptions were obeyed.

However, when considering cases outside of those covered by the underlying assumptions of ANGIM, the accuracy deteriorated quickly, thus limiting the applicability of the tool. The core ANGIM tool was initially developed without any calibrations. The authors of [112] noted that by adding suitable calibrating factors, the accuracy of ANGIM could be improved for conditions outside of the assumptions. For example, it was proposed that the relationship between the noise response and the airport elevation could be modeled, thereby negating the sea-level assumption.

The errors introduced by the assumptions were quantified using a comprehensive 94 airport study in subsequent research [113]. The annual flight schedules for the year 2015 were computed in AEDT and were used as the validation data. Diverging ground tracks were included in the validation data, as were two different atmospheric attenuation models. The noise results for all airports were then repeated in ANGIM by matching aircraft types and runway assignments. It was observed that for nearly all airports, the noise results for ANGIM were underestimating the noise levels, likely due to the sea-level assumption which led to a higher atmospheric density value. It was also observed that the assumption of standard day performance and straight ground track together resulted in a net over-prediction of noise results.

In summary, although the baseline ANGIM tool greatly sped up the process of aviation noise quantification, it did so partly by making simplifying assumptions to narrow down the aforementioned input space. Thus, while the tool was accurate and fast for a sea-level airport with straight ground tracks on standard day conditions, it was not applicable at other conditions. Noting this, researchers tried to make improvements to ANGIM by addressing some of these assumptions which are discussed in subsection 2.2.2.

Observation 4: The use of pre-computed noise grids greatly increases the speed of noise computation, but does not scale well to the complete input space due to storage requirements.

2.2.2 Enhancements to the Airport Noise Grid Interpolation Method

This section describes the various efforts undertaken by researchers to improve upon the basic ANGIM process. Note that while these improvements were motivated by a desire to improve ANGIM, they are not necessarily tied-in to the ANGIM process. Results and methodologies may be used for stand-alone analyses if appropriate.

Average generic vehicles

One way to speed up the computation even further is to make use of representative aircraft which stand in for all aircraft within a certain class. For example, the Boeing 737-700 can be used to represent all aircraft in the 150-180 passenger class. LeVine et al. [114] further improved on this by creating average generic vehicles which are better representations of an aircraft set than any individual aircraft within than set. The development of these representative average aircraft involved combining Environmental Design Space (EDS) with ANGIM. EDS is a modeling and simulation environment created for the design and evaluation of subsonic aircraft by integrating several industry standard tools into one framework [115, 116, 117]. To create average generic vehicle definitions, the overall process is shown in Figure 2.8 and described below –

1. Environmental metrics for each aircraft were computed – total mission fuel burn, total mission NO_x emission, Terminal area NO_x emission for departure and arrival, SEL contour areas, lengths, and widths.

2. Aircraft level metrics were converted to airport level metrics by aggregating the fuel burn and NO_x emissions, and by converting the SEL noise grids to DNL noise grids.

3. Next, linear discriminant analysis was used to refine the baseline classification which was based on passenger seat capacity. The linear discriminant analysis method predicts mis-classification among a-priori groups by using techniques from linear algebra, principal component analysis, and multiresponse permutation tests.

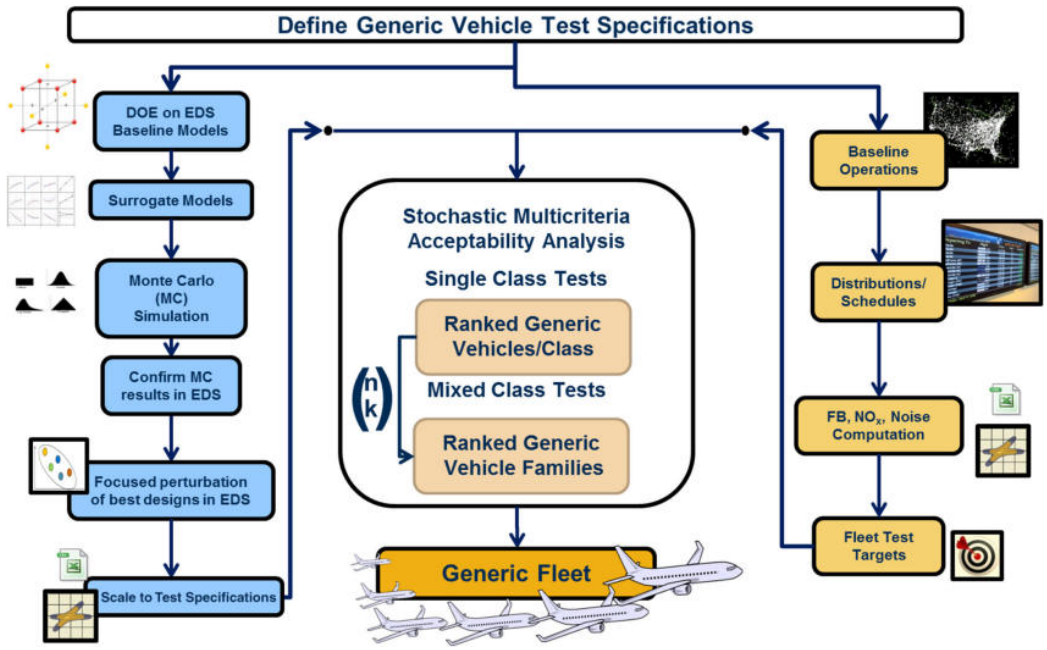

Figure 2.8: Process overview of creating average generic vehicles [114]

4. Targets were created for each environmental metric to represent the aggregate performance per the generic vehicle class.

5. A main effects screening test was performed to identify the most influential input variables for the relevant aircraft level metrics.

6. A design of experiments was created from the reduced set of influential input variable settings.

7. The created design of experiments was evaluated in a high fidelity aircraft-level model and the relevant environmental metrics were recorded for each design.

8. Surrogate models were created to map the computed metrics to the designs.

9. An optimization exercise was performed to optimize the input variables and obtain the best match to the average generic targets.

10. The optimal design was evaluated in the high fidelity model for verification.

It was observed that creating the average generic vehicle definitions depended primarily on the thermodynamic cycle design and sizing of the engine. The best designs per class featured similar engine OPR, BPR, and sea-level static thrust. The researchers were able to improve on the traditional method of using representative in-class vehicle, by making the representation more accurate while retaining the computational benefits.

Runway utilization

Instead of assigning each operation to a specific runway end, ANGIM included a feature where utilization ratios could be used instead. These ratios were envisioned to be useful when actual runway assignments were unknown. However, without additional guidance on the actual values of these ratios, the value would default to an equal utilization assumption where each runway end was assumed to be used equally. This does not reflect real-world runway utilization where often one runway end is prioritized due to prevailing winds or traffic flow patterns. Researchers in [113] used 2015 airport schedule information to derive unique runway utilization factors for approaches and departures for 94 airports. In addition to improving the computational speed by not requiring computations for each operation-runway assignment combination, the computed ratios also improved the accuracy compared to the scenario of assuming equal runway utilization. These ratios are also useful for evaluating future scenarios, where runway assignments cannot be known ahead of time.

Curved ground tracks

The original conception of ANGIM used straight-in and straight-out ground tracks for arrivals and departures respectively. This assumptions was made in part so that the resulting noise grids would be symmetric, thus requiring only half of the pre-computed grid to be stored. Consequently, many real-world operations could not be modeled accurately as real-world ground tracks often depart from the runway axis.

To address this limitation, a parameterization of ground tracks paired with a surrogate

model was proposed [118]. A demonstration case-study was performed by creating twenty alternative ground tracks using a parametric definition of a baseline ground track involving two left turns. The parametric definition decomposed the baseline track into five segments, with varying lengths and turn radii. These lengths and turn radii were used as parameters to generate alternate ground tracks. Treating the SEL value at a specific grid point as the response, an Artificial Neural Network (ANN) with 2 hidden layers of 1 Gaussian nodes each was trained. It was reported that with fewer nodes, the model was not sufficiently accurate. On the other hand, increasing the number of nodes greatly increased the model training and model evaluation times. The inputs to this ANN were the track parameters, the X-Y location of the noise grid receptor, and the SEL value of the baseline ground track.

The predicted SEL grid was calculated using the surrogate model and compared against data set aside for model validation. These results were used to compute noise contours which were compared as shown in Figure 2.9. It is observed that although the model was accurate for the 65 dB-SEL contours, the accuracy deteriorated quickly for higher dB levels. For the 80 dB-SEL contours, the contour shape could not be recreated accurately. Due to the nature of overlap, the error in contour area was lower than the distortion of the contour shape.

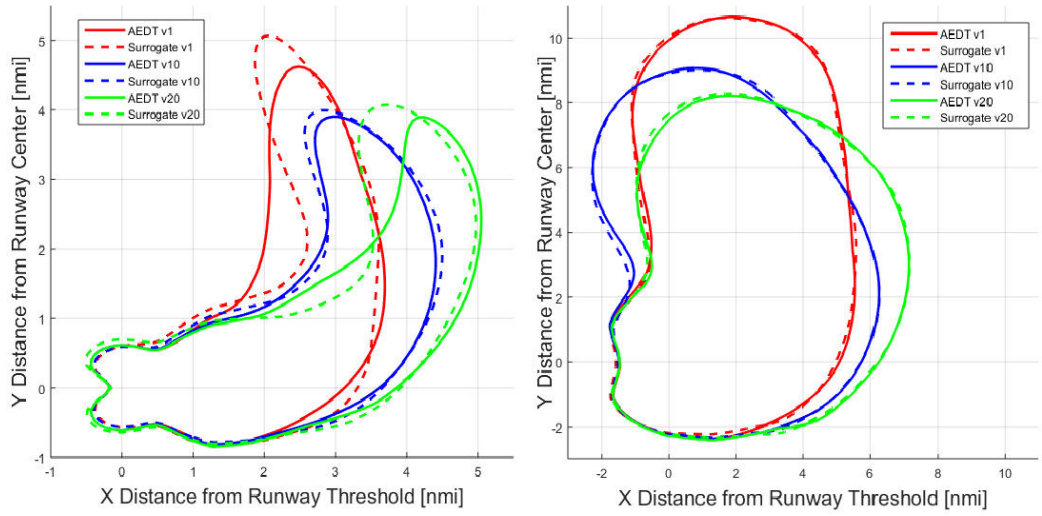

Figure 2.9: Comparison of validation testing results of ANN-based surrogate model for curved ground tracks [118]. 80 dB-SEL (left) and 65 dB-SEL (right).

The results obtained in this study point to the complexity of accounting for curved ground tracks in aviation noise analyses. Although accuracy could be improved further by adding more nodes to the ANN structure, it was computationally prohibitive. Thus, when curved ground tracks need to be modeled, the only suitable alternative is a full order model, like AEDT.

Calibration to atmospheric uncertainties

The use of standard day sea-level weather was identified as a key source of error when using ANGIM to model real world airports [113]. To address this problem, researchers tried to develop methods to perform the calibration of the pre-computed baseline weather noise grids at other weather conditions [119]. The dependency of SEL noise grids to weather was attributed to two main reasons – the aircraft performance and sound propagation. The takeoff and climb performance of an aircraft is highly dependent on ambient weather conditions. Additionally, the speed of sound and atmospheric absorption also depend on the ambient conditions. These ambient conditions were identified to be temperature, pressure, density, and humidity. The goal of the calibration exercise was to develop a surrogate model which could operate on the sea level SEL grids to obtain better estimations of noise results over a range of weather conditions.

Training and validation data for the surrogate model fit was generated for the B737-800 with CFM56-7B26 engines. The design space of atmospheric variables was explored by creating a latin hypercube design of experiments. This design of experiments was run through the full order model (AEDT). Fifty cases were used to train the model and an additional four cases were used for validation.

Several different surrogate modeling architectures were explored in order to identify the most suitable. Initial efforts using Procrustes analysis and superimposition was deemed unsuitable due to the non-linear grid scaling. Response Surface Equations (RSEs) were also tried, but the 2nd order RSEs proved to be inaccurate, whereas higher order RSEs were too

computationally expensive to train and evaluate. The interpolation technique called Kriging which leverages spatial correlations and Gaussian processes for estimating response values was another candidate. This method required the inversion of a correlation matrix, which was computationally intractable as the number of points increased.

The final method to be tested was an Artificial Neural Network. Initial single layer ANNs were not accurate, but two layer ANNs were deemed to be suitable with 15 Gaussian nodes in each layer as shown in Figure 2.10. The obtained results were largely positive, with R^2 values of the order of 0.999 and root-mean-squared errors between 0.10 and 0.15. However, when looking at the residuals between predictions and full order model "truth" data, it was observed that the error grew for higher SEL dB values. For high dB SEL values, the error could be as high as ± 2 dB. This trend is undesirable because when performing noise analyses, it is the higher decibel values which are the most important. It was also noted that one of the four validation cases showed an overall grid error of 18.86%. It was noted that this validation case was characterized by a very low ambient temperature and a very high atmospheric pressure, thus suggesting that the ANN based surrogate model may break down at the edges of the design space.

Summary of improvements to ANGIM

While several research efforts have been made to improve beyond the initial conception of ANGIM, the improvements have largely been limited to extending the capability to certain parameters instead of the complete input space. In most cases, the efforts to improve upon ANGIM resulted in slight computational cost increases, after the upfront cost of initial training of the surrogate models.

When trying to account for variations in atmospheric weather conditions and curved ground tracks, the accuracy of predictions varied greatly depending on the specific use-case. Traditional surrogate modeling methods were either inaccurate or too computationally expensive. Additionally, when ANNs were utilized, they produced unacceptable level of

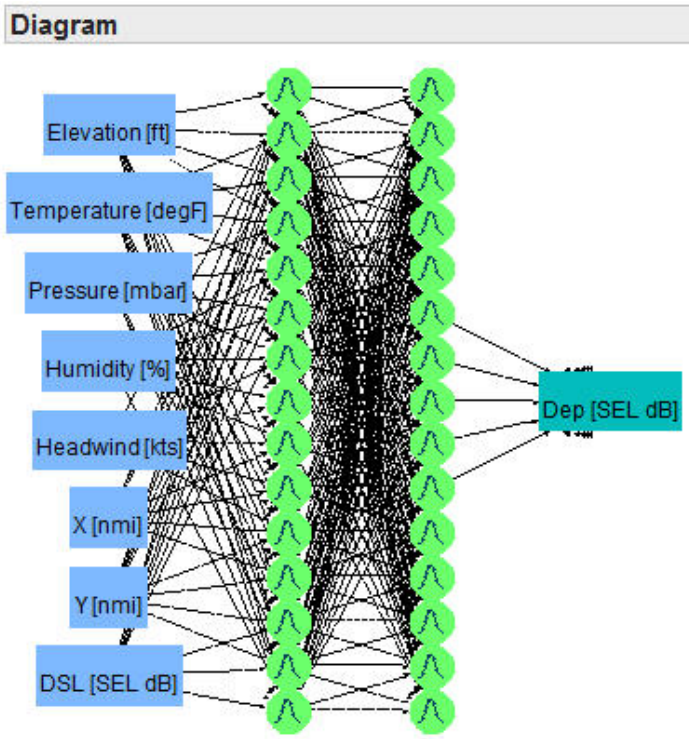

Figure 2.10: Neural Network Architecture for weather calibration [119]

errors at the edge cases. Finally, it is also noted that while many "hyperplanes" of the input space were explored, the arrival and departure trajectories were always kept constant. At this stage, the following observations are noted –

Observation 5: Traditional surrogate modeling methods based on scalar valued surrogates do not work well for replicating noise grids of full order models.

2.2.3 Rapid Environmental Impact on Airport Community Tradeoff Environment

Monteiro et al. [92, 120, 121] recognized that the state-of-the-art modeling software do not meet three main requirements that are essential for rapid noise exposure analysis – rapid assessment, forecasting ability, and parametric interactivity. To address this problem, they created the Rapid Environmental Impact on Airport Community Tradeoff Environment (REACT). The modeling architecture for REACT built upon ANGIM and the Global and Regional Environmental Aviation Tradeoff (GREAT) [122] tools, and is shown in

Figure 2.11.

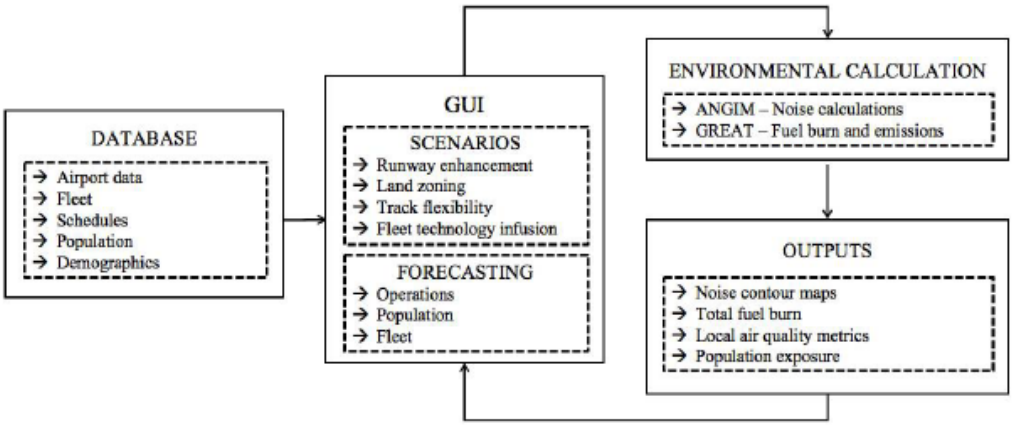

Figure 2.11: Modeling architecture of the REACT environment [92]

The goal of REACT was to create individual airport specific trade-off environments, which would tailor the database to each airport. This was necessary as community noise exposure is a very airport specific problem due to the uniqye population distributions and airport runway geometries. Two airports were selected to be used as case-studies within REACT – Kansas City International Airport (MCI) and Dallas-Fort Worth International Airport (DFW). The individual components which made up the environment are enumerated below –

1. Airport data – The data which is unique to each airport and most relevant for noise calculation are the runway geometries and atmospheric conditions. For runway configurations, the ANGIM referencing method was utilized. Atmospheric data in the form of temperature, pressure, humidity, and wind was extracted from the AEDT 2c database.

2. Fleet and Operations data – This contained information about the type of aircraft and the flight schedules (time of operation, runway assignment etc.). Operations were referenced to an averaged day in 2015 with data being obtained from airport partners.

3. Operations forecasting – The method outlined in the FAA Terminal Area Forecast (TAF) 2015 model [123] was used. The FAA's TAF is the official tool for forecasting commercial, general aviation, military, and commuter operations at all US airports.

4. Flight Track Parameterization – The definition used by AEDT to create curved and straight vector ground tracks was used. A generic ground track definition is used consisting of five segments described by nine parameters, as shown in Figure 2.12. The parametric track was later converted to a set of sequential points to generate the necessary shape files for the tool interface.

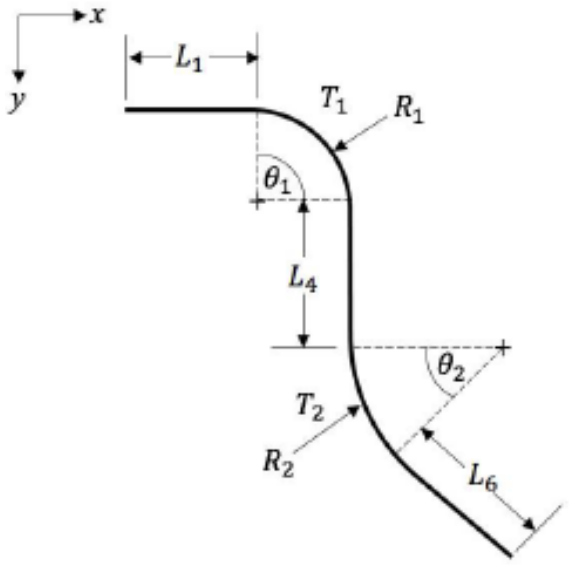

Figure 2.12: Parametric definition of curved ground tracks [92]

5. Population Database and Forecasting – Baseline population densities were obtained from the 2010 US Census data, which has a high resolution. Census county block level data was downloaded for each airport surrounding and imported into the tool. To forecast population trends, the Ratio Based Postcensal Small Area Projections method [124] was used which is a derivative of the Cohort Component Method [125].

6. Noise mitigation strategies – REACT was developed with the capability to create strategies for land planning by population block density control, operational changes

through forecasted years, track flexibility, and the simulation of technology advancements.

7. Environmental calculations – AEDT was used as a benchmark for validation of results generated by REACT. The fundamental benefit of ANGIM (pre-computed noise grids) was used along with aircraft substitutions to make the tool computationally efficient.

The components of REACT were integrated into an environment programmed using the ArcGIS for Developers SDK for Java. The validation results for REACT showed that the full order model results from AEDT were recreated accurately for a fraction of the computation time. However, there was a significant upfront cost involved in creating the environment itself, and adding the airport specific data.

2.2.4 Reduced Order Modeling applied to AEDT

Almost all literature on the creation of rapid noise modeling methods has been based on scalar surrogate modeling techniques which try to fit a model for the noise response treating various sets of parameters as inputs. The most common models used were Response Surface Equations, Kriging Interpolation, and Artificial Neural Networks. Kim et al. [126] recognized that such scalar valued surrogate models were more suited to outputs such as aggregate fuel burn or emissions related to an operation, but less so for noise grids. Thus, they focused their efforts on the use of a different class of surrogate models which are capable of dealing with high dimensional data by transforming it into a low dimensional space. Their method was based on a Reduced Order Model created by performing a Proper Orthogonal Decomposition (POD) of noise data coupled with a Kriging interpolation scheme in the lower dimensional latent space.

The first step of this process was to use the POD method to extract a set of orthonormal basis vectors which could be used to construct the lower dimensional space. The noise grid

computations from AEDT were projected onto this lower dimensional space coordinates. Thus, after projection, each noise grid could be identified by its coordinates along the basis vectors. These coordinates were then fit into a Kriging model with respect to the input parameters. The input parameters used in this case were weather conditions – elevation, temperature, pressure, humidity and headwind.

A total of 512 cases were run through the full order model and the noise results were recorded on a rectangular grid covering 32 by 16 nautical miles with a resolution of 0.08 nautical miles. The POD results found that the first three basis vectors were sufficient to recreate the full order results with an accuracy of 99.78%. The researchers noted remarkable improvements in computation time – 0.0042 seconds as compared to about 7 seconds taken by AEDT to simulate a single departure or arrival flights. It was also noted, however, that setting up the ROM and the interpolation scheme entailed a significant one-time upfront cost of 2.13 hours. The researchers also noted that ROM based noise computation methods could be extended to different aircraft types, flight tracks, and trip lengths.

2.2.5 Summary of methods for rapid noise evaluation

This section presented literature on the efforts of researchers to improve the computational efficiency of the aviation noise computation process. Several different methods were documented, all based on the idea of training a surrogate model which would be significantly faster to evaluate, once the upfront burden of training the model was complete. Most methods included some combination of simplifying assumptions, pre-computed and stored intermediate data, and scalar surrogate models. One method documented the use of Reduced Order Models instead of scalar-valued models and showed encouraging results.

Observation 6: The use of Reduced Order Modeling methods shows significant advantages over traditional scalar surrogate modeling methods seen in literature for aviation noise computation.

Each of the methods described previously demonstrated their method on a subset of the overall input space of the noise problem. These included some combination of varying weather conditions, parametric definitions of ground tracks, generic vehicle definitions, and population distributions. However, no study accounted for variations in the aircraft operations profiles – how the aircraft is flown by the pilot. Indeed, only the effect of aircraft weight on the trajectory and performance was studied by accounting for multiple stage lengths. Given that operational profiles are a significant influencer of noise impacts by affecting both trajectory and performance characteristics, this is a key gap in existing research.

Observation 7: Rapid noise quantification methods in the literature have explored various parts of the input space such as ground tracks, weather, aircraft model, community population etc. However, variations in operational profiles have not been included.

2.3 Parametric representation of the aviation noise quantification problem

An important part of creating a rapid noise quantification and optimization method is the ability to represent the problem using parameters. A parametric definition is advantageous over other definitions for a number of reasons. Firstly, a parametric definition allows many different and unique problems to be mapped onto a generic representation. If this mapping is known, then only the parameter values need to be stored and input to the overall model, instead of storing unique definitions of each problem. For example, ANGIM was able to approximate the layout of any airport by creating a parametric definition based on the runway ends, heading angles, and relative positions. Another advantage is that if an object consisting of categorical variables can be parameterized numerically, the parameters can serve as the basis for the creation of surrogate models. Categorical variables do not typically do well in surrogate models, typically requiring a separate surrogate model to be trained per setting of the categorical variable, thus eliminating it as one of the variables. Finally, parametric definitions are useful for understanding the isolated and combined

effects of parameters on the output, and are therefore useful for sensitivity analysis and optimization studies.

This section reviews existing literature on the parametric definition of the aircraft noise quantification problem. Due to the vast size of the input space of this problem, researchers have focused their efforts on smaller subsets of the complete problem. Each of these subsets are reviewed in the following subsections.

2.3.1 Airport representation

The representation of airports primarily concerns runway placement and orientation, ground tracks, airport elevation and baseline weather, and population distribution in the vicinity. For the context of this research, quantifying population exposure is excluded from the core methodology and treated as a post-processing step.

The parametric representation of runways was covered sufficiently in the original conception of ANGIM [38]. The curved ground track definition included in AEDT [107] and in an improved implementation of ANGIM [118] makes use of 5 segments represented by 9 parameters as shown in Figure 2.9. The airport elevation can be treated as a single parameter represented numerically by the elevation above mean sea level. The elevation is important because higher elevation airports have thinner atmospheres, which affects both aircraft performance and noise propagation.

The treatment of baseline weather is covered in subsection 2.3.2.

2.3.2 Weather definition

Weather conditions play a significant role in aviation noise metrics by affecting both aircraft performance and noise propagation [127]. Fundamental characteristics of aircraft performance such as lift, drag, and thrust forces are all highly dependent on atmospheric density. Additionally, thrust production by the engines is also dependent on the ambient temperature.

These factors, along with humidity also affect noise propagation and atmospheric absorption of sound. Thus, to accurately model noise metrics, all of these parameters have to defined and accounted for. Within AEDT, there are three levels of fidelity available for weather modeling. The two lower fidelity levels are based on a baseline weather definition with a lapse model used to determine the weather at different altitudes. The baseline weather can be the International Standard Atmosphere or, more accurately, be an averaged weather condition defined for each airport. At the highest fidelity level, the weather can be defined at multiple points in space and time, if such data is available.

To define the weather, six parameters are typically used in AEDT, and have also been adopted for use in various research [107, 119, 126]. These parameters are Sea-level Pressure, Station Pressure, Temperature, Relative Humidity, Dew Point Temperature, and Wind Speed. These inter-dependent parameters form a complete but non-unique weather definition. For example, the same definition can also be described by using absolute humidity in place of relative humidity. Also, although wind direction should be a factor, most noise models do not consider the effect of crosswinds. Thus, in this definition, only the wind speed is required and is applied as a headwind, regardless of the heading of the aircraft.

2.3.3 Aircraft definition

Most noise tools rely on a library of empirical data for each aircraft in their database. This data is obtained from real-world experiments and flight testing, and thus is typically only available for existing aircraft. Noise-Power-Distance tables, engine performance coefficients, aerodynamic coefficients etc. are part of such datasets. Treating these tables and coefficient values as parameters is a logical choice, although such treatment could not be found in literature. Instead, aircraft-engine combinations are treated as categorical variables representing a set of table and parameter values specific to that aircraft.

A second group of noise prediction tools permit the evaluation by new aircraft or

engine concepts by supplementing empirical data with physics-based models. In such models, major noise sources are modeled individually as parametric and semi-empirical noise sources. Thus, the effects of geometry and operating conditions can be accounted for. A prominent example of this is NASA's ANOPP tool [103] which is described in subsection 2.1.2.

The DLR Institute of Aerodynamics and Flow Technology developed the Parametric Aircraft Noise Analysis Module (PANAM) [128, 129] to perform overall noise prediction at the aircraft conceptual design stage. This was achieved by modeling individual components with semi-empirical and parametric source models which captured the major physical effects and correlations. Additionally, PANAM was developed to be modular for easy integration into upstream and downstream tools. For example, PANAM could be integrated with a flight simulation platform to design noise abatement operations. An application of PANAM to design a spiraling approach noise abatement procedure is documented in [130].

2.3.4 Trajectory definition

The trajectory and performance characteristics of an aircraft performing a landing or takeoff operation is a key influencer of noise metrics. There are typically two ways of describing this data – a time-series point-based representation or an event-based representation. Noise computation tools can typically handle one or both representations. In AEDT, a time-series representation is modeled as a Fixed-Point Profile (FPP) and an event-based representation is modeled as a procedural profile.

Time-series representation

A time-series representation treats the continuous trajectory of the aircraft as a sequence of points in the sky. These points are identified by their 4-D location – latitude, longitude, altitude, and time. Then, each point is associated with the aircraft performance characteristics – the instantaneous thrust, speed, climb rate, weight etc. Such data is

typically recorded in a tabular format.

There are many potential sources for this data, both aircraft-based and ground-based, which are described below –

1. Automatic Dependent Surveillance–Broadcast (ADS–B) based systems use periodic "pings" from the aircraft which report the aircraft's identification, altitude, position, and velocity [131]. The data transmitted by the aircraft is picked up by ground-based receivers and can be processed to recreate the aircraft's trajectory. There are several websites which utilize a large network of receivers to recreate trajectories such as FlightAware [132] and Flightradar24 [133]. Although this type of data is highly accessible, it is often low resolution, which leads to the loss of information about the aircraft's actual position over periods of time.

2. Ground-based radar systems such as those used by airports can also be used for recreation of trajectories. One of the most comprehensive of these systems is the Performance Data Analysis and Reporting System (PDARS) [134]. PDARS consists of several Air Route Traffic Control Centers (ARTCC's) and Terminal Radar Approach Control (TRACON) facilities.

3. Threaded Track developed by MITRE [135] makes use of geospatial data fusion techniques for aircraft flight trajectories. Threaded Track data is created by fusing data from a variety of sources including the aforementioned ADS-B, along with Airport Surface Detection Equipment, Model X (ASDE-X), the National Offload Program (NOP), and the Enhanced Traffic Management System (ETMS).

4. Flight Operational Quality Assurance (FOQA) data consists of data recorded by the airline operating the flight. The basis for the FOQA program is laid by the FAA Advisory Circular 120-82 which states " The value of FOQA programs is the early identification of adverse safety trends that, if uncorrected, could lead to accidents" [136]. To this effect, FOQA systems record large amount of data at a very

high frequency (typically at one recording per second, i.e. 1 Hz) and the data have been used for a number of safety related applications in prior work [137, 138, 139].

While point-based representations can be used directly for parametric implementations, there are a few key disadvantages. Firstly, real-world flight trajectories have many variations even among the same aircraft and missions due to real-world effects. This leads to a unique representation of each flight, which does not scale well to a large number of operations. Parametric variation is also difficult, while perturbations can be applied to the points, there is no guarantee that the resulting trajectory is actually flyable by the aircraft. Thus, every perturbed flight has to be verified by a performance model, at additional computational expense.

Observation 8: Point-based trajectory and performance representations are not conducive to rapid noise evaluation.

Event-based representation

An event-based representation is a description of the trajectory as intended by the pilot, which may be different that the actual trajectory due to real-world effects. In AEDT, this is defined by a procedural profile consisting of a sequence of steps reflecting pilot inputs. This procedural profile is then input to an aircraft performance model to compute the aircraft trajectory and performance in space and time. Note that because all output trajectories are produced by a performance model, there is no need to validate their flyability.

Procedural profiles can be used for both approach and arrival profiles. In fact, these can be extended to represent a complete flight, although the modeling of flights above the terminal area is usually inconsequential for subsonic aircraft. The steps which make up a typical procedural profile for departures is described below –

1. The profile starts with a takeoff ground roll with a given throttle and flap setting.

2. After lift-off the aircraft maintains its lift-off speed and climbs to a safe altitude.

3. At the safe altitude, the aircraft performs a thrust cutback from takeoff setting to climb setting.

4. After cutback, the aircraft starts accelerating wither immediately, or after reaching a higher altitude.

5. As the aircraft accelerates, the high-lift devices are retracted as per the flap schedule.

6. After reaching clean configuration, the aircraft continues accelerating to the final climbout speed either immediately, or after reaching a higher altitude.

7. Once the final climbout speed is attained (usually 250 knots calibrated airspeed (KCAS)), the aircraft stops accelerating and continues to climb to the end of terminal airspace (usually 10,000 ft MSL).

Procedural profiles are typically developed by airlines under guidance from ICAO and FAA [140, 141]. The FAA's Advisory Circular 91-53A outlines the development of two Noise Abatement Departure Profiles (NADPs) – one for benefits to the close-in community and another for distant communities. Some safety guidelines are also provided such as the limit that no cutback may be performed below 800 ft AFE.

Airlines typically develop two profiles based on their specific needs, although on rare occasions, the airport being operated to/from may require the use of a third profile [142]. The two profiles are typically labeled as ICAO-A and ICAO-B or NADP-1 and NADP-2, and are treated as categorical variables in noise modeling tools. Based on a comprehensive literature review and interviews, Lim et al. [143, 144] proposed a method to model these profiles, collectively called the NADP Library. This library consists of 20 profiles and their definitions for implementation in AEDT. The profiles differ in their cutback initiation, flap-retraction acceleration initiation, and final climbout speed acceleration initiation. The effect of these profiles on the SEL noise metric was also documented [145, 146]. The development of the NADP Library is helpful in expanding the options available to modelers, but it not a true parametric representation.

2.3.5 Summary of parametric representations

Researchers have studied various parts of the noise quantification problem and have successfully come up with parametric definitions for some of those parts. The parametric definitions identified in literature for airport, aircraft, and weather definitions seem to be well-suited for the creation of a rapid noise assessment model. However, flight profiles are typically still treated as categorical variables in the literature and are without a true parametric definition. Additionally, although point-based representations of aircraft trajectories can be created, they necessitate the inclusion of a performance validation model which would add computation time and cost to the process.

Observation 9: Many aspects of the noise quantification problem have been parameterized, but a parametric definition of aircraft trajectories remains elusive.

2.4 Optimization of Aviation Noise

Various methods of noise management and mitigation were discussed briefly in subsection 1.2.2. These solutions are typically classified into three categories – source noise reduction with new technologies, land-use planning and management, and noise abatement procedures and operational changes. Although new technologies can significantly reduce noise impacts, the process of developing a new technology is capital and time intensive, making them a long-term solution. On the other hand, land-use planning is difficult to implement, especially for older airports with significant residential areas in the vicinity.

In the short term, operational changes and noise abatement procedures seem to hold the most promise. Noise abatement procedures typically do not require any physical changes to the aircraft, and different procedures can be programmed into the flight management software. Typically, the scope for improvement in arrival operations is more limited than that for departures [147]. This is due to the 3°glideslope angle which almost all arrival operations converge on to during their final approach. The fundamental benefit of noise

abatement procedures emanates from the trade-off between the trajectory of the aircraft and the thrust variation. When the aircraft uses less thrust, the noise generated at the source is lower, but the aircraft's excess power is also lower leading to a trajectory closer to the ground. Similarly, an aircraft may aim to climb as fast as possible, usually at the compromise of higher noise at source due to higher thrust levels.

Indeed, this trade-off has been studied as far back as 1969, by Erzberger and Lee at NASA [148]. While the optimum trajectories were found to depend on the choice of noise criterion as well as other factors, a few similarities were observed across the cases. The computed optimum trajectories all had a period of acceleration as early as permissible after lift-off. It was suggested that prioritizing acceleration over climb rates may lead to a lower trajectory over sensitive areas, which may reduce the overall noise exposure if the clean configuration is achieved. Additionally, a maximum thrust reduction was performed upon reaching the noise sensitive area. If the noise sensitive area was more than four miles away from point of brake release, the initial acceleration permitted the complete retraction of flaps. It should be noted that aircraft and engine technology has changed significantly since 1969, and the results observed may not be directly applicable for modern aircraft.

In 1997, Clark [149] made use of a tool which combined a flight simulation model, a noise model, and a GIS model to evaluate aircraft's noise impacts. For approach profiles, it was found that a 3°decelerating approach provided the most significant noise reduction when compared to the baseline Instrument Landing System (ILS) approach. Studies of departure operations showed that the appropriate procedure depends heavily on the population distribution and should be developed on a case by case basis.

Initial research done by Visser et al. [150, 151, 152, 153] in the early 2000s used a similarly approach by combining a noise model, GIS model, and a dynamic trajectory optimization algorithm, later labeled as NOISHHH. The dynamic model could be used to optimize a very intricate trajectory comprising of precise turns and climb profiles to reduce awakenings on the ground. Multi-objective criteria were also sometimes included such as

fuel burn and noise contour areas. Such formulations made use of different weightings to prioritize the different objectives. One research article also noted that flying such complex trajectories may not be practical and instead used a procedural profile as a reference and then attempted to optimize deviations from this profile.

Subsequent research by Visser et al. focused on improvements to the NOISHHH tool and expansion of the framework's capabilities to new problems. By extending the scope from terminal area to full flight computations, a noise optimal runway-to-runway trajectory for a city-pair flight was created [154]. By extending the use-case from a single flight to multiple events, aggregated noise metrics could be optimized. Such an extension was applied to nightly flights at a major international airport and showed improvements to the number of people highly annoyed due to aircraft noise [155]. By changing the optimization scheme to a genetic algorithm based on parametric trajectory definitions, the process was made more efficient. This could be achieved by suitably choosing parameters to ensure compliance with operational requirements on departures, thereby avoiding infeasible solutions [156, 157, 158]. The approach was further extended into a two-step optimization framework for the design and selection of aircraft departure routes, and the allocation of flights to those routes [159, 160].

A similar problem was studied by Prats et al. as a non-linear multi-objective optimal control problem. Instead of using different weighting schemes for the multiple objectives, a Lexicographic optimization was performed instead [161]. This approach establishes a hierarchical order among the optimization objectives instead of assigning numeric and usually arbitrary weights. This technique was applied to to minimize noise annoyance with the maximum perceived noise metric at five different noise sensitive locations in [162]. This was later extended to include population data and results showed a dependency of the optimal trajectory on the type of aircraft and the hour of the day [163]. This optimization scheme was slightly adjusted by neglecting marginal benefits of noise reduction below a threshold value in [164]. Later, an optimization study revealed that if departure speed

constraints were removed, CO_2 emissions could be removed by 180 kg per flight at the cost of increased noise exposure below 70 dB [165].

A common theme across these optimization studies is that although they have been developed for generic use-cases, they have been applied to very specific scenarios. Typical demonstrations include modeling a single aircraft flying out of a specific airport. The effect of weather conditions or on the optimal trajectory is typically not studied. Thus, the optimized trajectories are not a comprehensive solution but are instead limited to a select few scenarios. The reason behind this can be linked back to the many-query nature of optimization studies – in order to evaluate optimum profiles across a variety of operating conditions, noise results have to be computed at each condition. However, these evaluations do not scale well with a large number of conditions due to the computation cost of the underlying physics based aircraft dynamic models and semi-empirical noise models.

Observation 10: Aircraft trajectory optimization efforts have been limited to specific instances, due to the difficulty in efficiently evaluating multiple scenarios using methods based on computationally expensive aircraft dynamics and performance models.

2.5 Reduced Order Modeling methods

In previous sections, it was observed that traditional surrogate modeling methods fall short when applied to even a moderately sized input subspace. It was also observed that there is extremely limited research on the application of Reduced Order Models to the aviation noise problems. The only application that could be found in literature showed promising results [126]. This section provides an overview of ROMs – what they are, how they work, and where they are typically used.

Is simple terms, Reduced Order Modeling or Model Order Reduction (MOR) is a method for reducing the computational complexity of mathematical models in numerical simulations [166, 167]. The fundamental idea of ROM/MOR is the identification and recreation of the underlying pattern of the data and not the complete replication. By

allowing for some data loss, the computational cost and time can be greatly reduced. This is especially useful in situations where there are many variables and models to consider, but the accuracy of full order models is not necessary. These situations typically arise in the early stages of a process, such as conceptual aircraft design.

The desire to replace or complement a complicated function with an approximation can be traced back to the early 19th century. In 1807, Fourier published the method of approximating any continuous function as a series of trigonometric terms [168]. The initial steps towards model reduction in linear algebra came in the form reducing a matrix to a tri-diagonal form or to a smaller matrix. Fundamental methods in the area of Model Order Reduction were published in 1980s and 1990s. One of the most commonly used method, Proper Orthogonal Decomposition (POD), was discovered independently by researchers in different disciplines, and is also known as Principal Component Analysis (PCA) or Karhunen-Loève decomposition.

Reduced Order Models have numerous applications in many different disciplines of science, engineering, and math. Within the realm of aerospace applications, the most popular application by far has been in advanced Computational Fluid Dynamics (CFD) applications involving unsteady aerodynamics, aero-elastic effects, hypersonic flow fields etc. [169, 170, 171, 172]. These models have also been used for multi-disciplinary design, analysis, and optimization applications, such as the design optimization of airfoils [173].

A useful classification of ROMs is whether they are projection-based or interpolation-based. Projection-based methods operate using the underlying governing equations and are also known as intrusive methods. These types of ROMs are advantageous because they retain the underlying physics of the problem, if the underlying equations are known. Interpolation-based methods, on the other hand, are "non-intrusive" and do not rely on knowledge of the underlying physics of the problem, and perform interpolation directly on the reduced space. Thus, interpolation-based methods offer greater flexibility and are better suited to aviation noise quantification.

An interpolation-based ROM has two major steps – the model order reduction step, and the creation of a surrogate model in the latent space. As with all surrogate models, a solution set is generated using the full order model. These solutions (also called snapshots) are then divided into two mutually exclusive subsets – one for training the ROM, and the other for validating the ROM. The training dataset is used to develop the surrogate model. Predictions made from the surrogate model are then compared to the validation dataset to assess whether the surrogate model has the desired accuracy. The process of training and validation is often iterative, until the desired accuracy is achieved.

2.6 Clustering of flight trajectories

As discussed in subsection 2.3.4, point-based representations of aircraft trajectories are unsuitable for parametric noise quantification models. One reason behind this is that point-based trajectories are often developed from aircraft recordings or ground-based RADAR systems. Each flight has a unique point-based trajectory, even if the pilot intends to fly a common, pre-defined operation. This is due to the introduction of real-world effects such as weather, and minor differences amongst aircraft of the same class.

Although the resultant trajectories and their point-based representations are unique, the differences among them are relatively minor. In such cases, collecting trajectories into a few self-similar groups can help reduce the amount of data to be stored, processed, and analyzed. The process of grouping entities based on similarity is known as *clustering*. Clustering is generally classified as an unsupervised Machine Learning (ML) technique, where the algorithm does not have a sample solution set with which to train the provided data.

Clustering techniques have been primarily used in safety applications, particularly in the terminal airspace. Gariel et al. [174] recognized that by grouping together similar trajectories, a knowledge base of typical operations and their variability could be generated. Current operations could then be monitored against the typical operations to detect

anomalies. This idea was conceived as a tool to monitor the instantaneous health of the airspace, with a "healthy" airspace being one in which all aircraft are flying as per typical operations. When an aircraft is not in conformance, more ATC attention is required to guide the flight. Similar work was done by Olive and Morio [175] to foster good understanding of traffic flow and structure, and enable a probabilistic approach to risk assessment in air traffic safety. Corrado et al. [176] introduced weighting functions to the standard Euclidean distance to address the limitation of skewed classification and inadequate identification. By trying different weighting methods, it was found that giving more weight to points closer to the boundary of the terminal airspace yielded more accurate clustering results. While clustering is usually done on similarity distance computations based on positions, times, and thematic attributes, not all may be equally relevant. This was recognized by Andrienko et al. [177] who proposed an analytical workflow in which relevance flags could be attached to different elements, and irrelevant elements could be ignored by the distance function. Basora et al. [178] created a trajectory clustering framework using minimal input parameters for application to real trajectories over a French area control center.

While several applications of trajectory clustering have been made in literature, these are largely limited to risk and safety identification. Applications to the evaluation of aviation environmental metrics are not observed in the literature. However, the core technique seems to hold promise for such applications as well.

2.7 Summary of Observations and Gaps

The observations drawn based on the initial literature review point towards the gaps in existing research. These gaps serve to narrow the focus of subsequent research, and addressing these gaps becomes the primary means of satisfying the research objective. These gaps represent the technical challenges that must be solved, and help to define the formal Research Questions for which Hypotheses can be posed and tested.

2.7.1 Gap 1 – Parametric definitions of aircraft trajectories

The first gap arises out of Observations 7, 8, and 9 which showed how existing representations of aircraft trajectories in literature are insufficient for building parametric models. In order to build a rapid and parametric modeling capability, a new representation has to be developed.

Gap 1: No parametric definition for aircraft trajectories exists which can be used to build the desired rapid aviation noise model.

2.7.2 Gap 2 – Field surrogate modeling capabilities

The second gap addresses the types of mathematical models that are used for noise quantification. Based on Observations 1, 2, 3, 4, 5, and 6, it is evident that methods in literature are inadequate in handling the entirety of the aviation noise quantification problem.

Gap 2: Current state-of-the-art tools and scalar valued surrogate models are unable to adequately address the inherent complexities of the noise problem.

2.7.3 Overall Gap – Parametric Aviation Noise Model

The Overall Gap that needs to be addressed is linked to Observation 10. The fulfilment of Gaps 1 and 2 will provide a path to the fulfilment of this Overall Gap.

Overall Gap: There is a lack of parametric aviation noise models which can enable rapid quantification, optimization, and other many-query applications.

In chapter 3, a formal problem formulation and a research plan is stated which aims to solve these gaps.

CHAPTER 3
RESEARCH FORMULATION

Building on the literature review, observations, and stated gaps in the previous chapter, this chapter focuses on formalizing the problem formulation and research questions, which eventually lead to the development of the methodology in response to the original research objective.

The observations and gaps from Chapter 2 are collected into two high-level research areas. Each area has certain requirements which must be addressed by the proposed methodology. These lead into the formal Research Questions which aim to tackle the identified gaps, and when answered, directly contribute to the Research Objective. Each Research Question is answered with a Hypothesis, which is supported with original research conducted by the author.

Finally, with the construction of the complete overall methodology, a demonstrative case study is performed on a suitable test case. The test case is designed to showcase the capabilities of the methodology, and thus demonstrate the contributions of this original research.

3.1 Research Objective

Before the formal research formulation, it is helpful to revisit the original Motivating Research Question and the overall Research Objective, which are stated here for reference
–

Motivating Research Question

How can the process of aviation noise quantification be improved to enable rapid quantification of noise metrics to facilitate parametric trade-off analyses and optimization efforts?

Research Objective

Develop a methodology to address inherent complexities in the aviation noise computation problem, thereby enabling rapid quantification of noise metrics in a variety of scenarios, thus facilitating parametric trade-off analyses and optimization efforts.

Without going into the details, the Research Objective lays out the basic requirements that any methodology must meet, in order for the objective to be satisfied. The end goal is to facilitate parametric trade-off analyses and optimization efforts. These type of efforts require the evaluation of many hypothetical scenarios which are compared to the current real-world scenario. This type of scaling up of analyses can only occur when the evaluation process is efficient on time and resources, which brings in the need to have rapid quantification capabilities. However, this type of rapid quantification can only occur when the inherent complexities of the aviation noise computation problem are addressed.

The inherent complexities mentioned in the research objective were evident from the literature review conducted in chapter 2. The observations from the literature review were organized into two formally stated Gaps, and corresponding research areas. Research Area 1 deals with the challenge of coming up with parametric definitions of the aviation noise modeling problem. This is a pre-requisite for the elimination of categorical variables and for handling complex aircraft trajectory data. Research Area 2 deals directly with the aviation noise modeling process and aims to enhance the surrogate modeling efforts observed in literature to achieve rapid noise modeling capabilities.

Based on this understanding, the identified Research Areas and their contributions to realizing the overall Research Objective are shown in Figure 3.1.

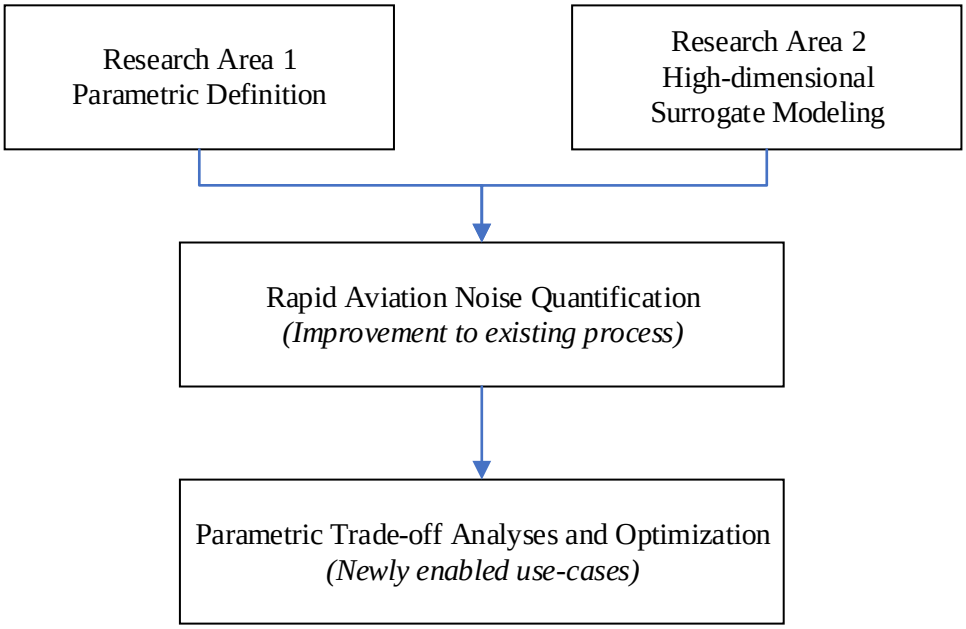

Figure 3.1: Break-down of the overall Research Objective

The remainder of this chapter is a deep dive into each Research Area. Within each area, specific Research Questions are posed to help address the identified Gaps. The problem is characterized and a separate literature review is conducted to attempt to answer each research question. A Hypothesis is formulated for each Research Question, and an Experiment is designed to test each Hypothesis. Depending on the results of the experiments, each Hypothesis is accepted or rejected. The methods of the accepted Hypothesis form the components of the Overall Methodology.

3.1.1 Scoping of the problem

The original Motivating Research Question and Research Objective were intentionally broad in their scope. With the conclusion of the subsequent literature review, it was discovered that different parts of the problem had been addressed to varying degrees, and

thus, more focused research areas emerged.

For example, various parts of the aviation noise modeling process have been assigned parametric definitions by literature, including airports [38, 107, 118], weather [107, 119, 126], and aircraft [101, 128, 129]. However, aircraft trajectory information remains resigned to either a high-dimensional time-series representation, or a categorical event-based representation.

Similarly, the computation of population exposure based on airport-level noise grids has been well studied and improvised in existing literature [92, 120, 121]. The process of computing airport-level noise grids themselves from aircraft-level single event noise metrics has also been adequately addressed in the literature [38, 112, 113]. However, obtaining those aircraft-level single event noise metrics in an accurate and rapid manner still poses a significant challenge and still remains an unsolved problem in the literature.

The scope of this research is thereby narrowed to a more specific purpose. Two key areas of research emerge within this domain of aircraft-level noise metric quantification – parametric representation of real-world aircraft trajectories and rapid modeling of aviation noise metrics.

3.2 Research Area 1 – Parametric Representation of Aircraft Trajectories

The first gap identified from literature review was about the lack of parametric aircraft trajectory representations. To fill this gap, the first high-level Research Question is posed –

Research Question 1
How can the input space of aircraft trajectories be represented to enable parametric quantification and optimization?

Based on this high-level research question, the following requirements arise which any solution must satisfy –

1. The first requirement is that of the representation itself. The solution must be able to provide a representation for aircraft trajectories that is better than existing representations. It must be a complete representation over the relevant domain, and consist entirely of numerical parameters. In addition to the representation, a method must also be provided to be able to convert real-world trajectory data into the proposed representation.

2. The second requirement is of relevance when real-world trajectories are evaluated for aviation noise. As noted previously, real-world trajectories are unique and thus cannot be efficiently modeled in large numbers using traditional methods. In order to effectively analyze such large datasets, the method must be scalable. If such scaling is not possible, a supplementary process must be designed.

3. Finally, in order to perform optimization and trade-off analyses, it is important to identify which parameters have the most influence on the noise results, so that they can be prioritized. Thus, the parameters which form the basis of the representation must be ranked in their order of influence so that their design space can be explored efficiently.

With these requirements, this research question can be further divided into three key parts that need to be addressed – representation, scalability, and exploration. These three parts lead to the three lower-level Research Questions.

3.2.1 Research Question 1.1 – Inverse Map of the aircraft performance model

It was previously noted that real-world aircraft trajectories are not well-suited for use with parametric models. Typical real-world flight data is usually available in a tabular format representing time-series information of various parameters.

When real-world data is unavailable, or cannot be modeled in large quantities, modelers have to rely on theoretical procedural profile definitions. As described in

subsection 2.3.4, these definitions are usually descriptive, and provide an enumeration of steps that collectively represent the departure or arrival operation. For example, the default departure procedure for a Boeing 737-800 aircraft (labeled as 'STANDARD'), as modeled by AEDT for a short stage length 1 mission is shown in Table 3.1 and detailed below –

1. The first step is the take-off ground roll, with the flaps set at 'T_05' setting and with the use of maximum available take-off thrust.

2. Once the aircraft is airborne, the aircraft maintains the flap and thrust settings and climbs with constant speed to an altitude of 1000 ft AFE.

3. After reaching 1000 ft altitude, the aircraft pitches over and starts to accelerate, while maintaining a positive vertical climb rate. The target altitude in this case is 181.7 knots calibrated airspeed, while maintaining a climb rate of 1885.7 ft/min. At the end of this step, the flaps are retracted from 'T_05' to 'T_01' setting.

4. Next, the aircraft continues to accelerate, this time with a target airspeed of 204.8 knots calibrate airspeed, while maintaining a climb rate of 2112.0 ft/min. At the end of this step, the flaps are retracted from 'T_01' to 'T_00' setting. The 'T_00' setting in this case implies a clean configuration.

5. Having completed the flap retraction, the aircraft maintains it's calibrated airspeed and climbs to an altitude of 3000 ft AFE. At this altitude, the aircraft performs a thrust cutback by changing the thrust setting from 'Max Takeoff' to 'Max Climb'.

6. Having performed the thrust cutback, the aircraft accelerates to its final climbout speed of 250 knots calibrated airspeed, while maintaining a climb rate of 1891.3 ft/min.

7. The final three steps are constant speed climbs up to 10,000 ft AFE with intermediate steps at 5500 ft AFE and 7500 ft AFE. These seemingly redundant intermediate steps are added for numerical conditioning of the tool's performance computations.

Table 3.1: Procedural definition of a departure operation for the Boeing 737-800 [107]

Step Number	Step Type	Flap ID	Thrust Level	Altitude AFE (ft)	Calibrated Airspeed (kt)	Climb Rate (ft/min)
1	Takeoff	T_05	Max Takeoff			
2	Climb	T_05	Max Takeoff	1000		
3	Accelerate	T_05	Max Takeoff		181.7	1885.7
4	Accelerate	T_01	Max Takeoff		204.8	2112
5	Climb	T_00	Max Takeoff	2040		
6	Climb	T_00	Max Climb	3000		
7	Accelerate	T_00	Max Climb		250	1891.3
8	Climb	T_00	Max Climb	5500		
9	Climb	T_00	Max Climb	7500		
10	Climb	T_00	Max Climb	10000		

These unsuitable and descriptive representations lead to Research Question 1.1.

Research Question 1.1

How can aircraft trajectories and performance characteristics be represented parametrically?

A procedural profile definition can be adapted to different operations by changing a few parameters – such as the rate of climb, or the altitude of thrust cutback. This was the basis of the creation of the NADP Library [143] which provided 20 profile definitions for departure operation implementation in noise modeling tools. However, these definitions are still descriptive, and contain a categorical variable in their treatment of the thrust cutback. This categorical variable takes on the value of “Before” if the thrust cutback is performed before the initiation of acceleration for flap retraction, and “After” if performed after flap retraction is complete.

Converting these descriptive definitions into a numeric parametric basis is relatively

straightforward if the structure of the description is fixed. If the underlying structure of the profile description – the number, order, and type of steps is held constant, then each profile differs only in numeric parameters such as altitude, target airspeed, and proxy labels of numeric parameters such as thrust setting.

With the conversion to a fixed structure and the replacement of proxy labels by their underlying numeric values, procedural profile definitions can be represented purely using numeric parameters. The bigger task at hand is to convert time-series operations to this set of parameters. These descriptive definitions of operations serve as inputs to a tool's performance computation model, with the output being a time-series dataset consisting of information about the aircraft's trajectory and performance characteristics. For example, the corresponding performance output for the profile described in Table 3.1 is depicted in Figure 3.2. The step numbers corresponding to each section of the trajectory are also labeled on the plot.

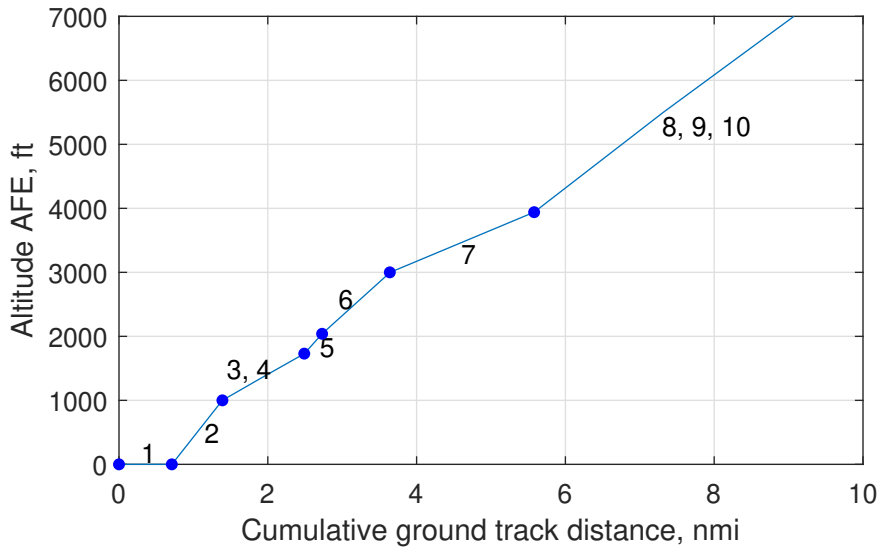

Figure 3.2: Visualization of resultant trajectory for the 737-800 aircraft for provided profile definition in Table 3.1

The fundamental modeling capability required here is an inverse model of an aircraft performance computation model, which can operate in the reverse direction, by taking in time-series data and giving a parametric profile definition as output. This desired capability

is summarized in Figure 3.3 and leads to Hypothesis 1.1.

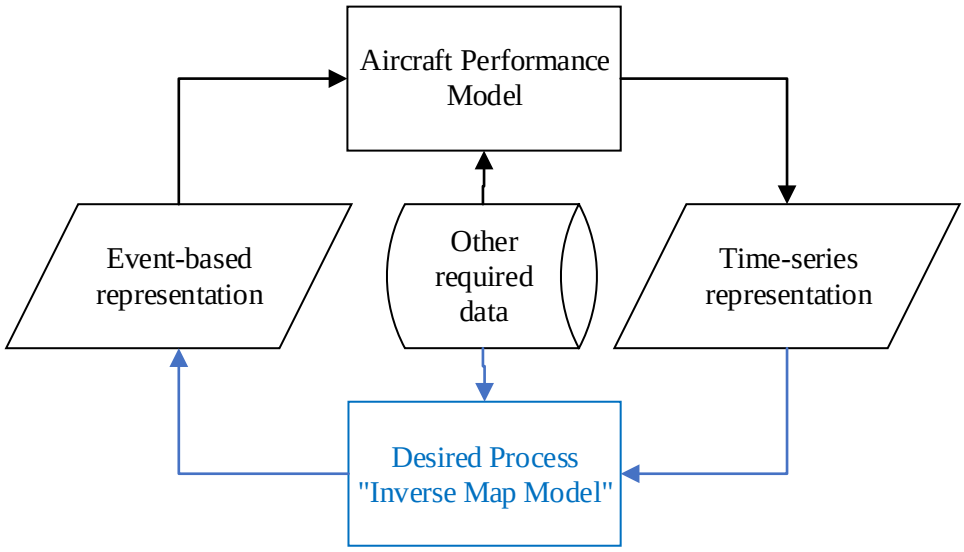

Figure 3.3: Desired inverse map model of an aircraft performance model

Hypothesis 1.1

If an inverse mapping of aircraft trajectory and performance calculations can be identified, then aircraft trajectories can be represented parametrically.

Formulation of the inverse map

First, it is helpful to note the following definitions –

- The numerical parameters that define an operation are represented by $\{p_i \mid i = 1, 2, \ldots, n\}$.
- Each operation x_i is therefore defined by the collection of parameter values as $x_i = \{p_1, p_2, \ldots, p_n\}$.
- The space of all possible sets of parameter values is $\mathbb{X}$.

- The corresponding trajectories and performance characteristics of an operation denoted by x_i is y_i.
- The space of all corresponding trajectories and performance characteristics is $\mathbb{Y}$.
- The Aircraft Performance Model is represented as $f_{APM} : \mathbb{X} \rightarrow \mathbb{Y}, f_{APM}(x_i) = y_i$.
- The desired inverse map of the Aircraft Performance Model is represented as $f_{APM}^{-1} : \mathbb{Y} \rightarrow \mathbb{X}, f_{APM}^{-1}(y_i) = x_i$.

To develop the formulation, the first step is to develop a set of known mappings $X \subset \mathbb{X}, Y \subset \mathbb{Y}$. Then, the question to be answered is, given a new trajectory $y_j \in \mathbb{Y}, \notin Y$, what is the corresponding parameter set x_j? As such, f_{APM} has a sequence of steps which uses standard equations and coefficients to convert the parameter set into the corresponding aircraft trajectory and performance. Therefore, f_{APM}^{-1} cannot be expected to have a closed form expression, and must instead be developed mathematically with the help of data analysis.

Given the nature of the problem, it is reasonable to assume that if two trajectories are very similar to each other, then their input parameters must also be similarly valued. That is,

$$y_j \approx y_i \implies x_j \approx x_i \tag{3.1}$$

Thus, if an approximately equal trajectory can be identified from the set Y, then an approximate inverse can also be identified from the set X. This brings the notion of trajectory similarity into question. To objectively compute the similarity between aircraft trajectories, a similarity function is proposed, which maps two input trajectories onto scalar similarity metrics. The similarity should be judged based on the relevant variables of the trajectory, such as the variation of aircraft altitude with ground track distance, the variation

of airspeed with altitude, and the variation of thrust with altitude. These three aspects are selected because of their strong influence on aviation noise, although it is rare to have thrust data available when using real-world data. Thus, when using k similarity metrics,

$$f_{similar} : \mathbb{Y} \times \mathbb{Y} \longrightarrow \mathbb{R}^k$$

To evaluate the similarity, each trajectory has to be interpolated to a new sampling basis. This basis is envisioned to be a linear space of cumulative ground track distance with equally spaced sampling points. The trajectory itself is terminated at 10,000 ft AFE. Once all trajectories have been re-sampled onto a common sampling basis, then the differences in altitude and airspeed are evaluated at each sampling point. These differences are then summarized using an appropriate summary statistic, such as the Root Mean Square. With this similarity metric computed, two trajectories can be judged on their "closeness" to each other. A low value of similarity metric indicates that profiles are similar.

With the construction of the similarity function, the inverse mapping process is now complete. The process for the creation of the inverse map is summarized here –

1. Create a library of operational profiles based on input parameters and compute their output trajectories and performance data.

2. Given a new trajectory, compute it's similarity to each of the profiles in the library.

3. Select the profile which is the most similar.

4. Assign the parameter values of the most similar profile.

In order to test Hypothesis 1.1, additional operations will be modeled using known parameter values and the results obtained from the inverse map will be compared. If the inverse mapped parameter values are sufficiently close to the known input parameter values, and the differences in corresponding noise results are acceptably small, then Hypothesis 1.1 is accepted.

3.2.2 Research Question 1.2 – Clustering of real-world trajectories

With the creation of the inverse map in RQ1.1, the first requirement 'representation' of the high-level RQ1 is satisfied. The next requirement is to be able to apply the developed method to real-world trajectories. The key problem in expanding to real-world trajectories is that of scalability. The calculation of the inverse map involves many steps, and is not necessarily computationally efficient. Applying the method developed in Hypothesis 1.1 to every real world operation may not necessarily be feasible, or even useful.

Additionally, even if there was a negligible cost associated with calculating the inverse, modeling each unique flight in a noise modeling tool would be impractical. Each flight would require the modeling of its unique parameter set, which would then go through the entire computationally expensive process of performance computation and noise metric calculation. As the number of flights to be modeled increase, the modeling effort increases linearly, and thus, for large sets of flights, this would inevitably be infeasible. As an example, even with the reduction is commercial aviation activity due to the Covid-19 pandemic, the top 10 busiest airports in the world still handled more than 1100 aircraft movements on average per day in 2020 [179].

This need for scalability leads to Research Question 1.2.

Research Question 1.2
How can real-world aircraft trajectories be efficiently mapped to a parametric definition?

To scale the process, a pre-processing step is proposed, where different real-world trajectories are first grouped together, and then a representative flight from within that group is used in the inverse mapping process. The obtained set of parameters is then considered to be representative of the entire group.

The grouping of objects based on their similarity is also called *clustering*. Clustering

is an unsupervised machine learning technique which groups similar objects based on their features. Thus, this technique can be adapted here for use with real-world trajectories. The similarities between different elements of the dataset are identified and used to cluster the dataset so that objects within a cluster are similar to each other and dissimilar to objects within another cluster.

Being an unsupervised learning technique, clustering does not require any prior knowledge about the similarity patterns within the dataset. By applying clustering algorithms to flight trajectory data, the dataset can be reduced to a few representative groups. Differences in flight trajectories that arise from various factors such as weather, load factor, pilot intent etc. form the basis of the separation into the groups.

Various algorithms exist for clustering, each with their own advantages and drawbacks. The application of this technique to aircraft data in the context of aviation safety has been documented in the literature. Using Flight Data Recorder datasets, researchers in [180] used clustering techniques to detect abnormal operations. Such research has also been conducted for General Aviation operations using energy metrics [181]. Other studies have focused on en-route trajectories [182], approach phase of flight [183], or in the selection of parameters for flight risk identification [184].

However, the use of clustering techniques has not been observed in literature for the purpose of aviation environmental impact assessment. It is proposed that the adaptation of the technique to this context will enable the efficient mapping of real-world trajectories onto a parametric definition. This leads to Hypothesis 1.2.

Hypothesis 1.2

If real-world aircraft trajectories are clustered into groups, then multiple trajectories within a group can linked to a single parametric definition using the inverse map of the cluster representative.

Formulation of the clustering process

The first step in performing clustering is to generate a quantitative method of judging the closeness or similarity of two objects. This requirement has strong parallels with the development of the similarity function for testing Hypothesis 1.1. In fact, the same similarity function which was developed there can be directly used here to assess the similarity between two real-world trajectories.

Thus the process for clustering real-world trajectory data is outlined below –

1. Obtain and pre-process set of real-world flight data.
2. Apply the similarity function for each pair of flights, thus obtaining the similarity of each flight to every other flight.
3. A clustering algorithm will be used to group flights based on their similarities. Different clustering algorithms will be researched and the appropriate algorithms will be deployed.
4. Pick a representative flight from each group.

The proposed process will be tested with different clustering algorithms and will likely require tuning of parameters associated with the algorithms. Hypothesis 1.2 is accepted if a sufficiently low error is obtained when substituting a real-world flight with its cluster representative.

3.2.3 Research Question 1.3 – Ranking of influential parameters

After the first two requirements of RQ1 are addressed, the final consideration of 'exploration' remains. The focus the shifts on parametric optimization, in which the objective is to design a theoretical optimal operational profile. This is in contrast to parametric quantification, where real operations had to be quantified accurately. Previously, the focus was on creating accurate parametric definitions of aircraft operations. Now, the parameters

are known, and therefore can be varied in appropriate ranges to generate theoretical candidate profiles for evaluation.

This leads to Research Question 1.3.

Research Question 1.3

How can the design space for aircraft trajectories be explored efficiently?

Given a set of parameters which influence the output to be optimized, it is very rarely the case that each parameter is equally influential on the output. In fact, a few key parameters usually drive the change in the output, an observation that is referred to as the Pareto Principle. Given this observation, it makes sense to focus on the important parameters and allocate more resources in order to evaluate more values of such parameters. This enables a richer and denser exploration of the design space where it matters the most.

The broader field of research in this context is called Global Sensitivity Analysis [185, 186, 187]. Some of the objectives of such analysis, which vary with application, are – assessment of similarity between the model and the underlying system, identification and screening of factor importance and function, location and characterization of regions of sensitivity, determination of factor interdependence, factor and model reduction, and quantitative uncertainty apportionment [188]. In this context, the objective is to is to idenify and screen the factors/parameters of importance.

Local sensitive analysis is focused on points within a much larger space, and makes use of partial derivatives to determine the sensitivities. These partial derivatives may be obtained either from analytically or numerically, depending on the type of model. On the other hand, GSA methods attempt to provide more general results by considering the entire domain of the model and characterizing the response sensitivity over it.

Hypothesis 1.3

If a screening test is performed and the primary drivers can be identified, the design space for aircraft trajectories can be explored efficiently.

Formulation of the screening test

The objective of RQ1.3 is to enable the efficient exploration of the design space of aircraft trajectories. The experiment performed here will involve modeling several combinations of parameters and assessing the importance of each parameter's influence on aviation noise metrics.

The following steps are proposed to text Hypothesis 1.3.

1. The identified list of parameters from RQ1.1 is used.
2. An appropriate range of variation for each parameter is to be determined using a literature review and domain knowledge.
3. These parameters are then sampled to create a design space of parameters, using a suitable Design Of Experiments.
4. The corresponding noise metrics of the obtained designs are evaluated. Any post processing if necessary is performed.
5. Statistical regression methods are used to perform the screening tests and identify parameter importance.

This information about the importance ranking of parameters is crucial to efficiently explore the trajectory design space. The higher ranked parameters are those which have a large influence on the noise metrics, and therefore must be sampled more finely. Additionally, when performing optimization, changing these higher ranked parameters will yield the most change in the objective function.

3.2.4 Summary of Research Area 1

Observations 7, 8, and 9 from literature review led to the identification of the first gap, which states that there are no available parameteric definitions of aircraft trajectories which can be used for developing rapid noise models. This motivated the first research area and the high-level Research Question 1 which aimed to develop a representation of the input space of aircraft trajectories to enable parametric quantification and optimization. This led to three requirements of representation, scalability, and exploration which were formulated with Research Questions 1.1, 1.2, and 1.3 respectively. This chain of reasoning is summarized in

With RQ1.1, it is shown that any trajectory can be transformed into a parametric definition. Since the parameter set is based on a procedural profile definition, it is ready for use in noise modeling tools such as AEDT. With RQ1.1, any source of aircraft trajectory data can be inverse-mapped onto a parametric definition and readily modeled to obtain noise metrics. With RQ1.2, the applicability of this inverse-mapping is expanded to be scalable to real-world flight data with use of a clustering technique which downsizes the number of real-world operations to be modeled. Finally, RQ1.3 helps inform efficient future optimization efforts based on the prioritization of the input parameters of the noise model.

3.3 Research Area 2 – Rapid modeling of aviation noise

The second gap identified in the literature was about the inability of current state-of-the-art tools and scalar valued surrogate models to adequately address the inherent complexities of the noise problem. This inability leads to computationally expensive physics-based and semi-empirical tools which are incompatible with rapid noise modeling applications.

Research Question 2

How can the process of computing aviation noise metrics be made more computationally efficient?

The primary complexity that most studies in literature are unable to address is the high dimensional output in the form of aviation noise metric grids that are generated. Noise results are typically quantified over a grid of points, so that contour shapes may be created for visualization. However, with the necessary resolution and size of the grid, the noise results become very high dimensional, often in the order of tens of thousands of points.

Scalar values surrogate models typically struggle with high dimensional data – either one surrogate model needs to be trained for each grid point, or a single model has to be trained which can differentiate between grid points based on their location. This leads to either inaccurate models which are fast, or accurate models which are slow. Models which are both fast and accurate are needed and preliminary research on Reduced Order Modeling of AEDT has shown promise [126].

So, the first problem to be tackled is that of dimensionality reduction. A process needs to be developed which can transform high dimensional noise grids into something which is easier to model. However, the process must also be reversible, so that actual noise grids can be recovered from the model. These two considerations led to the creation of the two specific research questions within this research area.

3.3.1 Research Question 2.1 – Model Order Reduction of noise results

The first key part is the reduction of dimensionality of the noise results from noise modeling tools. As noted previously, the high dimensionality of the noise results leads to inaccurate or impractical surrogate models. Thus, a pre-processing step is required to transform the high dimensional data before any accurate and rapid surrogate models can trained.

Research Question 2.1

How can the high dimension of the solution space be addressed?

In literature, the methods used for this purpose are collectively called Model Order Reduction techniques. By reducing the dimension of the data, an approximation of the original data is created, which is called a reduced order model. An approximation by definition involves errors, and the various techniques for Model Order Reduction in literature differ in their approaches towards minimizing this error.

Model order reduction methods have successfully been applied in numerous engineering disciplines and have been used to solve large-scale problems in areas such as control engineering [189, 190], signal processing [191, 192], image compression [193, 194], fluid mechanics [195, 196], power systems [197, 198], and earthquake engineering [199]. Specific to the field of aerospace engineering, applications have been found in design space exploration [200, 201, 202, 203], evaluation of aerodynamic loads [204, 205], solid mechanics and structural assessment [206, 207, 208, 209], aeroelasticity [210, 211], and design optimization [212, 213, 214, 215, 216].

With the numerous existing applications of Model Order Reduction in literature, it is a good candidate for application in this context of aviation noise metric data. This leads to Hypothesis 2.1.

Hypothesis 2.1

If Model Order Reduction techniques are used on the noise grid data, then the solution space can be projected onto a lower dimension space.

Formulation of the Model Order Reduction

There are three requirements that the MOR technique selected must satisfy –

1. Minimal error when projecting from the high dimensional space to the low dimen-

sional space.

2. Preservation of the underlying trends and properties of the data. This is needed so that the resultant reduced order model can be used effectively for surrogate modeling.

3. Ability to return to the high dimensional space, so that full noise grids can be recovered and used for analysis.

There are several different ways in which Model Order Reduction techniques can be classified –

- Parametric vs. Non-Parametric: Non-parametric reduced order models are typically used for applications when the simulation itself is computationally infeasible, such as for real-time control applications [217, 218]. Parametric reduced order models play the role of surrogate models for the prediction of fields (instead of scalars) as functions of input parameters [219, 220].

- Intrusive vs. Non-Intrusive: Intrusive reduced order models require access to the original full order model equations or matrix coefficients. Non-intrusive models work under constraint of having only output data available [221, 222].

- Projection based vs. Interpolation based: Projection-based models are a class of intrusive methods which work on governing equations directly. Interpolation based models are non-intrusive models which provide solutions at untested parameter combinations by directly interpolating in the reduced dimensional space.

A variety of methods exist for the creation of the reduced order space such as isomap, Fourier Model Reduction, Reduced-Basis method etc. One of the most commonly used method is the Proper Orthogonal Decomposition, also called Principal Component Analysis. The idea behind POD is that every point in the high dimensional space can be recreated using a linear combination of a basis vectors. The basis vectors are chosen such that almost all information can be captured with a very small number of basis vectors.

Thus, once the basis vectors have been computed, representing each high dimensional point becomes as easy as storing the coordinates along each basis vector.

For this experiment, the Proper Orthogonal Decomposition method is used to obtain the reduced order space due to two key reasons – first, the method has been proven to work with extensive engineering applications and is reliable for most field predictions Secondly, it is a method which is relatively easy to understand and implement. Given that there is scarce proven application of MOR techniques in this context, it makes sense to start with the method which is the most well understood.

The aim here is to demonstrate that the POD technique can be successfully adapted for the use of aviation noise modeling. The following steps are planned –

1. First, a large set of noise results will be obtained, collectively referred to as the *solution space*. A set of test cases similar to the one designed for testing Hypothesis 1.3 can be used. Each noise result here refers to a grid of receptor points at which a noise metric has been computed by AEDT. In the POD terminology, a single full-order solution is referred to as a *snapshot*.

2. The Proper Orthogonal Decomposition method will be used to map the full-order solutions onto a reduced space. The error for this step is defined as the *projection error* and is computed as aggregated difference in noise metric values across all receptor points between the reduced and original solution.

If the results of this experiment show that it is possible to reduce the dimension of the solution space and subsequently recreate full noise grids with acceptable error margins, then Hypothesis 2.1 will be accepted.

3.3.2 Research Question 2.2 – Field surrogate modeling

With the high dimensional solution space addressed using MOR techniques, the final piece of the puzzle is adapting the reduced solution space for surrogate modeling. The high

dimensional full order solution space was linked to the input space of the noise model by the noise modeling tool. Additionally, the reduced solution space is linked to the original solution space through the Model Order Reduction algorithm.

Research Question 2.2

How can the reduced solution space be mapped to the input space?

To map the reduced solution space to the input space, the coordinates of the reduced solution space need to be developed into functions of the input parameters. This type of surrogate model is referred to as *field* surrogate modeling, as it is able to work with field data such as high dimensional noise grids.

Hypothesis 2.2

If an interpolation/regression model is developed linking the solution in the latent space to the parameters, then the reduced solution space can be mapped to the input space.

Formulation of the Field Surrogate Model

This final experiment is based on the creation of regression or interpolation models of the coordinates of the latent space. If such a model is created, then the coordinates in the reduced solution space can be estimated given an input parameter set. This reduced order solution can then be transformed back into the high dimensional solution using the inverse of the Model Order Reduction process.

The steps for this experiment are –

1. A set of solutions in the reduced solution space are required. The projected high dimensional solutions from Experiment 2.1 is used here. The coordinates of these solutions in the reduced space created by the Proper Orthogonal Decomposition are

collected.

2. The input parameter values which led to the original high dimensional solution are collected. These serve as the independent variables which influence the dependent variables which are the coordinates in the reduced space.

3. Regression models are then created to build predictions of the reduced space coordinates based on input parameters. Different models will be tested including Response Surface Equations, Kriging (also known as Gaussian process regression), and various types of Artificial Neural Networks. The performance of these different models will be evaluated using metrics such as the error distribution, model fit error, and model prediction error.

If accurate surrogate models can be developed in this step, then the reduced space will successfully be mapped to the input parameters, and Hypothesis 2.2 will be accepted.

3.3.3 Summary of Research Area 2

Observations 1, 2, 3, 4, 5, and 6 from literature review led to the identification of the second gap, which states that current state-of-the-art tools and methods are unable to address the high-dimensional complexities of the noise quantification problem. This motivated the second research area and the high-level Research Question 2 which aimed to develop a computationally efficient process for the prediction of aviation noise metrics. This lead to two focused research tasks – the reduction of the dimensionality of the original high-dimensional data, and the creation of surrogate models in the lower-dimensional space.

With RQ2.1 it is shown how the high-dimensional can be handled and projected onto a lower-dimensional space with the use of a Model Order Reduction technique known as Proper Orthogonal Decomposition. With RQ2.2 it is shown how the coordinates of the high-dimensional data along the basis vectors can be predicted with surrogate models.

3.4 Overall Methodology

With the completion of the experiments, the overall methodology can now be constructed. The overall methodology represents a compilation of the methods, processes, and results obtained from executing the research plan. First, an Overarching Hypothesis is developed to answer the Motivating Research Question, and to satisfy the Research Objective.

Overarching Hypothesis

If a methodology is developed that

1. can efficiently represent real-world time-series flight trajectory data with a parametric definition obtained using an inverse map;
2. which is then used as an input to a field surrogate model developed using model order reduction;

then rapid quantification of noise metrics is enabled in a variety of scenarios, which facilitates parametric trade-off analyses and optimization efforts.

The Overarching Hypothesis is accepted if the requisite methodology can be developed. The developed methodology is developed in steps, with each step related to the research questions, hypotheses, and experiments. The verification of each hypothesis will lead contribute to the demonstration of the overall methodology and the acceptance of the Overarching Hypothesis.

Using the methods developed in the research plan, the overall methodology is formed as shown in Figure 3.4. The methodology is developed for two fundamental use-cases. The first use-case is for the quantification of real-world flights through the use of time-series trajectory data, and the second use-case is for many-query contexts such as optimization of noise metric footprints, parametric trade-off analyses etc.

The first research area is comprised of focused research questions which process

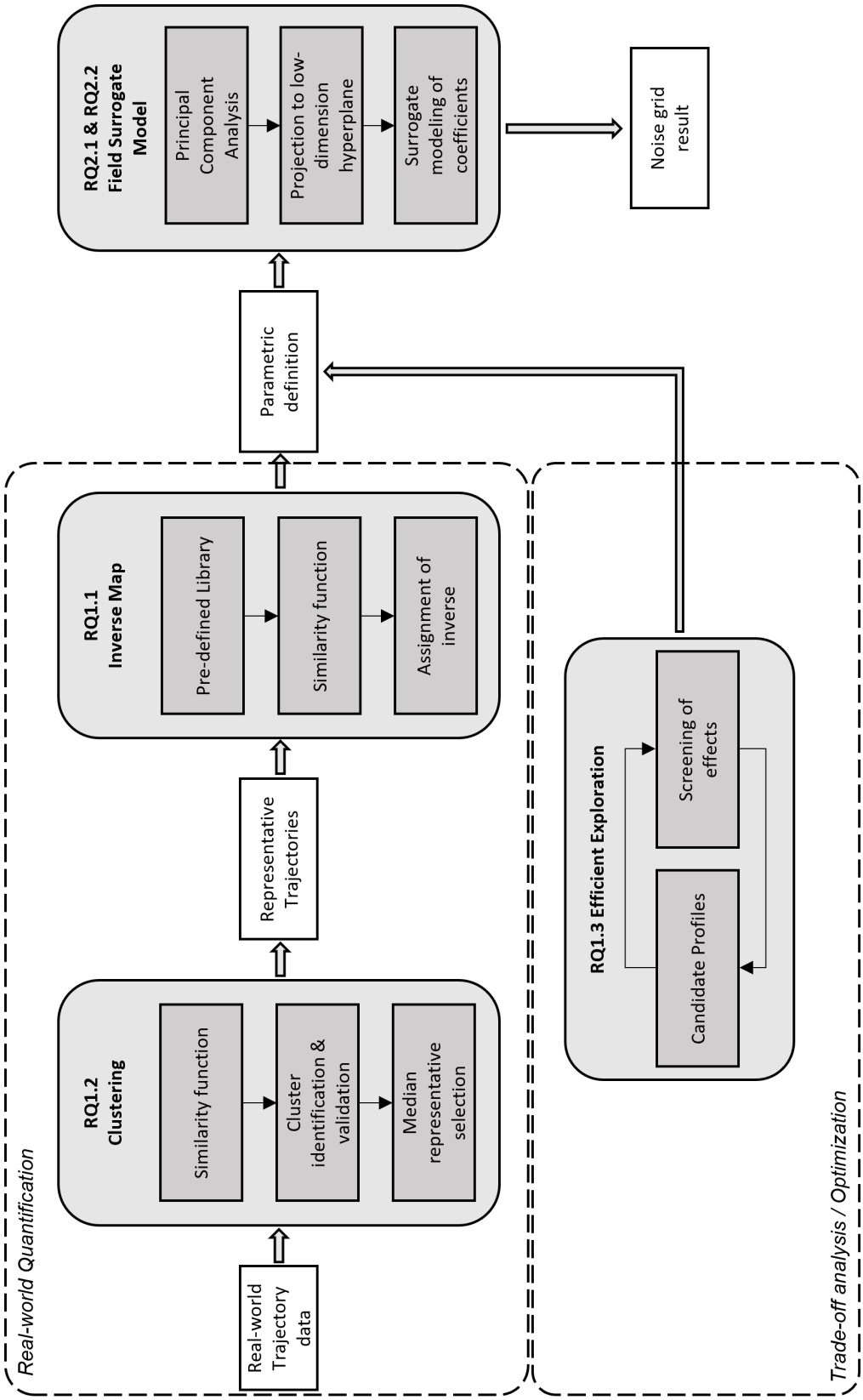

Figure 3.4: Overall Methodology

these two use-cases for parametric definitions of the aircraft trajectories and performance characteristics. RQ1.1 and RQ1.2 process real-world time-series data into parametric mappings. RQ1.3 provides guidance on how important each parameter is and how they should be varied. The second research area is comprised of focused research questions which take in parametric definitions (regardless of the use-case in which they originated) and rapidly model their noise impact. RQ2.1 and RQ2.2 together comprise of the field surrogate model which enables this rapid quantification of noise metrics.

The outcomes of the research plan are shown in chapter 4 and chapter 5. Details of the overall methodology are presented in chapter 6. Additionally, a practical case-study is also demonstrated using the developed methodology.

3.5 Test Problem Definition

The methods and processes proposed and developed in this Research Plan are fairly independent of specific use-cases, and can be easily adapted for a wide variety of scenarios. The overall methodology which is developed can be used both for rapid noise quantification of real-world flights, or for parametric trade-off analyses and optimization studies.

For the purposes of demonstration in each experiment, it is helpful to have practical examples and datasets. Therefore, suitable test cases must be identified which are appropriate to each experiment and facilitate the testing of the stated hypotheses.

3.5.1 Choice of Aircraft

The Boeing 737-800 is selected as the aircraft to be modeled for noise metrics, and for which real-world datasets are procured. The Boeing 737-800 is one of the most commonly used aircraft both within the US and globally. Data from the T-100 Segment database of the Bureau of Transportation Statistics for July 2018 is shown in Table 3.2 and shows that the Boeing 737-800 was used to perform more than 10% of all operations in the US [223, 224].

Table 3.2: Analysis of operational frequency of aircraft types in the US for July 2018 [223, 224]

Aircraft Name	Aircraft Category	Departures Scheduled		Departures Performed	
		Number	Percentage	Number	Percentage
Boeing 737 -700/700LR/Max 7	Narrow-body Jet	103323	10.53%	103954	10.59%
Boeing 737-800	Narrow-body Jet	94493	9.63%	101160	10.31%
Embraer ERJ-175	Regional Jet	66488	6.78%	68849	7.02%
Airbus Industrie A320-100/200	Narrow-body Jet	62802	6.40%	66996	6.83%
Canadair RJ -200ER /RJ-440	Regional Jet	55375	5.64%	55571	5.66%

There are two key advantages of choosing this frequently operated aircraft. Firstly, there is a larger quantity of real-world flight data available which can be analyzed. Secondly, the results obtained have more impact as they are relevant for a larger share of the total flight operations.

3.5.2 Choice of Operation

In this dissertation, the focus is on departure operations and not on arrival operations. One of the primary reasons for this is that arrival operations are usually much more constrained in their trajectory, especially at low altitudes, where all aircraft converge onto a typical 3° glideslope. Thus, there is little scope for parametric variation of the aircraft trajectory and its analysis. Parametric variations on the level-off height and distance have been performed in literature [147] and show that although variations in aviation noise results are observed, the changes are typically limited to very low SEL dB values, which are not always significant. Additionally, the contribution of airframe noise is especially important for arrivals, due to the range of configurations used and low thrust values [225]. Such effects cannot always be accurately modeled in current noise modeling tools.

Thus to observe the variability in aircraft trajectories and to develop useful parametric definitions, it is helpful to focus solely on departure operations. With suitable modifications, the methodology developed can certainly be adapted for arrival operations as well.

3.5.3 Choice of Noise metric

There are several possible noise metrics which can be modeled. Here, the Sound Exposure Level (SEL) is chosen for modeling. The SEL is an energy averaged metric which represents the A-weighted sound level over a duration of time by representing the total noise energy with a 1 second reference duration.

The most commonly used metric for community noise exposure is the Day-Night averaged Level (DNL). However, DNL is appropriate for use when a large number of operations are being modeled. For single events such as individual operations, which are being modeled in this dissertation, the SEL metric is appropriate. The DNL can be computed by aggregating SEL metrics if the time of the operation is known.

3.6 Chapter Summary

Starting with the original Motivating Research Question and the Research Objective, this chapter decomposed the problem into two high-level areas – parametric representations of real-world flight data, and rapid noise modeling. Within these research areas, three and two low level Research Questions were posed respectively. To answer these Research Questions, formal Hypotheses were stated. Finally, a formulation for each Hypothesis was created in order to test them.

The results from the formulated experiments in shown in chapter 4 and chapter 5. With the results from these experiments, the stated Hypothesis are accepted and satisfactorily answer their associated Research Questions. With the help of the developed techniques, both identified gaps are closed and the overall methodology is constructed. This overall methodology is the answer to the original Motivating Research Question and fulfils the

Research Objective.

CHAPTER 4

PARAMETRIC REPRESENTATION OF AIRCRAFT TRAJECTORIES

This chapter presents the research and findings from Research Area 1, i.e. the parametric representation of aircraft trajectories. As a quick recap, the high-level Research Question for this is mentioned below.

Research Question 1
How can the input space of aircraft trajectories be represented to enable parametric quantification and optimization?

This high-level Research Question led to three key requirements – representation, scalability, and exploration; which were addressed with three specific Research Questions and their associated Hypotheses. Each Hypothesis was then supplemented with a formulation to test the Hypothesis. This chapter will present the results of the Experiments which support each Hypothesis.

This chapter begins with section 4.1 which describes the real world dataset being used in Experiments 1.1 and 1.2. Following this, section 4.2, section 4.3, and section 4.4 provide the details of the experimental setup, obtained results, and analysis of the results. Finally section 4.5 provides a summary of the chapter.

4.1 Description of real-world dataset

The real-world aircraft trajectory and performance data used in this chapter is obtained from 'The OpenSky Network' which is a non-profit association based in Switzerland [226, 227]. Their goal is to provide open access to real-world air traffic data for research into the reliability, security, and efficiency of the air space usage. The intended target audience for

this dataset are university-affiliated researchers, governmental organizations, or aviation authorities. Data is available for download with SQL-like query interface and a public API. Python and MATLAB interfacing scripts are also available for data access and download.

The root source for all data hosted by OpenSky is the Automatic Dependent Surveillance-Broadcast (ADS-B). The ADS-B allows aircraft to broadcast their position and velocity information periodically. OpenSky operates a wide network of ADS-B receivers around the world and harvests the data which is then uploaded to their servers.

While there are several datasets which are available for download, the most comprehensive data tables combine most parameters into a single table and are called 'state vectors'. There is one state vector row per second in the table, representing a 1 Hz sampling frequency. A description of relevant parameters is mentioned in Table 4.1. A comprehensive list containing descriptions of all parameters is available on the OpenSky website [226].

4.1.1 Data pre-processing

It is important to note that while the OpenSky dataset is very useful, it is not a perfect dataset (as is the case with many real-world datasets which rely on sensor information). Therefore, before proceeding with any modeling, it is necessary to process the data to make it suitable for specific applications and also to clean the data to remove any 'erroneous' data points.

For the purposes of this study, a one-year timeframe was selected. Data pertaining to all airlines operating the Boeing 737-800 aircraft type at the San Francisco International Airport (KSFO) for the year 2019 (pre-pandemic) was selected for analysis. This dataset contained a total of 5070 flights operated by 10 airlines.

Due to the nature of this type of dataset, crucial information about the aircraft weight and thrust was missing. To mitigate this, the flight's great-circle-distance was computed using the origin-destination pair information. Given this information, the aircraft were

Table 4.1: List of important parameters included in the OpenSky dataset [226]

Group	Parameter	Unit	Description
Time	Time	seconds	Unix time, also known as POSIX or epoch time representing number of seconds elapsed since 00:00:00 UTC on 1 January 1970
IDs	ICAO transponder ID	6 digit hexadecimal string	24-bit ICAO transponder ID which can be used to track specific airframes over different flights
	Callsign	Alphanumeric string	Usually the airline and flight number
	Squawk code	4 digit octal number	Identification code used by ATC
Position	Latitude	degree	Last known latitude as decimal WGS84 coordinate
	Longitude	degree	Last known longitude as decimal WGS84 coordinate
	Barometer altitude	meters	Altitude measured by barometer, depends on weather
	Geometric altitude	meters	Altitude measured by GNSS/GPS sensor
Trajectory	Groundspeed	meters per second	Speed over ground
	Track angle	degree	Clockwise from geographic North
	Verticalspeed	meters per second	Climb/Descent rate of the aircraft

classified into different 'stage lengths', which is a commonly used proxy for aircraft weight in environmental analysis. This classification for trips up to 4500 nmi is shown in Table 4.2. The data was then further partitioned into sets representing a particular airline and stage combination as shown in Table 4.3. Not all combinations had flights associated with them.

Finally, the dataset was analyzed to remove anomalous flights. First, flights which did not cross 10,000 ft AFE within the first 25 nmi of ground track were removed. Next, flights which took more than 2 nmi of ground track distance for take-off ground roll were removed, which is the maximum runway length at SFO airport. With this, a total of 117 flights were

Table 4.2: Stage Length definition as a function of trip length

Stage Length	Trip Length, nmi	Representative Range, nmi
1	0–500	250
2	500–1000	850
3	1000–1500	1350
4	1500–2500	2200
5	2500–3500	3200
6	3500–4500	4200

Table 4.3: Grouping of real-world dataset by airline and stage length

	SL1	SL2	SL3	SL4	Total
Airline 1	999	442	302	**1361**	3104
Airline 2	83	0	117	345	545
Airline 3	78	126	54	74	332
Airline 4	39	51	0	193	283
Airline 5	163	51	0	0	214
Others			592		

identified as anomalous and were removed. Finally, all flights were re-sampled so that each row was exactly 0.167 nmi apart in cumulative ground track distance.

At the end of the data partitioning and cleaning, the most populous group of Airline 1 and SL4 containing 1361 flights was retained for further analysis. Each flight was then given a serialized label starting with "Flight 1" and ending with "Flight 1361". A small subset of randomly selected 30 flights from this dataset is visualized in Figure 4.1.

4.2 Experiment 1.1

In this section, the experimental setup and results for RQ1.1 are explained. For reference, RQ1.1 and H1.1 are repeated below –

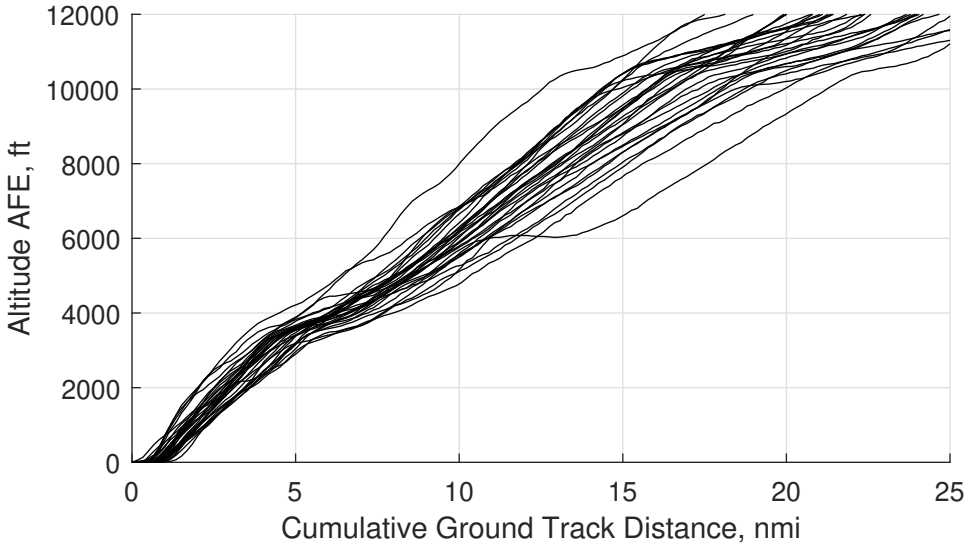

Figure 4.1: Visualization of real-world flight data for a small subset of flights

Research Question 1.1

How can aircraft trajectories and performance characteristics be represented parametrically?

Hypothesis 1.1

If an inverse mapping of aircraft trajectory and performance calculations can be identified, then aircraft trajectories can be represented parametrically.

The purpose of this experiment is to demonstrate that real-world flight data can be mapped onto a parametric definition. As noted previously, the procedural profile definitions as shown in Table 3.1 present a way to generate parametric profiles. Four parameters were identified in an attempt to reproduce the variation in real-world flights as well as possible. These parameters are explained below –

1. Takeoff weight – The takeoff weight of the aircraft of the aircraft represent a key variation observed in real-world operations, resulting from variations in both fuel weight (depends on the trip distance) and the payload weight (depends on the load

factor). Given that the chosen real-world dataset corresponds to stage length 4, the chosen parameter values here are the weights which correspond to stage length 3, 4, and 5 in AEDT.

2. Takeoff thrust reduction – Generally speaking, pilots do not always employ the maximum take-off thrust available. The choice of take-off thrust is a result of a multitude of factors such as runway length, weather conditions, weight of the aircraft etc. If safe to do so, pilots may elect to 'derate' the takeoff thrust in order to reduce engine maintenance [228]. Here, all four thrust derate options allowed in AEDT are included.

3. Altitude for acceleration initiation – This is the altitude at which the aircraft begins to pitch over and accelerate beyond its original lift-off speed. The minimum altitude for this is 800 ft as required by the FAA [141], though airlines may choose to delay it further. Here, five levels are used for this parameter ranging from 800 ft AFE to 1600 ft AFE in increments of 200 ft.

4. Energy share for acceleration – This parameter dictates how the aircraft allocates excess energy between climbing and accelerating. Given the maximum available acceleration G_m as a fraction of g (acceleration due to gravity), and A_p (the percent of thrust applied to acceleration), the climb gradient G can be found as –

$$G = G_m \left(1 - \frac{A_p}{100}\right) \tag{4.1}$$

This parameter is varied between 20%, 40%, 60%, and 80%. The extremity values are not used as 0% would indicate no acceleration, and 100% would indicate the aircraft leveling off to accelerate, which does not occur in commercial aviation.

The range of variation and parameter values identified for modeling are summarized in Table 4.4. There a total of $3 \times 4 \times 5 \times 4 = 240$ total possible combinations of these

parameters, which were all created as tabular profile definitions. These were then imported into AEDT and were modeled to obtain their performance outputs.

Table 4.4: Identified parameters and their ranges of variation

Parameter	Description	Possible values	Units
α_1	Takeoff weight (through Stage Length)	151100 (SL3), 162150 (SL4), 169950 (SL5)	lb_m
α_2	Takeoff thrust reduction	1.00, 0.95, 0.90, 0.85	multiplier
α_3	Altitude for acceleration	800, 1000, 1200, 1400, 1600	ft
α_4	Energy share percentages	20, 40, 60, 80	%

4.2.1 Flights modeled in AEDT

Once the real-world flights from OpenSky had been identified, a complementary dataset was required to build the inverse model. This dataset comes by modeling procedures created by using different combinations of the identified parameters. A total of 240 procedural profiles were created and modeled in the Aviation Environmental Design Tool. To be consistent with the real-world data, these operations were modeled at the SFO airport in AEDT, with take-off on runway 01R over the bay, which is consistent with SFO operations. The averaged airport weather definition in AEDT for this airport was used. The complete set of trajectories is shown in Figure 4.2. It is observed that a rich variety of trajectories were captured by the chosen parametric definition and the ranges on those parameters.

Once the results from AEDT were obtained, they had to be re-sampled so that the cumulative ground track distance points were consistent with the OpenSky real-world data. The process of resampling consists of simple 1-D interpolation to the two nearest points on either side of the sampled point. This method contructs piecewise linear functions for the interpolation. Any required value p_j at new sampling point x_j can be found using the

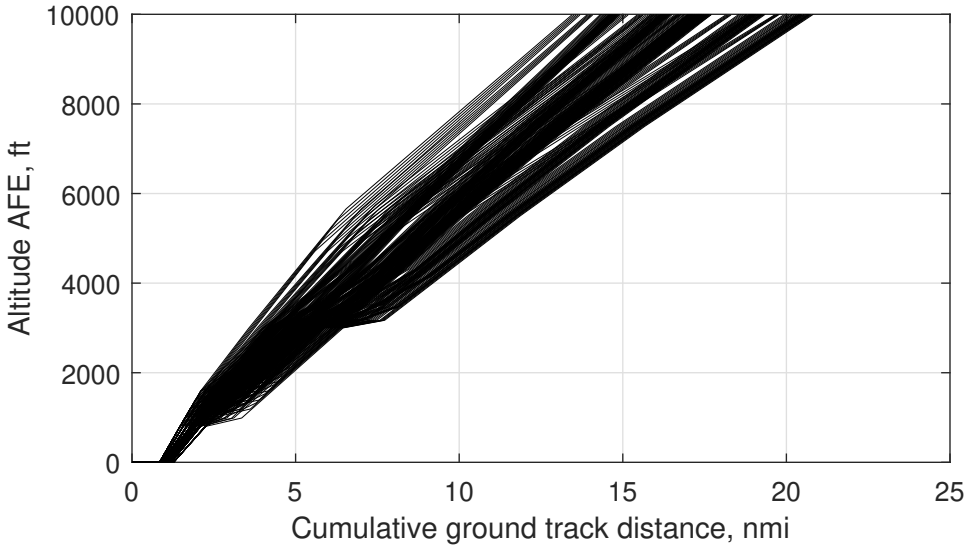

Figure 4.2: Visualization of all 240 trajectories obtained from AEDT

values p_i, p_{i+1} at points x_i, x_{i+1} if $x_i < x_j < x_{i+1}$ using the following formula –

$$y_j = y_i \left(\frac{x_{i+1} - x_j}{x_{i+1} - x_i} \right) + y_{i+1} \left(\frac{x_j - x_i}{x_{i+1} - x_i} \right) \tag{4.2}$$

The process of resampling is visualized in Figure 4.3. For better clarity, only the first 3 nmi of ground track is shown. It is evident that the linear interpolation works well to convert the data onto a consistent sampling basis, while ensuring that the 'shape' of the original data is retained.

4.2.2 Development of the similarity function

With the sampling basis of the real-world flight data and AEDT output performance data made consistent, the similarity function between two flights can be evaluated. Each real-world flight is compared to each of the 240 flights modeled in AEDT. The comparison is made by computing the 'trajectory score' of the two flights. The process of comparing the trajectory scores between two real world flights is detailed below –

1. Obtain the vectors for cumulative ground track distance g_{RW}, g_{AEDT} for the real-world flight and the AEDT modeled flight respectively. Also obtain their correspond-

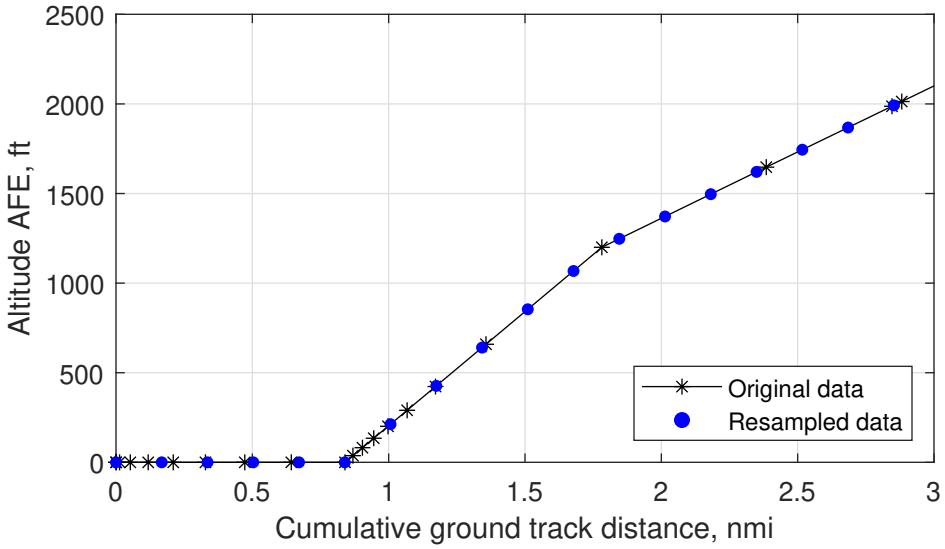

Figure 4.3: Visualization of the resampling process

ing altitude vectors h_{RW}, h_{AEDT}. Note that while the ground track distance vectors have the same resolution, they are not necessarily of the same length.

2. Identify the smaller dataset. The trajectory score is computed between the two flights up to the length of the smaller dataset L.

$$L = \min\{length\left(g_{RW}\right), length\left(g_{AEDT}\right)\} \tag{4.3}$$

3. The trajectory score t is then computed by taking the differences in altitude, and aggregating the differences into a single number with the Root Mean Square formula.

$$t = \sqrt{\frac{1}{L}\sum_{i=1}^{L}\left(h_{RW,i} - h_{AEDT,i}\right)^2} \tag{4.4}$$

Figure 4.4 shows a zoomed-in plot for this process over the first 3 nmi. The trajectory score is the Root Mean Square value of the lengths of all red line segments. This process is then repeated for all 1361 real-world flights, with comparisons to all 240 operations and is stored in a matrix $T_{1361\times240}$, with element $t_{i,j}$ representing the trajectory score between

real-world flight i and AEDT modeled flight j.

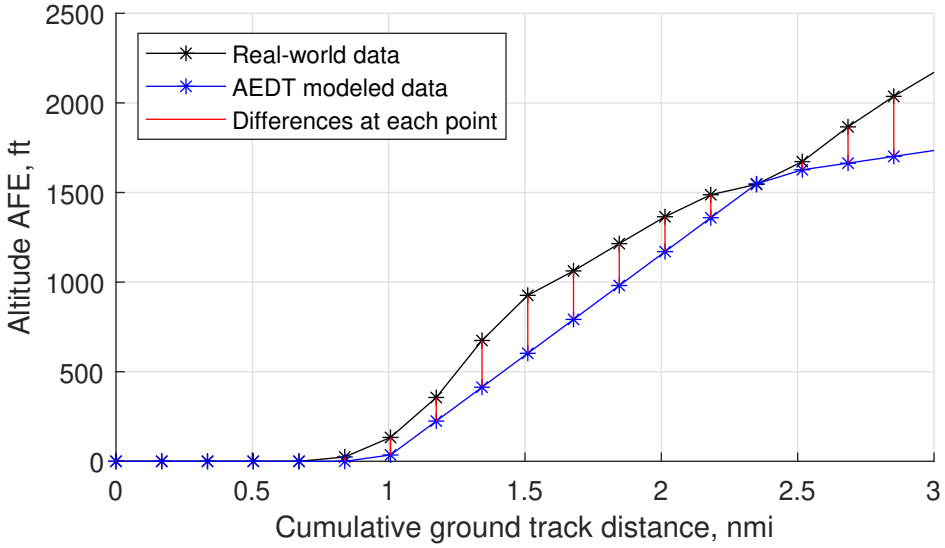

Figure 4.4: Sample calculation of the trajectory score between a real-world flight and AEDT modeled flight

4.2.3 Generating the inverse map

With the trajectory score matrix T computed, the inverse map assignments can be made. A row of matrix T represents the score of a real-world flight when compared against all AEDT modeled flights. To find the AEDT modeled flight which best represents the real-world flight, the trajectory score should be minimized for each row. In other words, AEDT modeled flight j is the best representation of real-world flight i, if the following holds true –

$$j = \arg\min \{t_{i,j} \mid i = 1, 2, \ldots, 240\} \tag{4.5}$$

With the best representation found, the assignment of the inverse map is trivial. The parameter values which resulted in the closest matching trajectory from AEDT are assigned to the real-world operation. With this assignment, the construction of the inverse map is complete.

4.2.4 Results

With the inverse map complete, each real-world flight is assigned to a parametric definition. However, there has not yet been any measure defined to check the 'goodness' of this assignment. After all, the process by itself only guarantees that each flight will be assigned to a parametric definition. It does not necessarily guarantee that the assignment will be reasonable. To assess this reasonability, the following error metric is proposed –

$$e_{invmap} = \sqrt{\frac{1}{L}\sum_{i=1}^{L}\left(\frac{h_{RW,i} - h_{AEDT,i}}{\frac{h_{RW,i}+h_{AEDT,i}}{2}}\right)^2} \tag{4.6}$$

This error definition is helpful in a few key ways. It is non-dimensional, so the error can be expressed in terms of percentages. Additionally, it is closely related to the trajectory score definition. A low trajectory score implies a good match between the two flights, and thus a lower error. Finally, due to the normalization by vector length, the error is independent of the amount of data points in each flight comparison, which can vary significantly.

One potential drawback of this error computation is for points when both flights are on the ground, where the operation can become indeterminate due to a division by zero attempt. Similarly, when the aircraft is close to the ground, the denominator is quite small which can cause the error to be artificially large. Hence, the error formulation needs to be updated to exclude such points. Let k be the first point where both flights have crossed 500 ft altitude. Then, the error computation can be modified as –

$$k = \min i \quad \text{such that} \quad h_{RW,i}, h_{AEDT,i} > 500 \tag{4.7}$$

$$e_{invmap} = \sqrt{\frac{1}{L}\sum_{i=k}^{L}\left(\frac{h_{RW,i} - h_{AEDT,i}}{\frac{h_{RW,i}+h_{AEDT,i}}{2}}\right)^2} \tag{4.8}$$

The error metric is computed for each real-world flight, and is shown in Figure 4.5a,

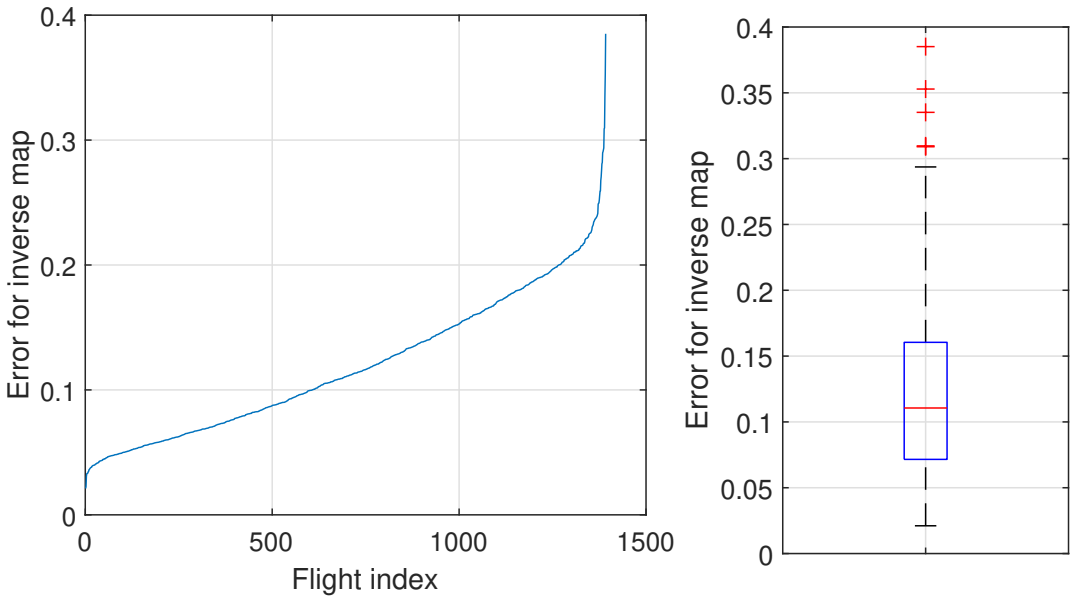

(a) Error in ascending order

(b) Error boxplot

Figure 4.5: Error involved in the inverse map

when sorted from the flight with the least error to the most error. The accompanying boxplot in Figure 4.5b shows the distribution of this error metric. It is observed that for most flights, the mapping resulted in an error of between 2% and 22%. While this may seem large, it is important to note the context in which these errors appear. Real-world flights with time series data have numerous deviations from the ideally modeled theoretical procedural profiles in AEDT. Nevertheless, in most cases, the parametric definitions do a good enough job of approximating the real-world flight, which can be seen in the visualizations in the following subsections.

Flights with least mapping error

The best six mappings obtained with the least error are discussed in this section. Figure 4.6 shows the visualization of these six flights and their respective mapped AEDT modeled flight. Their respective mappings to parametric definitions, trajectory scores, and errors are tabulated in Table 4.5.

With visual observation, it is evident that the AEDT modeled flights have accurately

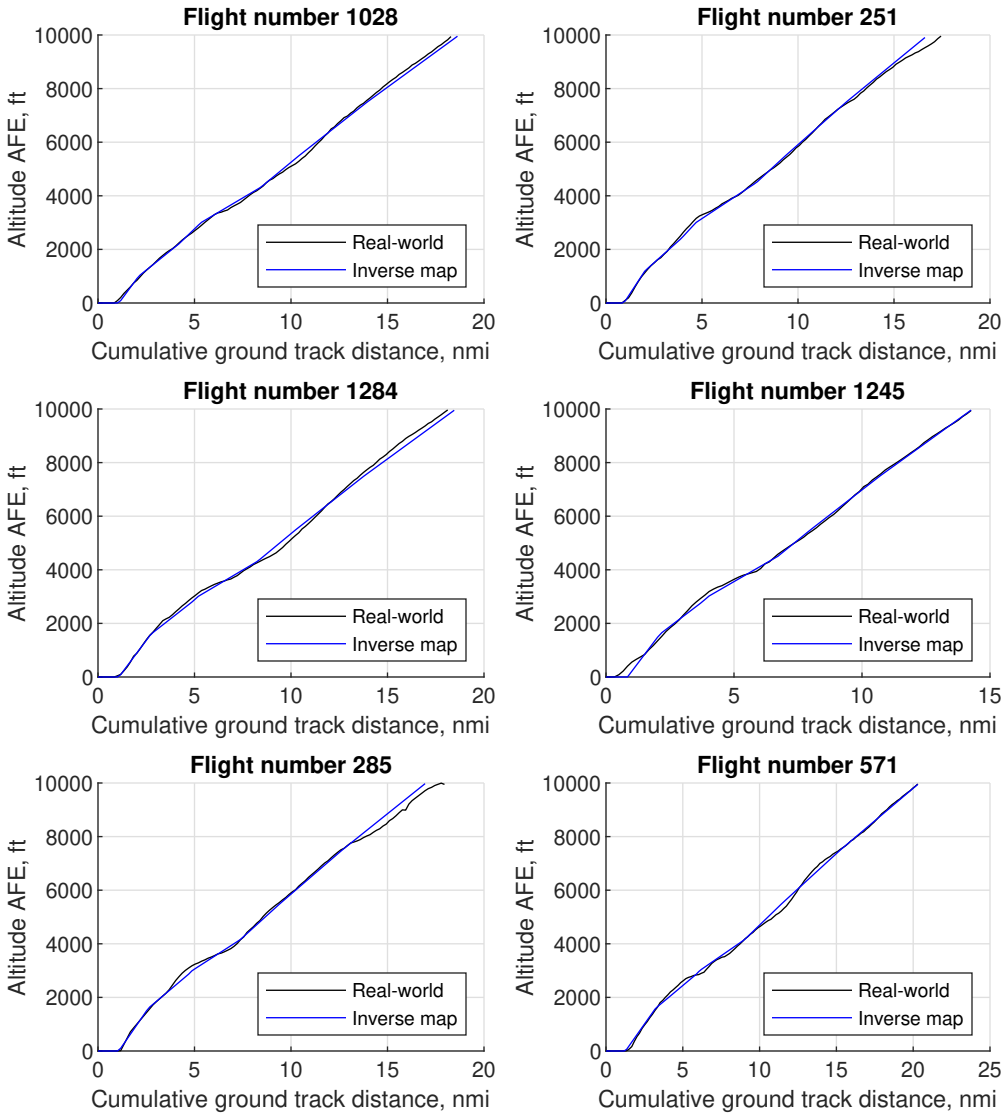

Figure 4.6: Top six flights with the best mappings

represented the real-world trajectories. With the exception of Flight 1245, all flights were also able to accurately recreate the lift-off point for each flight. For a majority of the distance, the two trajectories are co-incident, which is consistent with the low trajectory scores and error values associated with them. The parametric mappings shown in Table 4.5 also show good variation in takeoff weight, and takeoff thrust reduction, indicating that many different operating conditions could be inverse mapped successfully. The constant Energy Share percentage of 40% is reflective of that fact that most pilots tend to split excess energy evenly between acceleration and climb.

Table 4.5: Inverse mapping of best six flights to parameters

Real-world data	Inverse map				Mapping scores	
Flight #	Takeoff Weight, lb_m	Takeoff thrust reduction, multiplier	Altitude for acceleration, ft	Energy Share, %	Trajectory Score, ft	Error, %
1028	162150	0.90	1000	40	98.15	2.109%
251	151100	0.90	1200	40	106.36	2.278%
1284	162150	0.90	1600	40	145.53	3.082%
1245	151100	1.00	1600	40	99.47	3.293%
285	169950	1.00	1600	40	150.93	3.314%
571	169950	0.85	1600	40	103.64	3.318%

It is noted here that for these mappings which are quite accurate, the quantified trajectory scores range from about 100 ft to 150 ft. This indicates that on average over the complete departure up to 10,000 ft AFE, the two flights were about 100 ft to 150 ft apart vertically. Correspondingly, the error metric ranges from about 2.1% to 3.3%.

Flights with median mapping error

The median six mappings obtained with error values around the median are discussed in this section. Figure 4.7 shows the visualization of these six flights and their respective mapped AEDT modeled flight. Their respective mappings to parametric definitions, trajectory scores, and errors are tabulated in Table 4.6.

With this set of flights, larger differences in the AEDT modeled flights and the real-world trajectory represented by them can be observed. With the exception of Flight 369, all comparisons seem to show at least one cross-over point, where the trajectory which was previously higher dips below the other trajectory. Additionally, with the exception of Flight 369, differences in the liftoff point can also be observed. In fact, the real-world data for Flight 645 shows no take-off ground roll, which indicates an incomplete dataset for that

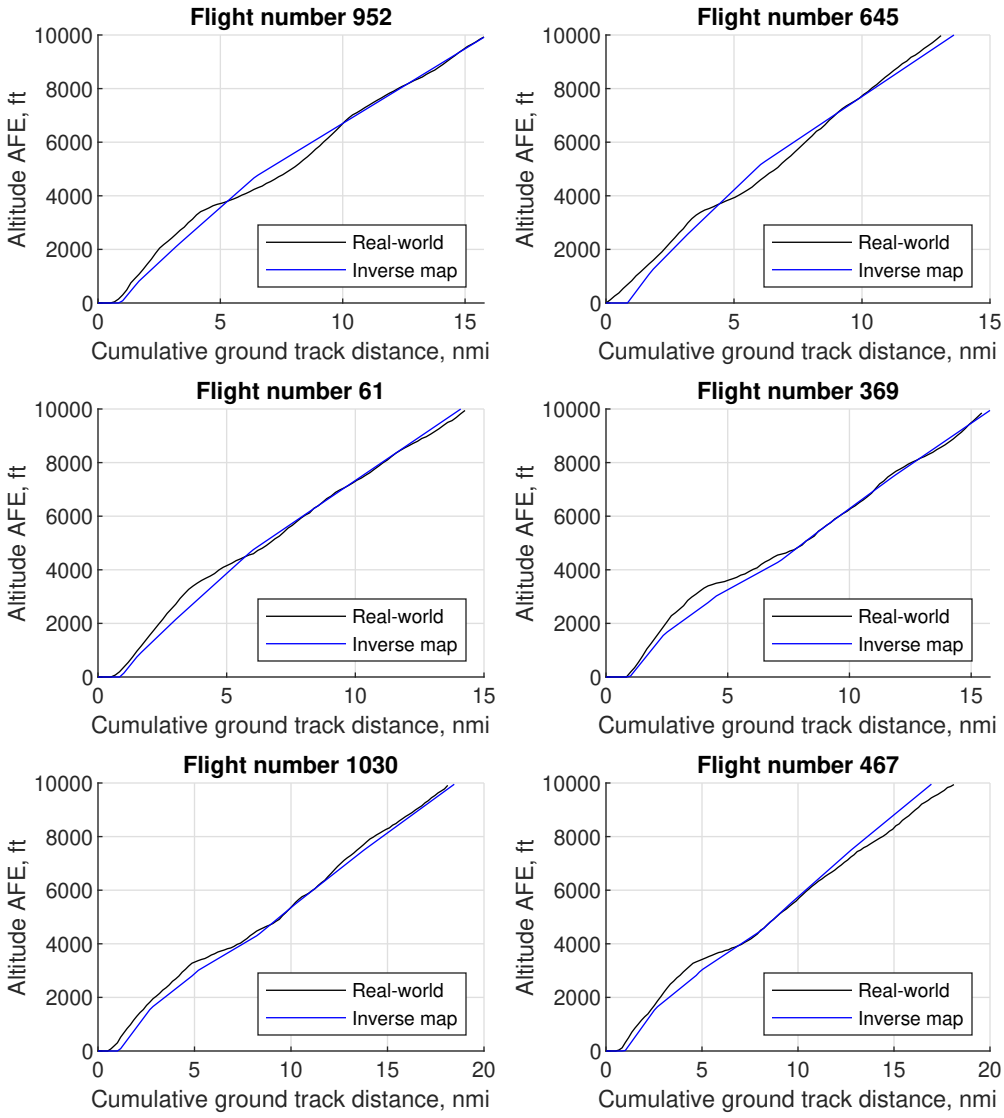

Figure 4.7: Median six flights with their respective mappings

flight. Differences in the liftoff point have a significant influence on the trajectory scores and error as they case the entire trajectory to be laterally shifted. The parametric mappings shown similarly show good variation in the takeoff weight, takeoff thrust reduction, and altitude for acceleration initiation.

For these set of flights representing the median error among the entire real-world dataset, the trajectory scores range from about 220 ft to 320 ft. This indicates that on average over the complete departure up to 10,000 ft AFE, the two trajectories were about 220 ft to 330 ft apart vertically. Correspondingly, the error metric is about 11%.

Table 4.6: Inverse mapping of median six flights to parameters

Real-world data	Inverse map				Mapping scores	
Flight #	Takeoff Weight, lb_m	Takeoff thrust reduction, multiplier	Altitude for acceleration, ft	Energy Share, %	Trajectory Score, ft	Error, %
952	151100	0.90	800	20	302.62	11.004%
645	151100	1.00	1200	20	313.91	11.026%
61	151100	0.95	800	20	264.89	11.049%
369	162150	1.00	1600	40	258.78	11.050%
1030	162150	0.90	1600	40	223.48	11.056%
467	151100	0.85	1600	40	306.13	11.059%

Flights with significant error

The worst six mappings obtained with the highest error are discussed in this section. Figure 4.8 shows the visualization of these six flights and their respective mapped AEDT modeled flight. As the inverse function did not do a good job of mapping the real-world trajectories to parametric definitions, the table outlining their parametric definition is not included. The trajectory scores, and errors are tabulated in Table 4.7.

Table 4.7: Inverse mapping of worst six flights

Real-world data	Mapping scores	
Flight #	Trajectory Score, ft	Error, %
432	1042.53	29.370%
1250	1025.24	30.903%
73	1242.96	30.970%
949	1429.66	33.517%
430	1541.48	35.287%
1099	1837.52	38.510%

It is quite evident visually that no flight among the 240 modeled in AEDT using

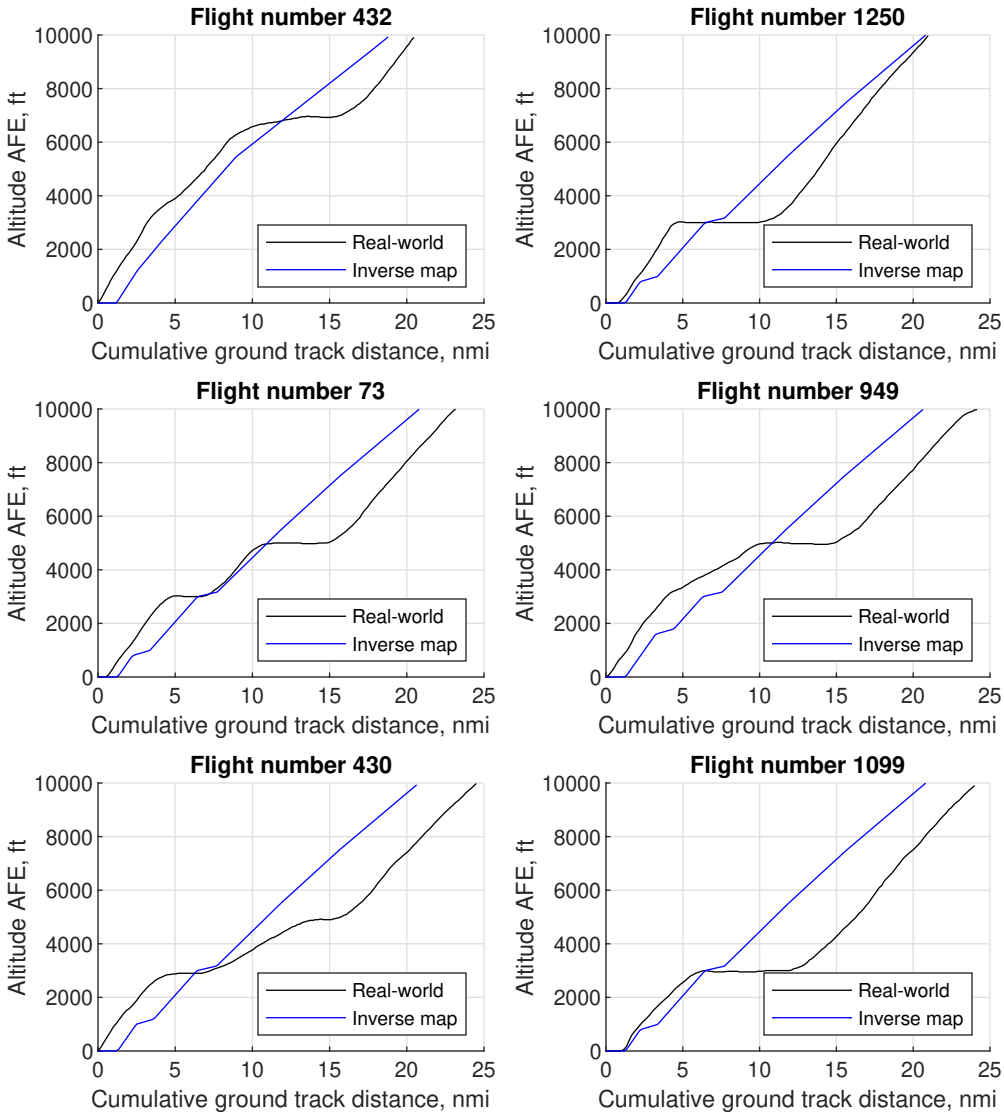

Figure 4.8: Bottom six flights with the worst mappings

parametric definitions could accurately represent any of these real-world flights. Most of these flights do not follow a 'nominal' trajectory which would be expected from a departure operation. For starters, three of the six flights (Flight 432, Flight 949, and Flight 430) did not have any takeoff ground roll data. Additionally, all six flights show at least one phase of flight where the altitude is held constant, with Flight 73 and Flight 949 showing two such level-off segments. While common for arrival operations, such level-off segments are highly unusual for departures. As these flights are outliers in the real-world dataset, there is little hope of the inverse map providing an accurate parametric definition for them. In

fact, the procedural profile definition used in AEDT does not allow for level-off steps to be defined for departure operations.

Unsurprisingly, the trajectory scores for these flights are quite high, ranging from about 1000 ft to 1800 ft. Correspondingly, the errors are quite high as well, ranging from about 29% to 39%.

To gain further insight into the inability of the inverse map function to create accurate parametric definitions for these flights, Flight 1099 is visually compared to all 240 AEDT modeled flights in Figure 4.9. It can be seen from the plot that due to the almost 6 nmi long level-off segment, the flight trajectory was shifted considerably out of the range which could be modeled in AEDT. This shift explains the poor inverse map performance and the large error for this flight and for the other outliers.

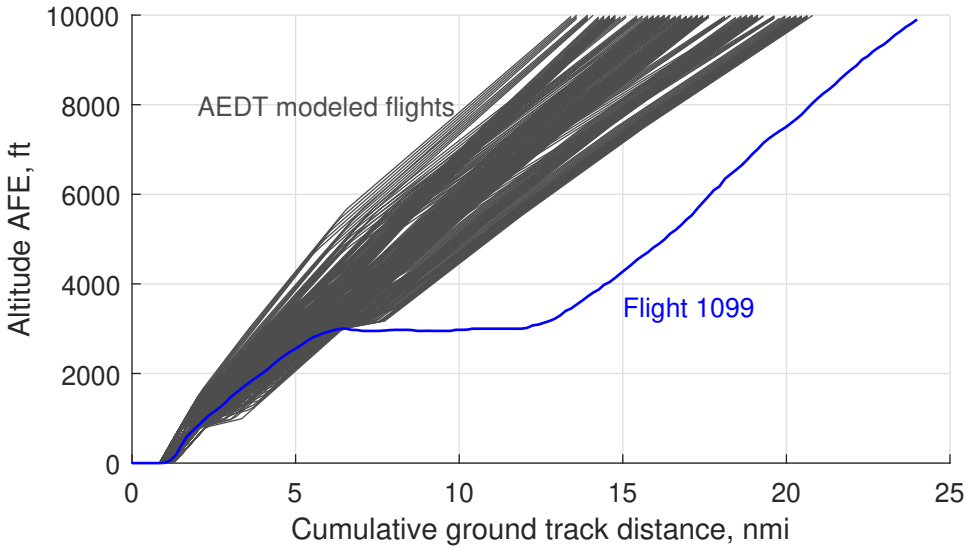

Figure 4.9: Comparison of outlier flight to AEDT modeled flights

4.2.5 Summary and evaluation of Hypothesis

The first experiment was designed to create an inverse mapping of real-world trajectory time-series data on to parametric definitions. The real-world data was obtained from OpenSky and processed to include 1361 flights departing out of San Francisco with a trip distance of 1500 to 2500 nmi (stage length 4). The complementary set to these flights was

created in AEDT by making use of the procedural profile definition. Four parameters were identified and varied between suitable values for a total 240 possible combinations. Each flight was modeled in AEDT at the SFO airport and the resulting performance report was exported.

The real-world flights were then compared to each AEDT modeled flight and a trajectory score was computed. Each pair of real-world and AEDT flight was assigned a trajectory score, with a lower score indicating more similarity between the flights. Each real-world flight was then mapped onto that AEDT modeled flight which minimized the trajectory score, and by extension to the underlying parametric definition.

To verify the 'goodness' of these mappings, an error metric was defined and computed. Several flights and their assigned mapping were analyzed for different values of the error. While most flights could be reasonably mapped onto a parametric definition, some flights showed large errors. The cause of these large errors was identified and the flights were found to have level-off segments, which made them outliers.

There are some potential avenues to further improve the mapping. The first area of improvement should be the correct identification of the lift-off point along the cumulative ground track distance. With the lift-off point correctly identified, the trajectories can be aligned to start at the same origin. This improves the validity of the trajectory score being computed. Additionally, a larger library of profiles can potentially lead to more accurate mappings as there are more options available for comparison.

For the purposes of RQ1.1, however, these potential improvements are considered out of scope and are recommended for future work. Revisiting Hypothesis 1.1, the primary requirement was the identification of an inverse map of aircraft trajectory and performance calculations. With the designed experiment, it was shown how such an inverse map can be constructed and deployed on real-world data. Therefore, Experiment 1.1 is considered successful and Hypothesis 1.1 is accepted.

4.3 Experiment 1.2

In this section, the experimental setup and results for RQ1.2 are explained[1]. For reference, RQ1.2 ans H1.2 are repeated below –

Research Question 1.2

How can real-world aircraft trajectories be efficiently mapped to a parametric definition?

Hypothesis 1.2

If real-world aircraft trajectories are clustered into groups, then multiple trajectories within a group can linked to a single parametric definition using the inverse map of the cluster representative.

During the research formulation stage, it was previously noted that the technique developed in RQ1.1 may not necessarily be feasible to directly use on large sets of data. Indeed, while the method worked well on datasets up to about 1000 flights, scaling it up further would be challenging. Additionally, the process of modeling all inverse mapped flights uniquely for aviation noise metrics may not be useful, as the desire is to retain high-level variability, and not the small perturbations between otherwise similar trajectories. In Experiment 1.1, it was observed that the inverse-mapping is a many-to-one mapping,

[1] Parts of the research described in this section are documented in the following publications –

- A. Behere, L. Isakson, T. G. Puranik, Y. Li, M. Kirby, and D. Mavris, "Aircraft landing and takeoff operations clustering for efficient environmental impact assessment," in *AIAA AVIATION 2020 FORUM*, Jun. 2020. DOI: 10.2514/6.2020-2583. eprint: https://arc.aiaa.org/doi/pdf/10.2514/6.2020-2583. [Online]. Available: https://arc.aiaa.org/doi/abs/10.2514/6.2020-2583 [229]
- A. Behere, J. Bhanpato, T. G. Puranik, M. Kirby, and D. N. Mavris, "Data-driven approach to environmental impact assessment of real-world operations," in *AIAA Scitech 2021 Forum*, Jan. 2021. DOI: 10.2514/6.2021-0008. eprint: https://arc.aiaa.org/doi/pdf/10.2514/6.2021-0008. [Online]. Available: https://arc.aiaa.org/doi/abs/10.2514/6.2021-0008 [230]

with many real-world flights being mapped onto the same parametric definition. These observations from Experiment 1.1 further reinforce the motivation behind RQ1.2.

The purpose of Experiment 1.2 is to demonstrate that instead of mapping each real-world trajectory onto a parametric definition, it is computationally efficient to first group the real-world flights and then map a single representative of each group onto its corresponding parametric definition. Then, instead of modeling the noise metrics for a large number of real-world flights, only a handful need to be modeled and the resultant noise metrics can be scaled up accordingly.

4.3.1 Clustering algorithms & validation measures

Clustering is an unsupervised Machine Learning technique that can be utilized to identify hidden trends and patterns within datasets. In order to cluster the dataset such that objects within a cluster are similar to each other and dissimilar to objects in other datasets, the similarities among objects must be identified. Being an unsupervised ML technique, clustering does not require any prior knowledge of grouping inherent within the dataset. Therefore, the application of clustering algorithms to flight trajectory data is relatively straightforward regardless of whether underlying similarities are known a-priori.

The underlying differences in flight operations can be the result of many factors, not all of which are recorded within the dataset. Some examples are the ambient weather, load factor and weight of the aircraft, piloting actions, air traffic constraints, and so on. The idea behind clustering is that with the correct choice of features and the correct similarity metric based on those features, similar objects can be successfully grouped.

Various algorithms for clustering exist in literature, with different formulations and use-cases. It is therefore important to evaluate and compare these algorithms before selecting the appropriate one for this use-case. There were three clustering algorithms which were considered –

1. K-Means Clustering [231, 232]: The K-Means algorithm is a method that aims to

partition objects into a pre-determined number of clusters. It is an iterative algorithm in which each object can be thought of a point in some "space" of data. Starting with a random selection of points as clusters, more points are added based on their proximity to the currently selected cluster centroids. This proximity (and cluster centroids) can be evaluated using different distance functions, such as Euclidean distance. In each iteration, the newly added points shift the centroid of each cluster. The iteration ends when all points have been assigned to a cluster and the cluster definitions are stable.

The K-Means algorithm is easy to understand and to implement. However, there are certain drawbacks to this algorithm. Firstly, the number of clusters K has to be known or guessed before the algorithm can start clustering, which is not always straightforward. Often, various different values of K are tried and the results are evaluated using some evaluation metric. Additionally, the choice of initial random assignment can influence the final outcome. Thus, the resultant cluster distributions are not guaranteed to be optimum. The algorithm itself also requires a large number of computations, so some heuristics are needed to supplement the method to make it efficient.

2. Kernel K-means Clustering [233, 234]: This algorithm is similar to the original K-means algorithm but makes use of a transformation to project data onto a higher dimensional space. This is done with the help of a kernel function prior to deploying the K-means algorithm. They key advantage of this method is that it addresses one of the disadvantages of the K-means algorithm, which is the inability to work correctly with irregularly shaped data which are not linearly separable. For non-linearly separable data, it is beneficial to transform the data to a high dimensional space where it is linearly separable. Thus K-means can be deployed successfully on the transformed data.

   However, the other drawbacks from Kernel K-means remain. Additionally, applying

the Kernel function is not always feasible for very large datasets due to its time complexity. In addition to still needing to specify a pre-determined number of clusters to the algorithm, various Kernel functions which can be used for transformation need to be tested to determine their appropriateness for the data.

3. Agglomerative Hierarchical Clustering [235, 236]: This type of clustering is also known as bottom-up hierarchical clustering. In this algorithm, all individual data points are considered to be their own singleton clusters in the first step. The algorithm then successively merges or agglomerates pairs of clusters until all the clusters have been merged into a single cluster containing the entire dataset. Then, depending on the number of clusters desires or the number that makes sense, the final few merges can be undone.

   Due to the bottom-up approach, clusters of various sizes can be identified. Additionally, this clustering algorithm does not require any specification of the number of clusters before the algorithm can be employed. However, due to the nature of the algorithm, all points are assigned to clusters, and therefore the algorithm is susceptible to outliers.

As clustering is an unsupervised technique, typically there is no available data against which the obtained clusters can be validated. Additionally, given that the obtained clusters may need user input (as with K-means and Kernel K-means) and that different resuls can be obtained based on the initialization cluster (which is often done randomly with some heuristics), cluster validation is of increasing importance. For example, the goal here is to cluster real-world data into groups so that the environmental impacts can be assessed efficiently. There is no 'ground truth' data available against which the obtained groupings can be validated. Some data labels such as the airline and stage length were already identified and used to segregate the data before any clustering is performed. Hence, the use of cluster validation measures is important [237, 238].

It is important to remember that the original goal of clustering is to identify hidden patterns in the data by grouping similar objects together while ensuring groups are dissimilar to each other. Thus, the effectivity of a clustering algorithm can be assessed by measuring the compactness of each cluster in some n-dimensional space (known as *cohesion*) and by the dissimilarity between clusters (known as *separation*). The measure of compactness and separation is performed by many of the same distance functions utilized by the clustering algorithms. Three different validation measures (also known as scores or indices) which were used are detailed below. All measures were evaluated using the Euclidean distance function.

1. Silhouette score [239]: This score makes use of pairwise comparisons of cohesion and separation for each point in the dataset. The measure itself is normalized to lie in the range $[-1, +1]$, with the ideal score being $+1$. Values closer to -1 indicate that many samples have been incorrectly placed in the wrong cluster. Values closer to 0 indicate spatial overlap in the n-dimensional space between clusters.

   Given $d(x, y)$ as the distance between data points x and y, C_i representing cluster i, and n_i being the number of data points in C_i, the mean intra-cluster distance $a(x)$ and mean nearest cluster distance $b(x)$ can be calculated.

$$a(x) = \frac{1}{n_i - 1} \sum_{y \in C_i, y \neq x} d(x, y) \tag{4.9}$$

$$b(x) = \min_{j, j \neq i} \left[\frac{1}{n_j} \sum_{y \in C_j} d(x, y) \right] \tag{4.10}$$

   Note that the scores $a(x)$ and $b(x)$ are computed for each data point individually. To assess the accuracy of the clustering algorithm, these scores have to be aggregated across all data points. Given N total number of clusters, this aggregated score S_{sil} is

computed.

$$S_{sil} = \frac{1}{N} \sum_{i} \left[\frac{1}{n_i} \sum_{x \in C_i} \frac{b(x) - a(x)}{\max \{a(x), b(x)\}} \right] \tag{4.11}$$

From the formulation, it is clear that when $b(x) > a(x)$, the score will tend towards $+1$. This is the desired outcome where a good cluster will have the mean intra-cluster distance much smaller than the mean distance to the nearest cluster.

2. Davies-Bouldin score [240]: This score is defined as the average similarity of each cluster with its most similar cluster. Similarity in this score is defined as the ratio of intra-cluster distances to inter-cluster distances. A better score occurs when clusters are compact and far apart from their nearest cluster. The minimum score for this cluster is 0, and smaller scores indicate better clustering.

   Using the same notation as above, and introducing c_i as the centroid of cluster C_i, the Davies-Bouldin score can be computed.

$$S_{DB} = \frac{1}{N} \sum_{i} \max_{j, j \neq i} \left[\frac{\frac{1}{n_i} \sum_{x \in C_i} d(x, c_i) + \frac{1}{n_j} \sum_{x \in C_j} d(x, c_j)}{d(c_i, c_j)} \right] \tag{4.12}$$

3. Calinski-Harabasz score [238]: Also known as the Variance Ratio criterion, this score measures the ratio of the sum of inter-cluster dispersion and intra-cluster dispersion. The dispersion is quantified as the sum of squares of distances. A higher score indicates better defined clusters with more compactness and with higher separation between cluster centers.

   Using the same notation as above, and introducing c as the centroid of the complete dataset, and n as the total number of samples in the dataset, the Calinski-Harabasz

score can be computed.

$$S_{CH} = \frac{\sum_i n_i d^2(c_i, c)}{\sum_i \sum_{x \in C_i} d^2(x, c_i)} \frac{n - N}{N - 1} \tag{4.13}$$

4.3.2 Data pre-processing and clustering setup

In order to implement clustering algorithms, the typical approach for unsupervised machine learning techniques was followed. Starting with the dataset outlined in section 4.1 and grouping by airline and stage length, the steps are – generation of feature vectors and their scaling, computation of distance functions, assignment to clusters, and evaluation of cluster validation measures.

Feature vector generation and scaling

The first step in the clustering process is to generate a feature vector. A feature vector consists of parameters or variables which are relevant for the assessment of similarity. For the evaluation of aviation noise, the trajectory and thrust of the aircraft are of utmost importance. As noted previously, various trajectory and performance parameters are known in the OpenSky dataset, with the notable exception of thrust. In addition to the altitude at each ground track point, the horizontal and vertical speeds of the aircraft were also identified as features for clustering. The horizontal speed is available as the ground speed, and the vertical speed is available as the rate of climb/descent.

The three identified parameters are then rearranged as a single vector which acts as the feature vector for the flight. Given p as the total number of points in the flight, and $m_j^{(i)}$ as the value of parameter i at location j, the feature vector f is given below –

$$f = \begin{bmatrix} m_1^{(1)} & \dots & m_p^{(1)} & m_1^{(2)} & \dots & m_p^{(2)} & m_1^{(3)} & \dots & m_p^{(3)} \end{bmatrix} \tag{4.14}$$

As noted previously, every flight data record was resampled to be on a consistent basis

for cumulative ground track distance. Further, flight lengths were truncated as necessary to ensure a consistent basis across all flights. Each flight was represented by a feature vector of 450 elements, with 150 values of each of the three parameter. 150 sample points also represent 25 nmi of cumulative ground track distance. The variation of these feature values over the departure phase for a single flight is shown in Figure 4.10.

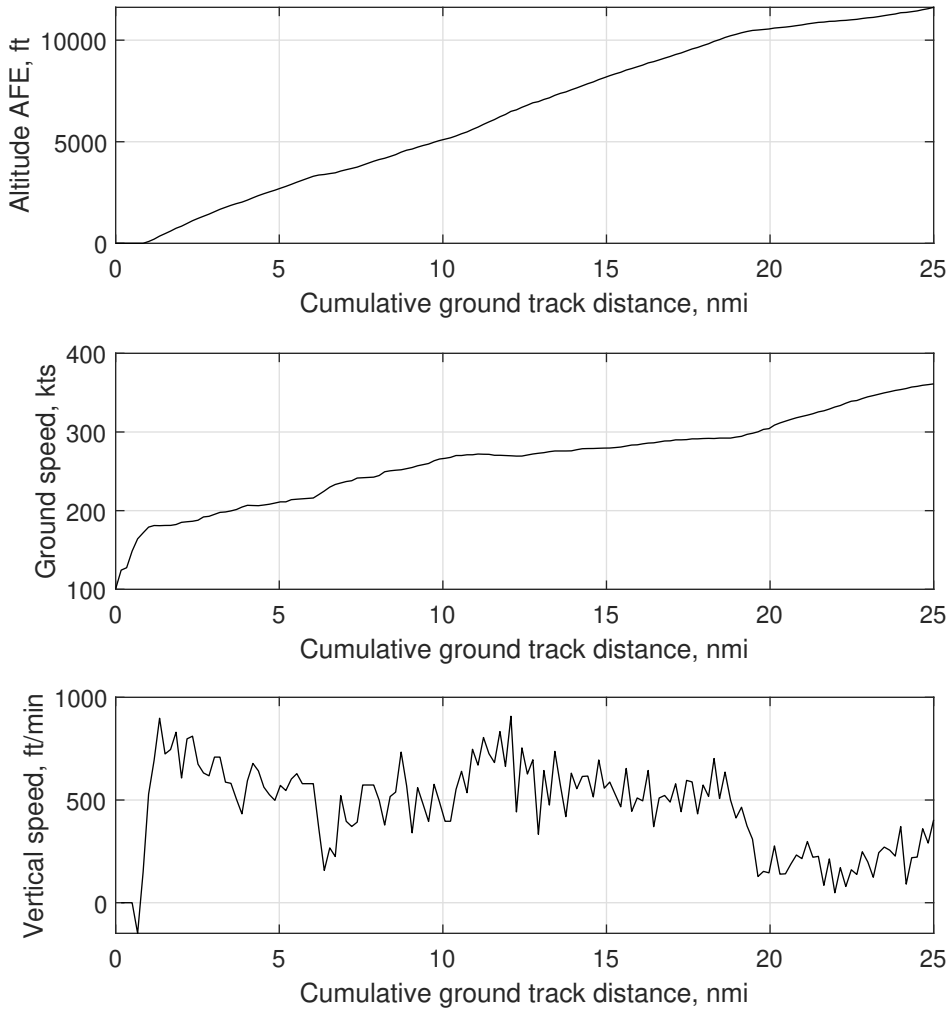

Figure 4.10: Identified features used for clustering

Due to the nature of the features and their units, their scale is quite different. As is evident from Figure 4.10, the ground speed varies from 100 to 400 knots, whereas altitude varies from 0 to 10000 ft AFE. The problem here is that one feature can overshadow the clustering computations simply due to the units being used. Such features can bias the

clustering results, and therefore, the influence of units must be removed. To mitigate this influence of magnitide, the feature vectors were scaled to be on the range of $[0, 1]$ using a *MinMaxScaler*.

Each element of the feature vector was scaled independently. Given values $m_{j,1}^{(i)}, m_{j,2}^{(i)}, \ldots, m_{j,n}^{(i)}$ of parameter i for all n flights in the dataset, at point j in the departure. The scaled value for the first parameter $m_{j,1}^{(i)}$ is given by –

$$\hat{m}_{j,1}^{(i)} = \frac{m_{j,1}^{(i)} - \min\left\{m_{j,1}^{(i)}, m_{j,2}^{(i)}, \ldots, m_{j,n}^{(i)}\right\}}{\max\left\{m_{j,1}^{(i)}, m_{j,2}^{(i)}, \ldots, m_{j,n}^{(i)}\right\} - \min\left\{m_{j,1}^{(i)}, m_{j,2}^{(i)}, \ldots, m_{j,n}^{(i)}\right\}} \tag{4.15}$$

The formula ensures that each element of the feature vector is scaled to the range $[0, 1]$. Additionally, it also ensures that the minimum value is scaled to 0 and the maximum value is scaled to 1.

Distance function computation

After the features have been identified and scaled appropriately, the next step is the evaluation of the distance function. For the K-means and Agglomerative clustering algorithms, the Euclidean distance function is used. Other measures of distance include weighted Euclidean distance, Manhattan distance etc. Euclidean distance is suitable when the vectors are of equal length. When feature vectors are not of equal length or have an uneven sampling basis, more complex distance computation is required such as shape-based or warping-based distance [241].

Given two feature vectors x, y corresponding to two different flights, the Euclidean distance is calculated as –

$$d(x, y) = \|x - y\| = \sqrt{\sum_{i=1}^{p} (x_i - y_i)^2} \tag{4.16}$$

For the Kernel K-means algorithm, the distance computation takes place in a trans-

formed space [233, 234]. The two Kernel functions employed in this experiment are –

1. Cosine Similarity Kernel: This makes use of the dot product of two feature vectors.

$$k(x, y) = \frac{x^T y}{\|x\|\|y\|} \tag{4.17}$$

2. Gaussian/Radial Basis Function Kernel: This uses an exponential function to evaluate similarity with σ as a hyperparameter.

$$k(x, y) = \exp\left(\frac{-\|x - y\|^2}{2\sigma^2}\right) \tag{4.18}$$

This concludes the data processing and clustering setup which is required before deploying the clustering algorithms. The algorithms and the cluster scoring metrics are implemented in Python using the scikit-learn toolbox [242].

4.3.3 Results from clustering

Evaluation of cluster validation measures

The three clustering methods mentioned were deployed on the data with both Kernel functions being used for Kernel K-means. The resulting 4 sets of results were evaluated with the three cluster validation scores. The cluster validation scores and their variation with number of clusters ranging from 2 to 19 is shown in Figure 4.11. The Silhouette score is observed to decrease with increasing number of clusters. A similar trend is observed for the Calinski-Harabasz score, whereas the Davies-Bouldin scores have more fluctuation. The agglomerative clustering algorithm seems to outperform the others in two score metrics and underperform in the third. Based on this observation, the remainder of section will present results from the Agglomerative Hierarchical clustering algorithm.

Once the algorithm has been down-selected, the number of clusters has to be determined. Ideally, the number of clusters should maximize the Silhouette and Calinski-

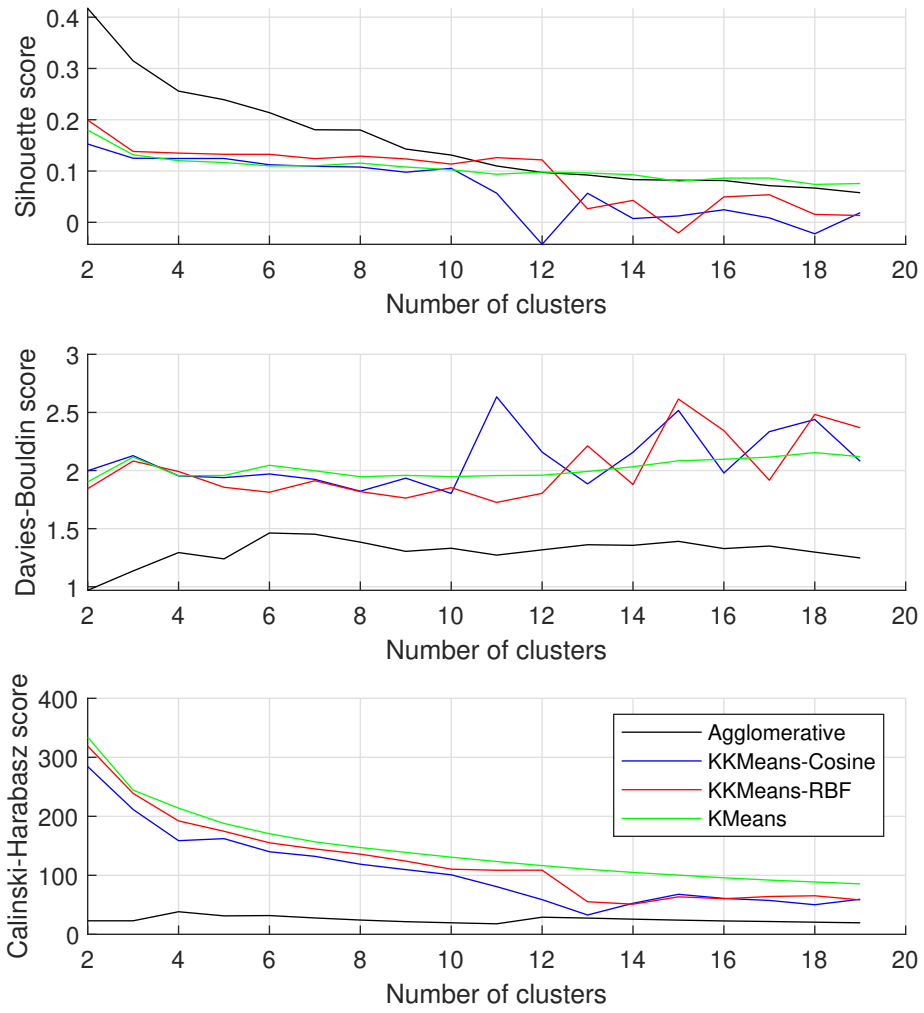

Figure 4.11: Comparison of clustering algorithms across three validation measures

Harabasz score and minimize the Davies-Bouldin score. Monotonically increasing or decreasing scores do not seem to suggest the preference of any one cluster solution over the other. Ideally, it is preferable to have a number of clusters which shows a local optimum. On closer inspection, it is observed that when choosing the number of clusters to be 4, there is local minima for the Davies-Bouldin score and a local maxima for the Calinski-Harabasz score. Therefore the analysis is performed with four clusters. It should be noted here that there is no one clear solution for the selection of number of clusters. Often, it comes down to heuristics and to subject matter expertise.

Cluster assignment

With the number of clusters identified, the flights belonging to each cluster can be identified. The variation of the three features across four clusters is visualized in Figure 4.12. The corresponding number of flights within each cluster is also shown in the figure. It is observed that most flights were clustered into a single group (Cluster A), with the other three clusters showing some key differences. Cluster B represents flights which are consistently higher than those observed in other clusters. Cluster C represents several flights which have a level-off segment. These flights were previously identified in Experiment 1.1 as being outliers.

With the visual observations, it is evident that the clustering algorithm was able to identify and separate out flights with markedly different characteristics from those with more nominal behavior. Indeed the purpose of clustering was to identify groups of flights which will have similar noise impacts. The employed clustering algorithm was able to segregate flights based on their overall flight profile. For example, flights in Cluster C which have level-off segments are expected to have significantly different noise results than from those in other clusters.

Selection of representative flights

With the identification of clusters and the corresponding flight assignments, the process of clustering is complete. However, for this use-case, the intention is to identify a representative cluster for each group, which can then act as a stand-in for all other flights within that group when evaluating noise metrics. The ideal representative flight should produce minimal error when compared to other flights in the same cluster. Such a requirement naturally leads to the notion of an average or median flight.

A simple approach to constructing such a representative flight can be to simply take the average or median of all feature vectors within a cluster. However, there is no guarantee that the obtained representative actually represents a valid flight, which can physically be

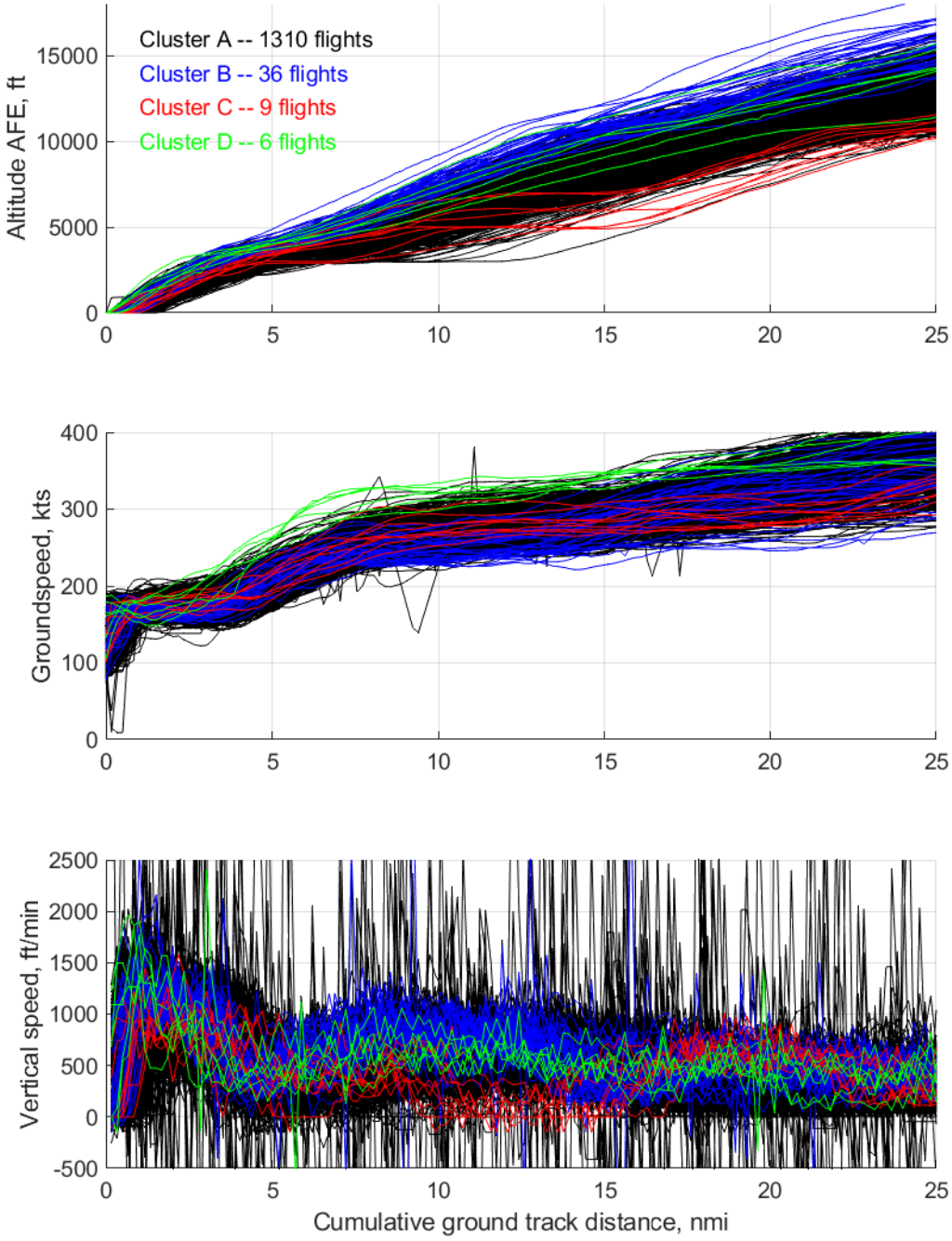

Figure 4.12: Visualization of flight assignment to four clusters

flown. To ensure a physics-consistent representative, the following process is proposed –

1. First, the ideal median feature vector for each cluster is obtained. Each element of this vector represents the median for that element across all flights.

2. Next, all flights within the cluster are compared to this ideal median. The flight which is most similar, based on the distance function used for clustering is considered to be the representative for that cluster. Given $\bar{x}_i$ as the ideal median for cluster C_i, the representative flight f_i is found as –

$$f_i = \arg \min_{x_j, x_j \in C_i} \|x_j - \bar{x}_i\| \tag{4.19}$$

Using this process, the representative flight for each cluster was obtained. As this representative is an actual real-world flight, there are no additional checks necessary to determine whether the chosen flight is actually feasible to be flown. The selected representatives for each cluster are visualized Figure 4.13. This visualization confirms that each median representative does a good job of being a stand-in for its cluster.

With the development of the median, the entire original dataset of 1361 flights has been reduced to only 4 flights, with Flight A representing Cluster A's 1310 flights, and so on. The task of modeling the environmental metrics for these real-world flights has been greatly simplified. Particularly, the computationally expensive noise metric quantification process only needs to be performed 4 times, as compared to 1361 times, which should take only 0.2939% of the resources. Scaling up each obtained noise result according to the number of flights in each cluster is a relatively simple process.

4.3.4 Summary and evaluation of Hypothesis

The second experiment was designed to create a process which supplemented the inverse map by which real-world aircraft trajectories could be efficiently mapped to a parametric definition. The same real-world dataset used in Experiment 1.1 was used, representing a

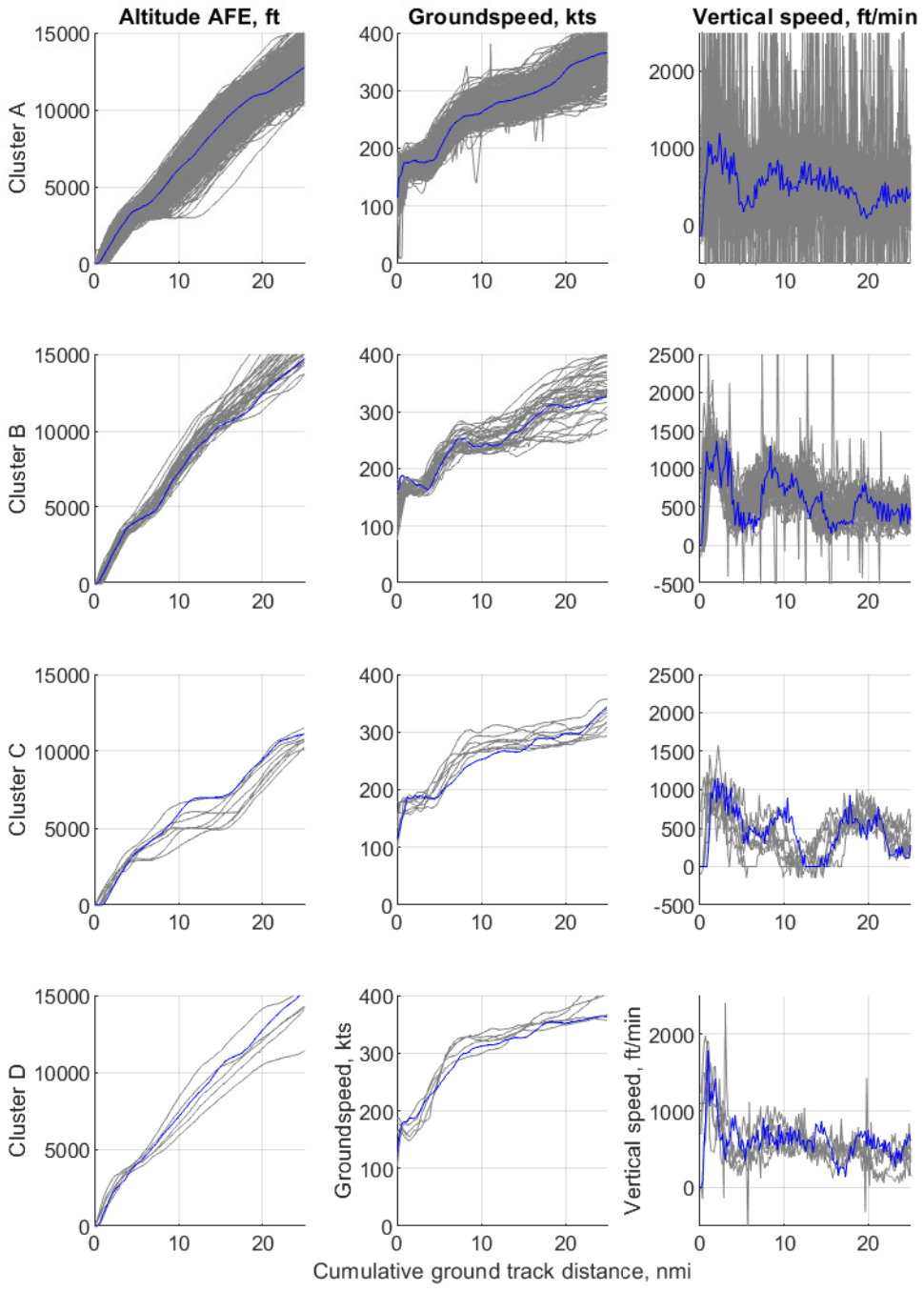

Figure 4.13: Median representative flight selection for each cluster

set of 5070 flights departing from San Francisco airport. Three clustering algorithms – K-Means, Kernel K-Means, and Agglomerative Hierarchical clustering were implemented and their performance on the datasets was evaluated using three cluster scoring methods – Silhouette score, Davies-Bouldin score, and the Calinski-Harabasz score. Due to a large number of potential combinations, only a small subset of results were shown for this Experiment.

The implementation of a clustering algorithm required the generation of feature vectors, where three parameters – altitude, ground speed, and vertical speed were identified and collected for each flight. The feature vectors were then scaled to remove any bias from parameters with naturally higher valued units. The distance function was then evaluated to ascertain the pair-wise similarity between flights. The clustering algorithms were then deployed with the number of clusters being a hyperparameter.

The 'goodness' of each cluster distribution was assessed using the three scores. In the example result shown, 4 clusters were chosen for the flight group representing 1361 flights from a single airline flying a stage length 4 mission. Next, the median representative flights for each cluster were computed. These median representatives serve as an efficient way to parametrically map the cluster to a parametric representation.

Revisiting Hypothesis 1.2, the requirement was to show that real-world trajectories could be clustered into groups in the context of aviation noise estimation. The accompanying experiment was designed to do exactly that and the obtained results confirm that such clustering is possible. Therefore, Experiment 1.2 is considered successful and Hypothesis 1.2 is accepted.

4.4 Experiment 1.3

In this section, the experimental setup and results for RQ1.3 are explained[2]. For reference, RQ1.3 and H1.3 are repeated below –

Research Question 1.3

How can the design space for aircraft trajectories be explored efficiently?

Hypothesis 1.3

If a screening test is performed and the primary drivers can be identified, the design space for aircraft trajectories can be explored efficiently.

The purpose of this experiment is to identify the primary drivers, if any, have the most significant contribution to aviation noise metrics so that the design space for aircraft trajectories can be explored efficiently for optimization or for trade-off studies. A screening test is proposed to identify the contribution of each parameter to the relevant noise metric. The objective of the screening test is to obtain a ranking of parameters, so that the most important parameters are prioritized when performing large-scale studies.

4.4.1 Methods for parameter screening

The overarching field of statistics which is applicable here is known as Global Sensitivity Analysis [185]. In a general sense, the objective of GSA is to provide measures of sensitivity of a model's output with respect to the model inputs. As the sensitivity of an output to a given input increases, so does the influence of that parameter on the model.

[2]Parts of the research described in this section are documented in the following publication –

- A. Behere, M. Kirby, and D. N. Mavris, "Relative importance of parameters in departure procedure design for lto noise, emission, and fuel burn minimization," in *AIAA AVIATION 2022 Forum*, Jun. 2022. DOI: 10.2514/6.2022-3916. eprint: https://arc.aiaa.org/doi/pdf/10.2514/6.2022-3916. [Online]. Available: https://arc.aiaa.org/doi/abs/10.2514/6.2022-3916 [243]

Conversely, if an output is not sensitive to a particular input, then that input does need to be sampled as densely.

With a fundamental understanding of the definition of sensitivity analysis, different methods in literature can be evaluated. Most methods in literature are based on partial derivatives. Indeed, this partial derivative $\frac{\partial Y_j}{\partial X_i}$ for a given output Y_i versus some input X_i can be thought as being the mathematical definition of sensitivity. However, partial derivative based methods have some major drawbacks. A key drawback is that the computed derivative is only useful and informative at the point at which it is computed. Thus, it is only suitable for a very narrow scope of local sensitivity analysis. Only in the case of linear models can the partial derivative be extended to the entire domain. However, most models are complex and non-linear.

Several methods for performing sensitivity analysis have been developed for different applications. One method which can be used with many different model types is called *step-wise regression*. Instead of being a separate method by itself, it is a modification to the standard process of fitting regression models. With regular regression modeling, typically all input variables will be used to fit the model. With step-wise regression, a procedure is used to determine which input variables will be included in the model.

Step-wise regression can be performed by either iteratively adding the most influential variables, or by removing the ones with the least influence. Statistical significance tests are performed to determine which variable should be included/excluded in the model. The process is repeated until a pre-defined stopping criteria is met. Using these two methods, there are three approaches for step-wise regression –

1. Forward selection involves starting with a constant valued model, and with no input variables included. Next, each possible inclusion to the model is tested and the the one whose inclusion provides the most statistically significant improvement is included. This process is continued until a convergence criteria is met. Typically, the convergence criteria is a check on whether the inclusion of any of the remaining

parameters can improve the model to a statistically significant extent.

2. Backward selection operates in an opposite manner, by first including all variables in the model and then iteratively eliminating the ones with least significance. The process is repeated until no variable can be removed without resulting in a statistically significant loss of model fit.

3. Bidirectional elimination uses a combination of the two selection approaches. At each step, variables are tested for inclusion or exclusion from the model.

Thus, by providing a subset of variables which are used to build the model, a reduced model can be constructed which leaves out the variables with negligible effect on the output. While this is certainly a useful application of step-wise regression, it is not the primary motive in this Research Question. Instead, rather than the subset itself, the order in which variables are included in the model provides a way to identify the primary drivers of the output.

4.4.2 Identified parameters

In Experiment 1.1, 1 list of 4 parameters was identified which were used to generate a set of 240 procedural profiles to be used with an aircraft performance model. These 4 parameters represented the design space of trajectories and associated performance characteristics. These parameters were sufficient for Experiments 1.1 as the outputs of relevance were the trajectories themselves.

However, when working with aviation noise metrics, a large number of external parameters are present which can influence the noise metrics. One of the most important parameters for the quantification of aviation noise is the ambient weather. Temperature in particular, has an impact on both the propagation of noise through the atmosphere, and on the aircraft performance itself. Therefore, an analysis of parameter influence on noise incomplete without the inclusion of ambient temperature as a factor.

In the aviation noise modeling AEDT, the ambient weather conditions are accounted for by specifying a set of six values representing six weather parameters. These parameters, along with their default values for the Atlanta airport are shown in Table 4.8. Several of these weather parameters have correlations and interdependencies. Therefore, they cannot all be set independently, and their dependencies have to be calculated to ensure a physically consistent weather definition. For example, among the set of $\{T, RH, DP\}$, only two need to be specified and the third can be solved as a function of the other two. There are several models proposed in literature to resolve the interdependency of these three variables [244].

Table 4.8: Weather vector definition in AEDT with example values at KATL airport

Weather parameter	Description	Example value	Units	Correlations
T	Ambient temperature	63.44	°F	with RH and DP
P_{st}	Station pressure	981.21	mbar	with P_{sl}
P_{sl}	Sea-level pressure	1018.00	mbar	with P_{st}
RH	Relative humidity	63.04	%	with DP and T
DP	Dew point temperature	50.64	F	with T and RH
W	Wind speed	6.79	knots	none

Including the ambient temperature as a variable, brings the total number of parameters to five. Of these parameters, the ambient temperature and takeoff weight can be considered as external factors, which are not controllable as part of the departure profile. Takeoff weight is usually a function of the payload of the aircraft and the fuel weight to be carried for the trip distance. On the other hand, the three remaining parameters, which are the takeoff thrust reduction, altitude for acceleration initiation, and the energy share percentage are all design variables for the profile.

Keeping in mind the computational resource constraints of the full-order aviation noise estimation tool AEDT, a set of values for each parameters was used to create a set of 960 results on which step-wise regression was to be performed. The parameters and their range of values is shown in Table 4.9.

Table 4.9: Identified parameters and their ranges of variation

Parameter	Description	Possible values	Units
α_1	Takeoff weight (through Stage Length)	151100 (SL3), 162150 (SL4), 169950 (SL5)	lb_m
α_2	Takeoff thrust reduction	1.00, 0.95, 0.90, 0.85	multiplier
α_3	Altitude for acceleration	800, 1000, 1200, 1400, 1600	ft
α_4	Energy share percentages	20, 40, 60, 80	%
α_5	Ambient temperature	40, 60, 80, 100	°F

The range of temperature variation was chosen to be aligned with the typical temperatures measured at the Atlanta airport. Additionally, the dew point temperature was updated during modeling to be ensure a constant relative humidity level was maintained. This ensured that the effects on the noise metric were isolated to those from the temperature only, and humidity effects could be controlled for.

The selected parameters all influence noise metrics either directly, or indirectly. The takeoff weight of the aircraft directly influences the trajectory of the departing aircraft. Given that takeoff and climb thrust levels are due to constant thrust settings, heavier aircraft have less excess energy to climb and accelerate. Thus, heavier aircraft are closer to the ground for a longer duration than lighter aircraft and thus their resulting noise footprint is higher. The effect of other parameters is more nuanced.

Takeoff thrust is directly correlated with engine noise, which is the largest component of noise for departures. Therefore, higher thrust levels should increase the noise footprint of the operation. However, a higher takeoff thrust also implies an ability to accelerate and climb faster, and hence at locations further down the ground track, the aircraft may be sufficiently far away that the noise impact is actually lower. Thus, the location is of importance when discussing the effects of the chosen parameters on noise metrics. Similarly, the choice of altitude for acceleration initiation, and energy share percent have a

complex effect on aviation noise metrics. Finally, the effect of temperature, as previously noted, is through both atmospheric propagation, and through influence on the aircraft performance.

4.4.3 Noise metric modeling

This subsection outlines the process from which the noise metric results were obtained and processed for model fitting.

Modeling setup

As mentioned previously, the Aviation Environmental Design Tool is used to model the noise metric results for this experiment. The process can be broken down into various steps outlined below –

1. First, the procedural profile definitions resulting from the 240 possible combinations of parameters $\{\alpha_1, \alpha_2, \alpha_3, \alpha_4\}$ were created and imported into AEDT.

2. Next, the four ambient temperature conditions were formatted into the appropriate weather definition and imported into AEDT. The dew-point temperature was varied appropriately to ensure that the relative humidity across the runs remained constant.

3. A set of SQL scripts were used to create a full factorial set of *jobs* in AEDT. Each job represented one operation being flown at a particular weather condition. All operations were modeled at the KATL airport, flying out of runway 09L with a East-bound heading along a straight ground track.

4. A set of noise receptors was created around the ground track along which the noise metric was evaluated. The set was set up as a 2D grid of receptor points, spaced 0.1 nmi along both the North-South and East-West directions. As the flight track was aligned with the East-West direction, more points were needed in that direction. 401 receptors were created along this 'longitudinal' direction, whereas 81 receptors were

created along the transverse direction. This led to a total of 32481 points at which the noise metric was computed. The grid itself was then positioned so that the start of the runway would be located at a position 4 nmi East and 4 nmi North from the Southwestern corner of the grid. The elevation of the grid was set to be the same elevation as the runway.

5. The Sound Exposure Level (SEL) noise metric was modeled on the noise grid for all jobs. While various noise metrics are relevant, the SEL is one of the most commonly used noise metrics used for aviation noise analysis. The Day-Night averaged Level (DNL) is the most commonly used metric, but is more relevant for groups of operations. For the noise evaluation of single operations, the SEL metric is more appropriate.

The modeled noise metrics are available in the noise report in AEDT. These reports were exported outside of AEDT for post-processing and analysis.

Post-processing

The raw noise metric results obtained in the noise report are in a tabular format. As a sample, Table 4.10 shows 5 consecutive rows (of 32481) for the noise report obtained for job number 437 (of 960) which consists of a procedural profile characterized by the parameters $\alpha_1 = 151100\ lb_m,\ \alpha_2 = 1.00,\ \alpha_3 = 1000\ ft,\ \alpha_4 = 40\%$ at temperature $\alpha_5 = 60\ ^\circ F$.

The raw noise reports were then aggregated into scalar metrics in the form of the areas and lengths of noise contours. Figure 4.14 shows the noise contours obtained from the noise report for job number 437 for four noise levels – 75 dB SEL, 80 dB SEL, 85 dB SEL, and 90 dB SEL. The noise levels are higher in the innermost contour and decrease in decrements of 5 dB SEL as one moves to the outward contours. Noise contours and their dimensions are one of the most commonly used metrics for aviation noise. The lengths and areas of the contours shown in Figure 4.14 are summarized in Table 4.11.

Table 4.10: Sample set of rows from a noise report obtained in AEDT

Receptor #	Latitude (deg)	Longitude (deg)	Elevation(ft)	Noise Level (dB)
⋮	⋮	⋮	⋮	⋮
11684	33.616334	-84.420027	1018.7	77.29
11685	33.616333	-84.418031	1018.7	77.68
11686	33.616333	-84.416035	1018.7	78.05
11687	33.616332	-84.414040	1018.7	78.37
11688	33.616332	-84.412044	1018.7	78.61
⋮	⋮	⋮	⋮	⋮

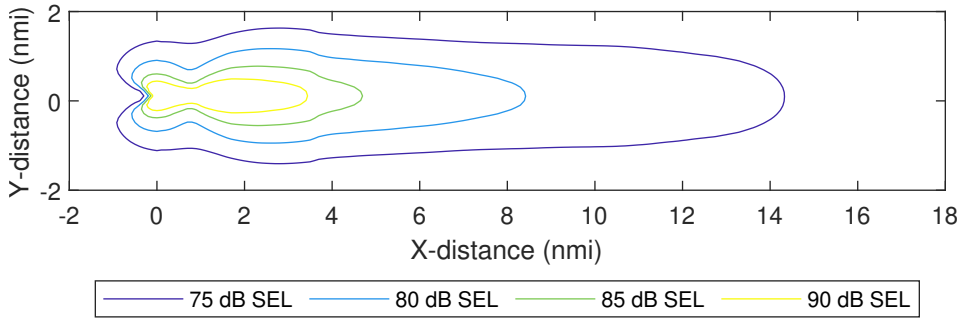

Figure 4.14: Noise contour visualization for a sample flight

The obtained contour dimensions in the form of area and length are used to build the regression models to perform the screening tests. In this case, the length of a contour is defined as the longer dimension of the smallest rectangular bounding box which can fully contain the contour. The area of the contour is obtained by dividing the contour into thin trapezoidal 'slices' aligned in the North-South direction and integrating the area of all such slices along the East-West direction.

Table 4.11: Contour dimensions for sample job 437

Noise Level	Length (nmi)	Area (nmi^2)
75 dB SEL	15.2453	35.2442
80 dB SEL	8.9931	13.2438
85 dB SEL	4.7853	4.7853
90 dB SEL	2.0966	2.0966

4.4.4 Results

With the contour dimensions constructed, the sensitivity of these dimensions with respect to the input parameters can be analyzed. Before moving onto the step-wise regression modeling, it is instructive to visually observe the effect of each of the five parameters on the noise contours.

One Factor At a Time analysis

A One Factor At a Time (OFAT) analysis is a type of sensitivity analysis in which the effects of only one input parameter is studied while the others are held constant. This type of sensitivity analysis can be considered to be halfway between a local and a global sensitivity analysis. It has a higher scope than local sensitivity analyses because the chosen parameter is varied not just within a small neighborhood, but across its entire range of permissible values. Of course, an OFAT analysis is still more limited than a global sensitivity analysis as it does not include variations of all parameters at the same time.

First, the variation of the noise contours with the aircraft weight is shown in Figure 4.15. In this case, the weight is varied between its three possible values, while the other parameters are held constant at their central values, $\alpha_2 = 0.90,\ \alpha_3 = 1200\ ft,\ \alpha_4 = 40\%,\ \alpha_5 = 60\ ^\circ F$. The corresponding values of the contour dimensions are shown in Table 4.12.

Table 4.12: Variation on contour dimensions with aircraft takeoff weight

Takeoff	Area, nmi^2				Length, nmi			
Weight	75	80	85	90	75	80	85	90
151100	29.40	10.49	3.91	1.48	15.28	8.44	4.88	3.44
162150	32.11	11.25	4.21	1.57	16.89	9.22	5.38	3.77
169950	34.15	11.82	4.49	1.63	18.09	9.82	5.81	4.01

From the figure, it is evident that the original expectation of a higher noise metric for a heavier takeoff weight has held true. Across the outer three contours, significant increases

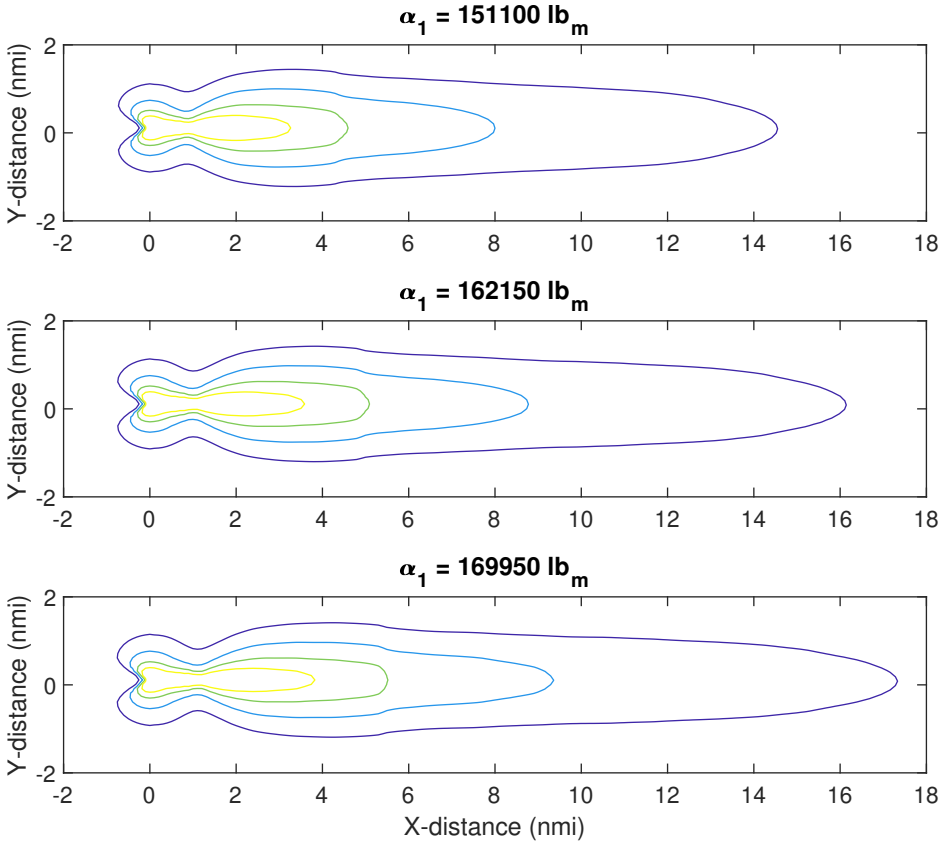

Figure 4.15: Variation of 75, 80, 85, and 90 dB SEL noise contours with aircraft takeoff weight

in the contour lengths, and consequently, contour areas can be observed. The change is less evident for the innermost contour representing 90 dB SEL. Nevertheless, inspecting the numbers for these two dimensions in Table 4.12 serves to confirm the visual observations.

The reason for this increase is noise metric levels is quite straightforward. With an increase in aircraft weight, the aircraft becomes less agile due to a lower thrust to weight ratio. Consequently, with a higher weight, the aircraft cannot climb or accelerate as fast as it can with a lower weight. Hence the aircraft trajectory ends up closer to the ground, which decreases the separation between the noise source and observer, leading to the higher values observed.

The variation of the noise contours with the aircraft takeoff thrust reduction is shown in Figure 4.16. In this case, the takeoff thrust is varied between its four possible values, while the other parameters are held constant at their central values, $\alpha_1 = 162150\, lb_m,\ \alpha_3 = 1200\ ft,\ \alpha_4 = 40\%,\ \alpha_5 = 60\,^\circ F$. The corresponding values of the contour dimensions are shown in Table 4.13.

Table 4.13: Variation on contour dimensions with aircraft takeoff thrust reduction

Takeoff	Area, nmi^2				Length, nmi			
Thrust multiplier	75	80	85	90	75	80	85	90
0.85	31.73	11.01	3.98	1.36	17.19	9.57	5.66	3.69
0.90	32.11	11.25	4.21	1.57	16.89	9.22	5.38	3.77
0.95	38.05	13.80	4.88	1.89	16.99	10.04	5.68	3.93
1.00	38.83	14.39	5.27	2.28	16.80	9.82	5.46	4.10

The effect of aircraft takeoff thrust reduction on the noise contours is a little more difficult to ascertain. There are two competing effects at play here, so it is difficult to intuitively expect what the outcome should be. The first effect is that with a higher thrust level, the aircraft is more agile and is better able to climb and accelerate. Therefore, the trajectory for higher thrust is also expected to be higher. On the other hand, due to a higher thrust, the noise produced at the source is higher. The level of noise at any grid point

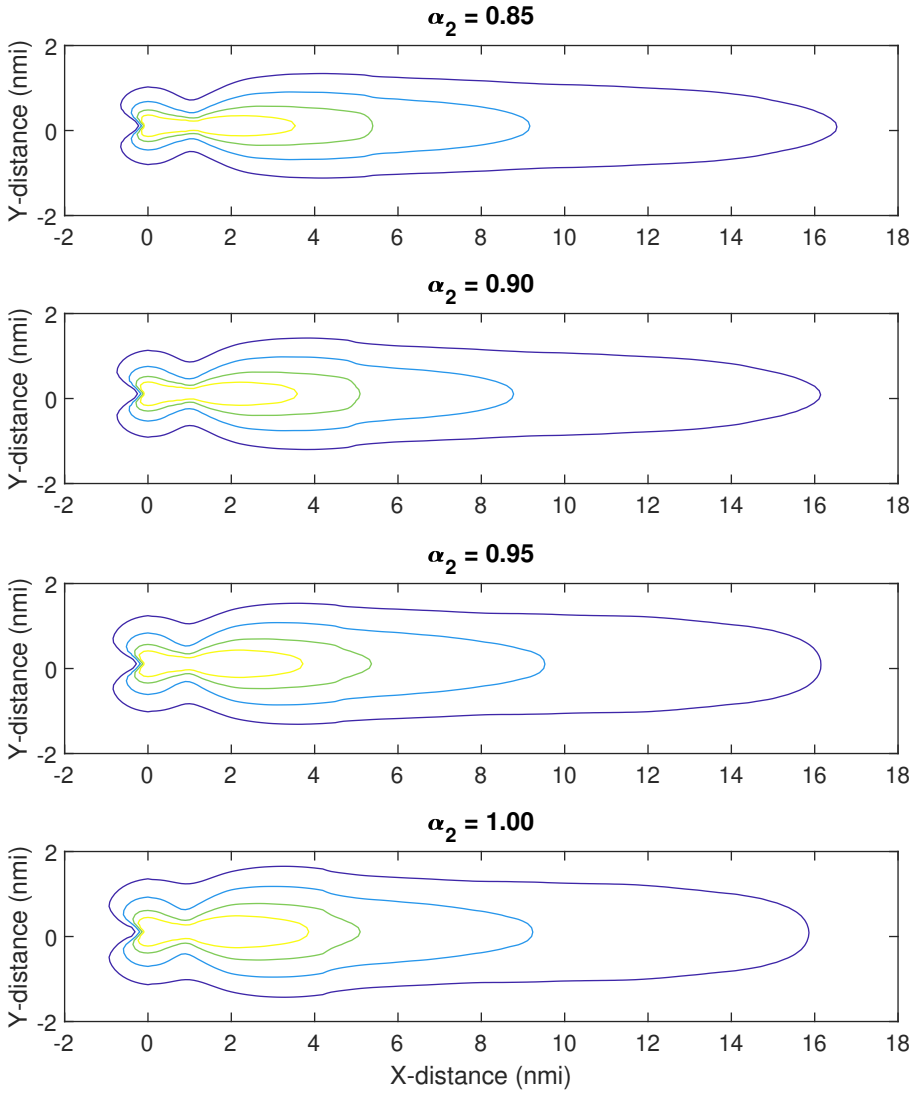

Figure 4.16: Variation of 75, 80, 85, and 90 dB SEL noise contours with aircraft takeoff thrust reduction

depends on which of these two competing effects is dominant.

From the figure, the length of contours tends to decrease with increasing thrust for the 75 dB contour, but increases for the 90 dB contour. The 90 dB contour is formed due to the noise energy at the very beginning stages of the profile. Hence, it makes sense that the higher noise source effect would be dominant. Conversely, the 75 dB contour is comprised of noise energy from the entire procedure. Here, the higher climb rate effect wins out as it has enough time to be significant. The contour area is less dependent on the climb rate effect, as the width of the contours are largely influenced by the thrust levels. Therefore, the area of all contours show a monotonic increase with higher takeoff thrust levels.

The variation of the noise contours with the altitude for acceleration initiation is shown in Figure 4.17. In this case, the altitude is varied between its five possible values, while the other parameters are held constant at their central values, $\alpha_1 = 162150\ lb_m,\ \alpha_2 = 0.90,\ \alpha_4 = 40\%,\ \alpha_5 = 60\ ^\circ F$. The corresponding values of the contour dimensions are shown in Table 4.14.

Table 4.14: Variation on contour dimensions with altitude of acceleration initiation

Altitude for	Area, nmi^2				Length, nmi			
acceleration	75	80	85	90	75	80	85	90
800	31.78	10.94	3.83	1.56	17.00	9.32	5.20	3.82
1000	31.95	11.10	4.02	1.57	16.95	9.28	5.26	3.80
1200	32.11	11.25	4.21	1.57	16.89	9.22	5.38	3.77
1400	32.29	11.41	4.42	1.57	16.85	9.17	5.54	3.76
1600	32.45	11.58	4.59	1.57	16.79	9.12	5.69	3.75

The effect of altitude of acceleration initiation on the noise contours is quite difficult to decipher from the figures alone. Very little variation among the contours is seen across the five levels for this parameter. The most notable distinction is that in the shape of the 80 dB contour. The shape is more tapered for the lower altitude values and becomes more rounded as the altitude increases. Based on the values in Table 4.14, it is observed that there is little variation in contour areas and lengths. The variation, however small, is observed to

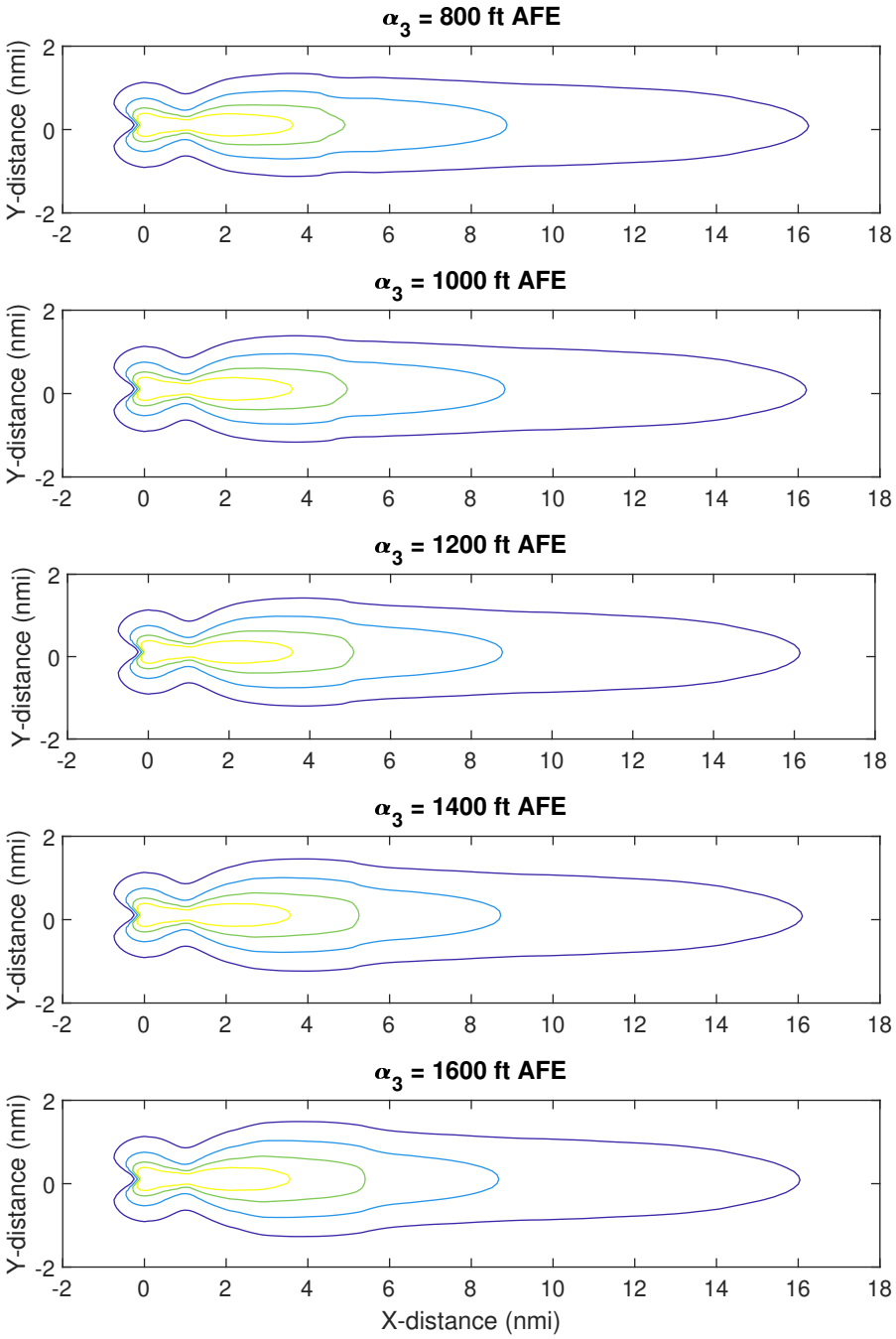

Figure 4.17: Variation of 75, 80, 85, and 90 dB SEL noise contours with altitude for acceleration initiation

be monotonic. The area of contours increases monotonically with altitude, and the length of the contours decrease monotonically.

The physical effect of the altitude of acceleration initiation is through the delaying of flap retraction and thrust cutback. By delaying these events, the aircraft is able to maximize its climb rate potential, with the caveat of having high thrust. Thus, the similar competing effects come into play which were observed for the takeoff thrust reduction percentage. Consequently, similar trends for contour areas and lengths are observed. However, it is noted that the variation introduced by this parameter is not as large as the other parameters. This will be confirmed in the next set of results from the step-wise regression model.

The variation of the noise contours with the energy share percentage is shown in Figure 4.18. In this case, the energy share percent is varied between its four possible values, while the other parameters are held constant at their central values, $\alpha_1 = 162150\ lb_m,\ \alpha_2 = 0.90,\ \alpha_3 = 1200\ ft,\ \alpha_5 = 60\ ^\circ F$. The corresponding values of the contour dimensions are shown in Table 4.15.

Table 4.15: Variation on contour dimensions with energy share percentage

Energy Share Percent	Area, nmi^2				Length, nmi			
	75	80	85	90	75	80	85	90
20	36.96	14.53	5.18	1.57	16.80	9.62	6.42	3.78
40	32.11	11.25	4.21	1.57	16.89	9.22	5.38	3.77
60	31.79	10.83	3.75	1.57	17.13	9.46	5.28	3.83
80	31.66	10.70	3.65	1.54	17.25	9.61	5.39	3.71

Next, the effect of energy share percentage on the noise contours is analyzed. The shape of the contours changes quite evidently across the four levels for this parameter. Although the length of the contours stays relatively constant, the width shows significant changes, which is carried over into the area of the contours as well. The contour for 20% energy share is quite smooth whereas the one for 80% energy share shows a wavy contour shape.

To explain this observation, it is helpful to first recall the definition of energy shape

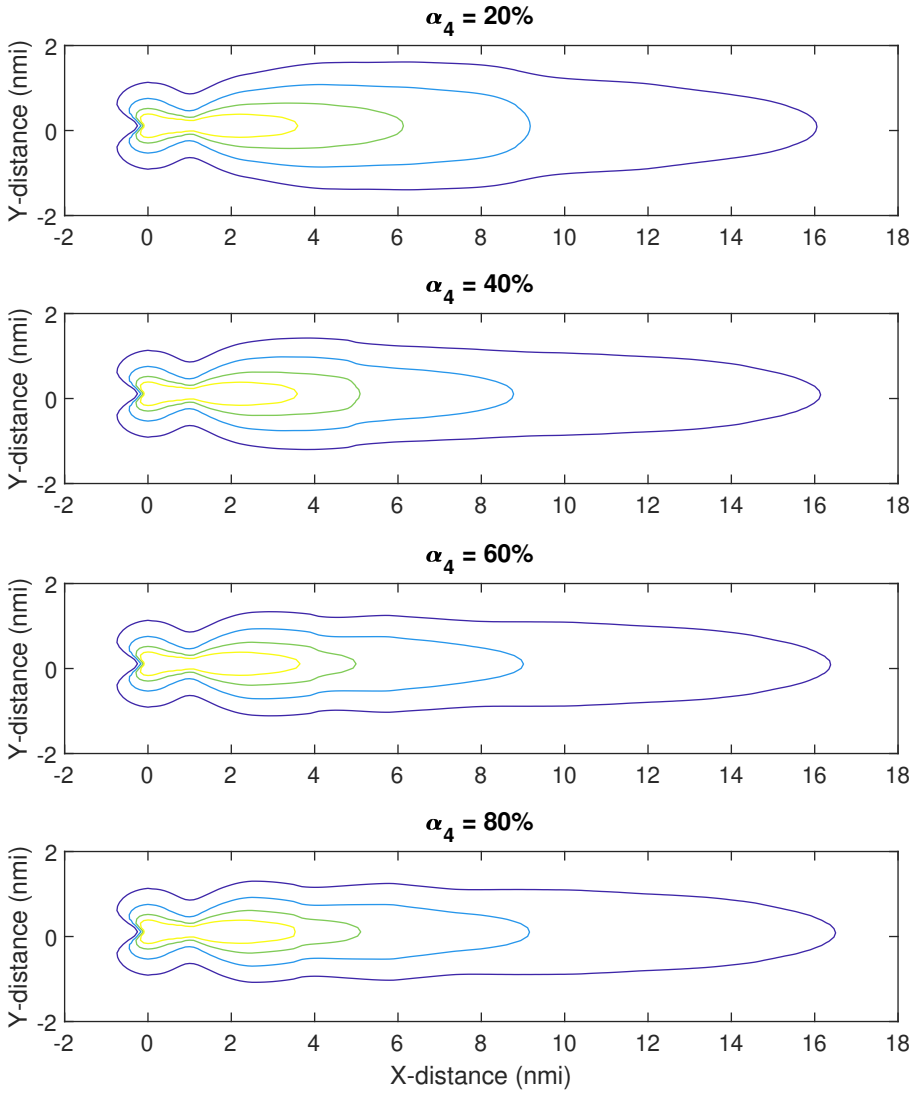

Figure 4.18: Variation of 75, 80, 85, and 90 dB SEL noise contours with energy share percentage

percent. A higher value indicates more energy is allocated for acceleration than climbing. Therefore, at higher values, the aircraft's climb gradient is quite low. There are three distinct acceleration steps in the procedural profile definition with a common value of energy share percentages across them. As the aircraft has an overall lower rate of climb, the transitions between these three acceleration steps occur at a lower altitude. Consequently, their effects are more pronounced on the noise contours. For the low energy share percent, the climb rate is higher and the transitions happen at a higher altitude, thus making their effect on the noise contour less pronounced.

Finally, the variation of the noise contours with the ambient temperature is shown in Figure 4.19. In this case, the temperature is varied between its four possible values, while the other parameters are held constant at their central values, $\alpha_1 = 162150\, lb_m,\ \alpha_2 = 0.90,\ \alpha_3 = 1200\ ft,\ \alpha_4 = 40\%$. The corresponding values of the contour dimensions are shown in Table 4.16.

Table 4.16: Variation on contour dimensions with ambient temprature

Ambient	Area, nmi^2				Length, nmi			
Temperature	75	80	85	90	75	80	85	90
40	42.02	12.59	4.31	1.58	19.18	9.81	5.34	3.75
60	32.11	11.25	4.21	1.57	16.89	9.22	5.38	3.77
80	22.38	8.32	3.55	1.30	13.86	7.92	5.28	3.48
100	19.06	6.86	3.13	1.10	12.49	6.78	5.17	3.27

Finally, the final parameter, ambient temperature, shows a strong effect on the noise contours. Both the length of the outer two contours and the areas of all contours show a inverse correlation with the ambient temperature. It is observed that at lower temperatures, the contour lengths are significantly higher for the 75 and 80 dB SEL contours. The entire contour for these two levels seems to shrink in both length and width at higher temperatures. This is confirmed by the values in Table 4.16, which show that the area of the 75 dB SEL contour for 40 °F is more than double that for 100 °F.

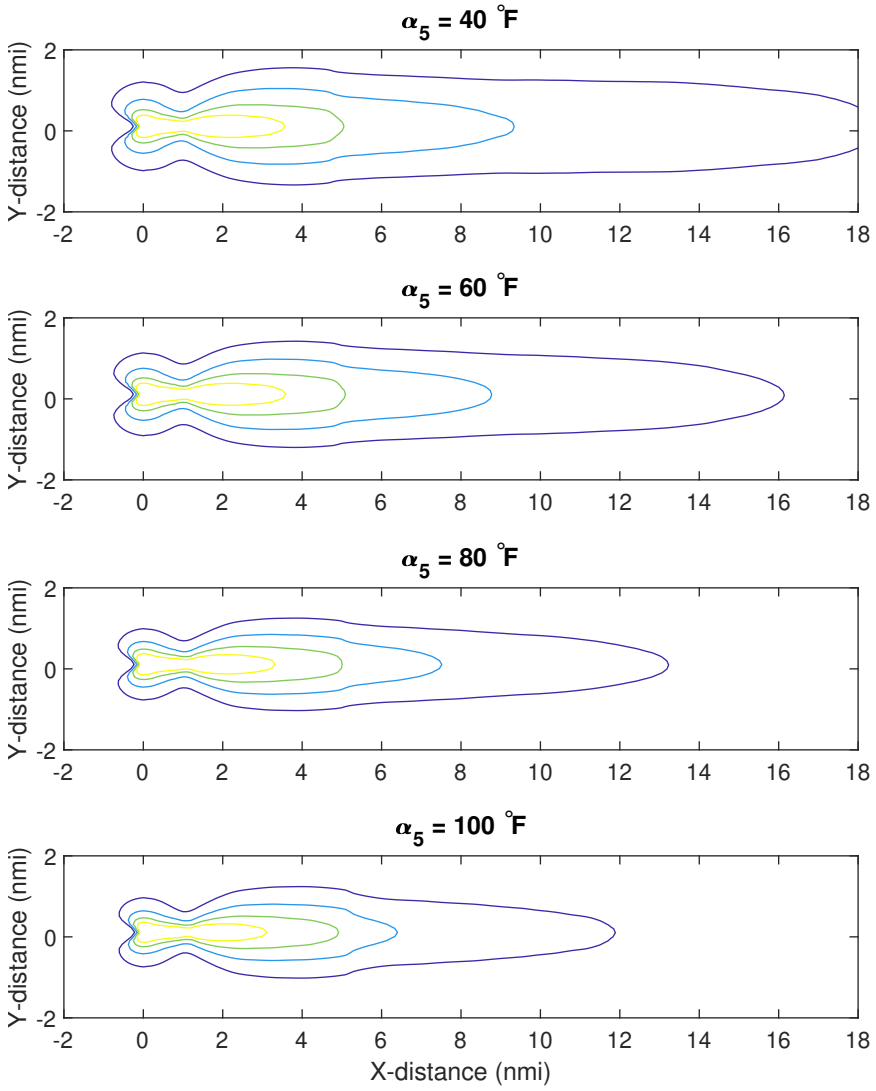

Figure 4.19: Variation of 75, 80, 85, and 90 dB SEL noise contours with ambient temperature

The explanation for this is that sound travels faster at lower temperatures and is less affected by atmospheric effects. Thus the noise is able to reach receptors faster and with higher amplitude at lower temperatures. This explains the trends observed in the contour areas and lengths. The effects of ambient temperature on noise propagation is explained by several adjustments, such as the acoustic impedance adjustment (AI_{ADJ}) in AEDT's technical manual [107].

Step-wise regression analysis

With the initial analysis using visualizations with the OFAT analysis complete, a more global sensitivity analysis can be conducted with a step-wise regression model. Before building a regression model however, it is generally recommended that the input and output variables of the model be scaled to be on a consistent basis.

The input parameters are all varied along linear scales, and thus a linear scaling is appropriate. The input parameters are scaled based on their minimum and maximum values to lie on a range of [0,1]. The formula for this scaling is –

$$\hat{\alpha}_i = \frac{\alpha_i - \min \alpha_i}{\max \alpha_i - \min \alpha_i} \tag{4.20}$$

The output parameters however are distributed similar to a normal distribution and Gaussian scaling is used for them instead. The effect of this scaling on the four contour areas and lengths is shown in Figure 4.20 and Figure 4.21.

$$\hat{Y}_i = \frac{Y_i - \mu(Y)}{\sigma(Y)} \tag{4.21}$$

These scaled/normalized inputs and outputs were then used to build regression models in JMP [245]. A step-wise regression model was built for each of the eight outputs. A response surface type of model was selected for fitting. A response surface includes linear, quadratic terms, and cross-terms. As there are five input parameters, a total of 21 terms are

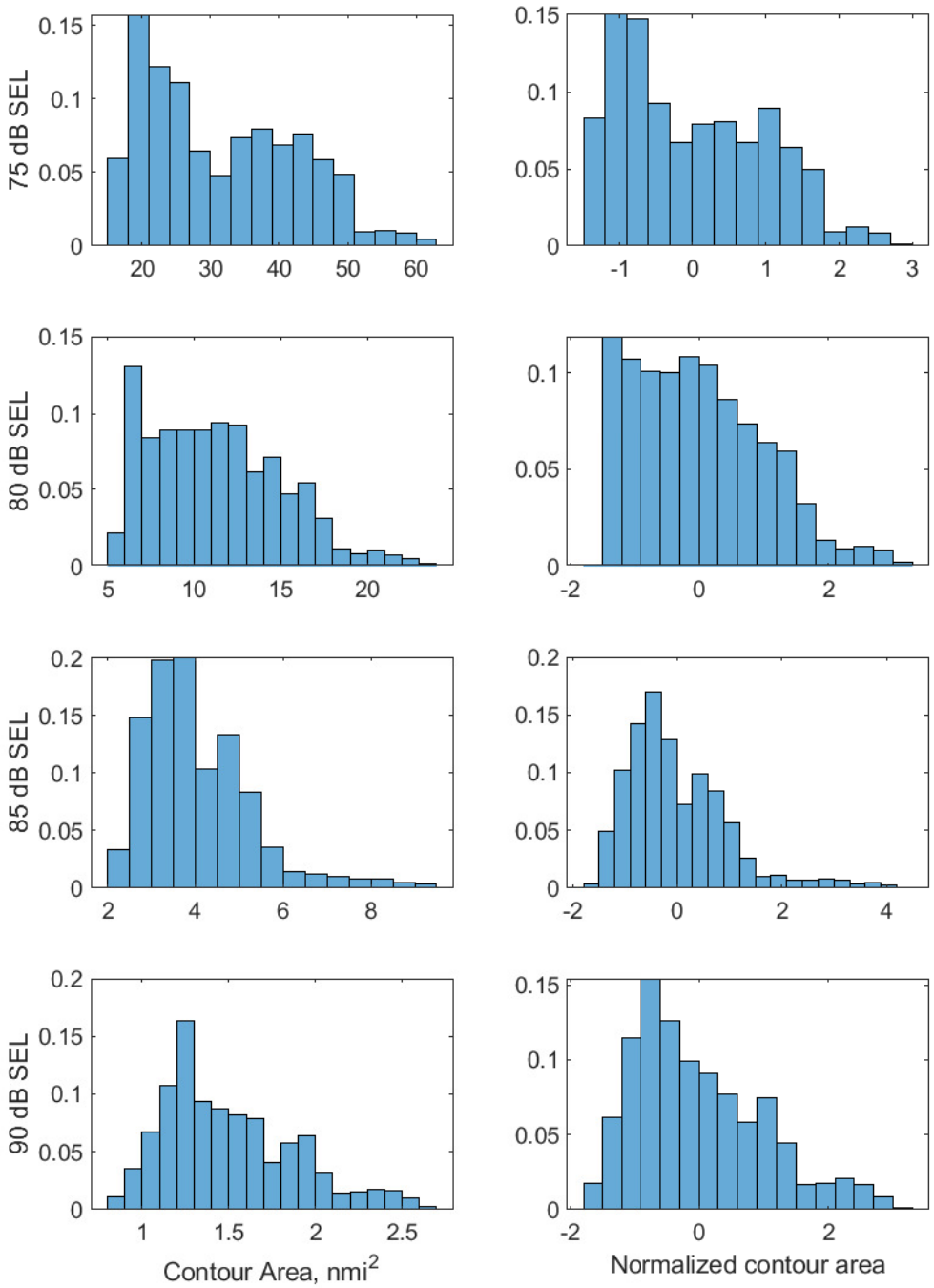

Figure 4.20: Normalization of contour areas

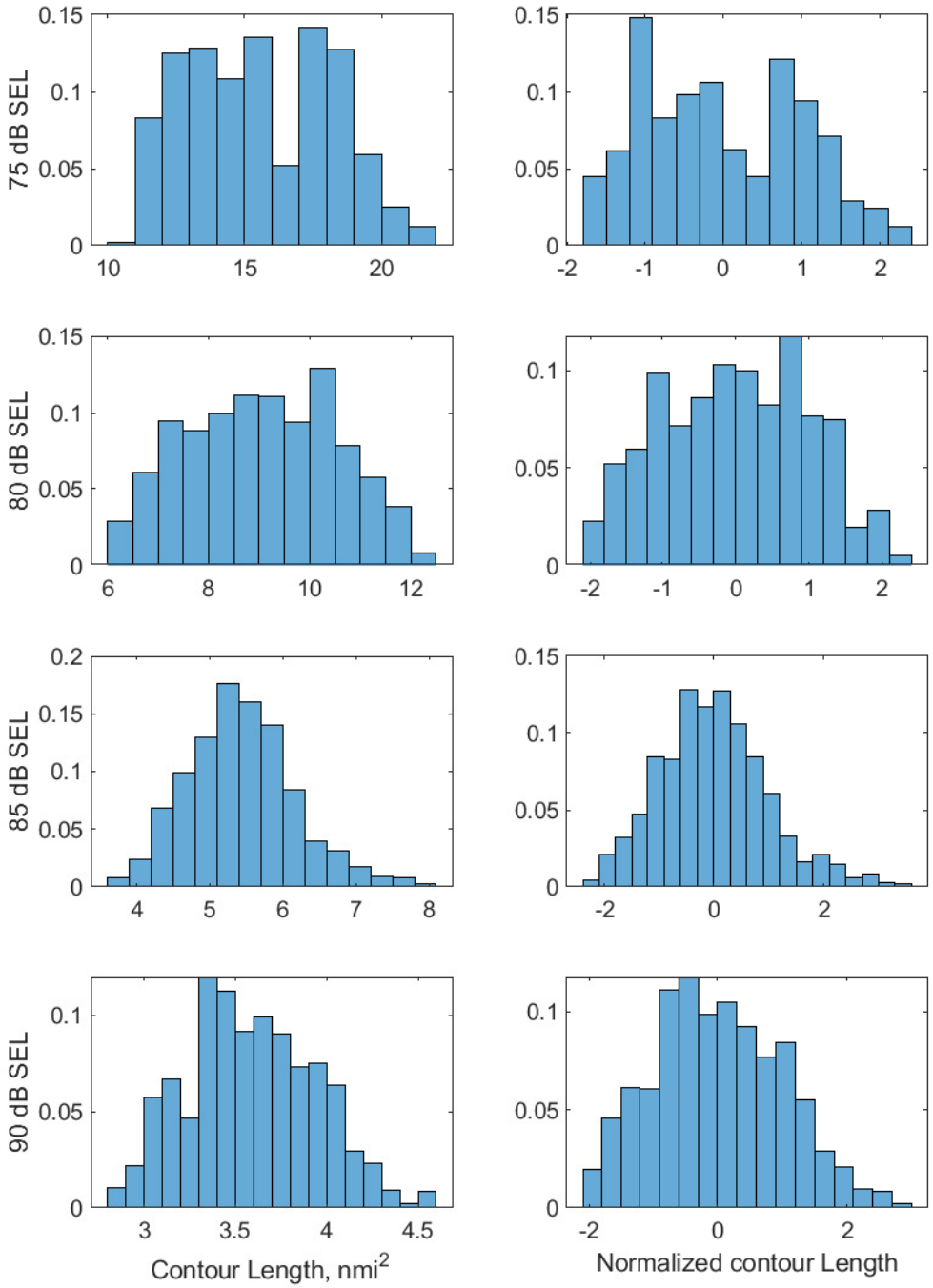

Figure 4.21: Normalization of contour lengths

possible, as shown in the following equation –

$$\begin{aligned} Y = {} & \beta_0 + \beta_1 X_1 + \beta_2 X_2 + \beta_3 X_3 + \beta_4 X_4 + + \beta_5 X_5 \\ & + \beta_{11} X_1^2 + \beta_{22} X_2^2 + \beta_{33} X_3^2 + \beta_{44} X_4^2 + \beta_{55} X_5^2 \\ & + \beta_{12} X_1 X_2 + \beta_{13} X_1 X_3 + \beta_{14} X_1 X_4 + \beta_{15} X_1 X_5 \\ & + \beta_{23} X_2 X_3 + \beta_{24} X_2 X_4 + \beta_{25} X_2 X_5 \\ & + \beta_{34} X_3 X_4 + \beta_{45} X_4 X_5 \\ & + \beta_{45} X_4 X_5 \end{aligned} \tag{4.22}$$

The step-wise model fit option in JMP implements different user options for direction of variable inclusion/exclusion and for different stopping criteria. Although not all options affected the model fit, these settings were investigated and the best options were selected which led to the most accurate model fit. For conciseness, only the model fitting outcomes for the 75 dB contour are presented here.

The general steps followed for model fitting are outlined below –

1. $\frac{1}{6}$th of the 960 total data points were randomly selected and set aside for model validation. The remaining 800 data points were used to train the model.

2. The selected Response Surface model was trained and the sequence of steps from the step-wise regression was saved. Each step contained information about the variable added, and the associated R_2 along with additional measures of statistical significance.

3. The obtained model was then evaluated at the validation points and the errors between the predicted and the actual values were analyzed. A good model has a high R^2, low Model Fit Error (MFE), and a low Model Representation Error (MRE).

The three goodness of fit metrics mentioned above are summarized in Table 4.17. The distribution of the Model Fit Error and Model Representation Error is visualized

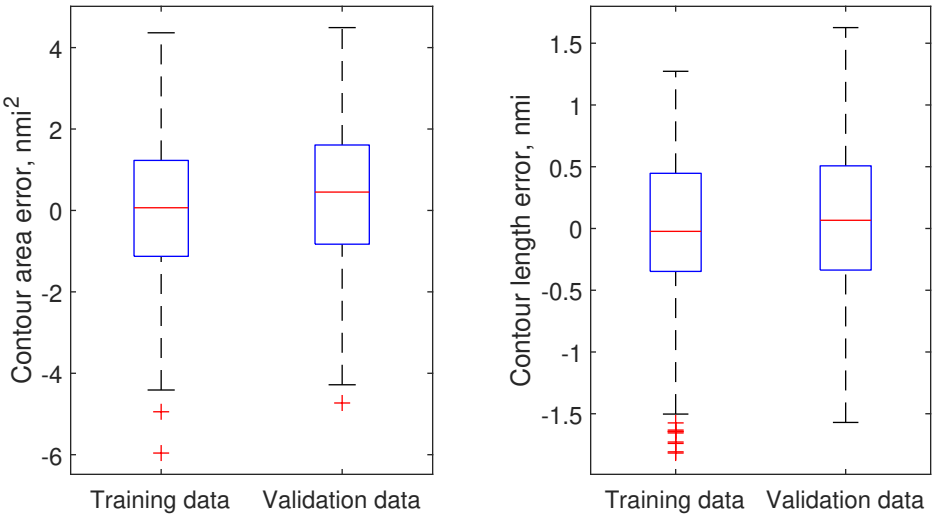

Figure 4.22: Distribution of the Model Fit Error and Model Representation error for the step-wise regression model

in Figure 4.22.

Table 4.17: Summary statistics for regression model errors

	75 dB SEL Area	75 dB SEL Length
R^2	0.9732	0.9540
MFE RMS	1.7443 nmi^2	0.5554 nmi
MRE RMS	1.8048 nmi^2	0.5915 nmi

With the regression models created for all eight contour dimension measures, the relative importance of each variable in the regression model was obtained. The top eight variables in terms of cumulative contribution to the R^2 value are shown in Table 4.18 with the variable labels described in Table 4.19. Not all variables are included as some such as the square of the altitude of acceleration initiation α_3^2 were not present in the list of any of the contour dimension regression models.

Some notable observations from Table 4.18 are listed below –

1. The single most important parameter which influences all contour dimensions is the ambient temperature. This is an important observation as departure operations are often not optimized for ambient conditions such as the temperature.

Table 4.18: Rankings of the top eight parameters for each contour dimension regression model

Variable	Area of SEL contour				Length of SEL contour			
	75 dB	80 dB	85 dB	90 dB	75 dB	80 dB	85 dB	90 dB
α_1	4	6	7	5	2	2	2	1
α_2	3	3	3	1	3			
α_3		7						
α_4	2	2	2				3	
α_5	1	1	1	2	1	1	1	2
α_2^2						8		
α_4^2	5	4	5		8	3	4	
α_5^2	6			4			7	5
$\alpha_1 \times \alpha_4$					7			
$\alpha_1 \times \alpha_5$	8				6	7		
$\alpha_2 \times \alpha_3$				8				6
$\alpha_2 \times \alpha_4$		8	6	6			5	3
$\alpha_2 \times \alpha_5$	7	5	4	3	4	5	6	
$\alpha_3 \times \alpha_4$						6	8	8
$\alpha_3 \times \alpha_5$								7
$\alpha_4 \times \alpha_5$			8	7	5	4		4

2. For contour areas, the next most important parameters are the energy share percentage values and the takeoff thrust reduction values. These observations are consistent with the findings from the OFAT sensitivity analysis. The remainder of the important variables depend on the noise level of the contour for which the regression is built.

3. For contour lengths, the next most important parameter is the takeoff weight. Again, this observation is consistent with the findings from the OFAT sensitivity analysis. As with the contour areas, the next important factors depend on the noise level of the contour.

4. During the OFAT analysis, the altitude for acceleration initiation was identified to not have much effect on noise contours. Here, the effects of this parameter do not

Table 4.19: Description of variables used to build regression models for contour dimensions

Variable	Description	Variable	Description
α_1	Weight	$\alpha_1 \times \alpha_2$	Weight $\times$ Thrust
α_2	Thrust	$\alpha_1 \times \alpha_3$	Weight $\times$ Altitude
α_3	Altitude	$\alpha_1 \times \alpha_4$	Weight $\times$ Energy Share
α_4	Energy Share	$\alpha_1 \times \alpha_5$	Weight $\times$ Temperature
α_5	Temperature	$\alpha_2 \times \alpha_3$	Thrust $\times$ Altitude
α_1^2	Weight^2	$\alpha_2 \times \alpha_4$	Thrust $\times$ Energy Share
α_2^2	Thrust^2	$\alpha_2 \times \alpha_5$	Thrust $\times$ Temperature
α_3^2	Altitude^2	$\alpha_3 \times \alpha_4$	Altitude $\times$ Energy Share
α_4^2	Energy Share ^{2}	$\alpha_3 \times \alpha_5$	Altitude $\times$ Temperature
α_5^2	Temperature ^{2}	$\alpha_4 \times \alpha_5$	Energy Share $\times$ Temperature

appear in the top 8 ranked important variables for most contour dimension regression models. Where they do appear, the ranking is quite low. For example, for the 80 dB SEL contour area, the altitude for acceleration initiation is the 7th most important factor.

The variation of the R^2 value for each contour dimension regression model with their respective top eight variables is visualized in Figure 4.23. As predicted, the inclusion of the first few top ranked parameter quickly accounts for most variance in the contour dimensions.

Notable, the inclusion of the top 4 variables accounts for an R^2 value of at least 0.80. In all cases except the 85 dB contour length, the inclusion of top 8 ranked variables yields an R^2 value of at least 0.90.

4.4.5 Summary and evaluation of Hypothesis

Experiment 1.3 was designed to evaluate and identify the primary drivers of aviation noise to enable the efficient exploration of the design space of aircraft trajectories. The original four parameters of procedural profile definition were paired with an additional parameter

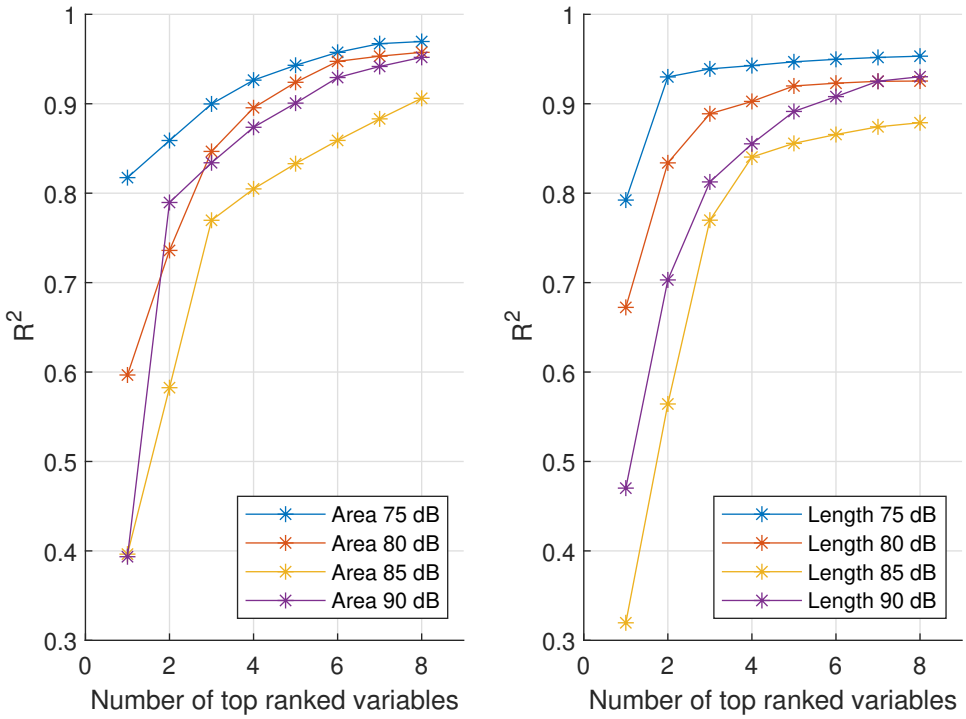

Figure 4.23: Variation of model R^2 with the top eight ranked variables

in the form of ambient temperature. This led to the creation of a set of 960 test cases, with each of the 240 possible procedural profiles being flown at 4 different ambient temperature conditions. A dependent variation of dew point temperature was added to hold the relative humidity at a constant level and control for effects of humidity.

This set of operations was then modeled in the Aviation Environmental Design Tool to obtain resultant noise metrics. The operations were modeled at the KATL airport and the Sound Exposure Level noise metric was modeled at a grid of receptor points. The grid was sized with appropriate dimensions, resolution, and alignment to ensure that the noise dB levels of interest would be captured correctly. Noise contours were then created as a post-processing step, and their dimensions in the form of contour area and contour length were computed.

Two types of sensitivity analysis were conducted. A One Factor At a Time analysis was conducted to get an understanding of the effect of individual parameters on the noise contours. An analysis was conducted with visual comparisons of contour plots and numeric

comparison of the contour dimensions. This type of sensitivity analysis was of a medium scope, lying between local and global sensitivity analyses.

The second analysis was conducted in the form of a step-wise regression. The collected contour dimensions and input variables were normalized to be on similar relative scaled. The JMP software was used to perform step-wise regression assuming a response surface model type. Each step of the step-wise regression provided insight into the parameters which had the most effect on the modeled dimension. It was observed that the ambient temperature was the most important parameter for the prediction of contour dimensions. Takeoff thrust and energy share percentage were important for the prediction of contour areas, whereas the takeoff weight was important for contour length. The two analyses also revealed that the altitude of acceleration initiation does not have a major impact on any of the modeled contour dimensions.

Revisiting Hypothesis 1.3, the requirement was to perform a screening test and identify the primary drivers behind aviation noise. The accompanying Experiment 1.3 performed two types of sensitivity analyses to identify the importance of parameters and confirm that such a screening is possible. Thus, Experiment 1.3 is considered successful and Hypothesis 1.3 is accepted.

4.5 Summary of Research Area 1

This chapter presented the findings from Experiments 1.1, 1.2, and 1.3 which supported their respective Hypotheses. All formulated Hypotheses were accepted, and the Research Questions leading to those hypotheses were answered.

The original high-level Research Question 1 is recapped below. The three requirements of representation, scalability, and exploration were addressed by Research Questions 1.1, 1.2, and 1.3 respectively.

Research Question 1

How can the input space of aircraft trajectories be represented to enable parametric quantification and optimization?

Research Question 1.1 led to the creation of a process in which real-world time-series based flight data could be represented as a set of parameters. This process was labeled as the *inverse map*, and was demonstrated on a set of 1361 real-world flights obtained from the OpenSky Network. The process involved the creation of a library of profiles with pre-defined parameter values and their resultant trajectories and performance. Real-world trajectories were then assessed in their similarity to this pre-defined library with the help of a defined similarity metric. The most similar pre-defined profile was then assigned as the inverse-mapped parametric definition for the real-world flight.

Research Question 1.2 led to the development of clustering processes to group similar flights together so that representative from each group could be efficiently modeled for environmental impact analyses. An advanced similarity metric was defined to determine the similarity between two real-world flights. Three different clustering algorithms were implemented and deployed on a set of 5070 flights. Cluster verification was also performed using three cluster scoring metrics. The process showed that with the help of clustering algorithms, real-world flight data could be grouped by similarity.

Research Question 1.3 was motivated by the desire to efficiently explore the design space of aircraft trajectories in the context of aviation noise. A set of 240 procedural profiles were modeled at 4 ambient temperature conditions. The resultant noise metrics were quantified on a grid of receptors and noise contours were created. The area and lengths of contours for 75, 80, 85, and 90 dB SEL were computed and fitted with a step-wise regression model. The model took the form of a Response Surface Equation and the independent variables were the five parameters, their squared terms, and their cross terms. The step-wise regression model showed a ranking of parameters based on their importance

for each regression model.

Together, these three RQs, their accompanying hypotheses, experiments, and the techniques developed in those experiments satisfied all requirements of the high-level Research Question 1. This concludes the discussion on Research Area 1.

CHAPTER 5

RAPID MODELING OF AVIATION NOISE

This chapter presents the research and findings from Research Area 2, i.e. the rapid modeling of aviation noise. As a quick recap, the high-level Research Question for this is mentioned below.

Research Question 2

How can the process of computing aviation noise metrics be made more computationally efficient?

Two focused research areas emerged from this high-level Research Question – the reduction of dimensionality of original high-dimensional data, and the creation of surrogate models in the lower-dimensional space. These areas were addressed with two specific Research Questions and their associated Hypotheses. Each Hypothesis was then supplemented with a formulation to test the Hypothesis. This chapter will present the results of the Experiments which support each Hypothesis.

This chapter begins with section 5.1 which describes the dataset being used in Experiments 2.1 and 2.2. Following this, section 5.2 and section 5.3 provide the details of the experimental setup, obtained results, and analysis of the results. The resulting Reduced Order Model or field surrogate model is described insection 5.4. Finally section 5.5 provides a summary of the chapter.

5.1 Description of dataset used

Before the creation of any models, the underlying data needs to be gathered. In Experiment 1.3, a large set of noise results was generated to determine the effects of different

parameters on the SEL aviation noise metric. A total of 960 cases were modeled in the Aviation Environmental Design Tool at the KATL airport. Each case resulted in the SEL noise metric dB value being computed on a receptor grid of $401 \times 81 = 32481$ points.

The analyses performed in Experiment 1.3 however, were limited to scalar valued aggregated metrics, instead of analyzing the entire grid as a whole. The sensitivity analysis based on step-wise regression modeling used eight aggregated scalar valued measures – the areas and lengths of contours for 75 dB SEL, 80 dB SEL, 85 dB SEL, and 90 dB SEL. Such type of analysis is typical in the field of aviation noise quantification and mitigation where aggregated measures are modeled and minimized.

Another type of common analysis focuses on the noise grid, but only at a select few locations. Thus, raw noise metrics can be quantified/optimized instead of their aggregated measures. A common example of this are the three locations for which noise certification is performed – flyover, sideline, and approach (see Figure 1.5).

There is a lot of information loss when such type of analyses are conducted, which greatly limits the usefulness of such analysis. In the two types of analyses mentioned above, information about different locations on the grid is lost or information about the contour shape is lost. Aggregated metrics such as contour areas and lengths do not retain information about the shape of the contour. In fact, different shapes of the contour can lead to the same area and length.

Although such analyses are of limited use, they are the best analyses which can be conducted on current state-of-the-art noise modeling capabilities. In order to scale analyses up to entire noise grids with tens of thousands of points, a whole new class of models is needed. One such modeling process making use of Model Order Reduction is described in Experiments 2.1 and 2.2[1].

[1]Parts of the research described in this chapter are documented in the following publication –

- A. Behere, D. Rajaram, T. G. Puranik, M. Kirby, and D. N. Mavris, "Reduced order modeling methods for aviation noise estimation," *Sustainability*, vol. 13, no. 3, 2021, ISSN: 2071-1050. DOI: 10.3390/su13031120. [Online]. Available: https://www.mdpi.com/2071-1050/13/3/1120 [246]

5.1.1 Dimensionality of noise metric modeling

Throughout this dissertation, it has been noted on several occasions that the quantification of aviation noise is a complex process with the involvement of many high-dimensional datasets. Before proceeding with the experiments, it is helpful to make a clear distinction in which high-dimensional dataset is being addressed.

The input space of the aviation noise modeling process is one such high-dimensional dataset. As noted in Observation 3 from subsection 2.1.2, there are a very large number of parameters and their possible values which influence aviation noise metrics. Some of these include external factors which cannot be controlled such as ambient temperature, humidity, wind speed and direction etc., and pilot-controllable factors such as the choice of thrust, procedure being flown etc. The input space being high-dimensional is a problem only when the model itself is computationally expensive, as is the case with aviation noise computation.

The process itself is computationally expensive because the output space of this problem is also high-dimensional. This dimensionality is directly related to the typical size of noise grids. Noise grids have to be defined so that – (a) their overall dimensions sufficiently cover the area of interest, and (b) their resolution is sufficiently fine/dense, so that smooth contour lines can be created. This results in typical noise grids with $\mathbb{O}(10^5 - 10^6)$ points.

The dimensionality which is addressed in this chapter refers to the output space of the aviation noise quantification problem. The idea is that by addressing this dimensionality, the complexity of the noise quantification process can be reduced. This will allow for more points in the input space to be evaluated, thereby also helping address the dimensionality of the input space, albeit indirectly.

5.2 Experiment 2.1

In this section, the experimental setup and results for RQ2.1 are explained. For reference, RQ 2.1 and H2.1 are repeated below –

Research Question 2.1

How can the high dimension of the solution space be addressed?

Hypothesis 2.1

If Model Order Reduction techniques are used on the noise grid data, then the solution space can be projected onto a lower dimension space.

The purpose of this experiment is to demonstrate a method by which the high-dimensional data can be converted into a lower-dimensional space which is easier to model. By performing this conversion, the amount of outputs to be predicted by a noise quantification model is reduced drastically. Model Order Reduction (MOR) techniques from literature were researched and the Principal Component Analysis (PCA) or Proper Orthogonal Decomposition (POD) technique is proposed to be implemented here.

5.2.1 Principal Component Analysis

The PCA/POD method is a way of reframing a set of data along its principal axis. The method relies on the Singular Value Decomposition (SVD), which is a generalized form of the well-known Eigendecomposition of square matrices. The method relies on identifying orthogonal directions of variation in the dataset which are linearly uncorrelated. Any datapoint can then be represented by a set of coordinates along each such orthogonal direction. Typically, it is observed that the first few directions are sufficient to adequately recreate the original datapoint with acceptably low errors. Thus, a high dimensional

data point is easily represented by its coordinates along a handful of principal orthogonal directions.

5.2.2 Formulation of PCA for aviation noise

The first step in performing PCA is to gather the data in a suitable format. Aviation noise grids are typically represented as 2D matrices, with a row of the matrix representing a row of receptor points in the East-West direction, and a column of the matrix representing a row of receptor points in the North-South direction. Even if an irregularly shaped grid of receptor points is available, the first step is to vectorize the obtained noise metric values. The idea is to serialize the receptor points and collect all data into a single vector w. This process is shown in Figure 5.1.

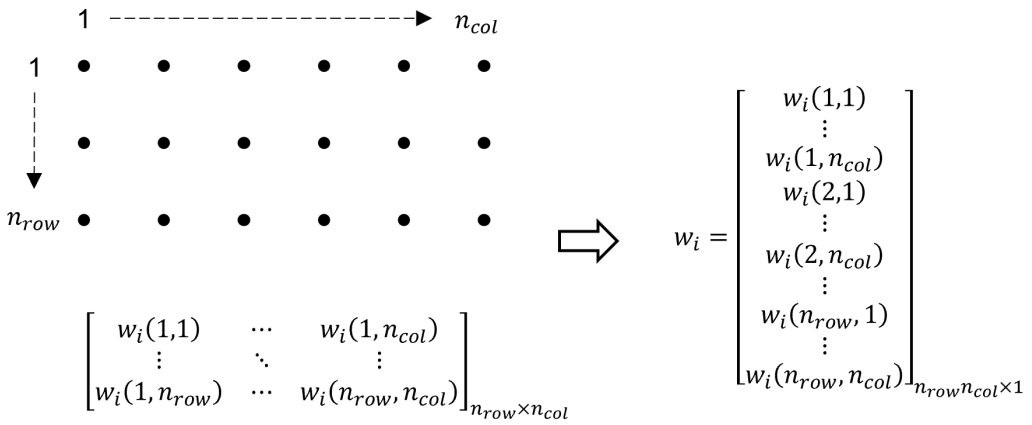

Figure 5.1: Representation of the conversion of 2D noise grid data matrix into a column vector

The obtained noise vector is a function of the entire input space of the aviation noise model. For the context of this experiment, the input space is considered to be the set of five parameters α_i, and their respective values. Here, let $\mu = \{\alpha_1, \alpha_2, \alpha_3, \alpha_4, \alpha_5\}$ represent the input space. Then, $w(\mu)$ represents the vectorized noise grid obtained as a function of the input space μ.

The following notation is used for the formulation of the PCA –

- $\mu \in \mathbb{R}^d$ represents the input space of dimension d. The dimension is nothing but the number of parameters which define the input space, which in this context is five.

- $w(\mu) \in \mathbb{R}^m$ represents the vectorized noise grid obtained of size $m \times 1$. w is the high dimensional output which has to be modeled, with $m \sim \mathbb{O}(10^5)$. Note that for brevity, the dependency of w on μ may not be explicitly mentioned. In such cases, w_i is understood to be $w(\mu_i)$. Such a noise grid is also referred to as the full-order solution.

- $W = [w(\mu_1)\ w(\mu_2)\ \ldots\ w(\mu_n)] \in \mathbb{R}^{m \times n}$ represents a set of n noise grids evaluated at the input parameters μ_i collected together as column vectors to form a matrix. In this context, $n = 960$. In the terminology of MOR, W is referred to as the *snapshot matrix* consisting of various *snapshots* w_i as column vectors.

With the notation and definitions complete, the steps for the PCA can be performed.

Step 1: Computation of principal components via Singular Value Decomposition

The starting point for this step is the snapshot matrix $W_{32481 \times 960}$ which is factorized using the Singular Value Decomposition –

$$W_{m \times n} = \Phi_{m \times m} \Sigma_{m \times n} V^T_{n \times n} \tag{5.1}$$

where Φ, V are real-valued square matrices, and Σ is a rectangular diagonal matrix with non negative real numbers on the diagonal. It is noted that apart from the possible rearrangement of the columns of Φ, V and the diagonal entries of Σ, the SVD is a unique decomposition. The matrices Φ, V are orthogonal matrices, implying that their columns and rows are mutually orthonormal. The diagonal entries of Σ are known as the singular

values σ_i of matrix W.

$$\Sigma_{m\times n} = \begin{bmatrix} \sigma_1 & 0 & \dots & 0 \\ 0 & \sigma_2 & \dots & 0 \\ \vdots & \vdots & \ddots & \vdots \\ 0 & \dots & 0 & \sigma_n \\ 0 & \dots & \dots & 0 \\ \vdots & \vdots & \vdots & \vdots \\ 0 & \dots & \dots & 0 \end{bmatrix}_{m\times n} \tag{5.2}$$

Typically, the diagonal entries of Σ are arranged in a descending order, so that $i < j \implies \sigma_i \geq \sigma_j$

Step 2: Selection of Principal Directions

The next step is to identify the principal directions so that the basis of the lower-dimensional space can be constructed. To aid in this, a selection criteria known as the Relative Information Content (RIC) is developed. The RIC is a measure which is used to rank the relative importance of columns of Φ.

$$RIC_i = \frac{\sum_{j=1}^{i} \sigma_j^2}{\sum_{j=1}^{n} \sigma_j^2} \tag{5.3}$$

By design, the RIC_i value increases from 0 to 1 as i increases. The idea is to select a particular value of i, say k such that RIC_k is at an acceptable threshold. By the nature of the PCA method, $k \ll m$. With a chosen k, the original snapshot matrix W can be

approximated as

$$W_{m\times n} \approx \Phi_k \Sigma_k V_k^T \tag{5.4}$$

where $\Phi_k \in \mathbb{R}^{m\times k}$, $\Sigma_k \in \mathbb{R}^{k\times k}$, and $V_k \in \mathbb{R}^{k\times n}$. This approximation of W is guaranteed to minimize the reconstruction error in the L_2 norm.

Step 3: Expressing noise grids in new basis

The principal directions obtained in Φ_k serve as the basis for the reduced order representation of full order solutions. Thus, any full order solution w can be represented by a linear combination of these basis vectors, plus some error. In practice, instead of projecting the complete full order solution w, only the difference from the mean $\bar{w}$ is projected. Note that this difference from the mean is still a high-dimensional vector.

$$\bar{w} = \frac{\sum_{i=1}^{n} w_i}{n} \tag{5.5}$$

$$w_i' = w_i - \bar{w} \tag{5.6}$$

Representing this deviation from the mean as a linear combination of the k basis vectors, the following expression is obtained

$$w_i' \approx a_{i,1}\phi_1 + a_{i,2}\phi_2 + \ldots + a_{i,k}\phi_k \tag{5.7}$$

$$= \sum_{j=1}^{k} a_{i,j}\phi_j + e_{proj,i} \tag{5.8}$$

Noting that w_i' is a shorthand for $w'(\mu_i)$, the coefficients of the linear combination are also functions of the input space, i.e. $a_{i,j} = a_j(\mu_i)$. Given that the basis of linear combination

are orthonormal, these coefficients are simply the component of w_i' along each basis vector.

$$a_j(\mu_i) = \langle w(\mu_i) - \bar{w}, \phi_j \rangle \tag{5.9}$$

$$= \langle w'(\mu_i), \phi_j \rangle \tag{5.10}$$

Note that with this projection, each full order solution w_i of size $m \times 1$ has been reduced to a collection of coordinates $\{a_{i,1}, a_{i,2}, \ldots, a_{i,k}\}$ along the chosen k principal directions. Given that $k \ll m$, the dimensionality reduction is complete.

Step 4: Quantifying the error due to projection

As noted in the equations above, the choice of neglecting the $k+1, k+2, \ldots m$ remaining principal directions leads to an error due to projection, labeled here as e_{proj}. This error can be thought of as the difference between the original high-dimensional vector and the projected lower-dimensional vector as shown in Figure 5.2. This error is computed as –

$$e_{proj,i} = w_i' - \sum_{j=1}^{k} a_{i,j}\phi_j \tag{5.11}$$

Step 5: Recreating high-dimensional noise grids

At any point, if the high-dimensional form of the noise grid is required, it can be approximated by the following equation –

$$w_{proj,i} = \bar{w} + \sum_{j=1}^{k} a_{i,j}\phi_j \tag{5.12}$$

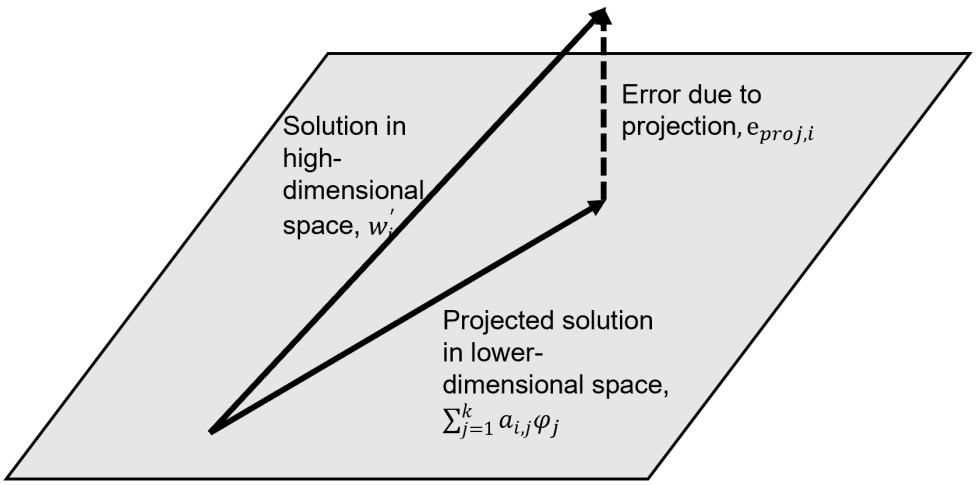

Figure 5.2: Visualization of projection from high-dimensional to lower-dimensional space

5.2.3 Results of Model Order Reduction

With the process formulation complete, this subsection presents the results from the application of the PCA method to the set of 960 noise results.

Choice of number of principal directions

The obtained noise results were compiled into a snapshot matrix $W_{32481\times960}$. The SVD of this matrix yielded the singular values, leading to the computation of the Relative Information Content (RIC). As expected, the RIC value quickly approached 1.00 with the first few principal directions, as shown in Figure 5.3. In fact, the first 12 principal directions were sufficient to produce the RIC value of 99.9%.

Projection to lower-dimensional space

With the 12 principal directions (also called basis vectors) were identified, the next step was to project each of the 960 noise results onto the space spanned by these 12 principal directions. The error resulting from these projections was computed. The relative error was

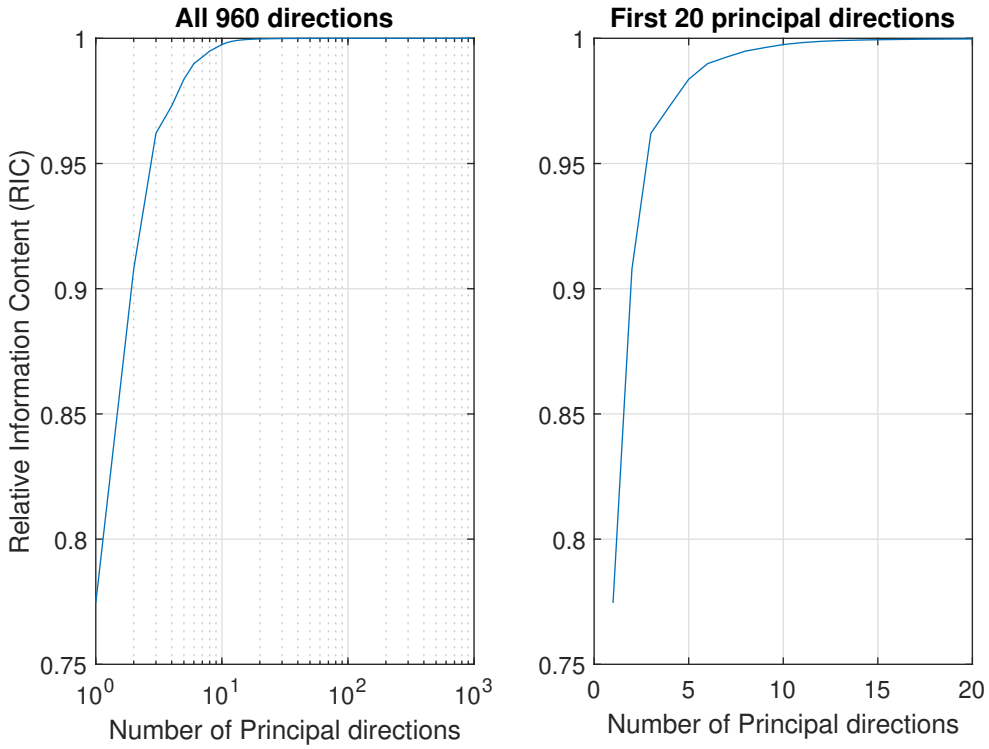

Figure 5.3: Variation of RIC with number of chosen principal directions

then computed with the following formula –

$$e_{proj,rel,i} = \frac{\|e_{proj,i}\|}{\|w_i\|} \tag{5.13}$$

The obtained relative projection error distribution is visualized in Figure 5.4 and summarized in Table 5.1. It is observed that most of the error variation is between the values of 0.12% to 0.38% with a few outliers. These low error values indicate that very little information was lost due to the projection, and that much of the original noise grid could be preserved by the projection. However, it is also noted that there were 44 outliers as indicated by the Boxplot, which need to be investigated further. While the error for these outliers was higher than the rest of the cases, the value of the relative error is still no more than 0.7%.

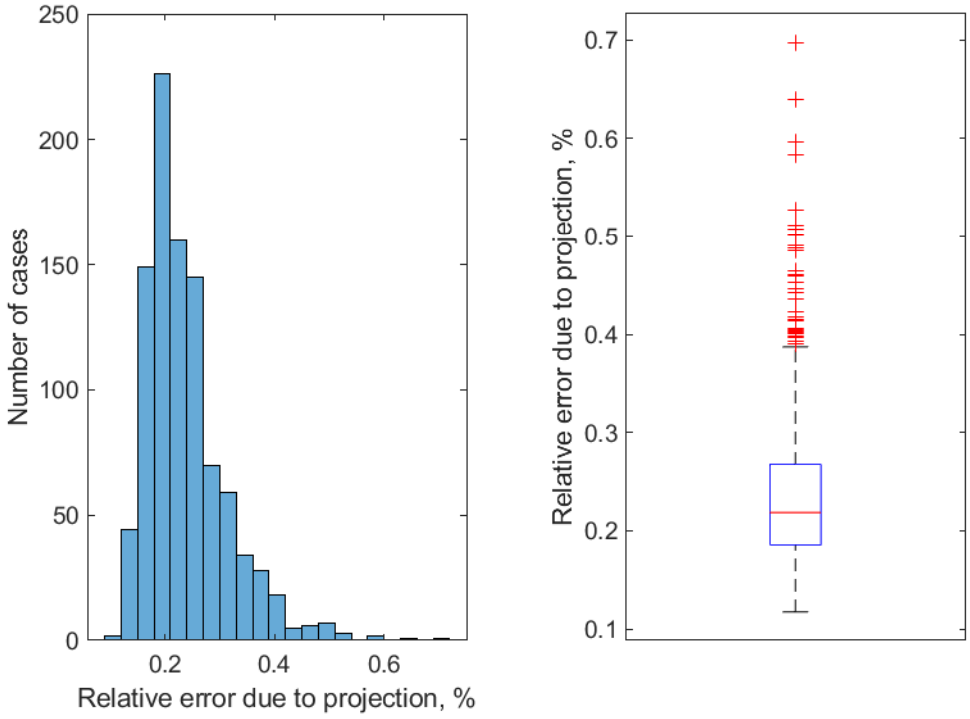

Figure 5.4: Relative error introduced by the projection to lower-dimensional space

Visualization of projected noise grids.

In addition to the analysis of the projection error, it is also helpful to visualize how the projection to lower-dimensional space affected the noise grids. Therefore, the two extreme cases of minimum and maximum projection error are visualized here.

As noted previously, the projected noise grid vectors are constructed as a linear combination of the twelve basis vectors. In other words, the noise grid vectors were represented by twelve coordinates in the twelve principal directions. Thus, the reconstructed grid can be thought of as a 12th order projection. In addition to this, the 1st, 4th, and 8th order projections are also visualized here which correspond to RIC values of 77.45%, 97.30%, and 99.49% respectively.

To visualize the reconstructed noise grid values and compare it to the original full-order solutions obtained from AEDT, a contour comparison plot it made with a colormap background. The features of this type of plot are outlined below –

Table 5.1: Summary statistics for relative error due to projection

Summary Statistic	Value
Minimum	0.12
Median	0.22
Mean	0.24
Maximum	0.7
Range	0.58
Standard Deviation	0.0752
Number of outliers	44

1. Solid contour lines represent the original solutions from the full-order model. 4 contour lines are presented representing the 90 dB SEL (innermost contour), 85 dB SEL, 80 dB SEL, and the 75 dB SEL (outermost).

2. Dashed contour lines represent the projected noise grid recreations, created in the same levels.

3. The background of the plots is a colormap showing which parts of the grid were underpredicted (blue colors) and which were overpredicted (red colors). The intensity of the color indicates the magnitude of difference. Light gray colors indicate a good match between predicted and original values, representing negligible errors. A colorbar is included to match the colors with the value of SEL dB difference.

The case with the lowest projection error is Job ID 217 and its recreation is shown in Figure 5.5. From the plot, it is observed that the 1st order projections are quite poor, but the quality of projections increases rapidly as the order of projection increases. At 4 basis vectors, the error is limited to ± 1 dB SEL. The inclusion of 8 and 12 basis vectors decreases the error across the grid to even lower values. At 12 basis vectors, the RIC crosses 99.9% and large sections of the noise grid are recreated with negligibly low error. The noise contours from the original noise grid and the projected noise grid are almost coincident at this stage.

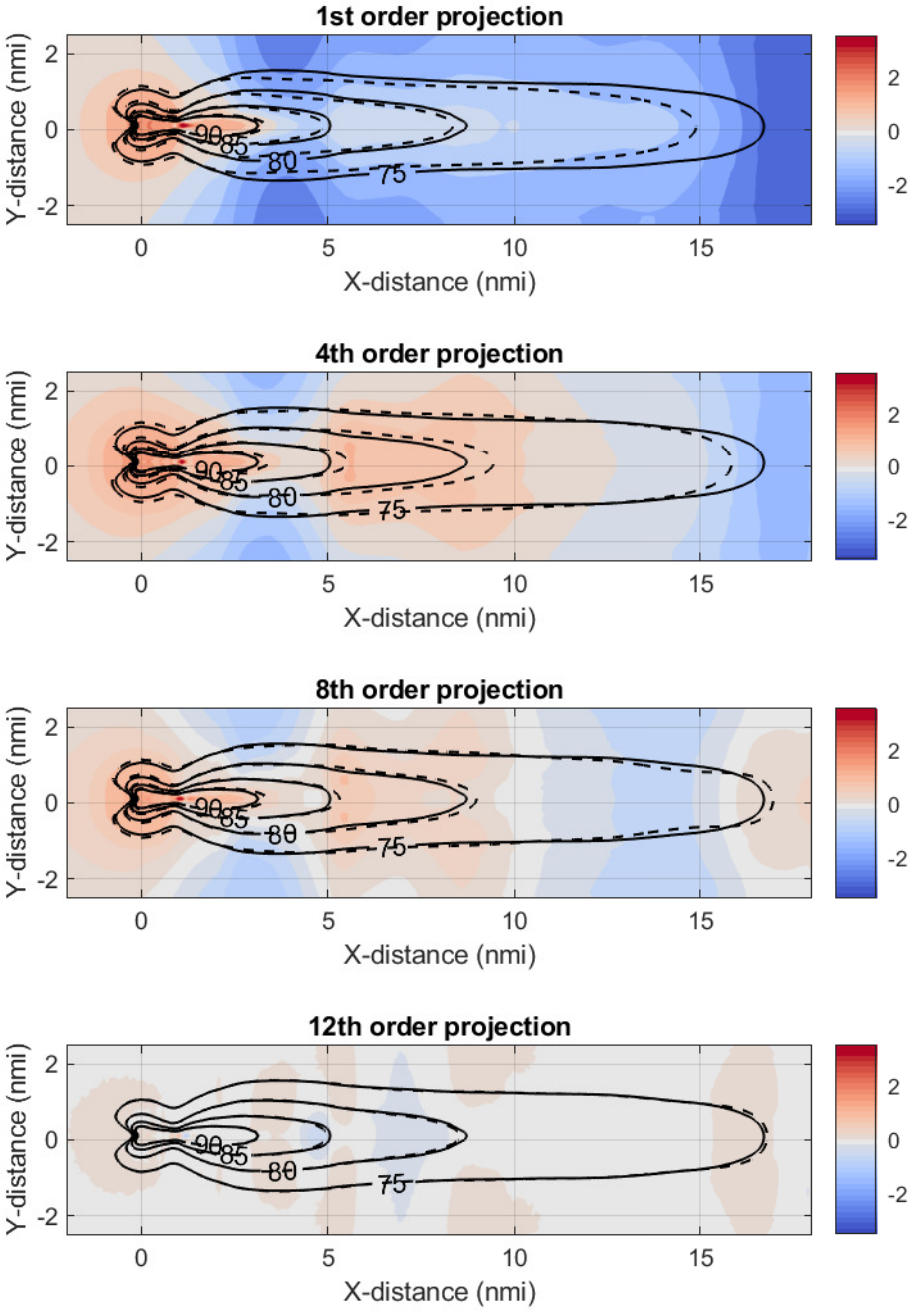

Figure 5.5: Projected noise grid recreation: least error

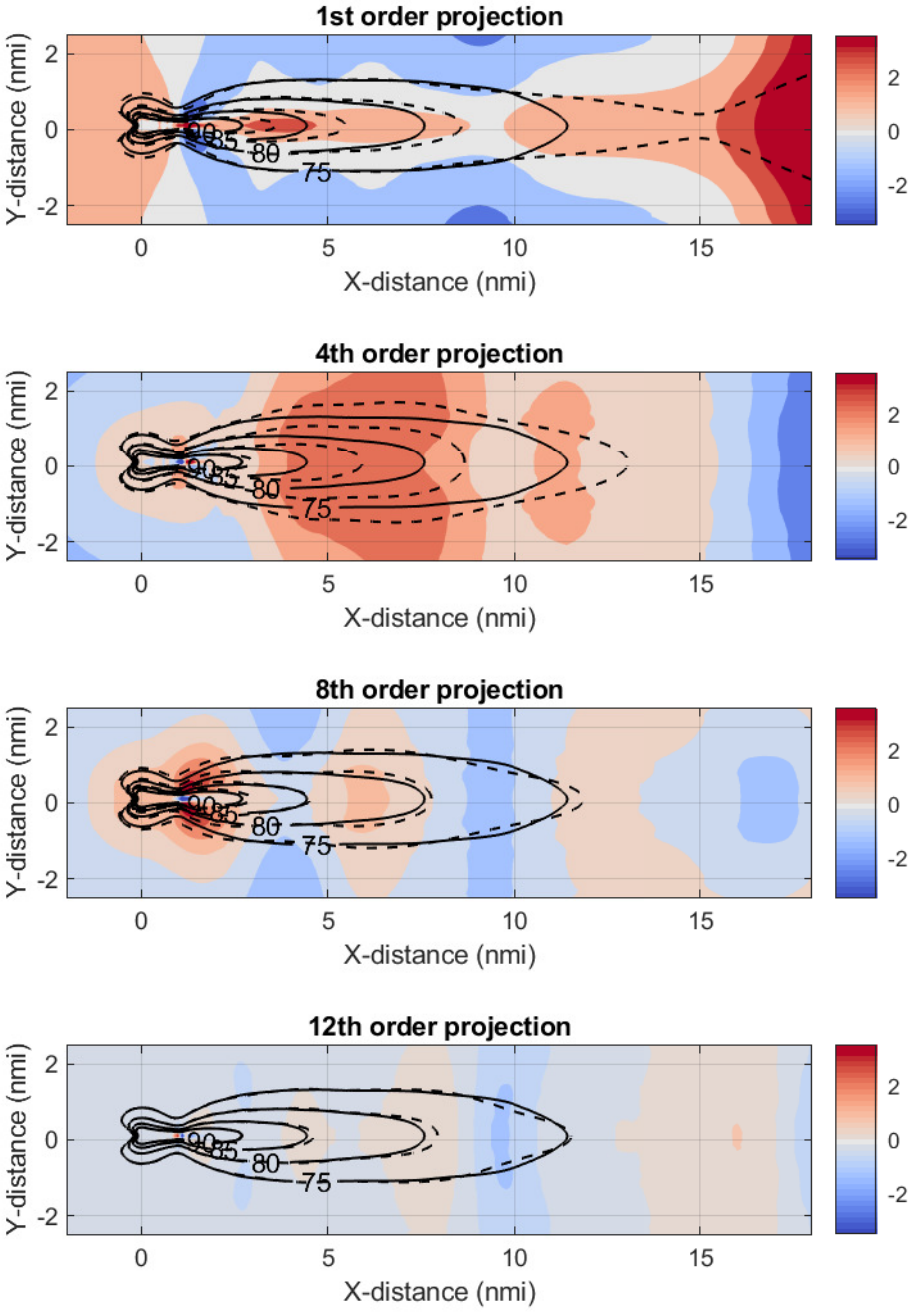

Figure 5.6: Projected noise grid recreation: highest error

The case with the highest projection error is Job ID 936 and its recreation is shown in Figure 5.6. Similar to the least error case, it is observed that the 1st order projections are inaccurate, but get better as the order of projection increases. At 4 basis vectors, the error is still quite high, with some regions exceeding ± 2 dB SEL. The inclusion of 8 and 12 basis vectors decreases the error across the grid to within ± 1 and ± 0.5 dB SEL respectively. At 12 basis vectors, the error across the noise grid is quite low and large sections of the noise grid are recreated with negligibly low error, although some pockets of higher error remain. The noise contours from the original noise grid and the projected noise grid are almost coincident at this stage, with some exceptions. The 80 dB and the 75 dB SEL contours show a deviation between the projected and the original noise grid.

It should be noted that although the worst case projection with most error is an outlier, large sections of the noise grid could still be recreated with minimal error. The error for most cases is much lower than the error for this outlier case.

5.2.4 Summary and evaluation of Hypothesis

Experiment 2.1 was designed to determine a process by which the high-dimensionality of the aviation noise grids could be managed. The Principal Component Analysis (also known as Proper Orthogonal Decomposition) was identified as a Model Order Reduction technique. The PCA method works by creating a vectorized representation of the full-order model data in some high dimensional space. By identifying principal axes (a generalized version of eigendirections), the data could be reoriented and represented as coordinates along the principal axes.

The dataset obtained in Experiment 1.3 was repurposed for this experiment. A total of 960 cases were evaluated for their SEL noise metric at a grid of receptors consisting of 401×81 receptors. With the identification of the principal axes, the Relative Information Content metric was computed to determine the appropriate number of directions to retain. A threshold requirement of 99.9% information retention led to the down-selection of the

first 12 principal directions.

The selected 12 directions formed the hyperplane onto which the high-dimensional data was projected. In this lower-order representation, each noise grid was represented simply by its coordinates along the 12 orthonormal basis vectors. Thus the original noise grid with 32481 values was reduced to just 12, representing an immense improvement. Although this reduction in dimensionality came with some error associated with the projection, the error was minimized through the construction and selection of the principal directions.

The best and worst cases with the least and highest error respectively were studied with visual comparisons of the noise grids and contours. It was observed that although minor errors remained, a vast majority of the region of noise grid could be recreated with negligibly small error. Most noise contours could also be recreated correctly.

Revisiting Hypothesis 2.1, the requirement was to show how the full-order solutions could be projected onto a lower dimensional space. The designed Experiment 2.1 demonstrated that the Model Order Reduction technique called PCA could successfully be adapted for use with aviation noise metrics. The change in dimensions from 32481 to just 12 with minimal loss of information demonstrated how effective Model Order Reductions can be for the aviation noise quantification process. Thus, Experiment 2.1 is considered successful and Hypothesis 2.1 is accepted.

5.3 Experiment 2.2

In this section, the experimental setup and results for RQ2.2 are explained. For reference, RQ2.2 and H2.1 are repeated below –

Research Question 2.2
How can the reduced solution space be mapped to the input space?

Hypothesis 2.2

If an interpolation/regression model is developed linking the solution in the latent space to the parameters, then the reduced solution space can be mapped to the input space.

In RQ2.1, a process was shown by which the high-dimensional noise grid data could be projected onto a much lower dimensional space. While the reduction of dimension is certainly helpful in terms of compression and storage, a new problem arises when the noise impacts of a previously unseen parameter have to be obtained. In such a case, there is no pre-existing full-order or reduced-order data. Hence, to complete the second half of the problem, a method needs to be generated by which the coordinates of a lower-order solution can be directly predicted as functions of the input parameters. The high-dimensional noise grid can then be generated from the lower-order solution coordinates using the orthonormal basis vectors.

5.3.1 Surrogate modeling setup

The entire surrogate modeling effort in this experiment was performed in JMP. The outputs to be modeled are the twelve coefficients $\{a_1, a_2, \ldots, a_{12}\}$ which represent the components of a full-order solution is the lower-dimensional space. The input parameters are the set of five parameters $\{\alpha_1, \alpha_2, \ldots, \alpha_5\}$ which represent the takeoff weight, takeoff thrust reduction, altitude of acceleration initiation, energy share percentage, and the ambient temperature respectively. Consistent with the step-wise regression modeling performed in Experiment 1.3, the cross-term factors and quadratic factors were also included in the modeling. Let $\hat{a}_i$ be the approximate surrogate model of coefficient a_i. Then, the regression

model can be represented as

$$\hat{a}_i \approx a_i \tag{5.14}$$

$$\hat{a}_i = f_i(\alpha_1, \alpha_2, \alpha_3, \alpha_4, \alpha_5) \tag{5.15}$$

Also consistent with the process followed in Experiment 1.3, the five input parameters and twelve outputs were normalized before any surrogate modeling was attempted.

Training and Validation data

As with any surrogate modeling exercise, it is important to set aside a subset of the available data for model validation. Model validation is done with data which were not used to train the model. In this experiment, 25% of cases are set aside of model validation (240 of 960). The remaining 720 cases are used to train the model. This split was done randomly to prevent any selection biases from affecting the modeling process.

Models considered

Numerous models are available for evaluation within JMP and a subset of those were selected for evaluation on the dataset. Each model is described here briefly. Hyperparameters which are required for some models were set to their default values, or to values recommended by JMP.

1. Bootstrap Forest – This type of model makes use of many decision trees and takes their average to form the final model. Each decision tree is fit to a bootstrap sample of the training dataset. The predicted output from this model is the average of the predicted values for that output over all decision trees.

2. Boosted Tree – The process of 'boosting' a tree involves the building of a larger decision tree by fitting a sequence of smaller decision trees which are called layers.

The final predicted output is the of predicted residuals for an observation over all layets.

3. K-Nearest Neighbors – The KNN algorithm assumes that objects which are similar in the dataset will be close to each other. Therefore, this supervised learning method predicts the output as some average of k nearest neighbors to the sampled point.

4. Neural Networks – Artificial Neural Networks are a class of models used for regression that are inspired by biological neural networks. ANNs make use of hidden layers of nodes which act as intermediaries between the inputs and the outputs. Many possible combinations of the number of layers and the number of nodes within a layer are possible.

5. Support Vector Machines – SVM methods are used in data classification, regression, and outlier identification. The methods make use of hyperplanes in the high-dimensional space.

6. Least Squares Fit – Common model fitting method in which the sum of squares of errors is minimized.

5.3.2 Results of surrogate model

All models described above were evaluated in JMP to assess their suitability for building the surrogate model. A comparison of the different models for the outputs is shown in this subsection. Based on the comparison, a single class of model was selected. The performance of that model on the validation dataset is also shown.

Model comparison and selection

The selected six regression models and their performance on the twelve coefficients to be modeled is shown in Figure 5.7.

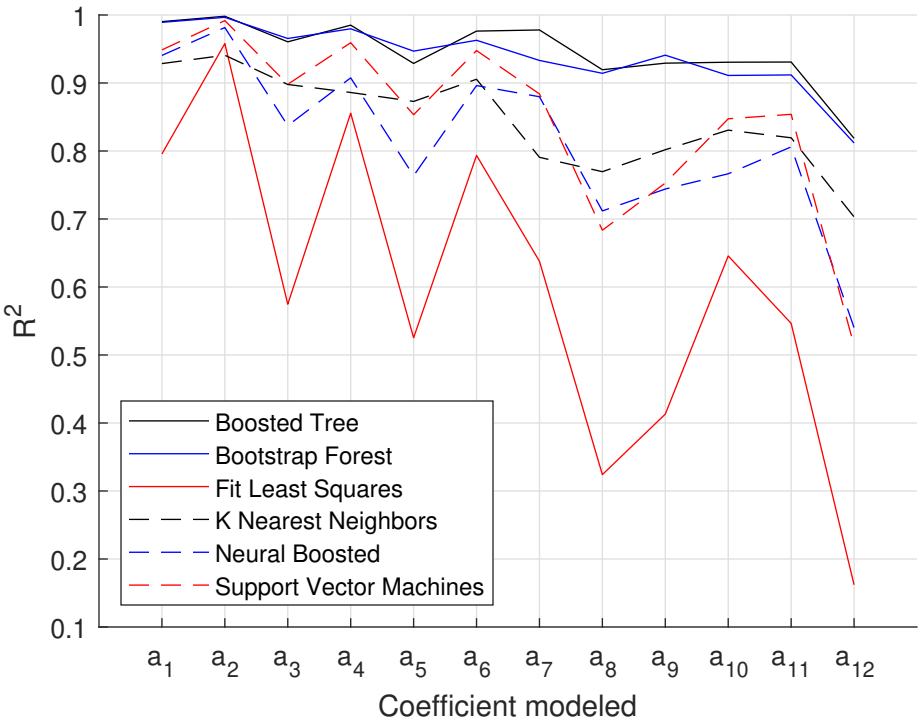

Figure 5.7: Comparison of regression model performance

It is observed that the best two methods are the Boosted Tree and the Bootstrap Forest methods, with the former showing slightly better performance overall, with higher R^2 values for a_6, a_7, a_10, and a_11. The other methods do not seem to work as well, with the Least Squares fit consistently performing the worst of all methods. Further, the R^2 value has a slight downward trend as the coefficient to be modeled changes from a_1 to a_{12}, with a sharp fall-off for the final coefficient. This can be explained by bringing back the notion of the Relative Information Content. As the index of the coefficient increases, the information stored by that coefficient decreases. In other words, there is far less information being held by coefficient a_{12} than by coefficient a_1. This decrease in information content explains the slight downward trend in R^2 values.

Based on the observations from Figure 5.7, the Boosted Tree algorithm for selected for further analysis.

Evaluation of selected model

Once the Boosted Tree algorithm was selected, additional evaluation were performed to determine the accuracy and goodness of the model fit. First, the model was evaluated on the validation points, and the resulting R^2 values are shown in Figure 5.8.

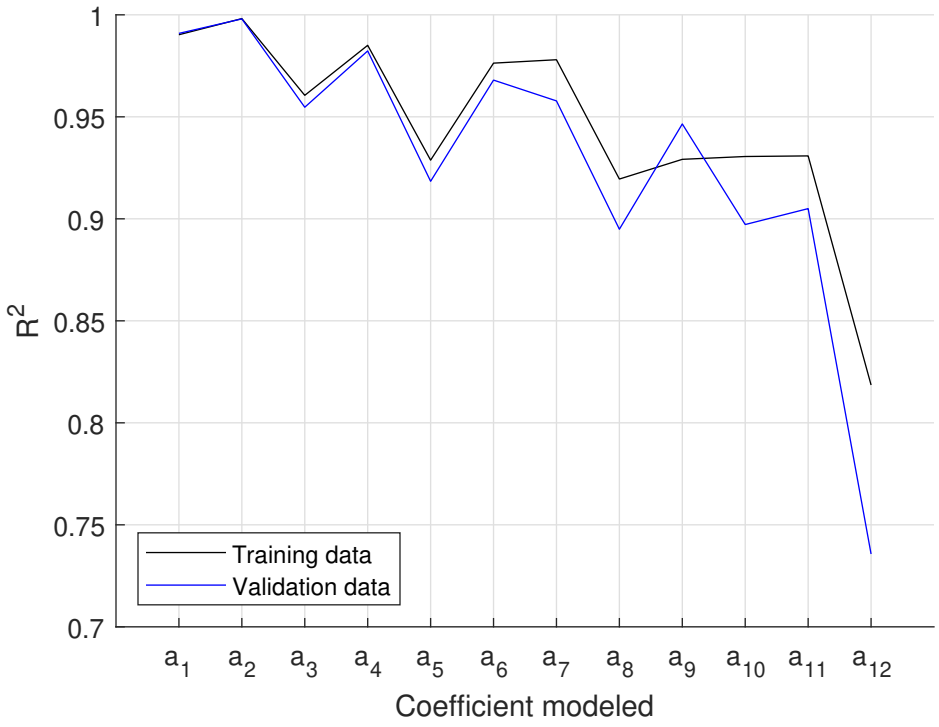

Figure 5.8: Comparison of R^2 values for training and validation data

The overall trends between the training and the validation datasets is similar, with the model performing better for the first few coefficients and with a marked decrease in performance for the latter coefficients. With one exception, the R^2 values for the validation dataset are lower than those for the training dataset.

Next, the predicted values are plotted as function of the actual values for each of the twelve coefficients in Figure 5.9. In an ideal model fit, all of these plots would look like a straight and thin $y = x$ lines. For most of the subplots, the expected behavior is observed, with the cloud of points aligned in the expected direction. A larger spread of points in the transverse direction indicates larger error in the predictions. Notably, the coefficient a_{12} which had resulted in a poor R^2 score deviates significantly from the $y = x$ behavior.

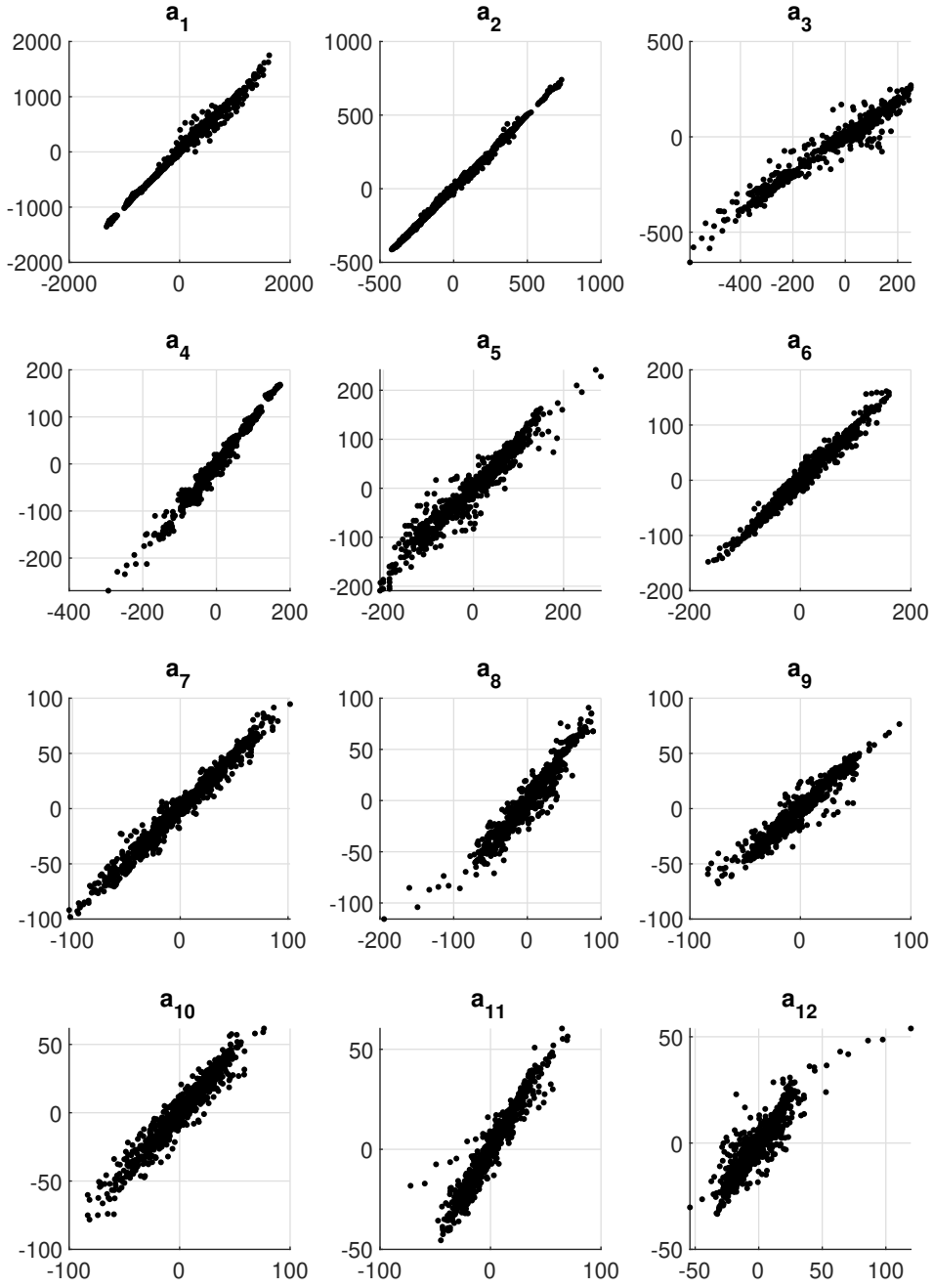

Figure 5.9: Predicted by True values for the 12 coefficients

The next step of plots is shown in Figure 5.10. Each subplot in this figure shows the absolute error against the true value of the coefficient. An ideal shape here is a cloud of points centered around the origin, with no discernible distortions in a particular direction. Again, the notable exception here is coefficient a_12 which shows a downward slope indicating that when the true coefficient values are high, they tend to be underpredicted. Conversely, when the true coefficient values are low, they tend to be overpredicted. The magnitude of this error is also quite large, however, as this is the final coefficient representing the component along the least important chosen principal axis, the error for a_{12} should not significantly impact the final noise grid predictions.

The distributions of the absolute and relative errors in the prediction of coefficients a_i are shown in Figure 5.11. From the boxplots, it is evident that there are a large number of outliers indicating that at some data points, the coefficients could not be predicted with a sufficiently low error. Discarding the outliers, the relative error is quite low for the first two coefficients a_1 and a_2, but increase for the other coefficients.

5.3.3 Predicted noise grids

With the error metrics and goodness of fit measures evaluated for the regression model, the focus shifts on the prediction of the noise grids. The end goal of this experiment, is to determine the noise grid results as a function of the input parameters.

The predicted noise grid is constructed using the predicted coefficient values of $a_1, a_2, \ldots, a_{12}$ obtained by evaluating the model at the validation parameter conditions. It should be noted that the predictions $w_{pred,i}$ are being performed in the lower-dimensional space, and hence the comparison is also made to the projected noise grids $w_{proj,i}$. The

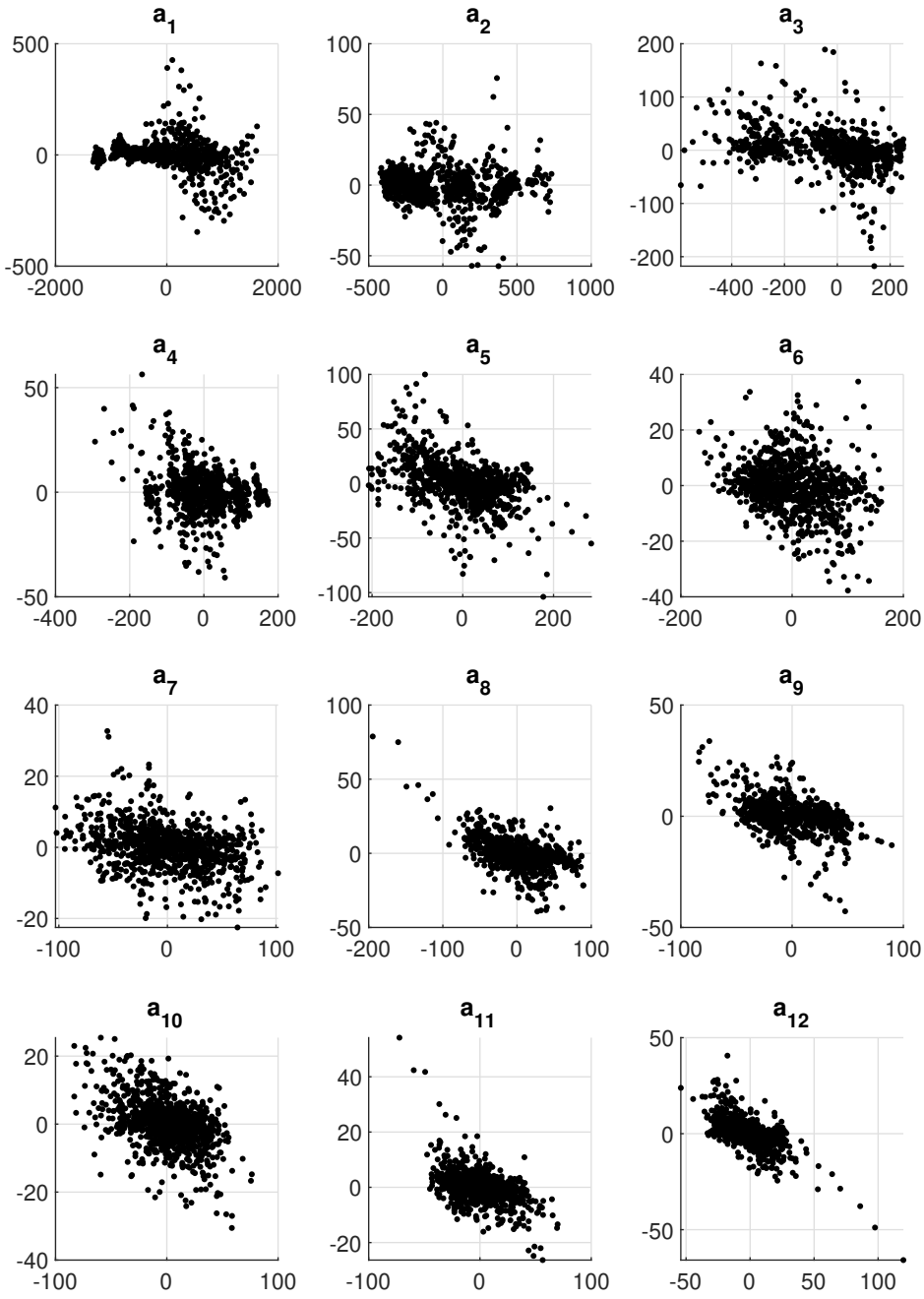

Figure 5.10: Absolute Error by True values for the 12 coefficients

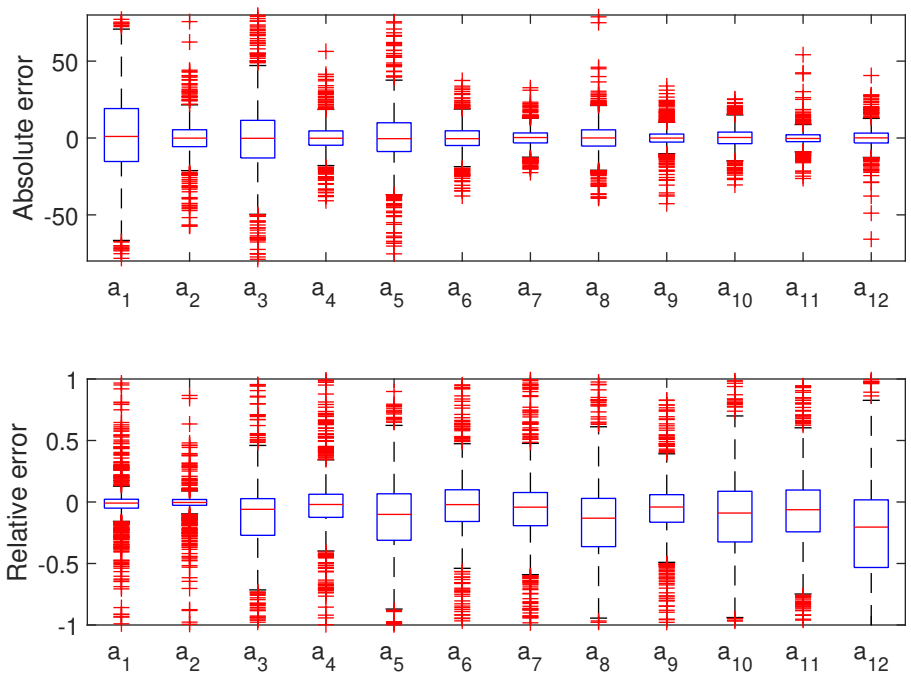

Figure 5.11: Distribution of the absolute and relative errors in the prediction of coefficients

formula for reconstruction is given by –

$$w_{proj,i} = \bar{w} + \sum_{j=1}^{k} a_{i,j} \tag{5.16}$$

$$w_{pred,i} = \bar{w} + \sum_{j=1}^{k} \hat{a}_{i,j}\phi_j \tag{5.17}$$

The two cases with the minimum and maximum projection error, Job ID 217 and 936 respectively are recalled at this stage for comparison. The comparison is made between the predicted and the projected noise grids, and not between the predicted and the true noise grids. Thus, the predictions are judged solely by their ability to recreate the projected noise grids, and not the original noise grids, regardless of how accurate the projected grids actually are when compared to the original noise grids.

The same features of the comparison plot are used which were explained in subsubsection 5.2.3. Here, the solid contour lines show the original projected data and the dotted contour lines show the predicted projected data.

The comparison for Job ID 217 is shown in Figure 5.12. The same four subplots showing the contour recreation with 1, 4, 8, and 12 basis vectors. It is observed that the recreation of the 1st order projection could be done very accurately with coincident contour lines and very low error across the noise grid. Most of the grid was recreated accurately or with a slight overprediction. This accurate recreation is to be expected, as only the $\hat{a}_1$ model is being used, which did have a high R^2 value and low errors.

As additional basis vectors are added, the quality of the prediction decreases. This is due to the poorer fitting models for the latter coefficients, for example $\hat{a}_8$ and $\hat{a}_{12}$. With 8th and 12th order projections, the predicted noise contours start to show some deviation at the East end of the 75 dB and 80 dB SEL contours, although they do remain coincident for large sections of the grid. Additionally, regions of the grid may show underprediction or overprediction, but the magnitude of this difference is limited to within ± 0.4 dB SEL.

The comparison for Job ID 936 is shown in Figure 5.13. The predictions in this case seem to perform worse than the predictions for Job ID 217. The trend of prediction quality remains, the prediction is more accurate for the 1st order projections, and worsens as additional basis vectors are included in the projection. The contours could accurately be recreated in the top subplot, but started to diverge especially at the East ends of the contours. The overall noise grid also shows regions of both underprediction and overprediction with the magnitude limited to ± 1.5 dB SEL. For the 12th order projection, the majority of the noise grid is overpredicted, although a small region near the 'neck' of the contours (near x location 1.5 nmi and y location 0 nmi) shows underprediction.

5.3.4 Summary and evaluation of Hypothesis

Experiment 2.2 was designed to develop a surrogate model which could link the original set of parameters $\{\alpha_1, \alpha_2, \alpha_3, \alpha_4, \alpha_5\}$ to the coefficients of projection in the lower-dimensional representation. The experiment started where E2.1 left-off, with the projected coordinates for each of the 960 evaluated jobs along the 12 identified basis vectors.

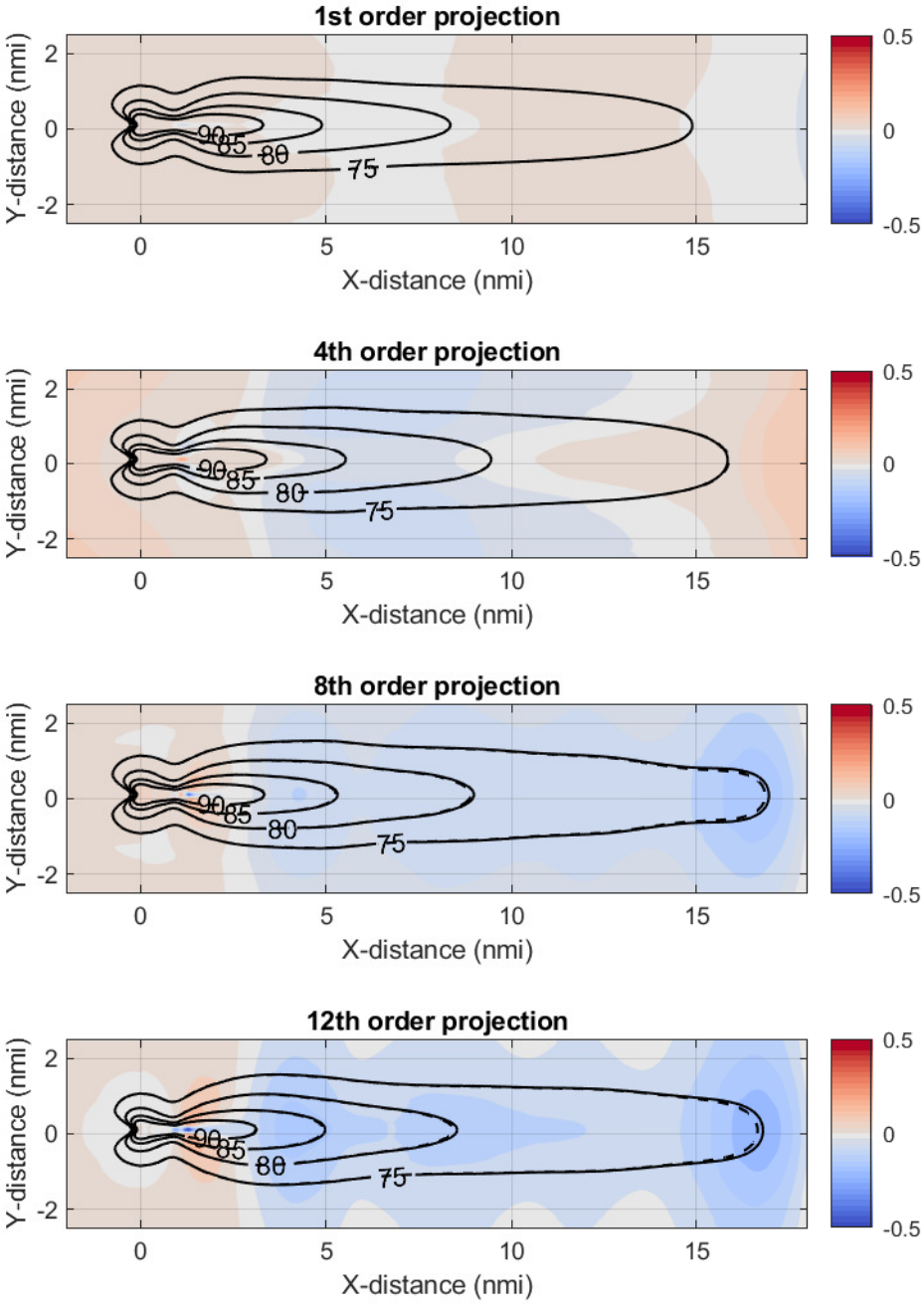

Figure 5.12: Prediction of projected noise grid with least projection error

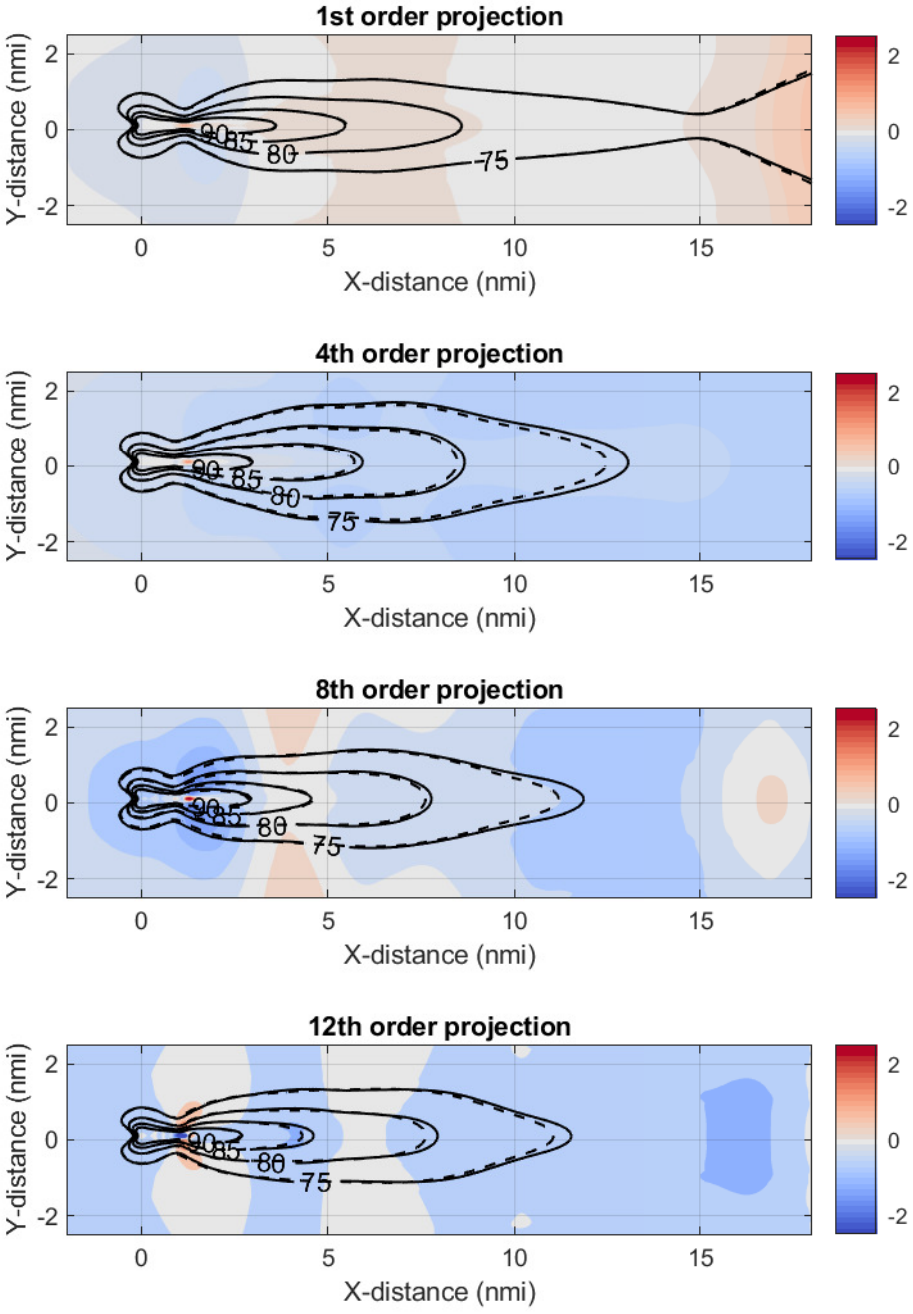

Figure 5.13: Prediction of projected noise grid with highest projection error

Various different surrogate modeling techniques were evaluated, and the best performing overall was determined to be the Boosted Tree method. The chosen technique was then used to fit the prediction models for all 12 coefficients individually. 240 cases were set aside for validation purposes and were not used to train the model. Various goodness of fit measures were employed to ensure that the 12 coefficients could be predicted reasonably well by the trained models. Nevertheless, the performance of the surrogate model decreased for coefficients of the latter basis vectors. This drop in performance was explained by the decrease in information content for the latter basis vectors. With more information contained within the data, there is a hidden pattern that can actually be captured by the surrogate model.

After the evaluation of the model fit, actual noise grids were compared. The same two cases from Experiment 2.1 were visualized to determine whether the noise grids could accurately be recreated by the surrogate model in the projected space. The visualization was constructed with 4 different choices of basis vectors, and provided insight into the dependence of accuracy of predictions on the basis vector being modeled. Generally, the 1st order projections could be predicted quite accurately due to the accurately fit models for the first coefficient a_1. As additional basis vectors were included, the error increased. It was noted that this error increase was only due to the prediction. The projection error, as noted in Experiment 2.1, does decrease when more basis vectors are included.

Revisiting Hypothesis 2.2, the requirement was to develop a model/process by which the solution in the projected space could be linked to the original input parameters to the noise quantification tool. This requirement was fulfiled by the creation of surrogate models for the coefficients along the twelve identified principal directions identified in Experiment 2.1. Therefore, the original input parameter alues could be linked to the twelve coefficients, which could then provide a noise grid solution in the projected space. Thus, Experiment 2.2 is considered successful, and Hypothesis 2.2 is accepted.

5.4 Integration of MOR and surrogate modeling

With the conclusion of Experiments 2.1 and 2.2, separate capabilities were developed to (a) project high-dimensional noise grid data onto a lower-dimensional representation and (b) link the projected data to the input parameters. The experiments also showed visualizations of noise grids as they are projected, and then predicted in the projected space. This section combines the Model Order Reduction step with the surrogate modeling step into a process which is called Reduced Order Modeling.

By integrating both experiments into a single process, the overall results obtained from predictions in the projected space can be compared to the original full-order solutions. This will help in understanding the total error which will be introduced when such Reduced Order Modeling is performed. The visualization of the original high-dimensional data, lower-order projection, and prediction in lower-dimensional space accompanied by the projection, prediction, and total errors is shown in Figure 5.14. The total error here is defined as the vector sum of errors resulting from projection and prediction –

$$e_{total,i} = e_{pred,i} + e_{proj,i} \tag{5.18}$$

$$= (w_{pred,i} - w_{proj,i}) + (w_{proj,i} - w_i) \tag{5.19}$$

$$= w_{pred,i} - w_i \tag{5.20}$$

This total error is a vector which shows the error at each point in the noise grid. The relative total error can be obtained by making use of vector norms –

$$e_{total,rel,i} = \frac{\|e_{total,i}\|}{\|w_i\|} \tag{5.21}$$

The distribution of total error across the entire grid for for Job ID 217 and 936 is shown in Figure 5.15. It is observed that the overall quality of prediction increases with the use of higher order projections, as indicated by the lower error values. The first order predictions

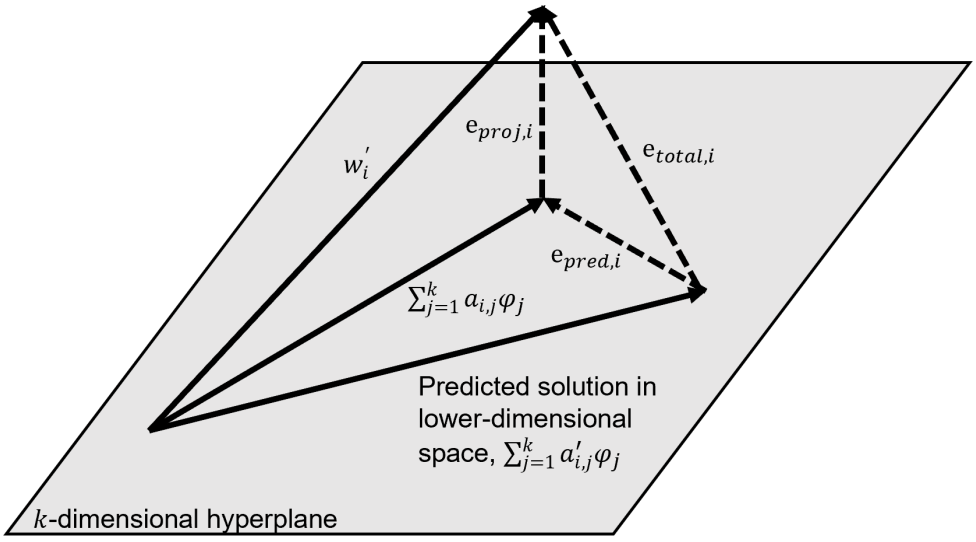

Figure 5.14: Visualization of prediction in lower-dimensional space and errors

do not do a good job of recreating the true noise grid, with differences as large as ± 8 dB SEL for the Job ID 936 without considering any outliers.

Finally, the predicted projected noise grids are compared to the true noise grids. This is the comparison which shows how well the Reduced Order Model (combination of projection from high-dimensional space to lower-dimensional space and prediction of coefficients in the lower-dimensional space) performed when compared to the full-order model predictions.

The comparison of predicted noise contours for Job ID 217 is shown in Figure 5.16. This case had the least projection error among all 960 cases. For this case, it is observed that the prediction quality improved significantly as more basis vectors/principal directions were used. With the use of 12 basis vectors corresponding to 99.9% RIC, the noise grid could be recreated quite accurately. The noise contours could mostly be recreated exactly, although some minor divergences were observed with the 80 dB SEL and 85 dB SEL contours.

The comparison of predicted noise contours for Job ID 936 is shown in Figure 5.17. This case had the highest projection error among all 960 cases. As with the previous case,

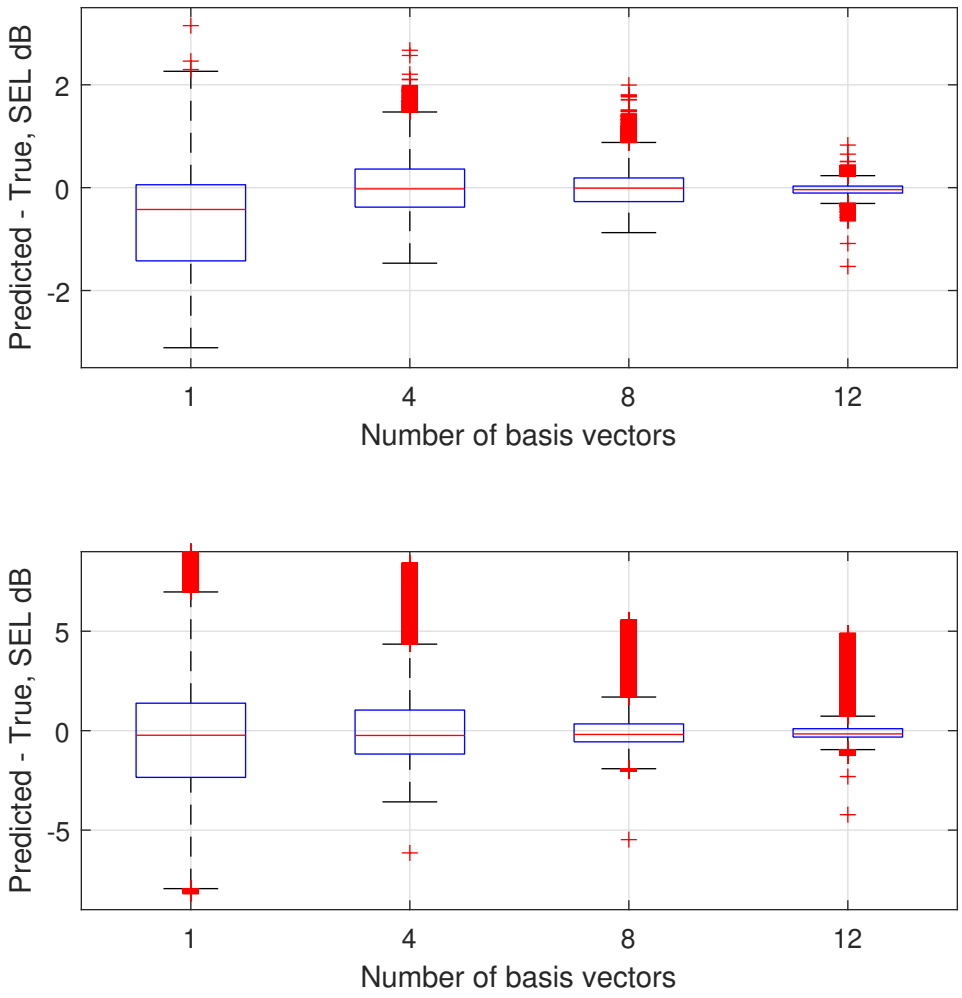

Figure 5.15: Box plot showing the distribution of error across the noise grid for predictions of different order projections

the quality of prediction improved considerably with the inclusion of a higher number of basis vectors. The 75 dB SEL contour showed more apparent deviations from the true contour. Additionally, the entire noise grid seemed to be slightly underpredicted, as indicated by the various shades of blue color on the colormap. However, the magnitude of difference was quite low for large sections of the grid, which is particularly impressive given that this case was an outlier with a 7% relative projection error.

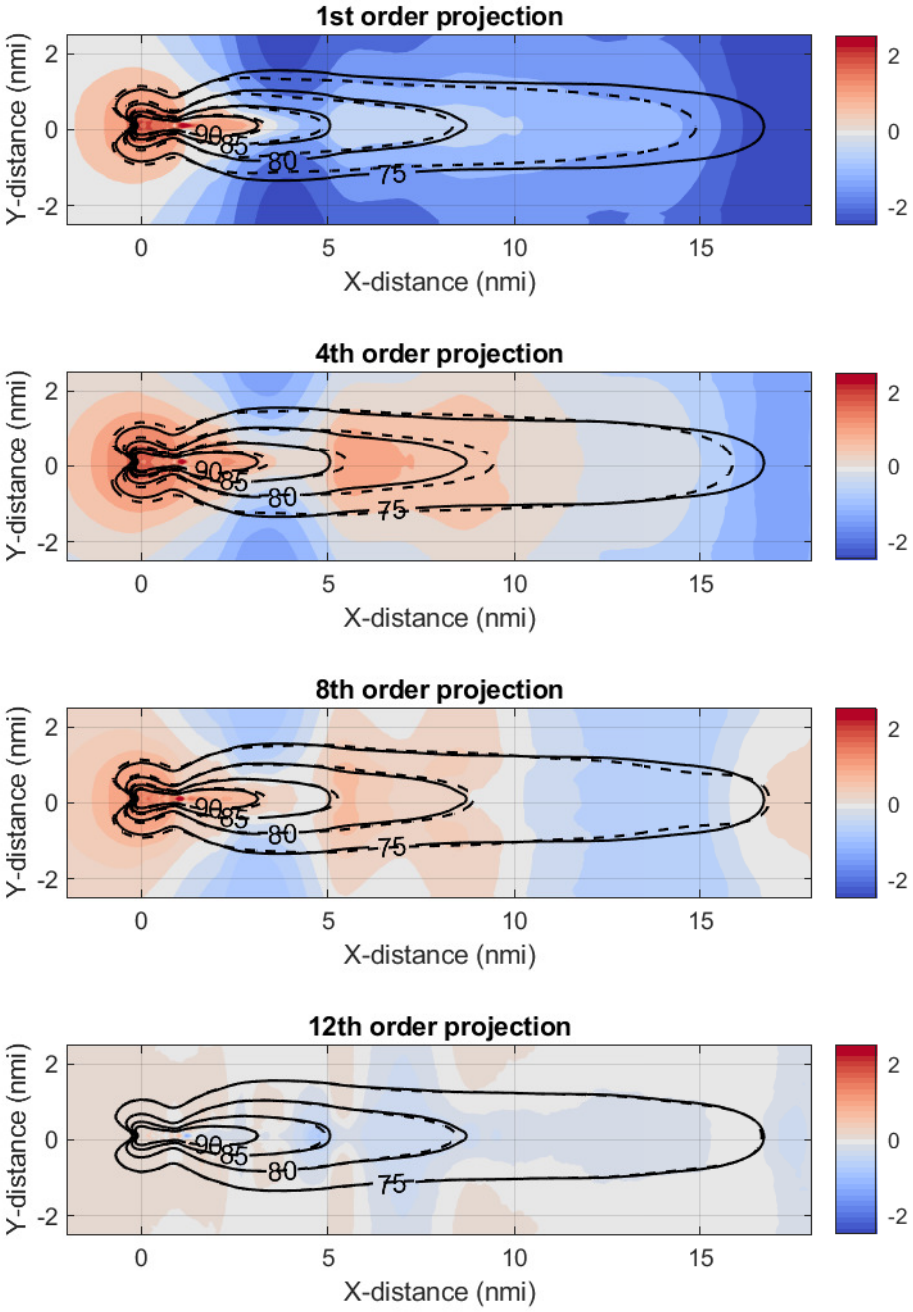

Figure 5.16: Comparison of predicted noise grids in projected space to original true noise grids, Case 217

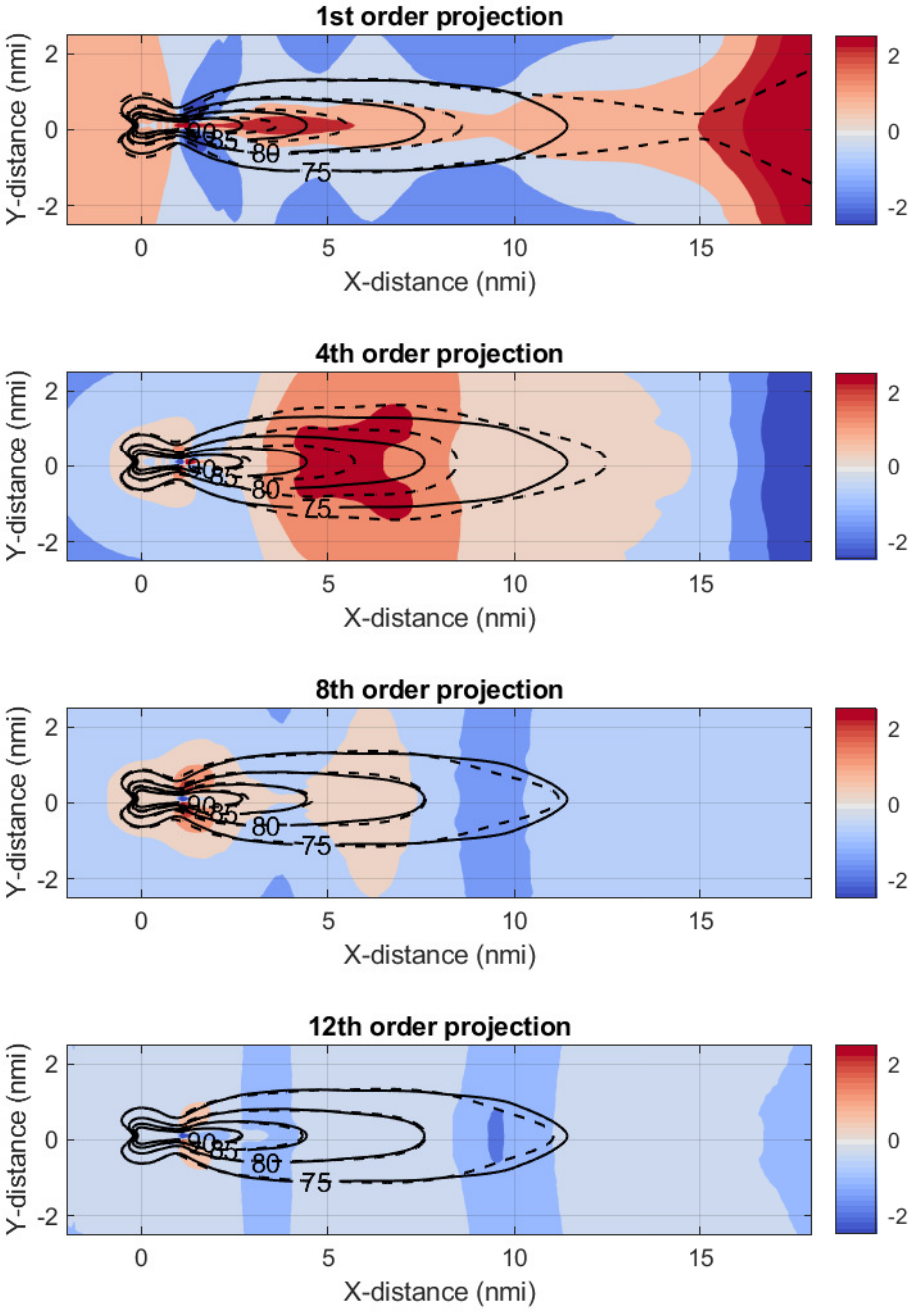

Figure 5.17: Comparison of predicted noise grids in projected space to original true noise grids, Case 936

5.5 Summary of Research Area 2

This chapter presented the findings from Experiments 2.1 and 2.2, which supported their respective Hypotheses. All formulated Hypotheses were accepted, and the Research Questions leading to those hypotheses were answered.

The original high-level Research Question 2 is recapped below. This led to the requirements of model order reduction and surrogate modeling which were addressed by Research Questions 2.1 and 2.2 respectively.

Research Question 2
How can the process of computing aviation noise metrics be made more computationally efficient?

Research Question 2.1 led to the creation of a Model Order Reduction process in which the high-dimensional noise grid data could be projected onto a lower dimensional space. The Principal Component Analysis method was successfully adapted for this application. A set of 960 noise results, each representing a high-dimensional noise grid was successfully projected onto a lower-dimensional space which could be represented much more compactly. The error associated with this projection was quantified and analyzed to ensure that the original full-order noise grids could still be recovered accurately.

Research Question 2.2 led to the creation of a surrogate model in the lower-dimensional space. This model was developed to link the original input parameters of the noise quantification process to the coefficients representing the components along each of the chosen principal directions. This enabled the prediction of noise grids for previously unseen parameter values, without ever needing to run the full-order model. The error associated with this prediction was quantified and analyzed to ensure the correct type of model was being fit.

The methods and processes obtained from Experiments 2.1 and 2.2 were then combined

to produce a Reduced Order Model. The predictions of this Reduced Order Model were then compared to the original full-order predictions to analyze the accuracy of predictions. It was determined that the ROM could reproduce the original result accurately for almost all cases. For some outlier cases, the contours could not be reproduced exactly and showed minor deviations in small regions of the noise grid.

Together, these two RQs, their accompanying hypotheses, experiments, and the techniques developed in those experiments satisfied all requirements of the high-level Research Question 2. This concludes the discussion on Research Area 2.

CHAPTER 6

OVERALL METHODOLOGY AND DEMONSTRATION

With the conclusion of the Research Plan execution, the overall methodology can be assembled. The overall methodology is presented in this chapter and a small application of the developed methodology is demonstrated.

6.1 Methodology Objectives

It is helpful to revisit the original Motivating Research Question which was posed in chapter 1.

Motivating Research Question

How can the process of aviation noise quantification be improved to enable rapid quantification of noise metrics to facilitate parametric trade-off analyses and optimization efforts?

The Research Objective, also first seen in chapter 1, was designed as a goal to address the Motivating Research Question.

Research Objective

Develop a methodology to address inherent complexities in the aviation noise computation problem, thereby enabling rapid quantification of noise metrics in a variety of scenarios, thus facilitating parametric trade-off analyses and optimization efforts.

The inherent complexities of the aviation noise quantification problem were identified to be linked to the dimensionality of the problem. It was observed that both the input and

the output space of any aviation noise quantification process were high-dimensional. In the input space, it was observed that aircraft trajectories, which are crucial to determining noise impacts, could not be suitably represented using a set of parameters. On the output side, it was observed that due to the nature of noise analysis which is fundamentally based on grids of noise metrics, the quantification process was computationally expensive.

An Overarching Hypothesis was developed to answer the Motivating Research Question, and to satisfy the Research Objective.

Overarching Hypothesis

If a methodology is developed that

1. can efficiently represent real-world time-series flight trajectory data with a parametric definition obtained using an inverse map;
2. which is then used as an input to a field surrogate model developed using model order reduction;

then rapid quantification of noise metrics is enabled in a variety of scenarios, which facilitates parametric trade-off analyses and optimization efforts.

The methodology envisioned in the Overall Hypothesis can be constructed with the research formulations, experiments, and findings contained in this dissertation. Based on the Research Objective, the following requirements are stated for this methodology –

1. Rapid quantification of noise metrics in both real-world and hypothetical scenarios. Real-world scenarios refer to the situation when a large amount of real-world flight data, obtained from either ground or aircraft sources are available, and an accurate noise impact assessment must be made. Hypothetical scenarios refers to a situation in which theoretical profiles or trajectory designs are being evaluated.
2. Parametric trade-off analyses and optimization, which do not rely on assumed or

averaged conditions. This required the elimination of categorical variables and the creation of parametric definitions of aircraft trajectories.

6.2 Components of Methodology

The overall methodology is shown in Figure 6.1. The complete methodology can be decomposed into three modules, which are related to the research plan identified in chapter 3.

1. The Real-World Quantification module is used when a large number of real-world flight data in the form of time-series is available and the resultant noise metrics must be evaluated. The clustering process developed in RQ1.2 and the inverse mapping process developed in RQ1.1 are present in this module. The output from this module is a set of parameter values which can accurately represent the entire set of real-world trajectories.

2. The Trade-off analysis/Optimization module is used when theoretical profiles are being designed. The factor screening process helps with the identification of important parameters which influences candidate profile design. The process itself can be repeated until the user is satisfied with the selection of candidate profiles. The output of this module is the parametric definition of the chosen candidate profiles.

3. The Field Surrogate Modeling module is used to then rapidly model the noise metrics of any given input parameter combination. When using the methodology, it is assumed that the field surrogate model as already been developed, i.e. the *offline* cost has been incurred. The *online* cost of obtaining noise grids for the given input parameters is then done with practically real-time speed.

Thus, there are two modes in which the methodology can be deployed. The first use-case is for the rapid and accurate evaluation of real-world time-series flight data, and the

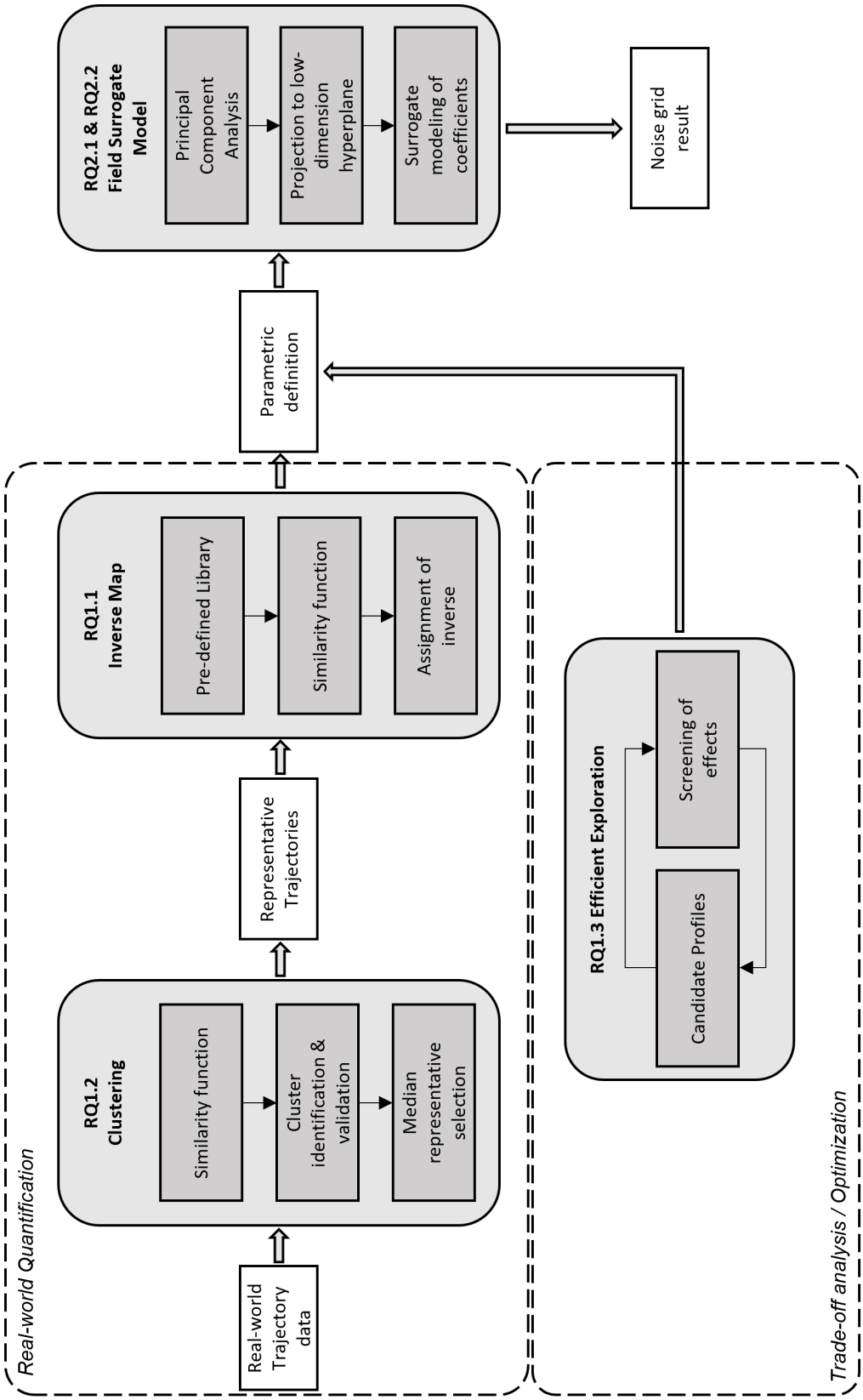

Figure 6.1: Overall Methodology

second use-case is for many-query applications such as parametric trade-off analyses and optimization, where many inputs have to be evaluated.

6.3 Demonstration of Methodology

Although every component of the methodology has been demonstrated individually through the various experiments, these experiments often used different sets of data. The interconnections of the different modules have not yet been shown. With the overall methodology now constructed, it is demonstrated on a practical case study, where the noise impacts of a large number of real-world flights will be quantified.

6.3.1 Real-world quantification

The first mode of use for the methodology is for the quantification of aviation noise impacts for real-world time-series flight trajectory data. Before deploying the methodology, it is helpful to note what the existing challenges for performing such impact analysis are –

- Real-world time-series trajectory data are uniquely represented. Thus, a set of 1000 flights, would need a 1000 evaluations of a noise model, which traditionally is prohibitively expensive in terms of computation cost.
- Almost all real-world flight data, whether it is based on ground-based RADAR, or aircraft-based sensors, lacks information about the aircraft weight and thrust. While weight is relatively easy to estimate, the variation of thrust throughout the aircraft trajectory is difficult to estimate.

Step 1: Collection of real-world data

The first step is to collected the real-world data and pre-process it. Here, the dataset which was introduced in Experiment 1.1 is used. To recap, this dataset represents a set of 1361 departure operations flown by the Boeing 737-800 aircraft out of the SFO airport, by a

single airline. The data is obtained from the OpenSky Network. These flights represent trip distances between 1500 and 2500 nmi. The complete set of flights is visualized in Figure 6.2.

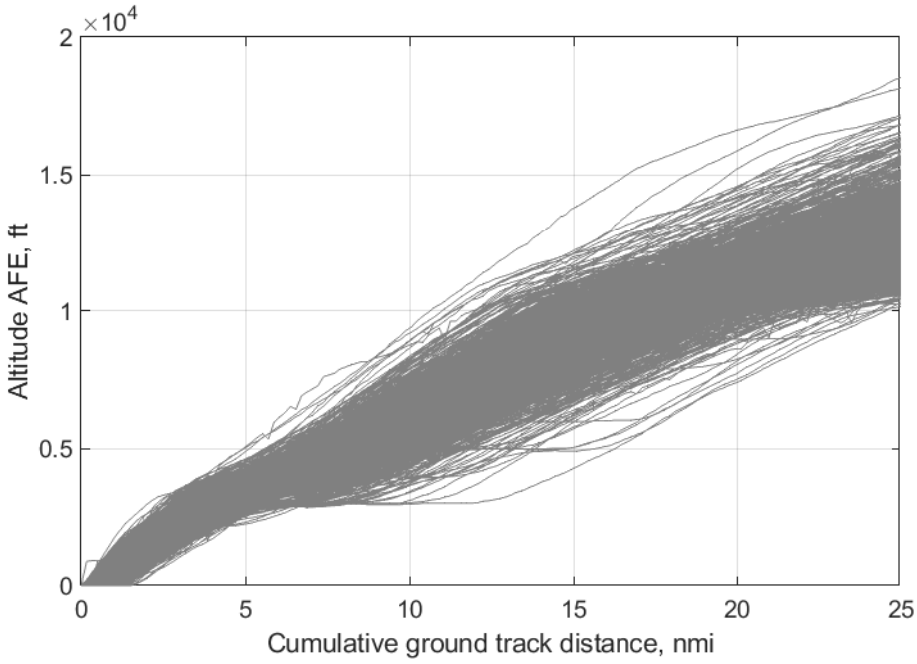

Figure 6.2: Visualization of 1361 flights from OpenSky dataset

Starting with this set of real-world data, the objective is to quantify the noise impact of each of these flights. Traditionally, capturing the variation in real-world trajectories has been difficult due to the need to model each flight uniquely. However, with the developed methodology, each flight does not have to be modeled.

Step 2: Trajectory clustering

Next, the collected flights were put through the clustering process outlined in RQ1.2. This process included the resampling of data to a consistent basis, evaluation of similarity function, creation of clusters and validation of created groupings, and the identification of representative medians for each cluster. The identified groupings and their representative medians are visualized in Figure 6.3.

The size of clusters is important as it impacts the scaling of the noise results obtained

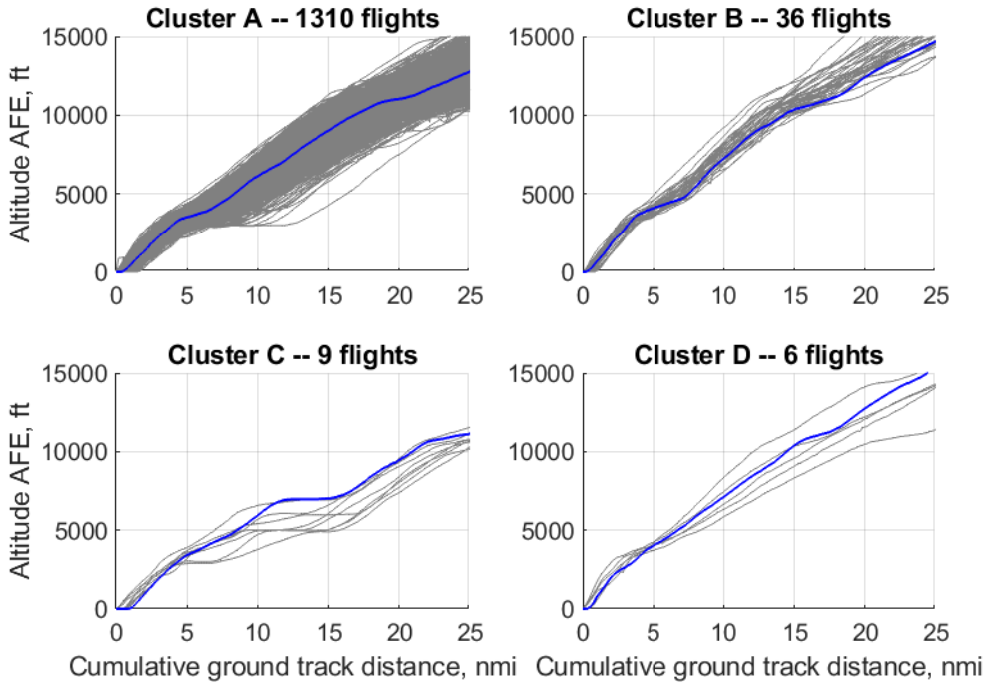

Figure 6.3: Visualization of the four identified clusters and their median

for each median further downstream in the process. For example, to obtain the DNL noise metric result, the noise contribution of each individual flight is aggregated. Therefore, in this case, the noise contributions of the representative flights would need to be scaled by the number of flights before adding the contributions of each representative to obtain an airport level noise result.

Step 3: Inverse mapping of cluster medians

Next, the identified median representative of each flight inverse mapped onto a set of four procedural profile parameters. The median representative for each cluster and its closest matching flight which yields the inverse map are shown in Figure 6.4. These identified parametric definitions are summarized in Table 6.1.

It is observed that although the numeric error values are high, the visualizations confirm that the best suitable match for each median representative flight was identified. Thus at this stage, every single real-world flight has been converted to a parametric definition through

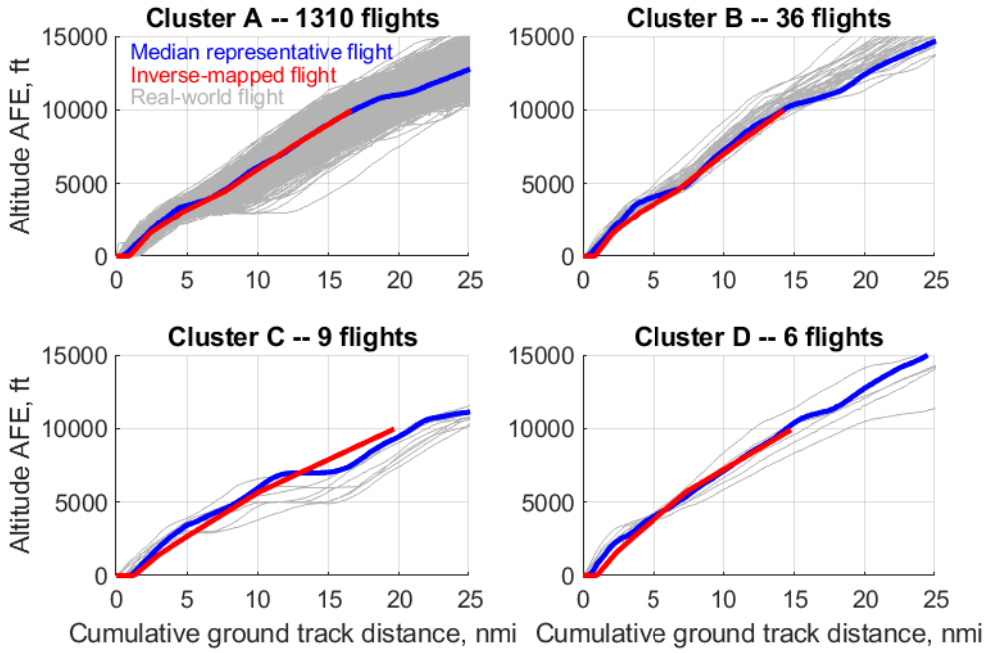

Figure 6.4: Visualization of the four identified clusters, their medians, and respective inverse mappings

the inverse map of its representative median cluster flight.

Step 4: Evaluation of noise metrics

With the determination of the parameters, only one final step remains. The constructed field surrogate model, or Reduced Order Model in chapter 5 is used to evaluate the SEL noise metric of each of the four representative median flights. The ROM needs an input for temperature, in addition to the four parameters. Here, the temperature is assumed to be 60 °F. The separate SEL noise grids representing the single median flight from each cluster is shown in Figure 6.5.

Summary

With the obtained noise grids and contours, the methodology is complete. Over the four steps outlined above, the methodology was able to receive a large number of real-world time-series flight data and obtain the noise metrics and contours for each real flight by

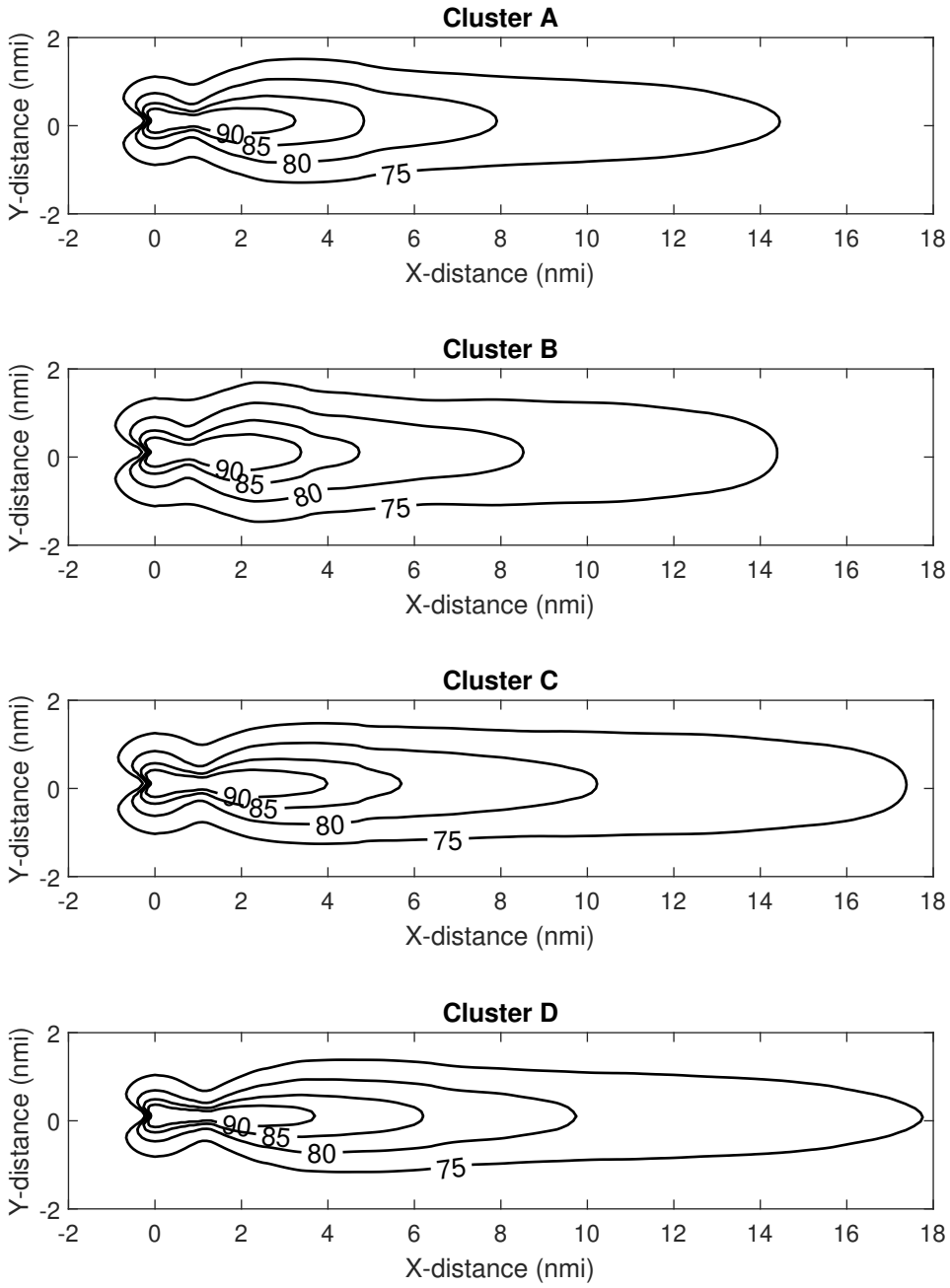

Figure 6.5: Noise contours for each of the four cluster median representative flights

Table 6.1: Inverse parametric mappings of the four cluster median representative flights

Cluster	A	B	C	D
Number of flights in cluster	1310	36	9	6
Representative Median ID	969	1295	186	1380
Closest matched AEDT flight ID	195	90	150	238
Error of mapping process	8.24%	12.93%	16.09%	16.16%
Takeoff Weight, lb_m, α_1	151100	151100	169950	169950
Takeoff thrust reduction, α_2	0.90	1.00	0.95	0.85
Altitude of acceleration initiation, ft, α_3	1600	1600	1000	1600
Energy Share Percentage α_4	40	60	40	40

evaluating a field surrogate model on the parametric definition of the median representative flight for its cluster.

This demonstration of the methodology shows how the complexities of handling real-world flight data and the high dimensional noise grid outputs was addressed. With the constructed methodology, rapid quantification of aviation noise is made possible, thus facilitating parametric trade-off analyses and optimization efforts. The original Research Objective is therefore considered to be fulfilled.

6.4 Discussion on improvements to current modeling methods and tools

With the overall methodology now developed and demonstrated, it is helpful to revisit the state-of-the-art modeling methods and tools and see how the developed methodology improves upon them. Both use-cases are discussed here.

6.4.1 Improvements to real-world quantification

First, consider a situation where a large number of real-world trajectories have to be analyzed for their noise impact. Such type of analysis is often required for airport-level noise contours where an averaged day of operations might need to be modeled. There are two possible processes by which such modeling might be carried out in a tool like AEDT.

The first option is to simply use the pre-defined default departure operation which removes all variation in the real-world trajectory. This pre-defined departure operation is created to represent real-world variation in an averaged sense, and thus gets rid of the variability in the real-world dataset that might be desirable.

The other option is to model each real-world flight uniquely by directly using its trajectory and performance as a fixed-point profile. There are two shortcomings to this method. Firstly, the thrust variation along the trajectory must be known and specified in this method. As noted earlier, many real-world data sources based on ADS-B or RADAR do not contain thrust information. Second, modeling each flight uniquely is feasible only for a small number of flights. As each flight needs to be properly formatted and processed to get the noise results, the process does not scale well to large number of flights.

These two modeling options can be thought of as the two end points of a spectrum. On one side, the default departure operation is fast to use but cannot provide variability. On the other side, fixed-point profiles can be used to retain variability but do not scale well for large number of flights. The methodology developed here provides a suitable compromise – variability is retained by having multiple clusters, and scalability is provided by only modeling the representatives of each cluster. This represents an improvement on the current state-of-the-art and using this method may lead to more accurate noise quantification analyses for real-world flights.

6.4.2 Improvements to optimization

Second, consider the situation where an airline or airport is trying to minimize the noise footprint from their operations. Given the modeling scenario (aircraft, weight, runway orientation), the objective would be to minimize the noise impact. In addition to the profile design, this noise impact is dependent on external conditions such as the elevation of the airport, ambient temperature, ambient humidity etc. Thus, to do a true optimization effort, a comprehensive study of all possible scenarios must be conducted.

As noted in the literature review, this comprehensive study is infeasible with existing methods and tools. At present, such studies would require subject matter expert input and some heuristics would be used to narrow the scope of analyses. A common method for scoping down is limiting the consideration to a single elevation (such as a sea-level airport) or to a single weather condition (airport average or standard day). Typically, a handful of profiles would be designed and evaluated for their noise impact. The best performing of these alternatives would then be chosen as the 'optimal'. Although this type of optimization is limited in its scope, it is the best that current methods and tools can support.

The switch to field surrogate modeling, as shown in the developed methodology introduces rapid noise quantification capabilities and enables true optimization. While the fundamental improvement in speed is certainly important, the facilitation of new type of analyses is the main benefit. External conditions such as ambient weather can be included, and many thousands of candidate profiles can be evaluated, instead of just a handful. Additionally, due to the nature of the parametric model, the design space of profiles can be explored efficiently. Thus, the developed methodology represents an improvement over the current state-of-the-art and using it enables more comprehensive optimization studies.

6.5 Expansion of methodology capabilities

The methodology developed in this dissertation had a focus on improving the traditional noise modeling process. By surveying the literature, it was identified that improving the modeling capabilities for aircraft level noise impacts by replacing physics-based and semi-empirical models with parametric field surrogate models would provide the most benefit. This section provides a discussion on how the developed methodology interfaces with existing literature, and how it can be used to improve airport-level noise modeling.

6.5.1 Modeling of additional/generic aircraft types

The experiments throughout this dissertation used the Boeing 737-800 aircraft as an example aircraft type for the various processes developed. The methods developed here, however are quite agnostic of the aircraft type and can be adapted for use with other aircraft types for which existing noise modeling capabilities exist. For example, AEDT contains the relevant equations, coefficients, and data to model the noise impacts of almost all commercial aircraft. To adapt this method to work with a different aircraft type, such as an Airbus A320, the process must be repeated using data specific to that aircraft.

The inverse map developed in RQ1.1 for example uses a pre-computed library of trajectories which must match the aircraft for which real-world data is available. Using the same parametric definition, the A320 can be modeled to obtain the pre-computed library. Then real-world trajectories of the A320 can be compared using the similarity metric to obtain the inverse mapping. Similarly, the field surrogate model must also be updated to be based on the full-order model results corresponding the the A320 aircraft.

Another approach can be to develop generic models of different aircraft categories, such as regional, narrow-body, and wide-body instead of using specific models of aircraft. AEDT does not provide generic aircraft modeling capabilities, however some studies in literature have attempted to build generic aircraft models for the purposes of aircraft noise estimation [247]. For example, the GENERICA method developed by LeVine et. al. [114] provides such generic aircraft definitions for which this methodology could be built. By using appropriately designed generic vehicles, the amount of data in the pre-computed inverse-map library and the field surrogate model can be greatly reduced while simultaneously expanding the applicability of the methodology.

6.5.2 Improving airport-level noise computations

Another enhancement of this methodology is to link it with airport-level analyses. In literature, airport-level analyses have been made rapid by maintaining a library of pre-

computed vehicle-level noise grids. By rotating and combining these pre-computed grids, an airport level grid could be obtained. This process was developed by Bernardo et. al. and is called the Airport Noise Grid Interpolation Method (ANGIM) [38, 112, 113]. The key limitation of this was that vehicle-level grids were not sensitive to the aircraft trajectory, ambient weather, airport elevation etc.

Choosing to include those sensitivities would have implied expanding the pre-computed library by a factor of 10 to 100, which would be impractical due to storage requirements. Noise grid information is high-dimensional data with many thousands of points per grid. The methodology developed here solves the problem by providing a rapid method of obtaining the vehicle-level noise grids in a variety of scenarios. Thus, by merging this methodology with ANGIM, airport-level noise analyses can be conducted rapidly – rapid vehicle-level noise quantification from this methodology, and rapid airport-level noise quantification with ANGIM.

CHAPTER 7
SUMMARY AND CONCLUSIONS

This chapter concludes the dissertation with a summary of each Research Question formulation and accompanying experiments, key contributions resulting from this research, and the identification of potential avenues for future work which can draw from the work presented in this dissertation.

Starting with the high-level Motivating Research Question and Research Objectives, an initial literature review was performed and key observations were highlighted. The observations led to the discovery of two formally stated Gaps in modeling capabilities. Each Gap was addressed by a high-level Research Question, which in turn was decomposed into five specific Research Questions. These then led to another round of review of methods and processes which helped in the formation of Hypothesis. To determine whether each Hypothesis could be accepted, detailed Experiments were proposed and performed. With the conclusion of all experiments, the Research Plan was complete, and the overall methodology could be constructed, which fulfilled the Research Objective.

7.1 Summary of Research Plan

The Research Plan was divided into two key areas, which are summarized here. The overall research formulation of this dissertation is presented in Figure 7.1.

7.1.1 Summary of Research Area 1

The first research area was identified to deal with the problem of parametric representation of aircraft trajectories. First, RQ1.1 solved the problem of representation, RQ1.2 solved the problem of scalability, and RQ1.3 solved the problem of efficient exploration.

In Research Question 1.1, a parametric representation for aircraft trajectories and

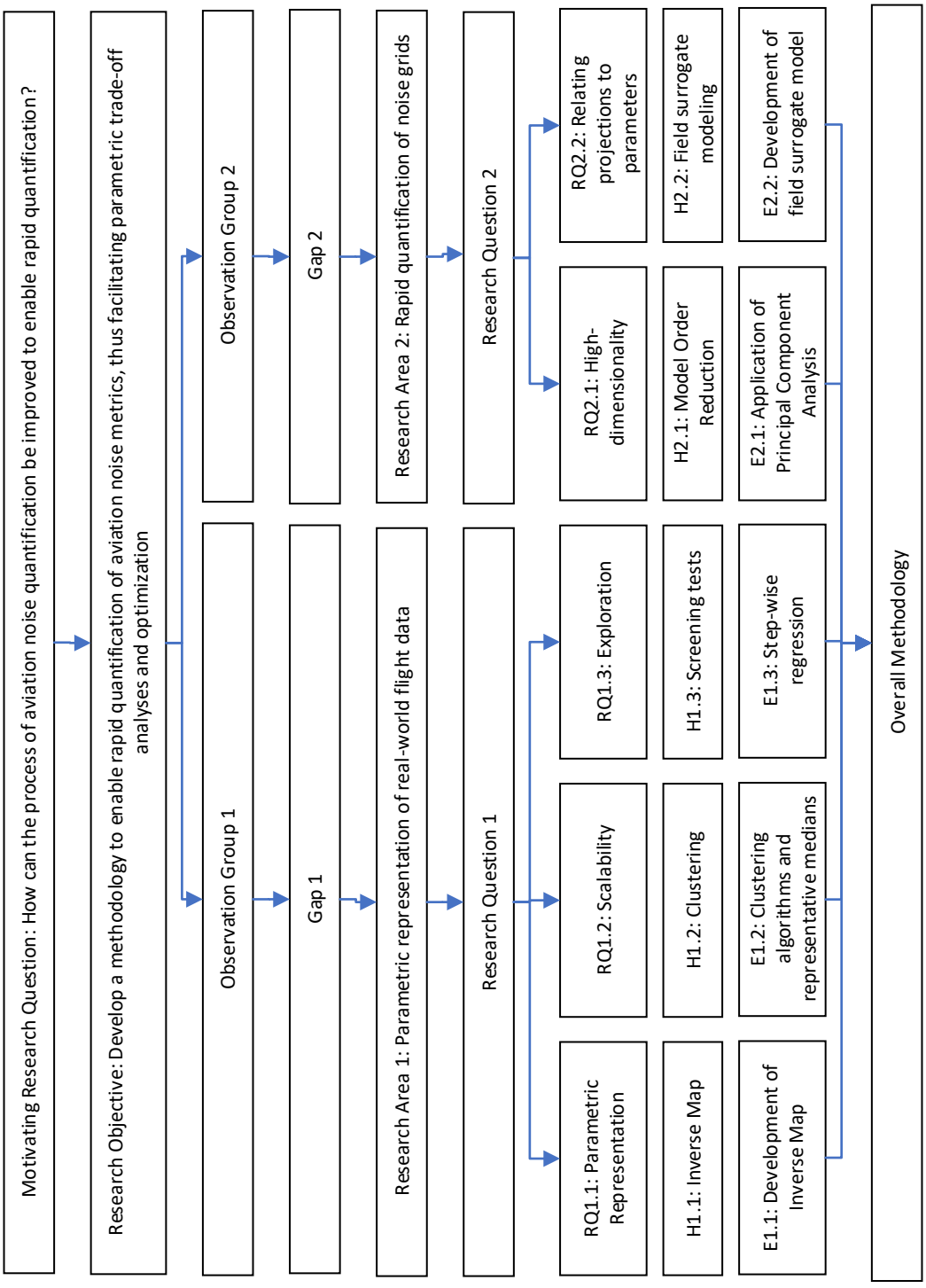

Figure 7.1: Overview of the Research Formulation

performance characteristics was proposed and an inverse-map method was developed in order to create parametric representations of real-world time-series flight data. The inverse-map was developed on the notion of trajectory similarity, and the evaluation of such similarity on a pre-computed library of trajectories. Thus, a real-world flight was assigned the parametric definition of the pre-defined trajectory it was most closely aligned with.

In Research Question 1.2, a supplementary method was proposed to make the inverse-mapping and subsequent noise quantification process more efficient for large real-world flight datasets. A clustering process was developed to group flights together based on their similarities in altitude, ground speed, and vertical speed over ground track distance. Once clusters had been identified, a representative flight from each cluster was chosen. This chosen representative was then put through the inverse map process, to obtain a parametric definition for all flights within the parent cluster.

In Research Question 1.3, the focus shifted from real-world noise quantification, to theoretical procedural profile design. In addition to the four profile parameters, an external parameter in the form of ambient temperature was added. A large set of noise results were obtained, and the raw results were converted into the aggregated metrics of contour length and area. These aggregated metrics were then used to build parameter screening models to help identify the relative importance of each of the five input parameters on each of the aggregated contour metrics. The obtained rankings showed which parameters were most influential, and which did not appreciably influence any given metric.

7.1.2 Summary of Research Area 2

The second research area was identified to deal with the problem of high-dimensionality of the output noise grids from any noise quantification process. First, RQ2.2 solved the problem of model order reduction and RQ2.2 solved the problem of linking solutions to the input parameters.

In Research Question 2.1, a model order reduction technique called Principal Compo-

nent Analysis was adapted for use with aviation noise grids. This technique projected the high dimensional data along a new set of principal directions computed using the singular value decomposition method. In this projected hyperplane, each noise grid could be accurately represented with only a handful of coordinates along each of the chosen principal directions. Thus, the dimensionality of noise grids was greatly reduced while minimizing the loss of information due to the projection.

In Research Question 2.2, a prediction model for the projected data was constructed to link the input parameters directly to the coordinates in the projected hyperplane. Thus, the complete process of aviation noise estimation could be bypassed, after the construction of the prediction surrogate model. By using the predicted coordinates in the lower-dimensional space, it was demonstrated how the original high-dimensional noise grids could be reconstructed. In combination with the projection step, this developed model was referred to as a Reduced Order Model or a field surrogate model.

7.2 Contributions

The primary contribution of this dissertation is the creation and demonstration of a methodology for the rapid and accurate quantification of aviation noise metrics. In particular, the developed methodology showed that it was possible to rapidly predict entire noise grids using field surrogate modeling, instead of relying on scalar-valued surrogate models of aggregated metrics such as contour areas. This represents a significant improvement from noise modeling techniques in literature, where either speed is compromised for accuracy or vice-versa. A salient feature of the developed methodology is the adaptation of Model Order Reduction techniques for the aviation noise quantification problem, which represents a significant shift away from traditional modeling paradigms in this domain of research and represents the core improvement which enabled rapid and accurate modeling.

The theoretical improvements of this new paradigm of models was also demonstrated using a large and comprehensive set of noise results obtained by the state-of-the-art

Aviation Environmental Design Tool. With the projection and prediction techniques developed in the second research area, the process of constructing, validating, and using the field surrogate model was documented.

The second set of contributions from this dissertation are the data-driven techniques created for the parametric representation of aircraft trajectories. Existing environmental modeling options for real-world flights were significantly limited in their scope and/or accuracy. With the absence of thrust data, most real-world flights had to be approximated by a single averaged procedural profile. However, a single averaged flight could not possible represent the wide range of variation observed in real-world trajectories. This dissertation provides methods for both handling the large number of unique flights, and also for mapping such flights to a parametric representation. A key benefit of parametric representation is that it provides a way for thrust estimation of real-world flight data using only available trajectory and speed information. To the best of the author's knowledge, this dissertation is the first to document an inverse map process created to generate parametric definitions of real-world flight data, particularly in the context of aviation noise quantification.

The third and final contribution of this dissertation is the global sensitivity analysis of aviation noise metrics to the identified input parameters. The step-wise regression method used provided a ranking of parameters (and their interactions) in terms of their influence on the noise grids and contour dimensions. Additionally, it also identified parameters which were not influential on the output metrics of interest. This serves to provide a recommendation to future modeling studies, where only a limited number of designs may be potentially evaluated. In such restrictive conditions, the parameters identified with the most effect should be sampled more finely, whereas the ones with negligible impacts can safely be discarded or set to their default values.

In summary, the developed methodology and underlying techniques fill the gaps observed in literature by facilitating the rapid quantification of aviation noise metrics in

a variety of scenarios and thus enabling many-query applications such as parametric trade-off analyses and optimization studies. The developed framework can be deployed both for accurate real-world noise quantification, or for optimization studies such as those for the design of noise abatement departure procedures.

7.3 Recommendations for Future Work

Aviation sustainability is and will continue to be at the forefront of aviation research in the future. The successful mitigation of aviation noise is a key component of sustainability, and thus there will always be a need for the rapid evaluation of aviation noise metrics. Although the hypotheses tested in this dissertation have answered the posed Research Questions, closed the identified gaps, and fulfilled the Research Objective; there are a potential avenues for further improvement or extension of the developed methodology. These avenues are discussed here, in the order in which their relevant research question appears in this dissertation.

The inverse map was developed to provide a method for real-world aircraft data to be represented with a handful of parameter values. This proposed method made use of only the aircraft trajectory in the form of aircraft altitude and ground track distance, and worked well to identify the inverse mappings for a large number of real-world flights. However, some outlier flights could not be accurately mapped due the presence of unexpected flight events such as a level-off during the climb-out phase. Thus, the identification of outliers would be helpful in improving the accuracy of the inverse mapping. Another potential source of improvement would be the identification of the start of takeoff-ground roll. Some real-world flights have unexpectedly long ground roll segments, likely due to the inclusion of some pre-departure taxiing segments. Finally, this process may also benefit from the inclusion of additional parameters such as the speed of the aircraft or the time elapsed at various points through the flight.

Another key area of improvement would be the inclusion of the ground track of flights

throughout the methodology. Currently, only the variation in the 2D vertical profile of the flight is considered. However, including the ground track of the flights would make the methodology more accurate by expanding the analysis to 3D trajectories. Ground tracks can be defined parametrically by using their vector representations. A vector ground track is represented as a sequence of segments of varying lengths, radii of curvature and directions of curvature. Thus, the parametric definition of the flight trajectories could be expanded to include these additional ground track parameters. The field surrogate model can also be expanded to include sensitivities to ground track.

While the reduced order modeling capability demonstrated in this dissertation showed great promise, it was only tested with the SEL noise metric. The applicability of this method to other noise metrics remains to be seen. Even with the SEL noise metric, many outliers could be observed at the projection step. For these outliers, the projection from the original high-dimensional space to the identified lower-dimensional hyperplane resulted in significant errors. It is possible that the original cloud of high-dimensional data is not well suited for linear dimensionality reduction techniques such as the Principal Component Analysis. Therefore, non-linear Model Order Reduction techniques such as isomap and other manifold learning algorithms should be investigated. The application of these models to similar datasets may yield in more accurate dimensionality reduction with fewer outliers.

REFERENCES

[1] The Boeing Company, *Commercial Market Outlook 2021-2040*, 2021. [Online]. Available: https://www.boeing.com/commercial/market/commercial-market-outlook/.

[2] Airbus SAS, *Global Market Forecast 2021-2040*, 2021. [Online]. Available: https://www.airbus.com/aircraft/market/global-market-forecast.html.

[3] Federal Aviation Administration, *FAA Aerospace Forecast 2021-2041*, 2021. [Online]. Available: https://www.faa.gov/data_research/aviation/aerospace_forecasts.

[4] EUROCONTROL, *EUROCONTROL Aviation Outlook 2050, Flights and CO_2 forecasts*, Apr. 2022. [Online]. Available: https://www.eurocontrol.int/publication/eurocontrol-aviation-outlook-2050.

[5] Office of Inspector General, "Aviation Industry Performance, A Review of the Aviation Industry, 2008-2011," U.S. Department of Transportation, Report Number: CC-2012-029, Sep. 2012. [Online]. Available: https://www.oig.dot.gov/sites/default/files/Aviation%20Industry%20Performance%5E9-24-12.pdf.

[6] International Air Transport Association (IATA), *Air Passenger Numbers to Recover in 2024*, Press Release, Mar. 2022. [Online]. Available: https://www.iata.org/en/pressroom/2022-releases/2022-03-01-01/.

[7] EUROCONTROL, *EUROCONTROL Forecast Update 2021-2027*, Oct. 2021. [Online]. Available: https://www.eurocontrol.int/publication/eurocontrol-forecast-update-2021-2027.

[8] K. Dube, G. Nhamo, and D. Chikodzi, "Covid-19 pandemic and prospects for recovery of the global aviation industry," *Journal of Air Transport Management*, vol. 92, p. 102 022, 2021. DOI: https://doi.org/10.1016/j.jairtraman.2021.102022. [Online]. Available: https://www.sciencedirect.com/science/article/pii/S0969699721000053.

[9] S. Gudmundsson, M. Cattaneo, and R. Redondi, "Forecasting temporal world recovery in air transport markets in the presence of large economic shocks: The case of covid-19," *Journal of Air Transport Management*, vol. 91, p. 102 007, 2021. DOI: https://doi.org/10.1016/j.jairtraman.2020.102007. [Online]. Available: https://www.sciencedirect.com/science/article/pii/S0969699720305871.

[10] Statista, *Number of scheduled passengers boarded by the global airline industry from 2004 to 2022*, Oct. 2021. [Online]. Available: https://www.statista.com/statistics/564717/airline-industry-passenger-traffic-globally/.

[11] S. Rajendran, S. Srinivas, and T. Grimshaw, "Predicting demand for air taxi urban aviation services using machine learning algorithms," *Journal of Air Transport Management*, vol. 92, p. 102 043, 2021. DOI: https://doi.org/10.1016/j.jairtraman.2021.102043. [Online]. Available: https://www.sciencedirect.com/science/article/pii/S0969699721000260.

[12] L. A. Garrow, P. Mokhtarian, B. German, and S.-S. Boddupalli, "Commuting in the age of the jetsons: A market segmentation analysis of autonomous ground vehicles and air taxis in five large u.s. cities," in *AIAA AVIATION 2020 FORUM*, Jun. 2020. DOI: 10.2514/6.2020-3258. [Online]. Available: https://arc.aiaa.org/doi/abs/10.2514/6.2020-3258.

[13] S. Roy, M. T. K. Herniczek, B. German, and L. A. Garrow, "User base estimation methodology for an evtol business airport shuttle air taxi service," in *AIAA AVIATION 2020 FORUM*, Jun. 2020. DOI: 10.2514/6.2020-3259. [Online]. Available: https://arc.aiaa.org/doi/abs/10.2514/6.2020-3259.

[14] National Aeronautics and Space Administration (NASA), *UAM Overview*, Aug. 2019. [Online]. Available: https://www.nasa.gov/uam-overview/.

[15] M. V. Bendarkar, D. Sarojini, and D. N. Mavris, "Off-nominal performance and reliability of novel aircraft concepts during early design," *Journal of Aircraft*, vol. 59, no. 2, pp. 400–414, 2022. DOI: 10.2514/1.C036395.

[16] M. V. Bendarkar, A. Behere, S. I. Briceno, and D. N. Mavris, "A Bayesian Safety Assessment Methodology for Novel Aircraft Architectures and Technologies Using Continuous FHA," in *AIAA Aviation 2019 Forum*, Jun. 2019. DOI: 10.2514/6.2019-3123. [Online]. Available: https://arc.aiaa.org/doi/abs/10.2514/6.2019-3123.

[17] M. V. Bendarkar, D. Rajaram, Y. Cai, and D. N. Mavris, "Optimal paths for progressive aircraft subsystem electrification in early design," *Journal of Aircraft*, vol. 59, no. 1, pp. 219–232, 2022. DOI: 10.2514/1.C036085.

[18] M. V. Bendarkar, D. Rajaram, Y. Cai, S. I. Briceno, and D. N. Mavris, "Evaluating optimal paths for aircraft subsystem electrification in early design," in *AIAA Aviation 2019 Forum*, Jun. 2019. DOI: 10.2514/6.2019-2802. [Online]. Available: https://arc.aiaa.org/doi/10.2514/6.2019-2802.

[19] S. Jain, K. E. Ogunsina, H. Chao, W. A. Crossley, and D. A. DeLaurentis, "Predicting routes for, number of operations of, and fleet-level impacts of future commercial supersonic aircraft on routes touching the united states," in *AIAA AVIATION 2020 FORUM*, Jun. 2020. DOI: 10.2514/6.2020-2878. [Online]. Available: https://arc.aiaa.org/doi/abs/10.2514/6.2020-2878.

[20] B. Liebhardt, V. Gollnick, and K. Luetjens, "Estimation of the market potential for supersonic airliners via analysis of the global premium ticket market," in *11th AIAA Aviation Technology, Integration, and Operations (ATIO) Conference*, Jun. 2012. DOI: 10.2514/6.2011-6806. [Online]. Available: https://arc.aiaa.org/doi/abs/10.2514/6.2011-6806.

[21] B. Liebhardt and K. Lütjens, "An analysis of the market environment for supersonic business jets," in *DLRK 2011*, 2011. [Online]. Available: https://elib.dlr.de/75275/.

[22] Y. Sun and H. Smith, "Review and prospect of supersonic business jet design," *Progress in Aerospace Sciences*, vol. 90, pp. 12–38, 2017. DOI: https://doi.org/10.1016/j.paerosci.2016.12.003. [Online]. Available: https://www.sciencedirect.com/science/article/pii/S0376042116301002.

[23] J. Zhang, D. Wuebbles, D. Kinnison, and S. L. Baughcum, "Potential impacts of supersonic aircraft emissions on ozone and resulting forcing on climate: An update on historical analysis," *Journal of Geophysical Research: Atmospheres*, vol. 126, no. 6, e2020JD034130, 2021, e2020JD034130 2020JD034130. DOI: https://doi.org/10.1029/2020JD034130. [Online]. Available: https://agupubs.onlinelibrary.wiley.com/doi/abs/10.1029/2020JD034130.

[24] J. J. Berton, D. L. Huff, K. Geiselhart, and J. Seidel, "Supersonic technology concept aeroplanes for environmental studies," in *AIAA Scitech 2020 Forum*, Jan. 2020. DOI: 10.2514/6.2020-0263. [Online]. Available: https://arc.aiaa.org/doi/abs/10.2514/6.2020-0263.

[25] S. Jain, M. Mane, W. Crossley, and D. DeLaurentis, "Investigating How Commercial Supersonic Aircraft Operations Might Impact Subsonic Operations and Total CO_2 Emissions," in *AIAA AVIATION 2021 FORUM*, Jun. 2021. DOI: 10.2514/6.2021-3014. [Online]. Available: https://arc.aiaa.org/doi/abs/10.2514/6.2021-3014.

[26] A. Mahashabde *et al.*, "Assessing the environmental impacts of aircraft noise and emissions," *Progress in Aerospace Sciences*, vol. 47, no. 1, pp. 15–52, 2011. DOI: https://doi.org/10.1016/j.paerosci.2010.04.003. [Online]. Available: https://www.sciencedirect.com/science/article/pii/S0376042110000382.

[27] K. Moolchandani, P. Govindaraju, S. Roy, W. A. Crossley, and D. A. DeLaurentis, "Assessing effects of aircraft and fuel technology advancement on select aviation environmental impacts," *Journal of Aircraft*, vol. 54, no. 3, pp. 857–869, 2017. DOI: 10.2514/1.C033861. [Online]. Available: https://doi.org/10.2514/1.C033861.

[28] K. Moolchandani, D. B. Agusdinata, M. Mane, D. DeLaurentis, and W. Crossley, "Assessment of the effect of aircraft technological advancement on aviation environmental impacts," in *51st AIAA Aerospace Sciences Meeting including the*

New Horizons Forum and Aerospace Exposition, Jan. 2013. DOI: 10.2514/6.2013-652. [Online]. Available: https://arc.aiaa.org/doi/abs/10.2514/6.2013-652.

[29] K. B. Marais *et al.*, "Evaluation of potential near-term operational changes to mitigate environmental impacts of aviation," *Proceedings of the Institution of Mechanical Engineers, Part G: Journal of Aerospace Engineering*, vol. 227, no. 8, pp. 1277–1299, 2013. DOI: 10.1177/0954410012454095. [Online]. Available: https://doi.org/10.1177/0954410012454095.

[30] "Aviation emissions, impacts & mitigation: A primer," Federal Aviation Administration - Office of Environment and Energy, Jan. 2015. [Online]. Available: https://www.faa.gov/regulations_policies/policy_guidance/envir_policy/media/primer_jan2015.pdf.

[31] K. Suder, "Overview of the NASA Environmentally Responsible Aviation Project's Propulsion Technology Portfolio," in *48th AIAA/ASME/SAE/ASEE Joint Propulsion Conference & Exhibit*, Jul. 2012. DOI: 10.2514/6.2012-4038. [Online]. Available: https://arc.aiaa.org/doi/abs/10.2514/6.2012-4038.

[32] IATA, "Aircraft Technology Roadmap to 2050," IATA, Tech. Rep., 2009. [Online]. Available: https://www.iata.org/contentassets/8d19e716636a47c184e7221c77563c93/Technology-roadmap-2050.pdf.

[33] International Civil Aviation Organization, *ICAO Council adopts new CO2 emissions standard for aircraft*, 2017. [Online]. Available: https://www.icao.int/newsroom/pages/icao-council-adopts-new-co2-emissions-standard-for-aircraft.aspx.

[34] ——, *Global trends in Aircraft Noise*. [Online]. Available: https://www.icao.int/environmental-protection/Pages/Noise_Trends.aspx.

[35] National Academy of Engineering, *Technology for a Quieter America*. Washington, DC: The National Academies Press, 2010, ISBN: 978-0-309-15632-5. DOI: 10.17226/12928. [Online]. Available: https://nap.nationalacademies.org/catalog/12928/technology-for-a-quieter-america.

[36] ICAO, "ICAO 9829 – guidance on the balanced approach to aircraft noise management, 2nd edition," ICAO, Tech. Rep., Oct. 2010. [Online]. Available: https://global.ihs.com/doc_detail.cfm?&input_search_filter=ICAO&item_s_key=00507943&item_key_date=890221&input_doc_number=9829&input_doc_title=&org_code=ICAO.

[37] U. S. G. A. Office, "Aviation and the Environment, Systematically Addressing Environmental Impacts and Community Concerns Can Help Airports Reduce

Project Delays," United States Government Accountability Office, Government Report, Sep. 2010. [Online]. Available: https://www.gao.gov/assets/gao-10-50.pdf.

[38] J. E. Bernardo, "Formulation and Implementation of a Generic Fleet-level Noise Methodology," PhD dissertation, Georgia Institute of Technology, Atlanta, GA, USA, May 2013.

[39] M. Basner *et al.*, "Aviation Noise Impacts: State of the Science," *Noise & health*, vol. 19, no. 87, pp. 41–50, 2017, NoiseHealth_2017_19_87_41_204623[PII]. DOI: 10.4103/nah.NAH_104_16. [Online]. Available: https://doi.org/10.4103/nah.NAH_104_16.

[40] B. Berglund, T. Lindvall, and S. Nordin, "Adverse effects of aircraft noise," *Environment International*, vol. 16, no. 4, pp. 315–338, 1990, Public Health Implications of Environmental Noise. DOI: https://doi.org/10.1016/0160-4120(90)90002-N. [Online]. Available: https://www.sciencedirect.com/science/article/pii/016041209090002N.

[41] V. Sparrow *et al.*, "Aviation noise impacts white paper, state of the science 2019: Aviation noise impacts," ICAO, White Paper, 2019. [Online]. Available: https://www.icao.int/environmental-protection/Documents/ScientificUnderstanding/EnvReport2019-WhitePaper-Noise.pdf.

[42] Transportation Research Board and National Academies of Sciences, Engineering, and Medicine, *Effects of Aircraft Noise: Research Update on Select Topics*. Washington, DC: The National Academies Press, 2008. DOI: 10.17226/14177. [Online]. Available: https://www.nap.edu/catalog/14177/effects-of-aircraft-noise-research-update-on-select-topics.

[43] A. Rodríguez-Díaz, B. Adenso-Díaz, and P. González-Torre, "A review of the impact of noise restrictions at airports," *Transportation Research Part D: Transport and Environment*, vol. 50, pp. 144–153, 2017. DOI: https://doi.org/10.1016/j.trd.2016.10.025. [Online]. Available: https://www.sciencedirect.com/science/article/pii/S136192091630342X.

[44] A. W. Correia, J. L. Peters, J. I. Levy, S. Melly, and F. Dominici, "Residential exposure to aircraft noise and hospital admissions for cardiovascular diseases: Multi-airport retrospective study," *BMJ*, vol. 347, 2013. DOI: 10.1136/bmj.f5561. [Online]. Available: https://www.bmj.com/content/347/bmj.f5561.

[45] M. Basner, U. Müller, and E.-M. Elmenhorst, "Single and combined effects of air, road, and rail traffic noise on sleep and recuperation," *Sleep*, vol. 34, no. 1, pp. 11–23, Jan. 2011. DOI: https://doi.org/10.1093/sleep/34.1.11. [Online]. Available: https://pubmed.ncbi.nlm.nih.gov/21203365/.

[46] E. Ganić, J. Ivošević, and B. Mirković, "Impact of aircraft noise on communities near belgrade airport," *Promet – Traffic & Transportation*, vol. 33, no. 3, pp. 323–335, May 2021. DOI: 10.7307/ptt.v33i3.3692. [Online]. Available: https://traffic.fpz.hr/index.php/PROMTT/article/view/3692.

[47] S. A. Janssen, H. Vos, E. E. M. M. van Kempen, O. R. P. Breugelmans, and H. M. E. Miedema, "Trends in aircraft noise annoyance: The role of study and sample characteristics," *The Journal of the Acoustical Society of America*, vol. 129, no. 4, pp. 1956–62, Apr. 2011. DOI: https://doi.org/10.1121/1.3533739. [Online]. Available: https://pubmed.ncbi.nlm.nih.gov/21476651/.

[48] S. Fidell *et al.*, "A first-principles model for estimating the prevalence of annoyance with aircraft noise exposure," *The Journal of the Acoustical Society of America*, vol. 130, no. 2, pp. 791–806, Aug. 2011. DOI: https://doi.org/10.1121/1.3605673. [Online]. Available: https://pubmed.ncbi.nlm.nih.gov/21877795/.

[49] G. W. Evans, M. Bullinger, and S. Hygge, "Chronic noise exposure and physiological response: A prospective study of children living under environmental stress," *Psychological Science*, vol. 9, no. 1, pp. 75–77, 1998. [Online]. Available: http://www.jstor.org/stable/40063251.

[50] S. Hygge, G. W. Evans, and M. Bullinger, "A prospective study of some effects of aircraft noise on cognitive performance in schoolchildren," *Psychological Science*, vol. 13, no. 5, pp. 469–474, 2002. [Online]. Available: http://www.jstor.org/stable/40063882.

[51] C. B. Pepper, M. A. Nascarella, and R. J. Kendall, "A review of the effects of aircraft noise on wildlife and humans, current control mechanisms, and the need for further study," *Environmental Management*, vol. 32, no. 4, pp. 418–32, Oct. 2003. DOI: https://doi.org/10.1007/s00267-003-3024-4. [Online]. Available: https://pubmed.ncbi.nlm.nih.gov/14986892/.

[52] N. Kempf and O. Hüppop, "The effects of aircraft noise on wildlife: A review and comment," *Journal of Ornithology*, vol. 137, pp. 101–113, Jan. 1996.

[53] K. M. Manci, D. N. Gladwin, R. Villella, and M. G. Cavendish, "Effects of aircraft noise and sonic booms on domestic animals and wildlife: A literature synthesis," U.S. Fish and Wildlife Service, National Ecology Research Center, Fort Collins, CO, Jun. 1988. [Online]. Available: https://www.fs.fed.us/eng/techdev/IM/sound_measure/Manci_et_al_1988.pdf.

[54] R. Tam, "Application and Sensitivity of Airport Noise-Damage Costs," *Transportation Research Record*, vol. 2362, no. 1, pp. 35–41, 2013. DOI: 10.3141/2362-05. [Online]. Available: https://doi.org/10.3141/2362-05.

[55] P. Morrel and C. H.-Y. Lu, "Social Costs of Aircraft Noise and Engine Emissions: Case Study of Amsterdam's Schiphol Airport," *Transportation Research Record*, vol. 1703, no. 1, pp. 31–38, 2000. DOI: 10.3141/1703-05. [Online]. Available: https://doi.org/10.3141/1703-05.

[56] M. Frankel, "Aircraft noise and residential property values: Results of a survey study," *The Appraisal Journal*, vol. 59, 1 Jan. 1991.

[57] C. Lipscomb, "Small cities matter, too: The impacts of an airport and local infrastructure on housing prices in a small urban city," *Review of Urban & Regional Development Studies*, vol. 15, no. 3, pp. 255–273, 2003. DOI: https://doi.org/10.1111/j.1467-940X.2003.00076.x. [Online]. Available: https://onlinelibrary.wiley.com/doi/abs/10.1111/j.1467-940X.2003.00076.x.

[58] Federal Aviation Administration, *AIP and PFC Funding Summary for Noise Compatibility Projects*, https://www.faa.gov/airports/environmental/airport_noise/part_150/funding/, Accessed: 2021-10-04.

[59] F. Netjasov, "Contemporary measures for noise reduction in airport surroundings," *Applied Acoustics*, vol. 73, no. 10, pp. 1076–1085, 2012. DOI: https://doi.org/10.1016/j.apacoust.2012.03.010. [Online]. Available: https://www.sciencedirect.com/science/article/pii/S0003682X12000655.

[60] E. M. Ganic, F. Netjasov, and O. Babic, "Analysis of noise abatement measures on european airports," *Applied Acoustics*, vol. 92, pp. 115–123, 2015. DOI: https://doi.org/10.1016/j.apacoust.2015.01.010. [Online]. Available: https://www.sciencedirect.com/science/article/pii/S0003682X15000122.

[61] R. Girvin, "Aircraft noise-abatement and mitigation strategies," *Journal of Air Transport Management*, vol. 15, no. 1, pp. 14–22, 2009. DOI: https://doi.org/10.1016/j.jairtraman.2008.09.012. [Online]. Available: https://www.sciencedirect.com/science/article/pii/S0969699708001166.

[62] R. E. Caves, A. D. Kershaw, and D. P. Rhodes, "Options for airport approach noise control: Flight procedures, aircraft certification, and airport restrictions," *Transportation Research Record*, vol. 1662, no. 1, pp. 48–54, 1999. DOI: 10.3141/1662-06. [Online]. Available: https://doi.org/10.3141/1662-06.

[63] D. Casalino, F. Diozzi, R. Sannino, and A. Paonessa, "Aircraft noise reduction technologies: A bibliographic review," *Aerospace Science and Technology*, vol. 12, no. 1, pp. 1–17, 2008, Aircraft noise reduction. DOI: https://doi.org/10.1016/j.ast.2007.10.004. [Online]. Available: https://www.sciencedirect.com/science/article/pii/S1270963807001162.

[64] J. W. Posey, T. D. Norum, M. C. Brown, and T. R. S. Bhat, "Jet noise from ultrahigh bypass turbofan engines," *The Journal of the Acoustical Society of America*, vol. 111, no. 5, pp. 2448–2448, 2002. DOI: 10.1121/1.4778437. [Online]. Available: https://asa.scitation.org/doi/abs/10.1121/1.4778437.

[65] N. Antoine and I. Kroo, "Optimizing aircraft and operations for minimum noise," in *AIAA's Aircraft Technology, Integration, and Operations (ATIO) 2002 Technical Forum*, Oct. 2002. DOI: 10.2514/6.2002-5868. [Online]. Available: https://arc.aiaa.org/doi/abs/10.2514/6.2002-5868.

[66] H. Jimenez, H. Pfaender, B. Havrilesko, and D. Mavris, "Noise Assessment of NASA Environmentally Responsible Aviation (ERA) Technologies and Concepts," in *12th AIAA Aviation Technology, Integration, and Operations (ATIO) Conference and 14th AIAA/ISSMO Multidisciplinary Analysis and Optimization Conference*, Sep. 2012. DOI: 10.2514/6.2012-5409. [Online]. Available: https://arc.aiaa.org/doi/abs/10.2514/6.2012-5409.

[67] K. Kinzie, B. Henderson, and J. Whitmire, "Fluidic Chevrons for Jet Noise Reduction," NASA, Preprint, Sep. 2004.

[68] L. Bertsch, F. Wolters, W. Heinze, M. Pott-Pollenske, and J. Blinstrub, "System noise assessment of a tube-and-wing aircraft with geared turbofan engines," *Journal of Aircraft*, vol. 56, no. 4, pp. 1577–1596, 2019. DOI: 10.2514/1.C034935. [Online]. Available: https://doi.org/10.2514/1.C034935.

[69] W. E. Meyer and W. J. Willkie, "Noise contour comparison of stage 3 hushkit options for boeing 727-200," *Transportation Research Record*, vol. 1703, no. 1, pp. 39–44, 2000. DOI: 10.3141/1703-06. [Online]. Available: https://doi.org/10.3141/1703-06.

[70] S. Fidell and L. Silvati, "An assessment of the effect of residential acoustic insulation on prevalence of annoyance in an airport community," *The Journal of the Acoustical Society of America*, vol. 89, no. 1, pp. 244–247, 1991. DOI: 10.1121/1.400506. [Online]. Available: https://doi.org/10.1121/1.400506.

[71] C. Asensio, M. Recuero, and I. Pavón, "Citizens' perception of the efficacy of airport noise insulation programmes in spain," *Applied Acoustics*, vol. 84, pp. 107–115, 2014, Special Issue: Air transport noise. DOI: https://doi.org/10.1016/j.apacoust.2014.03.020. [Online]. Available: https://www.sciencedirect.com/science/article/pii/S0003682X1400084X.

[72] E. I. Feitelson, R. E. Hurd, and R. R. Mudge, "The impact of airport noise on willingness to pay for residences," *Transportation Research Part D: Transport and Environment*, vol. 1, no. 1, pp. 1–14, 1996. DOI: https://doi.org/10.1016/S1361-

9209(96)00004-1. [Online]. Available: https://www.sciencedirect.com/science/article/pii/S1361920996000041.

[73] M. Espey and H. Lopez, "The impact of airport noise and proximity on residential property values," *Growth and Change*, vol. 31, no. 3, pp. 408–419, 2000. DOI: https://doi.org/10.1111/0017-4815.00135. [Online]. Available: https://onlinelibrary.wiley.com/doi/abs/10.1111/0017-4815.00135.

[74] J. P. Cohen and C. C. Coughlin, "Spatial hedonic models of airport noise, proximity, and housing prices," *Journal of Regional Science*, vol. 48, no. 5, pp. 859–878, 2008. DOI: https://doi.org/10.1111/j.1467-9787.2008.00569.x. [Online]. Available: https://onlinelibrary.wiley.com/doi/abs/10.1111/j.1467-9787.2008.00569.x.

[75] M. Rahmatian and L. Cockerill, "Airport noise and residential housing valuation in southern california: A hedonic pricing approach," *International Journal of Environmental Science & Technology*, vol. 1, no. 1, pp. 17–25, Mar. 2004. DOI: 10.1007/BF03325812. [Online]. Available: https://doi.org/10.1007/BF03325812.

[76] F. Salata *et al.*, "A first approach to the optimization of landing and take-off operations through intelligent algorithms for compliance with the acoustic standards in multi-runway airports," *Applied Acoustics*, vol. 181, p. 108 138, 2021. DOI: https://doi.org/10.1016/j.apacoust.2021.108138. [Online]. Available: https://www.sciencedirect.com/science/article/pii/S0003682X21002322.

[77] E. Ganić, O. Babić, M. Čangalović, and M. Stanojević, "Air traffic assignment to reduce population noise exposure using activity-based approach," *Transportation Research Part D: Transport and Environment*, vol. 63, pp. 58–71, 2018. DOI: https://doi.org/10.1016/j.trd.2018.04.012. [Online]. Available: https://www.sciencedirect.com/science/article/pii/S1361920917307770.

[78] C.-I. Hsu and P.-H. Lin, "Performance assessment for airport noise charge policies and airline network adjustment response," *Transportation Research Part D: Transport and Environment*, vol. 10, no. 4, pp. 281–304, 2005. DOI: https://doi.org/10.1016/j.trd.2005.04.009. [Online]. Available: https://www.sciencedirect.com/science/article/pii/S1361920905000192.

[79] United States Code of Federal Regulations (CFR) Title 14 Part 36, *NOISE STANDARDS: AIRCRAFT TYPE AND AIRWORTHINESS CERTIFICATION*.

[80] Federal Aviation Administration, "AC 36-1H - Noise Levels for U.S. Certificated and Foreign aircraft," Advisory Circular, 2001.

[81] International Civil Aviation Organization, *Reduction of Noise at Source*, https://www.icao.int/environmental-protection/pages/reduction-of-noise-at-source.aspx, Accessed: 2022-06-22.

[82] G. Alonso, A. Benito, and L. Boto, "The efficiency of noise mitigation measures at european airports," *Transportation Research Procedia*, vol. 25, pp. 103–135, 2017, World Conference on Transport Research - WCTR 2016 Shanghai. 10-15 July 2016. DOI: https://doi.org/10.1016/j.trpro.2017.05.385. [Online]. Available: https://www.sciencedirect.com/science/article/pii/S2352146517306920.

[83] E. Ganic, M. Dobrota, and O. Babic, "Noise abatement measures at airports: Contributing factors and mutual dependence," *Applied Acoustics*, vol. 112, pp. 32–40, 2016. DOI: https://doi.org/10.1016/j.apacoust.2016.05.007. [Online]. Available: https://www.sciencedirect.com/science/article/pii/S0003682X16301220.

[84] London City Airport, *Noise Action Plan 2018-2023*, 2018. [Online]. Available: https : / / assets . ctfassets . net / ggj4kbqgcch2 / 5OvmkWej5kwQopprH5T90P / 995d6f59b252e1df2c92318e656c69bf/LCY_Noise_Action_Plan_2018-2023.pdf.

[85] K. S. Pearsons, D. S. Barber, B. G. Tabachnick, and S. Fidell, "Predicting noise-induced sleep disturbance," *The Journal of the Acoustical Society of America*, vol. 97, no. 1, pp. 331–338, 1995. DOI: 10.1121/1.412316. [Online]. Available: https://doi.org/10.1121/1.412316.

[86] S. Fidell, B. Tabachnick, V. Mestre, and L. Fidell, "Aircraft noise-induced awakenings are more reasonably predicted from relative than from absolute sound exposure levels," *The Journal of the Acoustical Society of America*, vol. 134, no. 5, pp. 3645–3653, 2013. DOI: 10.1121/1.4823838. [Online]. Available: https://doi.org/10.1121/1.4823838.

[87] W. Passchier-Vermeer and W. F. Passchier, "Noise exposure and public health.," *Environmental Health Perspectives*, vol. 108, no. suppl 1, pp. 123–131, 2000. DOI: 10.1289/ehp.00108s1123. [Online]. Available: https://ehp.niehs.nih.gov/doi/abs/10.1289/ehp.00108s1123.

[88] R. L. Bennett and K. S. Pearsons, "Handbook of aircraft noise metrics," NASA, Contractor Report, Mar. 1981.

[89] "A review of aviation noise metrics and measurement," Independent Commission on Civil Aviation Noise, Tech. Rep., Jul. 2020.

[90] S. R. More, "Aircraft noise characteristics and metrics," Ph.D. dissertation, Purdue University, West Lafayette, Indiana, Dec. 2010.

[91] Federal Aviation Administration, *Fundamentals of Noise and Sound*, https://www.faa.gov/regulations_policies/policy_guidance/noise/basics/, Accessed: 2021-10-04.

[92] D. J. Monteiro, S. Prem, M. Kirby, and D. N. Mavris, "React: A rapid environmental impact on airport community tradeoff environment," in *2018 AIAA Aerospace*

Sciences Meeting. DOI: 10.2514/6.2018-0263. eprint: https://arc.aiaa.org/doi/pdf/10.2514/6.2018-0263. [Online]. Available: https://arc.aiaa.org/doi/abs/10.2514/6.2018-0263.

[93] A. Gabrielian, "A Methodology to Capture the Acoustic Properties of Small Unmanned Aerial System Noise Using a Novel Frequency Weighting," M.S. thesis, Georgia Institute of Technology, Atlanta, GA, Aug. 2021.

[94] "Procedure for the calculation of airplane noise in the vicinity of airports," SAE International, SAE Standard, Sep. 1995.

[95] "Recommended Method for Computing Noise Contours Around Airports, Second Edition," International Civil Aviation Organization, Doc 9911, 2018.

[96] "Report on Standard Method of Computing Noise Contours around Civil Airports, Third edition," European Civil Aviation Conference, ECAC.CEAC Doc 29, 2005.

[97] "STAPES (SysTem for AirPort noise Exposure Studies)," EUROCONTROL, Final Report, Oct. 2009, Research Project EC TREN/05/ST/F2/36-2/2007-3/S07.77778.

[98] J. B. Ollerhead, "The CAA Aircraft Noise Contour Model: ANCON Version 1," Civil Aviation Authority, DORA Report 9120, Nov. 1992, https://publicapps.caa.co.uk/docs/33/ERCD9120.PDF.

[99] J. B. Ollerhead, D. P. Rhodes, M. S. Viinikainen, D. J. Monkman, and W. C. Woodley, "The UK Civil Aircraft Noise Contour Model ANCON: Improvements in Version 2," Civil Aviation Authority, Environmental Research and Consultancy Department, R&D Report 9842, Jun. 1999, https://publicapps.caa.co.uk/docs/33/ERCD9842.PDF.

[100] EUROCONTROL, *Integrated aircraft noise and emissions modelling platform*, https://www.eurocontrol.int/platform/integrated-aircraft-noise-and-emissions-modelling-platform, Accessed: 2021-08-07.

[101] L. Bertsch, S. Guerin, G. Looye, and M. Pott-Pollenske, "The parametric aircraft noise analysis module - status overview and recent applications," in *17th AIAA/CEAS Aeroacoustics Conference (32nd AIAA Aeroacoustics Conference)*, Jun. 2011. DOI: 10.2514/6.2011-2855. eprint: https://arc.aiaa.org/doi/pdf/10.2514/6.2011-2855. [Online]. Available: https://arc.aiaa.org/doi/abs/10.2514/6.2011-2855.

[102] M. Ahearn, E. R. Boeker, J. E. Rosenbaum, P. J. Gerbi, and C. J. Roof, "Analysis of modeling aircraft noise with the Nord2000 noise model," John A. Volpe National Transportation Systems Center (U.S.), Tech. Rep., Oct. 2012, https://rosap.ntl.bts.gov/view/dot/9687.

[103] L. V. Lopes and C. L. Burley, "ANOPP2 User's Manual: Version 1.2," NASA Langley Research Center, Technical Memorandum, Oct. 2016.

[104] B. He *et al.*, "Integrated Noise Model (INM) Version 7.0 User's Guide," United States. Federal Aviation Administration. Office of Environment et al., User Manual, Apr. 2007.

[105] E. R. Boeker *et al.*, "Integrated Noise Model (INM) Version 7.0 Technical Manual," Volpe National Transportation Systems Center, ATAC Corporation, and Federal Aviation Administration, Technical Manual, Jan. 2008.

[106] "Aviation Environmental Design Tool (AEDT) Version 3d User Manual," U.S. Department of Transportation Federal Aviation Administration, User Manual, Mar. 2021.

[107] "Aviation Environmental Design Tool (AEDT) Version 3d Technical Manual," U.S. Department of Transportation Federal Aviation Administration, Technical Manual, Mar. 2021.

[108] EUROCONTROL, *BADA – Base of aircraft data*, https://www.eurocontrol.int/model/bada/, Accessed: 2022-06-29.

[109] M. V. Bendarkar, J. Bhanpato, T. G. Puranik, M. Kirby, and D. N. Mavris, "Comparative assessment of aedt noise modeling assumptions using real-world data," in *AIAA AVIATION 2022 Forum*, Jun. 2022. DOI: 10.2514/6.2022-3917. eprint: https://arc.aiaa.org/doi/pdf/10.2514/6.2022-3917. [Online]. Available: https://arc.aiaa.org/doi/10.2514/6.2022-3917.

[110] A. Gabrielian, T. Puranik, M. Bendarkar, M. Kirby, and D. Mavris, "Validation of the aviation environmental design tool's noise model using high fidelity weather," in *INTER-NOISE and NOISE-CON Congress and Conference Proceedings*, vol. 263, 2021, pp. 4810–4822. DOI: 10.3397/IN-2021-2846.

[111] A. B. Gabrielian, T. G. Puranik, M. V. Bendarkar, M. Kirby, D. Mavris, and D. Monteiro, "Noise model validation using real world operations data," in *AIAA AVIATION 2021 FORUM*, Jun. 2021. DOI: 10.2514/6.2021-2136. [Online]. Available: https://arc.aiaa.org/doi/10.2514/6.2021-2136.

[112] J. E. Bernardo, M. Kirby, and D. Mavris, "Development of a Rapid Fleet-Level Noise Computation Model," *Journal of Aircraft*, vol. 52, no. 3, pp. 721–733, 2015. DOI: 10.2514/1.C032503. eprint: https://doi.org/10.2514/1.C032503. [Online]. Available: https://doi.org/10.2514/1.C032503.

[113] M. J. LeVine, D. Lim, Y. Li, M. Kirby, and D. N. Mavris, "Quantification of Error for Rapid Fleet-Level Noise Computation Model Assumptions," in *2018 Aviation*

Technology, Integration, and Operations Conference, 2018. DOI: 10.2514/6.2018-3993. eprint: https://arc.aiaa.org/doi/pdf/10.2514/6.2018-3993. [Online]. Available: https://arc.aiaa.org/doi/abs/10.2514/6.2018-3993.

[114] M. J. LeVine, J. E. Bernardo, M. Kirby, and D. N. Mavris, "Average Generic Vehicle Method for Fleet-Level Analysis of Noise and Emission Tradeoffs," *Journal of Aircraft*, vol. 55, no. 3, pp. 929–946, 2018. DOI: 10.2514/1.C034368. eprint: https://doi.org/10.2514/1.C034368. [Online]. Available: https://doi.org/10.2514/1.C034368.

[115] M. R. Kirby and D. N. Mavris, "The Environmental Design Space," in *26th International Congress of the Aeronautical Sciences*, Sep. 2008.

[116] "Environmental Design Space (EDS) Progress," Committee on Aviation Environmental Protection (CAEP) Seventh Meeting, Tech. Rep. CAEP/7-IP/23, Feb. 2007.

[117] L. S. Nunez, J. C. Tai, and D. N. Mavris, "The Environmental Design Space: Modeling and Performance Updates," in *AIAA Scitech 2021 Forum*. DOI: 10.2514/6.2021-1422. eprint: https://arc.aiaa.org/doi/pdf/10.2514/6.2021-1422. [Online]. Available: https://arc.aiaa.org/doi/abs/10.2514/6.2021-1422.

[118] P. Zanella, "Sensitivity Analysis for Noise and Emissions Based on Parametric Tracks," in *17th AIAA Aviation Technology, Integration, and Operations Conference*. DOI: 10.2514/6.2017-4449. eprint: https://arc.aiaa.org/doi/pdf/10.2514/6.2017-4449. [Online]. Available: https://arc.aiaa.org/doi/abs/10.2514/6.2017-4449.

[119] M. J. LeVine, A. Kaul, J. E. Bernardo, M. Kirby, and D. N. Mavris, "Methodology for Calibration of ANGIM Subjected to Atmospheric Uncertainties," in *2013 Aviation Technology, Integration, and Operations Conference*. DOI: 10.2514/6.2013-4321. eprint: https://arc.aiaa.org/doi/pdf/10.2514/6.2013-4321. [Online]. Available: https://arc.aiaa.org/doi/abs/10.2514/6.2013-4321.

[120] D. Monteiro, "Integrating Flexible Flight Tracks into a Rapid Airport Community Environmental Impact Tradeoff Environment," Georgia Institute of Technology, AE 8900 Special Problems Final Report, Advisor Prof. Dimitri Mavris, Jul. 2017.

[121] S. Prem, "The Expansion of a Tradeoff Environment on Rapid and Parametric Noise Modeling," Georgia Institute of Technology, AE 8900 Special Problems Final Report, Advisor Prof. Dimitri Mavris, Jul. 2017.

[122] M. Kirby, K. Becker, S. Isley, G. Burdette, and D. Mavris, "Development of an Interactive Capability to Trade Off New Technologies and Future Aircraft to Reduce Aviation Environmental Impacts," in *ICAS*, vol. 4, 2010, pp. 2–645.

[123] Federal Aviation Administration, *Terminal Area Forecast (TAF) website*, https://taf.faa.gov, Accessed: 2021-08-13.

[124] "The Small Area Population Projection and Distribution Methodology," GIS Associates Inc., The St. Johns River Water Management District, Palatka, FL, Tech. Rep. SJ2009-SP7, 2009.

[125] U.S. Census Bureau, *Population Projections*, https://www.census.gov/programs-surveys/popproj.html, Accessed: 2021-08-13.

[126] S. Kim, D. Lim, and K. Lee, "Reduced-order modeling applied to the aviation environmental design tool for rapid noise prediction," *Journal of Aerospace Engineering*, vol. 31, Jun. 2018. DOI: 10.1061/(ASCE)AS.1943-5525.0000860.

[127] M. J. Yaworski, E. P. Dinges, and R. J. Iovinelli, "High-Fidelity Weather Data Makes a Difference Calculating Environmental Consequences with FAA's Aviation Environmental Design Tool," in *Ninth USA/Europe Air Traffic Management Research and Development Seminar (ATM2011)*, Jun. 2011.

[128] L. Bertsch, S. Guerin, G. Looye, and M. Pott-Pollenske, "The Parametric Aircraft Noise Analysis Module - status overview and recent applications," in *17th AIAA/CEAS Aeroacoustics Conference (32nd AIAA Aeroacoustics Conference)*. DOI: 10.2514/6.2011-2855. eprint: https://arc.aiaa.org/doi/pdf/10.2514/6.2011-2855. [Online]. Available: https://arc.aiaa.org/doi/abs/10.2514/6.2011-2855.

[129] L. Bertsch, W. Dobrzynski, and S. Guérin, "Tool Development for Low-Noise Aircraft Design," *Journal of Aircraft*, vol. 47, no. 2, pp. 694–699, 2010. DOI: 10.2514/1.43188. eprint: https://doi.org/10.2514/1.43188. [Online]. Available: https://doi.org/10.2514/1.43188.

[130] L. Bertsch, G. Looye, E. Anton, and S. Schwanke, "Flyover noise measurements of a spiraling noise abatement approach procedure," *Journal of Aircraft*, vol. 48, no. 2, pp. 436–448, 2011. DOI: 10.2514/1.C001005. eprint: https://doi.org/10.2514/1.C001005. [Online]. Available: https://doi.org/10.2514/1.C001005.

[131] U.S. Federal Aviation Administration, *Automatic Dependent Surveillance-Broadcast (ADS-B)*, https://www.faa.gov/nextgen/programs/adsb/, Accessed: 2021-08-18.

[132] FlightAware, *FlightAware website*, https://flightaware.com/, Accessed: 2021-08-18.

[133] Flightradar24, *Flightradar24 website*, https://www.flightradar24.com/, Accessed: 2021-08-18.

[134] J. Browder, R. Gutterud, and J. Schade, "Performance Data Analysis Reporting System (PDARS) : a valuable addition to FAA managers' toolsets," 2011.

[135] A. Eckstein, C. Kurcz, and M. Silva, "Threaded track: Geospatial data fusion for aircraft flight trajectories," Tech. Rep., 2012. [Online]. Available: https://www.mitre.org/sites/default/files/publications/pr-17-3649-geospatial-data-threaded_track.pdf.

[136] *Advisory Circular, 120-82 - Flight Operational Quality Assurance*, url: https://www.faa.gov/regulations_policies/advisory_circulars/index.cfm/go/document.information/documentID/23227, Federal Aviation Administration, Apr. 2004.

[137] T. G. Puranik and D. N. Mavris, "Anomaly Detection in General-Aviation Operations Using Energy Metrics and Flight-Data Records," *Journal of Aerospace Information Systems*, vol. 15, no. 1, pp. 22–35, 2018. DOI: 10.2514/1.I010582.

[138] T. G. Puranik and D. N. Mavris, "Identification of Instantaneous Anomalies in General Aviation Operations Using Energy Metrics," *Journal of Aerospace Information Systems*, vol. 17, no. 1, pp. 51–65, 2020. DOI: 10.2514/1.I010772. eprint: https://doi.org/10.2514/1.I010772. [Online]. Available: https://doi.org/10.2514/1.I010772.

[139] H. Lee *et al.*, "Critical Parameter Identification for Safety Events in Commercial Aviation Using Machine Learning," *Aerospace*, vol. 7(6), p. 73, 2020. DOI: 10.3390/aerospace7060073.

[140] "Doc 8168 Procedures for Air Navigation Services – Aircraft Operations, Volume I – Flight Procedures," International Civil Aviation Organization, PANS-OPS Doc 8168, 2006.

[141] "AC 91-53A – Noise Abatement Departure Profiles," U.S. Federal Aviation Administration, Advisory Circular, Jul. 1993, https://www.faa.gov/documentLibrary/media/Advisory_Circular/ac91-53.pdf.

[142] Federal Aviation Administration, *FAA TV: New Departure Procedures at John Wayne Airport*, https://www.faa.gov/tv/?mediaId=1478, Accessed: 2021-10-04.

[143] D. Lim *et al.*, "Improved Noise Abatement Departure Procedure Modeling for Aviation Environmental Impact Assessment," in *AIAA Scitech 2020 Forum*, Jan. 2020. DOI: 10.2514/6.2020-1730. eprint: https://arc.aiaa.org/doi/pdf/10.2514/6.2020-1730. [Online]. Available: https://arc.aiaa.org/doi/abs/10.2514/6.2020-1730.

[144] A. Behere, D. Lim, M. Kirby, and D. N. Mavris, "Alternate departure procedures for takeoff noise mitigation at atlanta hartsfield-jackson international airport," in *AIAA Scitech 2019 Forum*, Jan. 2019. DOI: 10.2514/6.2019-2090. eprint: https:

//arc.aiaa.org/doi/pdf/10.2514/6.2019-2090. [Online]. Available: https://arc.aiaa.org/doi/abs/10.2514/6.2019-2090.

[145] A. Behere *et al.*, "Sensitivity Analysis of Airport level Environmental Impacts to Aircraft thrust, weight, and departure procedures," in *AIAA Scitech 2020 Forum*, Jan. 2020. DOI: 10.2514/6.2020-1731. eprint: https://arc.aiaa.org/doi/pdf/10.2514/6.2020-1731. [Online]. Available: https://arc.aiaa.org/doi/abs/10.2514/6.2020-1731.

[146] Z. Gao, A. Behere, Y. Li, D. Lim, M. Kirby, and D. N. Mavris, "Development and analysis of improved departure modeling for aviation environmental impact assessment," *Journal of Aircraft*, vol. 58, no. 4, pp. 847–857, 2021. DOI: 10.2514/1.C036105. eprint: https://doi.org/10.2514/1.C036105. [Online]. Available: https://doi.org/10.2514/1.C036105.

[147] A. Behere, T. G. Puranik, M. Kirby, and D. N. Mavris, "Parametric optimization of aircraft arrival trajectories for aviation noise mitigation using BADA4 performance model," in *Internoise 2021*, Aug. 2021. DOI: 10.3397/IN-2021-2783. [Online]. Available: https://doi.org/10.3397/IN-2021-2783.

[148] H. Erzberger and H. Q. Lee, "Technique for calculating optimum takeoff and climb out trajectories for noise abatement," NASA, Technical Note NASA-TN-D-5182, May 1969, https://ntrs.nasa.gov/citations/19690016816.

[149] J.-P. B. Clarke, "A systems analysis methodology for developing single event noise abatement procedures," http://hdl.handle.net/1721.1/10720, Sc.D. Thesis, Massachusetts Institute of Technology, Cambridge, MA, Feb. 1997.

[150] H. G. Visser and R. A. A. Wijnen, "Optimization of noise abatement departure trajectories," *Journal of Aircraft*, vol. 38, no. 4, pp. 620–627, 2001. DOI: 10.2514/2.2838. eprint: https://doi.org/10.2514/2.2838. [Online]. Available: https://doi.org/10.2514/2.2838.

[151] R. Wijnen and H. Visser, "Optimal departure trajectories with respect to sleep disturbance," in *7th AIAA/CEAS Aeroacoustics Conference and Exhibit*, Jun. 2001. DOI: 10.2514/6.2001-2260. eprint: https://arc.aiaa.org/doi/pdf/10.2514/6.2001-2260. [Online]. Available: https://arc.aiaa.org/doi/abs/10.2514/6.2001-2260.

[152] R. Wijnen and H. Visser, "Optimal departure trajectories with respect to sleep disturbance," *Aerospace Science and Technology*, vol. 7, no. 1, pp. 81–91, 2003. DOI: https://doi.org/10.1016/S1270-9638(02)01183-5. [Online]. Available: https://www.sciencedirect.com/science/article/pii/S1270963802011835.

[153] H. Visser, "Generic and site-specific criteria in the optimization of noise abatement trajectories," *Transportation Research Part D: Transport and Environment*, vol. 10,

no. 5, pp. 405–419, 2005. DOI: https://doi.org/10.1016/j.trd.2005.05.001. [Online]. Available: https://www.sciencedirect.com/science/article/pii/S1361920905000428.

[154] H. G. Visser and S. Hartjes, "Economic and environmental optimization of flight trajectories connecting a city-pair," *Proceedings of the Institution of Mechanical Engineers, Part G: Journal of Aerospace Engineering*, vol. 228, no. 6, pp. 980–993, 2014. DOI: 10.1177/0954410013485348. eprint: https://doi.org/10.1177/0954410013485348. [Online]. Available: https://doi.org/10.1177/0954410013485348.

[155] S. Hartjes, J. Dons, and H. G. Visser, "Optimization of area navigation arrival routes for cumulative noise exposure," *Journal of Aircraft*, vol. 51, no. 5, pp. 1432–1438, 2014. DOI: 10.2514/1.C032302. eprint: https://doi.org/10.2514/1.C032302. [Online]. Available: https://doi.org/10.2514/1.C032302.

[156] S. Hartjes and H. Visser, "Efficient trajectory parameterization for environmental optimization of departure flight paths using a genetic algorithm," *Proceedings of the Institution of Mechanical Engineers, Part G: Journal of Aerospace Engineering*, vol. 231, no. 6, pp. 1115–1123, 2017. DOI: 10.1177/0954410016648980. eprint: https://doi.org/10.1177/0954410016648980. [Online]. Available: https://doi.org/10.1177/0954410016648980.

[157] V. Ho-Huu, S. Hartjes, H. G. Visser, and R. Curran, "An efficient application of the moea/d algorithm for designing noise abatement departure trajectories," *Aerospace*, vol. 4, no. 4, 2017. DOI: 10.3390/aerospace4040054. [Online]. Available: https://www.mdpi.com/2226-4310/4/4/54.

[158] V. Ho-Huu, S. Hartjes, L. Geijselaers, H. Visser, and R. Curran, "Optimization of noise abatement aircraft terminal routes using a multi-objective evolutionary algorithm based on decomposition," *Transportation Research Procedia*, vol. 29, pp. 157–168, 2018, Aerospace Europe CEAS 2017 Conference. DOI: https://doi.org/10.1016/j.trpro.2018.02.014. [Online]. Available: https://www.sciencedirect.com/science/article/pii/S2352146518300188.

[159] V. Ho-Huu, S. Hartjes, H. Visser, and R. Curran, "An optimization framework for route design and allocation of aircraft to multiple departure routes," *Transportation Research Part D: Transport and Environment*, vol. 76, pp. 273–288, 2019. DOI: https://doi.org/10.1016/j.trd.2019.10.003. [Online]. Available: https://www.sciencedirect.com/science/article/pii/S1361920918310186.

[160] V. Ho-Huu, S. Hartjes, J. Pérez-Castán, H. Visser, and R. Curran, "A multilevel optimization approach to route design and flight allocation taking aircraft sequence and separation constraints into account," *Transportation Research Part C: Emerging Technologies*, vol. 117, p. 102 684, 2020. DOI: https://doi.org/10.1016/j.trc.

2020.102684. [Online]. Available: https://www.sciencedirect.com/science/article/pii/S0968090X20305994.

[161] X. Prats, V. Puig, J. Quevedo, and F. Nejjari, "Lexicographic optimisation for optimal departure aircraft trajectories," *Aerospace Science and Technology*, vol. 14, no. 1, pp. 26–37, 2010. DOI: https://doi.org/10.1016/j.ast.2009.11.003. [Online]. Available: https://www.sciencedirect.com/science/article/pii/S1270963809000856.

[162] X. Prats, V. Puig, J. Quevedo, and F. Nejjari, "Multi-objective optimisation for aircraft departure trajectories minimising noise annoyance," *Transportation Research Part C: Emerging Technologies*, vol. 18, no. 6, pp. 975–989, 2010, Special issue on Transportation Simulation Advances in Air Transportation Research. DOI: https://doi.org/10.1016/j.trc.2010.03.001. [Online]. Available: https://www.sciencedirect.com/science/article/pii/S0968090X10000276.

[163] X. Prats, V. Puig, and J. Quevedo, "A multi-objective optimization strategy for designing aircraft noise abatement procedures. case study at girona airport," *Transportation Research Part D: Transport and Environment*, vol. 16, no. 1, pp. 31–41, 2011. DOI: https://doi.org/10.1016/j.trd.2010.07.007. [Online]. Available: https://www.sciencedirect.com/science/article/pii/S1361920910001069.

[164] X. Prats, V. Puig, and J. Quevedo, "Equitable aircraft noise-abatement departure procedures," *Journal of Guidance, Control, and Dynamics*, vol. 34, no. 1, pp. 192–203, 2011. DOI: 10.2514/1.49530. eprint: https://doi.org/10.2514/1.49530. [Online]. Available: https://doi.org/10.2514/1.49530.

[165] D. Mitchell, H. Ekstrand, X. Prats, and T. Grönstedt, "An environmental assessment of air traffic speed constraints in the departure phase of flight: A case study at gothenburg landvetter airport, sweden," *Transportation Research Part D: Transport and Environment*, vol. 17, no. 8, pp. 610–618, 2012. DOI: https://doi.org/10.1016/j.trd.2012.07.006. [Online]. Available: https://www.sciencedirect.com/science/article/pii/S136192091200079X.

[166] W. Schilders, "Introduction to model order reduction," in *Model Order Reduction: Theory, Research Aspects and Applications*, W. H. A. Schilders, H. A. van der Vorst, and J. Rommes, Eds. Berlin, Heidelberg: Springer Berlin Heidelberg, 2008, pp. 3–32, ISBN: 978-3-540-78841-6. DOI: 10.1007/978-3-540-78841-6_1. [Online]. Available: https://doi.org/10.1007/978-3-540-78841-6_1.

[167] W. Schilders, H. van der Vorst, and J. Rommes, *Model Order Reduction: Theory, Research Aspects and Applications*, ser. Mathematics in Industry. Springer Berlin Heidelberg, 2008, ISBN: 9783540788416. [Online]. Available: https://books.google.com/books?id=WWi1evmAQPkC.

[168] F. Cajori, "A History of Mathematics," in Macmillan & Co., 1893, ch. EULER, LAGRANGE, AND LAPLACE. P. 283.

[169] P. LeGresley and J. Alonso, "Investigation of non-linear projection for pod based reduced order models for aerodynamics," in *39th Aerospace Sciences Meeting and Exhibit*, 2001. DOI: 10.2514/6.2001-926. eprint: https://arc.aiaa.org/doi/pdf/10.2514/6.2001-926. [Online]. Available: https://arc.aiaa.org/doi/abs/10.2514/6.2001-926.

[170] T. R. Smith, J. Moehlis, and P. Holmes, "Low-dimensional modelling of turbulence using the proper orthogonal decomposition: A tutorial," *Nonlinear Dynamics*, vol. 41, pp. 275–307, Aug. 2005. DOI: https://doi.org/10.1007/s11071-005-2823-y.

[171] J. Qian *et al.*, "Projection-based reduced-order modeling for spacecraft thermal analysis," *Journal of Spacecraft and Rockets*, vol. 52, no. 3, pp. 978–989, 2015. DOI: 10.2514/1.A33117. eprint: https://doi.org/10.2514/1.A33117. [Online]. Available: https://doi.org/10.2514/1.A33117.

[172] K. Decker, H. D. Schwartz, and D. Mavris, "Dimensionality reduction techniques applied to the design of hypersonic aerial systems," in *AIAA AVIATION 2020 FORUM*, 2020. DOI: 10.2514/6.2020-3003. eprint: https://arc.aiaa.org/doi/pdf/10.2514/6.2020-3003. [Online]. Available: https://arc.aiaa.org/doi/abs/10.2514/6.2020-3003.

[173] D. Amsallem, M. Zahr, Y. Choi, and C. Farhat, "Design optimization using hyper-reduced-order models," *Structural and Multidisciplinary Optimization*, vol. 51, pp. 919–940, Apr. 2014. DOI: 10.1007/s00158-014-1183-y.

[174] M. Gariel, A. N. Srivastava, and E. Feron, "Trajectory clustering and an application to airspace monitoring," *IEEE Transactions on Intelligent Transportation Systems*, vol. 12, no. 4, pp. 1511–1524, Dec. 2011. DOI: 10.1109/TITS.2011.2160628.

[175] X. Olive and J. Morio, ""trajectory clustering of air traffic flows around airports"," *Aerospace Science and Technology*, vol. 84, pp. 776–781, 2019. DOI: https://doi.org/10.1016/j.ast.2018.11.031. [Online]. Available: https://www.sciencedirect.com/science/article/pii/S127096381731129X.

[176] S. J. Corrado, T. G. Puranik, O. J. Pinon, and D. N. Mavris, ""trajectory clustering within the terminal airspace utilizing a weighted distance function"," *Proceedings*, vol. 59, no. 1, 2020. DOI: 10.3390/proceedings2020059007. [Online]. Available: https://www.mdpi.com/2504-3900/59/1/7.

[177] G. Andrienko, N. Andrienko, G. Fuchs, and J. M. C. Garcia, "Clustering trajectories by relevant parts for air traffic analysis," *IEEE Transactions on Visualization and*

Computer Graphics, vol. 24, no. 1, pp. 34–44, Jan. 2018. DOI: 10.1109/TVCG.2017.2744322.

[178] L. Basora, J. Morio, and C. Mailhot, "A Trajectory Clustering Framework to Analyse Air Traffic Flows," in *SID 2017, 7th SESAR Innovation Days*, Belgrade, Serbia, Nov. 2017. [Online]. Available: https://hal-enac.archives-ouvertes.fr/hal-01655747.

[179] Statista, *Leading airports worldwide in 2020, based on aircraft movements*, Apr. 2021. [Online]. Available: https://www.statista.com/statistics/226823/largest-airports-worldwide-by-flight-operations/.

[180] L. Li, S. Das, R. John Hansman, R. Palacios, and A. N. Srivastava, "Analysis of flight data using clustering techniques for detecting abnormal operations," *Journal of Aerospace Information Systems*, vol. 12, no. 9, pp. 587–598, 2015. DOI: 10.2514/1.I010329. eprint: https://doi.org/10.2514/1.I010329. [Online]. Available: https://doi.org/10.2514/1.I010329.

[181] T. G. Puranik, H. Jimenez, and D. N. Mavris, "Utilizing energy metrics and clustering techniques to identify anomalous general aviation operations," in *AIAA Information Systems-AIAA Infotech @ Aerospace*, Jan. 2017. DOI: 10.2514/6.2017-0789. [Online]. Available: https://arc.aiaa.org/doi/abs/10.2514/6.2017-0789.

[182] X. Olive and L. Basora, "Identifying Anomalies in past en-route Trajectories with Clustering and Anomaly Detection Methods," in *ATM Seminar 2019*, VIENNE, Austria, Jun. 2019. [Online]. Available: https://hal.archives-ouvertes.fr/hal-02345597.

[183] K. Sheridan, T. G. Puranik, E. Mangortey, O. J. Pinon-Fischer, M. Kirby, and D. N. Mavris, "An application of dbscan clustering for flight anomaly detection during the approach phase," in *AIAA Scitech 2020 Forum*, Jan. 2020. DOI: 10.2514/6.2020-1851. eprint: https://arc.aiaa.org/doi/pdf/10.2514/6.2020-1851. [Online]. Available: https://arc.aiaa.org/doi/abs/10.2514/6.2020-1851.

[184] E. Mangortey *et al.*, "Application of machine learning techniques to parameter selection for flight risk identification," in *AIAA Scitech 2020 Forum*, Jan. 2020. DOI: 10.2514/6.2020-1850. eprint: https://arc.aiaa.org/doi/pdf/10.2514/6.2020-1850. [Online]. Available: https://arc.aiaa.org/doi/abs/10.2514/6.2020-1850.

[185] A. Saltelli *et al.*, *Global sensitivity analysis: the primer*. West Sussex, England: John Wiley & Sons, 2008.

[186] I. Sobol', "Global sensitivity indices for nonlinear mathematical models and their monte carlo estimates," *Mathematics and Computers in Simulation*, vol. 55, no. 1, pp. 271–280, 2001, The Second IMACS Seminar on Monte Carlo Methods. DOI:

https://doi.org/10.1016/S0378-4754(00)00270-6. [Online]. Available: https://www.sciencedirect.com/science/article/pii/S0378475400002706.

[187] M. D. Morris, "Factorial sampling plans for preliminary computational experiments," *Technometrics*, vol. 33, no. 2, pp. 161–174, 1991. [Online]. Available: http://www.jstor.org/stable/1269043.

[188] S. Razavi and H. V. Gupta, "What do we mean by sensitivity analysis? the need for comprehensive characterization of "global" sensitivity in earth and environmental systems models," *Water Resources Research*, vol. 51, no. 5, pp. 3070–3092, 2015. DOI: https://doi.org/10.1002/2014WR016527. eprint: https://agupubs.onlinelibrary.wiley.com/doi/pdf/10.1002/2014WR016527. [Online]. Available: https://agupubs.onlinelibrary.wiley.com/doi/abs/10.1002/2014WR016527.

[189] A. J. Krener, "Reduced order modeling of nonlinear control systems," in *Analysis and Design of Nonlinear Control Systems: In Honor of Alberto Isidori*, A. Astolfi and L. Marconi, Eds. Berlin, Heidelberg: Springer Berlin Heidelberg, 2008, pp. 41–62, ISBN: 978-3-540-74358-3. DOI: 10.1007/978-3-540-74358-3_4. [Online]. Available: https://doi.org/10.1007/978-3-540-74358-3_4.

[190] L. Fortuna, G. Nunnari, and A. Gallo, *Model Order Reduction Techniques with Applications in Electrical Engineering*. Springer London, 1992. DOI: https://doi.org/10.1007/978-1-4471-3198-4.

[191] J. Roychowdhury, "Reduced-order modeling of time-varying systems," *IEEE Transactions on Circuits and Systems II: Analog and Digital Signal Processing*, vol. 46, no. 10, pp. 1273–1288, Oct. 1999. DOI: 10.1109/82.799678.

[192] D. L. Angwin and H. Kaufman, "Image restoration using reduced order models," *Signal Processing*, vol. 16, no. 1, pp. 21–28, 1989, Multidimensional Signal Processing. DOI: https://doi.org/10.1016/0165-1684(89)90110-2. [Online]. Available: https://www.sciencedirect.com/science/article/pii/0165168489901102.

[193] C. Chrysafis and A. Ortega, "Line-based, reduced memory, wavelet image compression," *IEEE Transactions on Image Processing*, vol. 9, no. 3, pp. 378–389, Mar. 2000. DOI: 10.1109/83.826776.

[194] L. Fortuna, G. Nunnari, and A. Gallo, *Model Order Reduction Techniques with Applications in Electrical Engineering*. Springer London, 1992. DOI: https://doi.org/10.1007/978-1-4471-3198-4.

[195] B. R. Noack, M. Morzynski, and G. Tadmor, *Reduced-Order Modelling for Flow Control*. Springer Publishing Company, Incorporated, 2013, ISBN: 3709111145.

[196] T. Lieu, C. Farhat, and M. Lesoinne, "Reduced-order fluid/structure modeling of a complete aircraft configuration," *Computer Methods in Applied Mechanics and Engineering*, vol. 195, no. 41, pp. 5730–5742, 2006, John H. Argyris Memorial Issue. Part II. DOI: https://doi.org/10.1016/j.cma.2005.08.026. [Online]. Available: https://www.sciencedirect.com/science/article/pii/S0045782505005153.

[197] I. Kamwa, R. Grondin, E. Dickinson, and S. Fortin, "A minimal realization approach to reduced-order modelling and modal analysis for power system response signals," *IEEE Transactions on Power Systems*, vol. 8, no. 3, pp. 1020–1029, Aug. 1993. DOI: 10.1109/59.260898.

[198] H. A. Pulgar-Painemal and P. W. Sauer, "Towards a wind farm reduced-order model," *Electric Power Systems Research*, vol. 81, no. 8, pp. 1688–1695, 2011. DOI: https://doi.org/10.1016/j.epsr.2011.03.022. [Online]. Available: https://www.sciencedirect.com/science/article/pii/S037877961100085X.

[199] F. Bamer, A. K. Amiri, and C. Bucher, "A new model order reduction strategy adapted to nonlinear problems in earthquake engineering," *Earthquake Engineering & Structural Dynamics*, vol. 46, no. 4, pp. 537–559, 2017. DOI: https://doi.org/10.1002/eqe.2802. eprint: https://onlinelibrary.wiley.com/doi/pdf/10.1002/eqe.2802. [Online]. Available: https://onlinelibrary.wiley.com/doi/abs/10.1002/eqe.2802.

[200] A. Bertram, C. Othmer, and R. Zimmermann, "Towards real-time vehicle aerodynamic design via multi-fidelity data-driven reduced order modeling," in *2018 AIAA/ASCE/AHS/ASC Structures, Structural Dynamics, and Materials Conference*, Jan. 2018. DOI: 10.2514/6.2018-0916. eprint: https://arc.aiaa.org/doi/pdf/10.2514/6.2018-0916. [Online]. Available: https://arc.aiaa.org/doi/abs/10.2514/6.2018-0916.

[201] T. Bui-Thanh, M. Damodaran, and K. Willcox, "Proper orthogonal decomposition extensions for parametric applications in compressible aerodynamics," in *21st AIAA Applied Aerodynamics Conference*, Jun. 2003. DOI: 10.2514/6.2003-4213. eprint: https://arc.aiaa.org/doi/pdf/10.2514/6.2003-4213. [Online]. Available: https://arc.aiaa.org/doi/abs/10.2514/6.2003-4213.

[202] W. Chen, J. S. Hesthaven, B. Junqiang, Y. Qiu, Z. Yang, and Y. Tihao, "Greedy nonintrusive reduced order model for fluid dynamics," *AIAA Journal*, vol. 56, no. 12, pp. 4927–4943, 2018. DOI: 10.2514/1.J056161. eprint: https://doi.org/10.2514/1.J056161. [Online]. Available: https://doi.org/10.2514/1.J056161.

[203] M. Ripepi *et al.*, "Reduced-order models for aerodynamic applications, loads and mdo," *CEAS Aeronautical Journal*, vol. 9, Feb. 2018. DOI: 10.1007/s13272-018-0283-6.

[204] M. Fossati, "Evaluation of aerodynamic loads via reduced-order methodology," *AIAA Journal*, vol. 53, no. 8, pp. 2389–2405, 2015. DOI: 10.2514/1.J053755. eprint: https://doi.org/10.2514/1.J053755. [Online]. Available: https://doi.org/10.2514/1.J053755.

[205] D. Rajaram *et al.*, "Deep gaussian process enabled surrogate models for aerodynamic flows," in *AIAA Scitech 2020 Forum*, Jan. 2020. DOI: 10.2514/6.2020-1640. eprint: https://arc.aiaa.org/doi/pdf/10.2514/6.2020-1640. [Online]. Available: https://arc.aiaa.org/doi/abs/10.2514/6.2020-1640.

[206] L. Mainini and K. Willcox, "Surrogate modeling approach to support real-time structural assessment and decision making," *AIAA Journal*, vol. 53, no. 6, pp. 1612–1626, 2015. DOI: 10.2514/1.J053464. eprint: https://doi.org/10.2514/1.J053464. [Online]. Available: https://doi.org/10.2514/1.J053464.

[207] M. J. Zahr, P. Avery, and C. Farhat, "A multilevel projection-based model order reduction framework for nonlinear dynamic multiscale problems in structural and solid mechanics," *International Journal for Numerical Methods in Engineering*, vol. 112, no. 8, pp. 855–881, 2017. DOI: https://doi.org/10.1002/nme.5535. eprint: https://onlinelibrary.wiley.com/doi/pdf/10.1002/nme.5535. [Online]. Available: https://onlinelibrary.wiley.com/doi/abs/10.1002/nme.5535.

[208] D. Sarojini, D. Rajaram, D. Solano, and D. N. Mavris, "Adjoint-based structural optimization for beam-like structures subjected to dynamic loads," in *AIAA Scitech 2020 Forum*, Jan. 2020. DOI: 10.2514/6.2020-0273. eprint: https://arc.aiaa.org/doi/pdf/10.2514/6.2020-0273. [Online]. Available: https://arc.aiaa.org/doi/abs/10.2514/6.2020-0273.

[209] C. Perron, D. Sarojini, D. Rajaram, J. Corman, and D. Mavris, "Manifold alignment-based multi-fidelity reduced-order modeling applied to structural analysis," *Structural and Multidisciplinary Optimization*, vol. 65, no. 236 (2022), 2022. DOI: 10.1007/s00158-022-03274-1. [Online]. Available: https://link.springer.com/article/10.1007/s00158-022-03274-1.

[210] D. Amsallem, J. Cortial, and C. Farhat, "Towards real-time computational-fluid-dynamics-based aeroelastic computations using a database of reduced-order information," *AIAA Journal*, vol. 48, no. 9, pp. 2029–2037, 2010. DOI: 10.2514/1.J050233. eprint: https://doi.org/10.2514/1.J050233. [Online]. Available: https://doi.org/10.2514/1.J050233.

[211] T. Lieu and M. Lesoinne, "Parameter adaptation of reduced order models for three-dimensional flutter analysis," in *42nd AIAA Aerospace Sciences Meeting and Exhibit*, Jan. 2004. DOI: 10.2514/6.2004-888. eprint: https://arc.aiaa.org/doi/pdf/10.2514/6.2004-888. [Online]. Available: https://arc.aiaa.org/doi/abs/10.2514/6.2004-888.

[212] A.-M. Leung and R. Khazaka, "Parametric model order reduction technique for design optimization," in *2005 IEEE International Symposium on Circuits and Systems (ISCAS)*, May 2005, 1290–1293 Vol. 2. DOI: 10.1109/ISCAS.2005.1464831.

[213] K. Carlberg and C. Farhat, "A compact proper orthogonal decomposition basis for optimization-oriented reduced-order models," in *12th AIAA/ISSMO Multidisciplinary Analysis and Optimization Conference*, Sep. 2008. DOI: 10.2514/6.2008-5964. eprint: https://arc.aiaa.org/doi/pdf/10.2514/6.2008-5964. [Online]. Available: https://arc.aiaa.org/doi/abs/10.2514/6.2008-5964.

[214] C. Gogu, "Improving the efficiency of large scale topology optimization through on-the-fly reduced order model construction," *International Journal for Numerical Methods in Engineering*, vol. 101, no. 4, pp. 281–304, 2015. DOI: https://doi.org/10.1002/nme.4797. eprint: https://onlinelibrary.wiley.com/doi/pdf/10.1002/nme.4797. [Online]. Available: https://onlinelibrary.wiley.com/doi/abs/10.1002/nme.4797.

[215] M. J. Zahr and C. Farhat, "Progressive construction of a parametric reduced-order model for pde-constrained optimization," *International Journal for Numerical Methods in Engineering*, vol. 102, no. 5, pp. 1111–1135, 2015. DOI: https://doi.org/10.1002/nme.4770. eprint: https://onlinelibrary.wiley.com/doi/pdf/10.1002/nme.4770. [Online]. Available: https://onlinelibrary.wiley.com/doi/abs/10.1002/nme.4770.

[216] Y. Cai, D. Rajaram, and D. N. Mavris, "Multi-mission multi-objective optimization in commercial aircraft conceptual design," in *AIAA Aviation 2019 Forum*, Jun. 2019. DOI: 10.2514/6.2019-3577. eprint: https://arc.aiaa.org/doi/pdf/10.2514/6.2019-3577. [Online]. Available: https://arc.aiaa.org/doi/abs/10.2514/6.2019-3577.

[217] A. C. Antoulas, *Approximation of Large-Scale Dynamical Systems*. Society for Industrial and Applied Mathematics, 2005. DOI: 10.1137/1.9780898718713. eprint: https://epubs.siam.org/doi/pdf/10.1137/1.9780898718713. [Online]. Available: https://epubs.siam.org/doi/abs/10.1137/1.9780898718713.

[218] P. Benner, M. Ohlberger, A. Cohen, and K. Willcox, *Model Reduction and Approximation*, P. Benner, M. Ohlberger, A. Cohen, and K. Willcox, Eds. Philadelphia, PA: Society for Industrial and Applied Mathematics, 2017. DOI: 10.1137/1.9781611974829. eprint: https://epubs.siam.org/doi/pdf/10.1137/1.9781611974829. [Online]. Available: https://epubs.siam.org/doi/abs/10.1137/1.9781611974829.

[219] P. Benner, S. Gugercin, and K. Willcox, "A survey of projection-based model reduction methods for parametric dynamical systems," *SIAM Review*, vol. 57, no. 4,

pp. 483–531, 2015. DOI: 10.1137/130932715. eprint: https://doi.org/10.1137/130932715. [Online]. Available: https://doi.org/10.1137/130932715.

[220] K. Lu *et al.*, "Review for order reduction based on proper orthogonal decomposition and outlooks of applications in mechanical systems," *Mechanical Systems and Signal Processing*, vol. 123, pp. 264–297, May 2019. DOI: 10.1016/j.ymssp.2019.01.018.

[221] C. Perron, D. Rajaram, and D. N. Mavris, "Multi-fidelity non-intrusive reduced-order modelling based on manifold alignment," *Proceedings of the Royal Society A: Mathematical, Physical and Engineering Sciences*, vol. 477, no. 2253, p. 20 210 495, 2021. DOI: 10.1098/rspa.2021.0495. eprint: https://royalsocietypublishing.org/doi/pdf/10.1098/rspa.2021.0495. [Online]. Available: https://royalsocietypublishing.org/doi/abs/10.1098/rspa.2021.0495.

[222] D. Rajaram, C. Perron, T. G. Puranik, and D. N. Mavris, ""randomized algorithms for non-intrusive parametric reduced order modeling"," *AIAA Journal*, vol. 58, no. 12, pp. 5389–5407, 2020. DOI: 10.2514/1.J059616. eprint: https://doi.org/10.2514/1.J059616. [Online]. Available: https://doi.org/10.2514/1.J059616.

[223] A. Behere and D. N. Mavris, "Optimization of takeoff departure procedures for airport noise mitigation," *Transportation Research Record*, vol. 2675, no. 9, pp. 81–92, 2021. DOI: 10.1177/03611981211004967. eprint: https://doi.org/10.1177/03611981211004967. [Online]. Available: https://doi.org/10.1177/03611981211004967.

[224] Bureau of Transportation Statistics, *Data Bank 28DS - T-100 Domestic Segment Data (World Area Code)*, https://www.bts.gov/browse-statistical-products-and-data/bts-publications/data-bank-28ds-t-100-domestic-segment-data, Accessed: 2022-07-11.

[225] M. Geissbuhler, A. Behere, D. Rajaram, M. Kirby, and D. N. Mavris, "Improving airport-level noise modeling by accounting for aircraft configuration-related noise at arrival," in *AIAA SCITECH 2022 Forum*, Jan. 2021. DOI: 10.2514/6.2022-1650. eprint: https://arc.aiaa.org/doi/pdf/10.2514/6.2022-1650. [Online]. Available: https://arc.aiaa.org/doi/abs/10.2514/6.2022-1650.

[226] OpenSky Network website, *The OpenSky Network – Open Air Traffic Data for Research*, https://opensky-network.org/, Accessed: 2022-07-11.

[227] M. Schäfer, M. Strohmeier, V. Lenders, I. Martinovic, and M. Wilhelm, "Bringing up opensky: A large-scale ads-b sensor network for research," in *IPSN-14 Proceedings of the 13th International Symposium on Information Processing in Sensor Networks*, Apr. 2014, pp. 83–94. DOI: 10.1109/IPSN.2014.6846743.

[228] S. Ackert, "Engine Maintenance Concepts for Financiers: Elements of Turbofan Shop Maintenance Costs," Handbook, Sep. 2011. [Online]. Available: http://www.aircraftmonitor.com/uploads/1/5/9/9/15993320/engine_mx_concepts_for_financiers___v2.pdf.

[229] A. Behere, L. Isakson, T. G. Puranik, Y. Li, M. Kirby, and D. Mavris, "Aircraft landing and takeoff operations clustering for efficient environmental impact assessment," in *AIAA AVIATION 2020 FORUM*, Jun. 2020. DOI: 10.2514/6.2020-2583. eprint: https://arc.aiaa.org/doi/pdf/10.2514/6.2020-2583. [Online]. Available: https://arc.aiaa.org/doi/abs/10.2514/6.2020-2583.

[230] A. Behere, J. Bhanpato, T. G. Puranik, M. Kirby, and D. N. Mavris, "Data-driven approach to environmental impact assessment of real-world operations," in *AIAA Scitech 2021 Forum*, Jan. 2021. DOI: 10.2514/6.2021-0008. eprint: https://arc.aiaa.org/doi/pdf/10.2514/6.2021-0008. [Online]. Available: https://arc.aiaa.org/doi/abs/10.2514/6.2021-0008.

[231] D. T. Pham, S. S. Dimov, and C. D. Nguyen, "Selection of k in k-means clustering," *Proceedings of the Institution of Mechanical Engineers, Part C: Journal of Mechanical Engineering Science*, vol. 219, no. 1, pp. 103–119, 2005. DOI: 10.1243/095440605X8298. eprint: https://doi.org/10.1243/095440605X8298. [Online]. Available: https://doi.org/10.1243/095440605X8298.

[232] A. Likas, N. Vlassis, and J. J. Verbeek, "The global k-means clustering algorithm," *Pattern Recognition*, vol. 36, no. 2, pp. 451–461, 2003, Biometrics. DOI: https://doi.org/10.1016/S0031-3203(02)00060-2. [Online]. Available: https://www.sciencedirect.com/science/article/pii/S0031320302000602.

[233] I. S. Dhillon, Y. Guan, and B. Kulis, "Kernel k-means: Spectral clustering and normalized cuts," in *Proceedings of the Tenth ACM SIGKDD International Conference on Knowledge Discovery and Data Mining*, ser. KDD '04, Seattle, WA, USA: Association for Computing Machinery, 2004, pp. 551–556, ISBN: 1581138881. DOI: 10.1145/1014052.1014118. [Online]. Available: https://doi.org/10.1145/1014052.1014118.

[234] G. Tzortzis and A. Likas, "The global kernel k-means clustering algorithm," in *2008 IEEE International Joint Conference on Neural Networks (IEEE World Congress on Computational Intelligence)*, Jun. 2008, pp. 1977–1984. DOI: 10.1109/IJCNN.2008.4634069.

[235] A. Bouguettaya, Q. Yu, X. Liu, X. Zhou, and A. Song, "Efficient agglomerative hierarchical clustering," *Expert Systems with Applications*, vol. 42, no. 5, pp. 2785–2797, 2015. DOI: https://doi.org/10.1016/j.eswa.2014.09.054. [Online]. Available: https://www.sciencedirect.com/science/article/pii/S0957417414006150.

[236] F. Murtagh and P. Contreras, "Algorithms for hierarchical clustering: An overview," *WIREs Data Mining and Knowledge Discovery*, vol. 2, no. 1, pp. 86–97, 2012. DOI: https://doi.org/10.1002/widm.53. eprint: https://wires.onlinelibrary.wiley.com/doi/pdf/10.1002/widm.53. [Online]. Available: https://wires.onlinelibrary.wiley.com/doi/abs/10.1002/widm.53.

[237] Y. Liu, Z. Li, H. Xiong, X. Gao, and J. Wu, "Understanding of internal clustering validation measures," in *2010 IEEE International Conference on Data Mining*, Dec. 2010, pp. 911–916. DOI: 10.1109/ICDM.2010.35.

[238] U. Maulik and S. Bandyopadhyay, "Performance evaluation of some clustering algorithms and validity indices," *IEEE Transactions on Pattern Analysis and Machine Intelligence*, vol. 24, no. 12, pp. 1650–1654, Dec. 2002. DOI: 10.1109/TPAMI.2002.1114856.

[239] P. J. Rousseeuw, "Silhouettes: A graphical aid to the interpretation and validation of cluster analysis," *Journal of Computational and Applied Mathematics*, vol. 20, pp. 53–65, 1987. DOI: https://doi.org/10.1016/0377-0427(87)90125-7. [Online]. Available: https://www.sciencedirect.com/science/article/pii/0377042787901257.

[240] D. L. Davies and D. W. Bouldin, "A cluster separation measure," *IEEE Transactions on Pattern Analysis and Machine Intelligence*, vol. PAMI-1, no. 2, pp. 224–227, Apr. 1979. DOI: 10.1109/TPAMI.1979.4766909.

[241] P. C. Besse, B. Guillouet, J.-M. Loubes, and F. Royer, "Review and perspective for distance-based clustering of vehicle trajectories," *IEEE Transactions on Intelligent Transportation Systems*, vol. 17, no. 11, pp. 3306–3317, Nov. 2016. DOI: 10.1109/TITS.2016.2547641.

[242] F. Pedregosa *et al.*, "Scikit-learn: Machine learning in Python," *Journal of Machine Learning Research*, vol. 12, pp. 2825–2830, 2011.

[243] A. Behere, M. Kirby, and D. N. Mavris, "Relative importance of parameters in departure procedure design for lto noise, emission, and fuel burn minimization," in *AIAA AVIATION 2022 Forum*, Jun. 2022. DOI: 10.2514/6.2022-3916. eprint: https://arc.aiaa.org/doi/pdf/10.2514/6.2022-3916. [Online]. Available: https://arc.aiaa.org/doi/abs/10.2514/6.2022-3916.

[244] M. G. Lawrence, "The relationship between relative humidity and the dewpoint temperature in moist air: A simple conversion and applications," *Bulletin of the American Meteorological Society*, vol. 86, no. 2, pp. 225–234, 2005. DOI: 10.1175/BAMS-86-2-225. [Online]. Available: https://journals.ametsoc.org/view/journals/bams/86/2/bams-86-2-225.xml.

[245] SAS Institute, *JMP Software*, https://www.jmp.com/en_us/home.html, Accessed: 2022-07-11.

[246] A. Behere, D. Rajaram, T. G. Puranik, M. Kirby, and D. N. Mavris, "Reduced order modeling methods for aviation noise estimation," *Sustainability*, vol. 13, no. 3, 2021. DOI: 10.3390/su13031120. [Online]. Available: https://www.mdpi.com/2071-1050/13/3/1120.

[247] Z. Gao, S. I. Kampezidou, A. Behere, T. G. Puranik, D. Rajaram, and D. N. Mavris, "Multi-level aircraft feature representation and selection for aviation environmental impact analysis," *Transportation Research Part C: Emerging Technologies*, vol. 143, p. 103 824, 2022. DOI: https://doi.org/10.1016/j.trc.2022.103824. [Online]. Available: https://www.sciencedirect.com/science/article/pii/S0968090X22002467.

VITA

Ameya Behere was born and raised in Mumbai, India. He received his Bachelor and Master of Technology in Aerospace Engineering in an integrated five-year dual-degree program from the Indian Institute of Technology, Bombay in 2016. In his time in undergrad, he was involved in various student activities, most notably being part of the leadership team of the Student Mentorship Program and Academic Mentorship Program. For his Masters thesis, he worked on analyzing the interactions between high-speed rail networks and aviation, and identifying avenues of competition and cooperation.

Ameya started graduate school at the Georgia Institute of Technology in 2016, where he obtained his doctorate degree in Aerospace Engineering in 2022. He also earned a Master of Science in Aerospace Engineering and Master of Science in Computational Science and Engineering in 2021. At the Aerospace Systems Design Lab, he has worked on various projects in aviation sustainability through the Federal Aviation Administration's ASCENT Center of Excellence. He is a recipient of the Airport Cooperative Research Program's Graduate Student Award fellowship from 2018-19. In addition to research, he also has experience in the industry and government, with internships at Gulfstream Aerospace in 2014 and 2017, and at the FAA Tech Center in 2018.

In his free time he enjoys hiking, photography, and playing racquet sports.